# ICOAM 2022

**6th International Conference on Optical Angular Momentum**
**12-17 June, 2022**

Tampere University, Finland

## Conference Booklet

# How to access the WiFi

As a guest of the higher education community, you can connect to the guest network if your own organization has not joined the https://www.eduroam.fi or https://www.roam.fi services.

Or you can use the TUNI-GUEST network:

The guest network is *unencrypted*. It is only recommended for temporary use.

- Connect to the TUNI-GUEST network with your device.
- Choose your e-mail address or phone number as the means to sign in.
- Familiarise yourself with the Terms of use of IT Services and auth.fi privacy statement in the activation form and tick the box where you commit to adhering to the terms.
- Fill in the information required in the activation form (e-mail address or phone number).
- Choose Proceed.
- You will receive the activation link by e-mail or text message.
- By opening the activation link you have access to the TUNI-GUEST visitor network for 12 hours.

# Registration

The registration will be on Monday morning starting around 8:45 am in the Main lobby of the main building (see campus map on page 7), after that one can still “self-register”, i.e., pick up the badges and ICOAM material in front of the auditorium.

# Streaming information

The conference will be streamed via ZOOM via the following link:
**https://tuni.zoom.us/j/62774513243?pwd=RVpYNUUrOFlySzN2QmZPeEhqdS8xQT09**

Meeting ID: 627 7451 3243
Passcode: 866128

In case you share the link with interested group members or colleagues, please note that while it will be possible to follow the presentations ICOAM 2022 is not a hybrid conference, i.e., there will no possibility for asking questions or giving comments.

**https://events.tuni.fi/icoam2022/**

**Official Hashtag: #ICOAM2022**

# Contents

# Tervetuloa Tampereelle

*If you want to know the future, look at the past (A. Einstein)*

ICOAM 2022 is the 6th of a series of conferences aimed at bringing together scientists with a common interest in electromagnetic, electronic, and matter fields with nontrivial spatiotemporal characteristics, that allow them, for example, to carry spin and angular momenta. Since its inception in 2010 in York (United Kingdom), where its aim was simply to *"bring together the practitioners and others interested to identify new developments and directions for further exploration of this rich field",* ICOAM has been hosted in many different countries, such as United Kingdom, United States, Italy, Canada, and this year, for its 6th iteration, in Finland. ICOAM has always been the occasion for an international and widespread community of scientists to meet, discuss, brainstorm and germinate ideas, as well as to have the chance to widen the community's research horizons, by learning about possible new research fields, that the community could explore and contribute to.

The true meaning and value of ICOAM resides in its ability to bring together the community, foster new collaborations, and meet old and new friends and colleagues. It is because of its unique atmosphere and community spirit, that when the pandemic struck in 2020, we decided to shift ICOAM by one year, from June 2021 to June 2022. We have done so with the aim in mind of giving our community the possibility to physically meet and listen to high-quality and interesting research, while at the same time spending quality time together and having fun!

As a good by-product of this decision, ICOAM will now be hosted in the year, in which the community is celebrating the 30th anniversary of the publication of the seminal work by Allen and Woerdman, by most addressed as *"the paper that started it all".* This year, then, ICOAM wants to take upon itself the double challenge of looking back at the achievements and lessons we have learned during these three decades, while at the same time opening its stage for new and potentially impactful research areas, such as topological photonics, gauge-gravity duality, and data science to name a few. We hope that ideas based on angular momentum and structured waves could also find a new fertile ground in this fields to grow and carry on further the legacy of our community.

For these reasons, and to fully embrace the spirit of its tagline, ICOAM is hosting for the very first time a panel discussion, involving some of the founding fathers of our community and aimed at looking back at the early days of our community, understand the evolution of our research field, and look forward to the challenges to come. This event will give the whole community a chance to reflect on itself, get inspired by its past achievements and lay down the foundations upon which the new generation of ICOAM scientists will build the future successes and breakthroughs of this thriving community!

Last, but not least, we would like to express our deepest gratitude to the scientific committee, for their guidance in preparing the scientific program of ICOAM, to all the speakers and students that participate to ICOAM, the Tampere Congress Office, and in particular Kristiina Kuokko, for helping us with the logistics and organisational things of ICOAM, and all the people that have helped us with the practical aspects ICOAM.

We hope you will enjoy the program of the 6th ICOAM and, in addition, find some time to relish the beautiful northern European nature along with its long days and white nights.

Yours,
Marco and Robert

# Locations & Social Events

## Conference:

Venue:
Tampere University
City Center Campus
Kalevantie 4, 33100 Tampere
Main building, Lecture hall A1 (follow the signs upstairs)

## Welcome reception
## Sunday, 12.06.22

Venue:
Ravintola Periscope
Vuolteenkatu 1, 33100 Tampere
Time: Start at 7pm
Additional information:

- incl. dinner buffet and welcome drink

## Sauna Party
## Tuesday, 14.06.22

Venue:
Varala Sauna
Varalankatu 36, 33240 Tampere
Time: Start at 6:15pm (at location), 6:00pm (transport to location)
Additional information:

- There will be buses bringing all participants to the location. The buses will leave at the conference venue in front of the main building at 6:00pm
- Please bring your swimsuits (non-private saunas are usually non-nude in Finland)
- Note that there will be mixed-gender saunas as well as gender-separated saunas and swimming possibilities
- Incl. BBQ style dinner and drinks
- Departure to conference venue by bus at 10:00pm

## Boat Trip & Conference Dinner
## Thursday, 16.06.22

Harbour:
Laukontori, 33200 Tampere
Dinner Venue:
Ravintola Viikinsaari
Viikinsaari 2, 33950 Tampere
Time: Departure from harbour at 6:00pm. Return after dinner at harbour: approx. 11pm
Additional information:

- You can either arrive at the harbour on your own, or you can join the organised walk (~20min) to the harbour together from the conference venue at 5:30pm.
- The dinner will start at around 7pm on Viikinsaari
- Incl. buffet style dinner and 2 drinks
- Departure to harbour by boat at 10:30pm

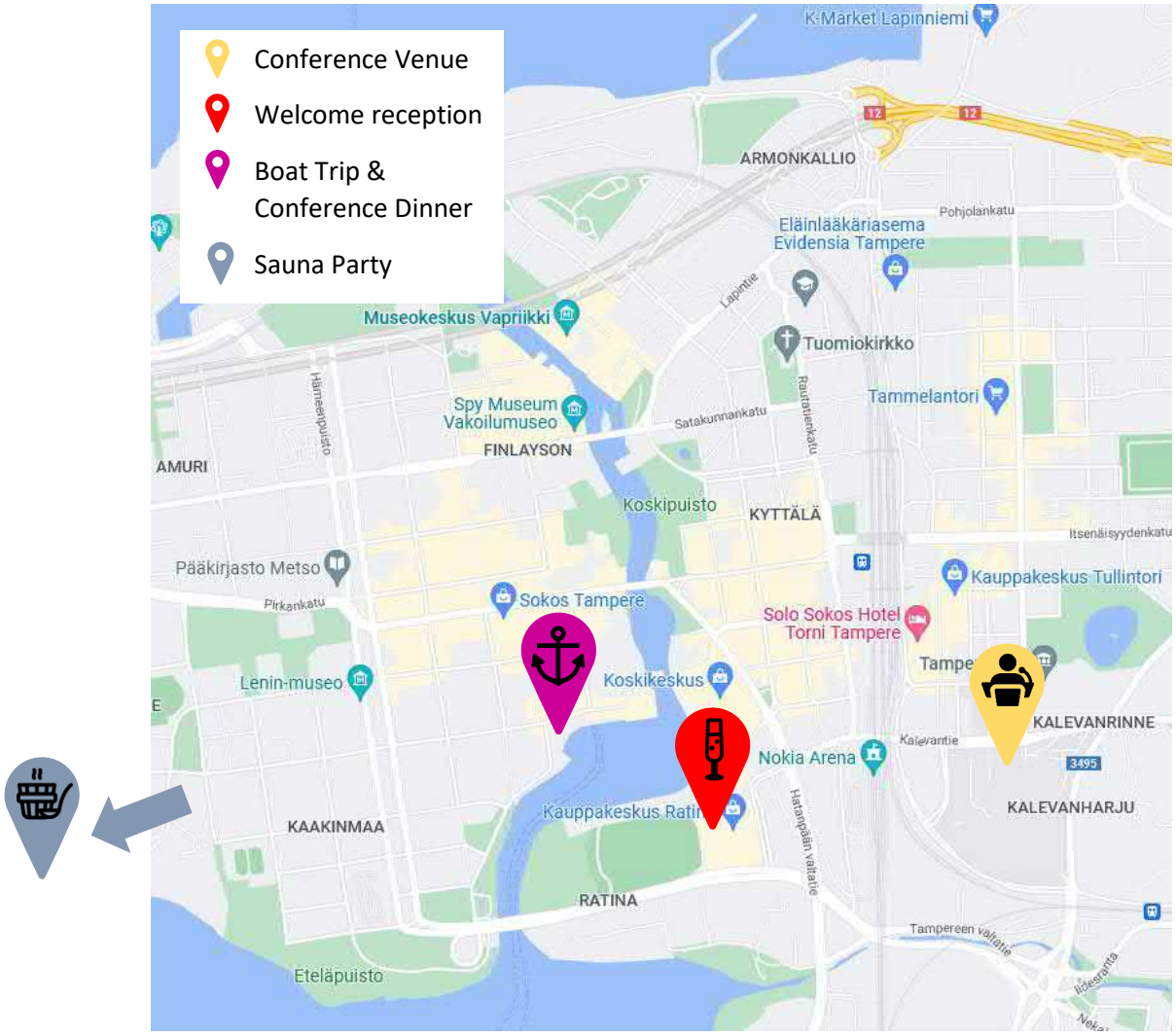
Conference Venue
Welcome reception
Boat Trip & Conference Dinner
Sauna Party
K-Market Lapinniemi
ARMONKALLIO
Pohjolankatu
Eläinlääkäriasema Evidensia Tampere
Lapintie
Museokeskus Vapriikki
Tuomiokirkko
Tammelantori
Rautatienkatu
Satakunnankatu
Spy Museum Vakoilumuseo
FINLAYSON
AMURI
Hämeenpuisto
Koskipuisto
KYTTÄLÄ
Itsenäisyydenkatu
Pääkirjasto Metso
Pirkankatu
Sokos Tampere
Kauppakeskus Tullintori
Solo Sokos Hotel Torni Tampere
Lenin-museo
Koskikeskus
KALEVANRINNE
Kalevantie
Nokia Arena
3495
KALEVANHARJU
Kauppakeskus Ratina
Hatanpään valtatie
KAAKINMAA
RATINA
Tampereen valtatie
Eteläpuisto

# Campus restaurants

Lunch **is included** for all participants at restaurant Minerva in the Pinni B building if you show your batch at the counter.

③ Pinni B building, 2nd floor, Restaurant Minerva

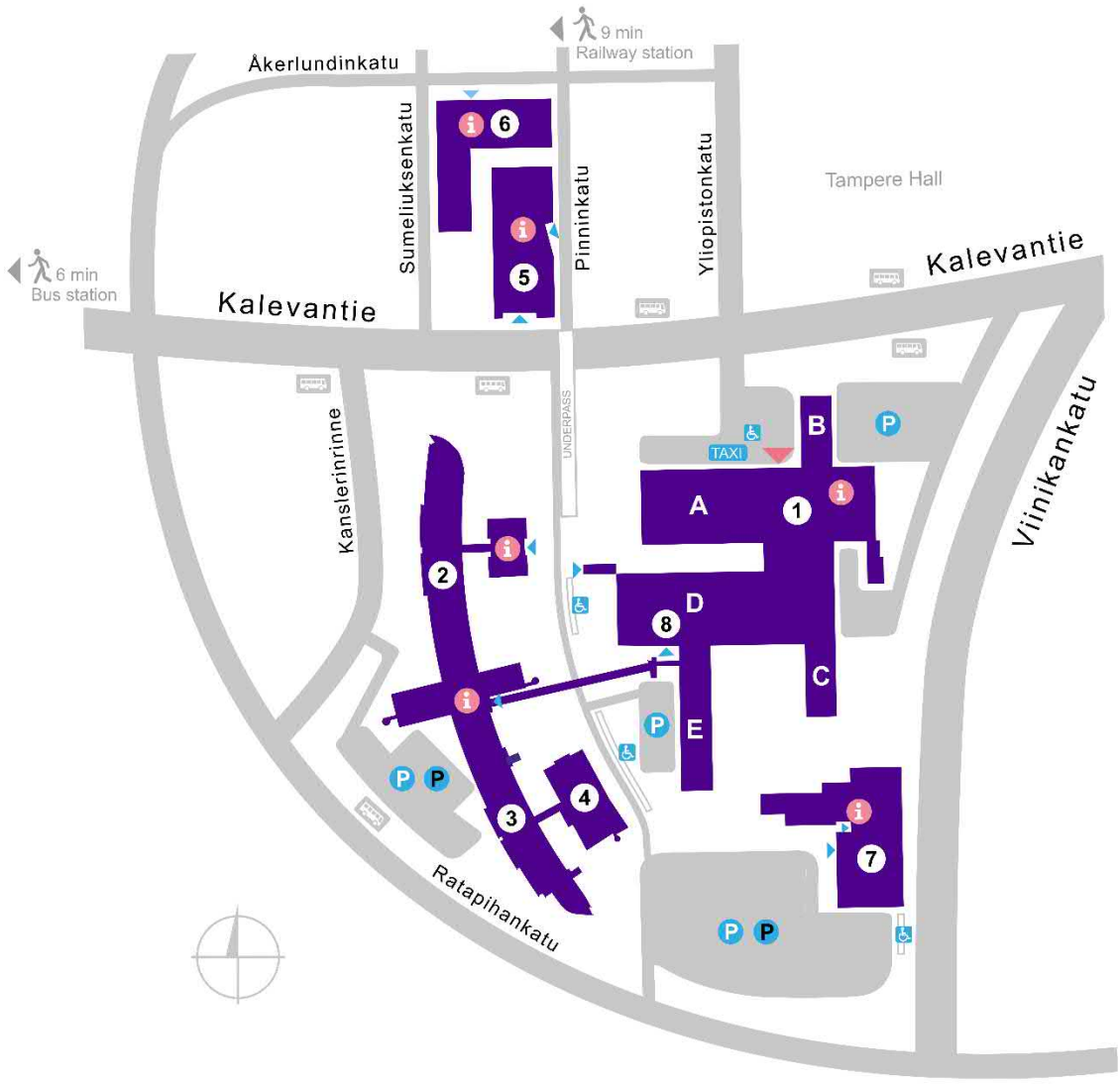

# Other restaurants close to the university

Restaurant Dabbal, Yliopistonkatu 44 (Lapland Hotel)

Restaurant Myllärit, Åkerlundinkatu 4

Restaurant Sasor, Yliopistonkatu 50

Restaurant Sorella, Vuolteenkatu 20

Restaurant Telakka, Tullikamarin aukio 3

Restaurant Tuhto, Yliopistonkatu 55 (Tampere Hall)

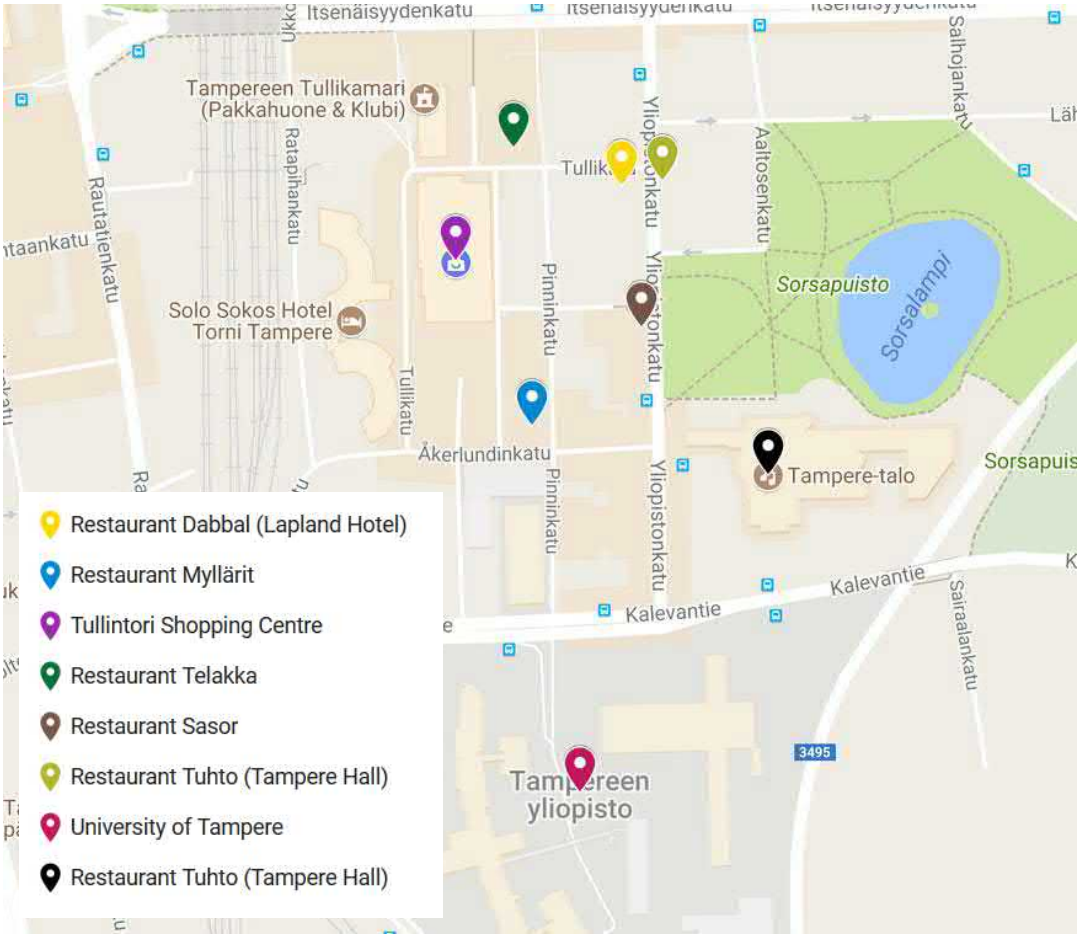


There is also plenty more restaurants in the city centre we hope you enjoy to discover.

# Tampere Highlights

Tampere offers plenty of things to do. Explore your options via the Visit Tampere webpages.

Download the **Tampere.Finland app** to find things to see and do. The app features guided tours, local bus and tram routes and timetables, the Tampere event calendar, as well as the Tampere Pass discount application (Tampere Tunnetuksi Passi). The application can be downloaded free of charge from Google Play Store and Apple App Store. You can find more information on the Tampere Pass here.

Watch the YouTube video on 5 reasons to visit Tampere.

You can check the weather forecast here.

## Our Recommendations:

- *Pyynikin Tower, Näkötorni and Munkki Café:* It offers a nice view and the best Munkkis (donuts)
- *Sauna's:*
  - The oldest Sauna in Finland: Rajaportti
  - The most modern Sauna at the city center: Kuuma
  - Saunas with nice beaches and swimming opportunities: Rauhaniemi or Kaupinoja

  Don't forget to take a swimsuit along. Mixed public saunas require you to wear a swimsuit!

- *Tampere Market Hall Kauppahalli*: This is a nice old building to explore the scents and tastes of Finnish treats and delicacies.

- *Outdoor market Tammelantori:* Find many fresh vegetables, fruits and plenty of small food stalls.

- *Nature activities:*
  - Kajak, Kanu, mountain bike rent: Hiking Travel, Hit (maps)
  - Hiking: Many trails start nearby the Hiking Travel location (info also on the webpage) or in Hervanta, which is reachable by public transport (Info on trails in/around Tampere). There are plenty of bonfire places at the trails where wood is provided (map for bonfire places).

- *Special Museums:*
  - The outdoor museum of Worker's Housing: Amurin museokortteli (maps)
  - The Moomin Museum for fans of the famous Finnish cartoon figure (maps)

# Conference Program Overview

| | Sunday 12.06.22 | Monday 13.06.22 | Tuesday 14.06.22 | Wednesday 15.06.22 | Thursday 16.06.22 | Friday 17.06.22 |
|---|---|---|---|---|---|---|
| **08:45-09:00** | | Registration | | | | **Concluding Remarks** |
| **09:00-09:25** | | **Opening Remarks** | **Sonja Franke-Arnold**<br>University of Glasgow, UK | **Daniel Leykam**<br>Institute for Basic Science, South Korea | **Filippo Cardano**<br>Università di Napoli Federico II, Italy | **Danilo Gomes Pires**<br>Duke University, USA |
| **09:25-09:50** | | **Cornelia Denz**<br>Universität Münster, Germany | **Ferdinand Schmidt-Kaler**<br>University of Mainz, Germany | **Fabio Biancalana**<br>Heriot-Watt University, UK | **Jonathan Leach**<br>Heriot-Watt University, UK | **Tyler Neely**<br>University of Queensland, Australia |
| **09:50-10:05** | | **Igor Meglinski**<br>University of Oulu, Finland | **Christian Schmiegelow**<br>Universidad de Buenos Aires, Argentina | **Takashige Omatsu**<br>Chiba University, Japan | **Jietai Jing**<br>East China Normal University, China | **Robert Bennet**<br>University of Glasgow, UK |
| **10:05-10:20** | | **Payvand Arjmand**<br>Université Paris Cité, France | **Andrei Afanasev**<br>George Washington University, USA | **Enrique Galvez**<br>Colgate University, USA | **Mujtaba Zahidy**<br>Technical University of Denmark, Denmark | **Andreas Norrman**<br>University of Eastern Finland, Finland |
| **10:20-10:50** | | Coffee Break | Coffee Break | Coffee Break | Coffee Break | Coffee Break |
| **10:50-11:15** | | **Qiwen Zhan**<br>University of Shanghai for Science & Technology, China | **Marcus Huber**<br>Technical University Vienna, Austria | **Lixiang Chen**<br>Xiamen University, China | **Vincenzo Grillo**<br>Istituto di Nanoscienze Cnr, Italy | **Jamal Berakdar**<br>Martin-Luther University, Germany |
| **11:15-11:40** | | **Howard Milchberg**<br>University of Maryland, USA | **Ebrahim Karimi**<br>University of Ottawa, Canada | **Jacquiline Romero**<br>University of Queensland, Australia | **Raphael Dahan**<br>Technion, Israel | **Joel Carpenter**<br>University of Queensland, Australia |
| **11:40-12:05** | | **Alison Yao**<br>University of Strathclyde, UK | **Bereneice Sephton**<br>University of Witwatersrand, South Africa | **Mehul Malik**<br>Heriot-Watt University, UK | **Dmitry Pushin**<br>University of Waterloo, Canada | **Miguel Alonso**<br>CNRS, Aix Marseille University, France |
| **12:05-12:30** | | **Peter Banzer**<br>Universität Graz, Austria | **Siddharth Ramachandran**<br>Boston University, USA | **Mark T. Lusk**<br>Colorado School of Mines, USA | **Konstantin Bliokh**<br>RIKEN, Japan | **Peter Mekhail**<br>University of Glasgow, UK |
| **12:30-14:00** | arrival | Lunch | Lunch | Lunch | Lunch | Lunch |
| **14:00-14:25** | | **Jaroslav Kysela**<br>IQOQI Vienna, Austria | **Jian Wang**<br>HUST - University of Science & Technology, China | Poster Session | Panel Discussion<br>**David Andrews**,<br>University of East Anglia, UK<br>**Mohamed Babiker**,<br>University of York, UK<br>**Stephen Barnett**,<br>University of Glasgow, UK<br>**Sir Micheal Berry**,<br>University of Bristol, UK<br>**Miles Padgett**,<br>University of Glasgow, UK<br>**Halina Rubinsztein-Dunlop**,<br>University of Queensland, Australia | **Mark Dennis**<br>University of Birmingham, UK |
| **14:25-14:50** | | **Girish Kulkarni**<br>University of Ottawa, Canada | **Flavio Capotondi**<br>Elettra (Synchrotron), Italy | | | **Jörg Götte**<br>University of Glasgow, UK |
| **14:50-15:15** | | **Antonio Khoury**<br>Universidad Federal Fluminense, Brazil | **Martin Lavery**<br>University of Glasgow, UK | | | **Kayn Forbes**<br>University of East Anglia, UK |
| **15:15-15:30** | | **Alba de la Heras**<br>Universidad de Salamanca, Spain | **Vincenzo D'Ambrosio**<br>Università di Napoli Federico II, Italy | | | **Emilio Pisanty**<br>King's College London, UK |
| **15:30-16:00** | | Coffee Break | Coffee Break | Enjoying Tampere | Coffee Break | departue |
| **16:00-16:25** | | **Etienne Brasselet**<br>University of Bordeaux, France | **Alexander Szameit**<br>Universität Rostock, Germay | | **Robert Cameron**<br>University of Strathclyde, UK | |
| **16:25-16:50** | | **Gianluca Ruffato**<br>University of Padova, Italy | **Ritesh Agarwal**<br>University of Pennsilvania, USA | | **Gabriel Molina** Terriza<br>Donostia International Physics Centre, Spain | |
| **16:50-17:15** | | **Federico Capasso**<br>Harvard university, USA | **Alan Willner**<br>University of Southern California, USA | | **Benjamin J. McMorran**<br>University of Oregon, USA | |
| **17:15-17:30** | | | **Thierry Ruchon**<br>Université Paris-Saclay, France | | | |
| | | | | | | |
| **18:00-20:00** | | Poster Session | | | | |
| **social events** | **Welcome Reception**<br>(start 19:00) | | **Sauna Party**<br>(departure to venue by bus 18:00,<br>start at venue 18:15,<br>return to campus by bus at around 22:00) | | **Boat Trip & Conference Dinner**<br>(walk to harbour 17:30,<br>departure at harbour by boat 18:00,<br>return to harbour at around 23:00) | |

# Conference Program

## Monday

| | |
|---|---|
| 8:45-9:00 | Registration |
| 9:00-9:25 | Opening Remarks |
| 9:00-10:20 | **Cornelia Denz**: Topology in three-dimensionally structured light |
| | **Igor Meglinski:** Orbital Angular Momentum for Biomedical Diagnosis and Tissues Characterization |
| | **Payvand Arjmand:** Compressive STED Microscopy with Speckles |
| 10:50-12:30 | **Qiwen Zhan:** Spatiotemporal Sculpturing of Ultrashort Pulses (Remote Presentation) |
| | **Howard Milchberg:** Spatio-temporal optical vortex (STOV) pulses: propagation and OAM conservation |
| | **Alison Yao:** Structuring light for controlled propagation of optical and atomic solitons |
| | **Peter Banzer:** Super Pixels – Phase and Polarization Sensitive Cameras Based on Integrated Photonics |
| 14:00-15:30 | **Jaroslav Kysela:** Engineering high-dimensional quantum entanglement via path identity |
| | **Girish Kulkarni:** A classical model of spontaneous parametric down-conversion |
| | **Antonio Khoury:** Spin to orbital angular momentum transfer in nonlinear wave mixing |
| | **Alba de la Heras:** Nonlinear up-conversion of scalar and vectorial vortices through high harmonic generation |
| 16:00-17:30 | **Etienne Brasselet:** Spin-independent geometric self-focusing of light driven by the photon spin |
| | **Gianluca Ruffato:** A general conformal framework for structured wavefields: from OAM algebra to multipoles analysis |
| | **Federico Capasso:** 3D Structuring of Light with Metaoptics (Remote Presentation) |
| 18:00-20:00 | Poster Session |

# Conference Program

## Tuesday

| | |
|---|---|
| 9:00-10:20 | **Sonja Franke-Arnold:** Shape-shifting cold atoms with vector light |
| | **Ferdinand Schmidt-Kaler:** Ion wavepackets interacting with vortex laser beams |
| | **Christian Schmiegelow:** Transfer of optical orbital angular momentum to the transverse motion of the center of mass of a single trapped ion |
| | **Andrei Afanasev:** Angular Momentum and Polarization Transfer from the Twisted Light to Atoms |
| 10:50-12:30 | **Marcus Huber:** High-dimensional entanglement for quantum communication (Remote Presentation) |
| | **Ebrahim Karimi:** Structured Photons – Their Application in Quantum Photonics (Remote Presentation) |
| | **Bereneice Sephton:** Teleporting high-dimensional OAM states |
| | **Siddharth Ramachandran:** High Dimensional Quantum Sources with Optical Fibers |
| 14:00-15:30 | **Jian Wang:** Tailoring Optical Angular Momentum with Fibers and Chips: Devices and Applications (Remote Presentation) |
| | **Flavio Capotondi:** Applications of XUV – OAM beams to image transient dynamics of plasmonic nanostructures and magnetic vortex |
| | **Martin Lavery:** Environmental and Fibre Sensing with Structured Light |
| | **Vincenzo D'Ambrosio:** Ultra-sensitive measurement of transverse displacements with linear photonic gears |
| 16:00-17:30 | **Alexander Szameit:** Nonlinear Photonic Topological Insulators (Remote Presentation) |
| | **Ritesh Agarwal:** On-chip OAM photodetectors: topological light meets topological materials |
| | **Alan Willner:** Advances in Utilizing OAM Multiplexing for Communication Systems in the THz and Mid-IR Frequency Bands (Remote Presentation) |
| | **Thierry Ruchon:** Magnetic Helicoidal Dichroism with XUV Light Carrying Orbital Angular Momentum |
| 18:00 | Sauna Party (departure to venue by bus 18:00, start at venue 18:15, return to campus by bus at around 22:00) |

# Conference Program

## Wednesday

9:00-10:20

**Daniel Leykam:** Singular Optics: From a Data Science Perspective (Remote Presentation)

**Fabio Biancalana:** Non-perturbative, fully quantum formulation of nonlinear optics in 2D media: the holographic principle

**Takashige Omatsu:** Optical vortex induced forward transfer for printed electronics and photonics (Remote Presentation)

**Enrique Galvez:** Einstein Beams: Light beams following gravitationally-lensed trajectories

10:50-12:30

**Lixiang Chen:** The Radial Momentum of Light (Remote Presentation)

**Jacquiline Romero:** Hiding Ignorance Using High Dimensions

**Mehul Malik:** Transport and Manipulation of High-Dimensional Entanglement through a Complex Medium

**Mark T. Lusk:** The Geometric Phase of Entanglement for Trapped Optical Vortices and Its Interpretation as an Information Measure

14:00-15:30 Poster Session

# Conference Program

## Thursday

9:00-10:20

**Filippo Cardano:** Ultra-long photonic quantum walks via spin-orbit metasurfaces

**Jonathan Leach:** Efficiently sorting overlapping quantum states of light

**Jietai Jing:** OAM multiplexed quantum entanglement and quantum teleportation (Remote Presentation)

**Mujtaba Zahidy:** Recent development of OAM mode generation for quantum communication

10:50-12:30

**Vincenzo Grillo:** Electrostatic OAM generation, detection and ghost imaging in electron microscopy

**Raphael Dahan:** Tunable Photon-Induced Spatial Modulation of Free Electron Wavepackets

**Dmitry Pushin:** Integrating structured wave techniques into neutron sciences

**Konstantin Bliokh:** Momentum and Angular Momentum of Sound, Water, and Plasma Waves

14:00-15:30 Panel Discussion

16:00-17:30

**Robert Cameron:** How to knot microwaves

**Gabriel Molina** Terriza**:** Classical and Quantum scattering of vortex beams from small particles

**Benjamin J. McMorran:** Quantum Interactions with Structured Electrons

18:00 Boat Trip and Conference Dinner
(walk to harbour 17:30, departure at harbour by boat 18:00, return to harbour at around 23:00)

# Conference Program

## Friday

8:45-9:00 Concluding remarks

9:00-10:20

**Danilo Gomes Pires:** Knots of darkness in turbulent media

**Tyler Neely:** DMD-based optical traps for stirring-up and observing Bose-Einstein condensate superfluid dynamics (Remote Presentation)

**Robert Bennet:** A condensate of light as a sensor of chirality

**Andreas Norrman:** Spin structures in random three-dimensional polarization states

10:50-12:30

**Jamal Berakdar:** Generation of structured fields via Spintronic THz emitters (Remote Presentation)

**Joel Carpenter:** Time reversed optical waves by arbitrary vector spatiotemporal field generation

**Miguel Alonso:** Geometry and topology in 3D Polarization

**Peter Mekhail:** 3D Time-of-Flight Imaging using Ultra-thin Endoscopy

14:00-15:30

**Mark Dennis:** Skyrmionic Hopfions: particle-like twisted topologies in light

**Jörg Götte:** Paraxial Skyrmionic Beams

**Kayn Forbes:** Chirality and optical activity of twisted light (Remote Presentation)

**Emilio Pisanty:** Three-dimensional polychromatic knots and skyrmionic textures via tightly-focused beams

# Overview Poster Session

| | |
|---|---|
| **Esra I. Albar:** | Generating Twisted Light using Archimedean Spirals: A Real-Space Real-Time Study |
| **Baghdasar Baghdasaryan:** | The Gouy Phase in Parametric Downconversion: Decoupling of Spatial and Spectral Degrees of Freedom |
| **Sarvesh Bansal:** | Detection of Singular Beams on Higher Order Poincare Sphere |
| **Rafael Barros:** | Observation of the quantum Gouy phase |
| **Ben W. Butler:** | Misalignment of spin densities in helicity lattices |
| **Carl E. Carlson:** | Micromanipulation using twisted photons to test superkicks and momentum Densities |
| **Claire M. Cisowski:** | Angular momentum redirection phases of vector beams |
| **Timothé Denys:** | Measuring the phase and polarization of structured vector beams with quadriwave lateral shearing interferometry |
| **Francesco Di Colandrea:** | Ultra-long photonic quantum walks via liquid-crystal metasurfaces |
| **Daniel Ehrmanntraut:** | Generation and measurement of volume-filling structures in paraxial light |
| **Matias Eriksson:** | Talbot self-imaging and two-photon interference in ring-core fibers |
| **Angelina Frank:** | Boosted Topological Domain Walls in 1D Photonic Waveguide Arrays |
| **Kapil K. Gangwar:** | Polarization Singularity Array Generation Using Dammann Grating |
| **Ana García-Cabrera:** | Multi-vortex high-harmonic beams from graphene's anisotropy |
| **Rodrigo Gutiérrez-Cuevas:** | Learning from the disorder in multimode fibers |
| **Vagharshak Hakobyan:** | Hyperspectral optical vortex modulation |
| **Grant Henderson:** | Propagation of coupled atom-light solitons carrying angular momentum in a Bose-Einstein Condensate |
| **Isael A. Herrera Hernandez:** | Role of supercritical angle fluorescence in CHIDO microscopy |
| **Natalia Herrera Valencia:** | Entangled ripples and twists of light: Radial and azimuthal Laguerre-Gaussian mode entanglement |
| **Markus Hiekkamäki:** | Photonic angular super-resolution using twisted N00N states |
| **Muhammad W. Iqbal:** | Non Circular Conical Diffraction with Fractional Optical Angular Momentum |

| | |
|---|---|
| **Felipe Isaule:** | Quantum phases of bosonic chiral molecules in helicity lattices |
| **Malcolm Kadodwala:** | Optical Angular Momentum For Dynamic Control of Material Properties (presented by Paula Laborda Lalaguna) |
| **Suman Karan:** | Controlled generation of high-dimensional OAM entangled state without postselection |
| **Matias Koivurova:** | Self-focusing vortex beams in turbulence |
| **Baby Komal:** | Complete self-healing of V-point singularities |
| **Lea Kopf:** | Spectral vector beams for high-speed spectroscopic measurements |
| **Oussama Korichi:** | High efficiency interface between multi-mode and single-mode fibers |
| **Neel Mackinnon:** | On the Differences between Helicity and Chirality |
| **Lewis Madden:** | A Unifying Approach to Spin and Orbital Angular Momentum for Vector Spherical Harmonics |
| **Manisha:** | Detection of Non-isotropic Partially Coherent Vector Vortex Beams |
| **David Marco Castillo:** | Nonparaxial optical fields containing all possible polarization ellipses in a 4D physical space-time |
| **Marcello H. Marques Passos:** | Spin-orbit X-states |
| **Kerr Maxwell:** | Semiclassical approximation of Zernike amplitudes via the Higgs oscillator |
| **Amy McWilliam:** | A practical approach to measuring paraxial optical Skyrmions |
| **Philip Menz:** | Orbital angular momentum-based pseudospin coupling in photonic lattices with higher-order conical intersections |
| **Björn Minneker:** | A geometric approach to tour-knot angular momentum in high harmonic radiation |
| **Satyajeet Patil:** | Anisotropic Spatial Entanglement |
| **Braian Pinheiro da Silva:** | Observation of triangular-lattice pattern in nonlinear wave mixing with optical vortices |
| **Shreyas Ramakrishna:** | Photo-excitation of atoms by vector Laguerre-Gaussian beams |
| **Valeria Rodríguez-Fajardo:** | Swinging and Rotating Pendulum Beams: 3D modal wavepackets that simulate the quantum-pendulum |
| **Filippo Romanato:** | Design and fabrication of silicon metasurfaces for control of structured light beams |
| **Keshaan Singh:** | Turbulence invariant basis for optical communication |

| | |
|---|---|
| **Afsoun Soltani:** | OAM Mode Conversion using Two Dimensional Multimode Interference (2D MMI) Couplers |
| **Lavi Somers:** | Integrated orbital angular momentum mode sorters on vortex fibers |
| **Felix Stopp:** | Transversal movement transfer of light carrying OAM to single trapped 40Ca+ ions |
| **Yaraslau Tamashevich:** | Inhomogeneous Dirac-Bloch Equations for Graphene Interacting with Structured Light |
| **Maurizio Verde:** | Optical super-resolution sensing of a trapped ion's wave packet size |
| **Alexander J. Vernon:** | Cold Spots: A Meeting Point for Polarisation Singularities, and their Complete Position Control |
| **Maddie Waller:** | Environment-modified Three-body Energy Transfer |
| **Niclas Westerberg:** | Helicity in a chiral Hopfield dielectric |
| **Zhujun Ye:** | Faraday effect for vector vortex beams |
| **Iuliia Zalesskaia:** | A double-clad ytterbium-doped tapered fiber with circular birefringence as a gain medium for structured light |

# Abstracts

## Invited Talks

# On-chip OAM photodetectors: topological light meets topological materials

**Ritesh Agarwal**[*1]

*1. Department of Materials Science and Engineering, University of Pennsylvania, Philadelphia, USA*

Photodetectors detect the presence of light and are important components for applications in spectroscopy, imaging, diagnostics and for driving our information technology infrastructure. Most conventional photodetectors detect optical power, i.e., convert the total number of photons impinging on the active area into a corresponding photocurrent. This approach of utilizing only a small subset of the entire information carrying capacity of light is highly limiting given the full vectorial description of light which endows it with many degrees of freedom that largely remain untapped for on-chip applications. Within the semiclassical picture, light-matter interactions can be designed to be extremely versatile to go beyond the simple intensity and wavelength characteristics, therefore taking the full advantage of different degrees of freedom of light, i.e., intensity, frequency, polarization and phase. There is a need to develop on-chip devices that can measure the polarization, intensity and phase gradients of light using direct photocurrent readout method for integrated photonics applications. Fabricating on-chip photonic devices that can detect complex optical modes representing different polarization and complex phase differences and gradients is not an easy task and requires an intricate interplay of symmetry and topology along with the optimization of the geometrical parameters of the device that is compatible with the underlying phase-dependent geometrical response of the material system. Hence, new advances in materials, fundamental understanding of complex light-matter interaction and innovative optical and device engineering are required to solve this problem for making photodetectors that can directly detect the complete vectorial nature of optical beams.

The development of on-chip chiral photonic devices requires fundamental investigations and manipulation of momentum space geometry and topology of materials and their coupling to the environment to engineer specific spin-orbit interactions to control and detect the vectorial states of light. We will first discuss our efforts to explore the properties of $Mo_x\ W_{1-x}Te_2$, which are type-II Weyl semimetals, i.e., gapless topological states of matter with broken inversion and/or time reversal symmetry. We observed spatially dispersive circular photogalvanic effect (s-CPGE) over a wide spectral region $(0.2-2.0$ eV range) by using optical beams with spatially inhomogeneous intensity profiles [1]. This effect shows exclusively in the Weyl phase and vanishes upon temperature induced topological phase change. We will describe how spatially inhomogeneous optical excitation along with unique symmetry, band structure and inversion, large Berry curvature and symmetry, band structure and inversion, large Berry curvature and topology of Weyl semimetals produces a strong S-CPGE response. We will then extend this idea to the orbital photogalvanic effect (OPGE), which is driven by the helical phase gradient of optical beam, that is characterized by a current winding around the optical beam axis with a magnitude proportional to its quantized OAM mode number [2]. OPGE accesses different properties of the material

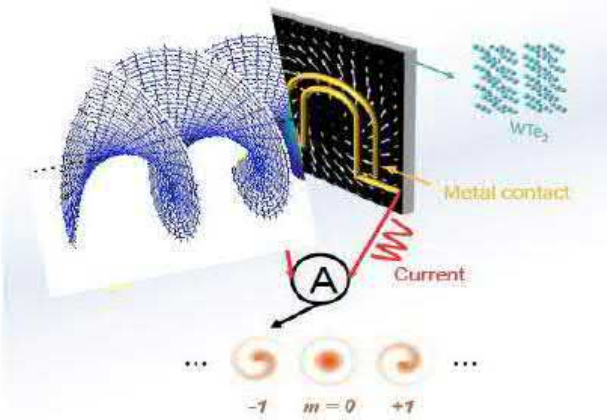


**Fig. 1:** Fig. 1. Schematic of photodetection of polarization and orbital angular momentum modes using WTe (room [2] temperature Weyl semimetal). The technique involves nonlocal photoresponse of the material to detect the OAM mode of light. via a more complex carrier excitation mechanism and symmetry characteristics and can lead to charge vortices in topological systems. The direct transduction of photocurrents mapped to various SAM-OAM (spin-orbital angular momentum) coupled states is engineered via nonlocal light-matter interactions that cannot be described within the electric-dipole approximation and requires a theoretical description accounting for the topology of electronic bands and light (OAM states with topological charge). Our studies on nonlocal CPGE provides a promising route towards the development of-chip detection of optical OAM modes, which can enable the development of next-generation chiral photonic circuits.

## References

[1] Ji, Zhurun; Liu, Gerui; Addison, Zachariah; Liu, Wenjing; Yu, Peng; Gao, Heng; Liu, Zheng; Rappe, Andrew M.; Kane, Charles L.; Mele, Eugene J.; Agarwal, Ritesh, "Spatially dispersive circular photogalvanic effect in a Weyl semimetal". Nat. Mater. 2019, 18 (9), 955-962.

[2] Ji, Zhurun; Liu, Gerui; Krylyuk, Sergiy; Fan, Xiaopeng; Zhang, Zhifeng ; Pan, Anlian; Feng, Liang; Davydov, Albert; Agarwal, Ritesh, "Photocurrent detection of the orbital angular momentum of light". Science **2020**, 368(6492), 763 – 767.

[*]Corresponding author: riteshag@seas.upenn.edu

# Geometry and topology in 3D Polarization

**Miguel A. Alonso**[*1,2]
*1. Aix Marseille Univ., CNRS, Centrale Marseille, Institut Fresnel, UMR 7249, 13397 Marseille Cedex 20, France*
*2. The Institute of Optics and Laboratory for Laser Energetics, University of Rochester, Rochester NY 14627, USA*

**Introduction:** The polarization of electromagnetic waves refers to the statistical description of the geometric behavior of the oscillations of the electric (or sometimes the magnetic) field vector for optical fields. The study of optical polarization and the implementation of techniques for measuring it have been mainly restricted to light with a well-defined local direction of propagation. This restriction is valid in many common situations, such as when the light source is distant and subtends a small range of angles at the point of observation, or when a collimated laser beam is considered. The transversality of the electric and magnetic fields then means that their component in the direction of propagation is much smaller than those normal to this direction and hence has a negligible effect on measurements. These longitudinal field components can therefore be ignored for most practical purposes.

In recent years, there has been growing interest in areas such as nano-optics, plasmonics and microscopy, in the polarization of light in cases where all three Cartesian field components can be significant. The aim of this talk is to present a summary of different theoretical descriptions of nonparaxial light as extensions to the standard treatment in the paraxial regime, with an emphasis on geometric interpretations. Much of the work presented here is contained in a tutorial in progress [1].

**Fully polarized fields:** For paraxial light, a useful abstract representation of polarization is given by the spherical coordinates of a point over the surface of a unit sphere, the Poincaré sphere: the two polar coordinates encode respectively the ellipticity and orientation of the polarization ellipse, and the Cartesian axes correspond to the normalized Stokes vectors.

**Partial polarization:** When the field is not purely monochromatic, the shape traced by the electric field is in general not periodic and is significantly more complex than an ellipse. However, the details of the oscillation are typically over a time scale inaccessible to detectors, and what can be measured are averages over the detector's integration time of quantities that have a quadratic dependence in the field. The polarization at a given point is then statistically described by the autocorrelation matrix of the field components, known as the polarization (or coherency) matrix. For paraxial light, only a $2 \times 2$ matrix is needed, and the coefficients of its expansion in terms of Pauli matrices are precisely the Stokes parameters. When normalized by the intensity, these Stokes parameters give coordinates over or inside the Poincaré sphere, and the distance to the origin is known as the degree of polarization.

For nonparaxial light, the polarization matrix is $3 \times 3$. Its decomposition in terms of the Gell-Mann matrices gives what is sometimes referred to a s the generalized Stokes parameters [4], which when normalized provide a description of polarization in terms of a point in an 8D abstract space. Several definitions for the degree of polarization have been proposed, one of which corresponds to the radial coordinate in this space. However, an important difference with the paraxial case is that not all points inside the hypersphere correspond to physical polarization states, the shape of the inhabitable region being quite complex [1]. Alternative and more intuitive representations can be formulated in terms of not one but a collection of points in 3D space.

**Measurements for fluorophores and spin textures:** Optical measurements of nonparaxial polarization typically imply the interaction of the field with a known small probe, whose scattered field is characterized. These techniques have been used for the experimental verification of interesting local polarization effects such as transverse spin [5]. Further, by scanning the probe, the spatial distribution of polarization can be detected, hence allowing the observation of extended topological features such as polarization Möbius bands [6], knotted structures [7] and skyrmions [8]. In this presentation we present a new and simple time-dependent field distribution that spans all possible states of full nonparaxial polarization over a unit cell in space and time. This field can be regarded as a 4D skyrmion.

An application for which nonparaxial polarization is of interest is fluorescence microscopy, where instead of elastic scattering nanoparticles one detects fluorescent molecules that label biological samples. Therefore, rather than the particle allowing the retrieval of local information about the field, the measured emitted field reveals information (3D position and orientation) about the particle. In particular, the measured nonparaxial polarization of the field emitted by each fluorophore provides information about its orientation and even whether it is static or "wobbling". We show results of a technique based on birefringent filtering within the Fourier plane in order to encode the information about the molecule's orientation (i.e. the polarization of the emitted light) and its height in the shape of the point spread function [9].

**Acknowledgments**: I'd like to thank many collaborators in work related to the main topic of this presentation and whose results are directly or indirectly discussed: L. Arturo Alemán Castañeda, R. Gutiérrez Cuevas, I. Herrera Hernández, Y.-T. Feng, S. Vo, A. J. Vella, V. Curcio, S. Brasselet, T. G. Brown, K. Bliokh, M. R. Dennis, E. Brasselet, J.S. Eismann, L.H. Nicholls, D.J. Roth, P. Banzer, F.J. Rodríguez Fortuño, A.V. Zayats, F. Nori, and P. Réfrégier.

## References

[1] M.A. Alonso, http://arxiv.org/abs/2008.02720 (2020).
[2] J.H. Hannay, J. Mod. Opt. 45, 1001-1008 (1998).
[3] K.Y. Bliokh, M.A. Alonso and M.R. Dennis, Rep. Prog. Phys. 82, 122401 (2019).
[4] C. Brosseau, Fundamentals of Polarized Light (Wiley, 1998).
[5] J.S. Eismann, L.H. Nicholls, D.J. Roth, M.A. Alonso, P. Banzer, F.J. Rodríguez-Fortuño, A.V. Zayats, F. Nori and K.Y. Bliokh, Nat. Phot. 15, 156161 (2021).
[6] T. Bauer, P. Banzer, E. Karimi, S, Orlov, A. Rubano, L. Marrucci, E. Santamato, R.W. Boyd, and G. Leuchs, Science 347, 964966 (2015).
[7] H. Larocque, D. Sugic, D. Mortimer, A.J. Taylor, R. Fickler, R.W. Boyd, M.R. Dennis, and E. Karimi, Nat. Phys. 14, 1079-1083 (2018).
[8] S. Tsesses, E. Ostrovsky, K. Cohen, B. Gjonaj, N.H. Lindner, and G. Bartal, Science 361, 993-996 (2018).
[9] V. Curcio, L.A. Alemán-Castañeda, T.G. Brown, S. Brasselet and M.A. Alonso, Nature Comm. 11, 5307 (2020).

[*]Corresponding author: miguel.alonso@fresnel.fr

# SuperPixels – Phase and Polarization Sensitive Cameras Based on Integrated Photonics

**Johannes Bütow** [1], **Jörg S. Eismann** [1,2,3], **Varun Sharma** [1], **Dorian Brandmüller** [1], **Peter Banzer**[*2,1]

*1. Institute of Physics, University of Graz, NAWI Graz, Austria*

*2. Max Planck Institute for the Science of Light, Erlangen, Germany*

*3. Institute of Optics, Information, and Photonics, University Erlangen-Nuremberg, Germany*

Standard cameras are usually insensitive for parameters different than intensity or power. To get access to the spatial distributions of parameters like phase and polarization, additional optical elements or methods are required. Reconfigurable integrated photonic circuits hold immense potential as actively controllable all-integrated on-chip detectors, if constructed and calibrated appropriately. We show that such novel integrated detectors are capable of simultaneously measuring light's spatial intensity, phase and polarization distributions [1]. They are a powerful addition to the existing detector toolbox. They pave the way towards intriguing applications in nano-optics [2], imaging, endoscopy, and optical communication. With their unique ability to also reemit and shape the light field [3], they are extremely versatile and flexible. In this presentation, we plan to introduce the corresponding photonic integrated architecture of SuperPixels, their building-blocks, and discuss selected applications.

Acknowledgement: We thank the Super-Pixels consortium for very valuable support and countless fruitful discussions. This project has received funding from the European Commission Horizon 2020 research and innovation programme under the Future and Emerging Technologies Open Grant Agreement Super-Pixels No. 829116.

## References

[1] J. Bütow, J. S. Eismann, M. Milanizadeh, F. Morichetti, A. Melloni, D. A. B. Miller, P. Banzer, Spatially resolving amplitude and phase of light with a reconfigurable photonic integrated circuit, arXiv:2204.09284 (2022)

[2] J. S. Eismann and P. Banzer, Sub-diffraction-limit Fourier plane laser scanning microscopy, Optica 9, 455-460 (2022)

[3] M. Milanizadeh, F. Toso, G. Ferrari, T. Jonuzi, D. A. B. Miller, A. Melloni, and F. Morichetti, Coherent self-control of free-space optical beams with integrated silicon photonic meshes, Photon. Res. 9, 2196-2204 (2021)

[*]Corresponding author: peter.banzer@uni-graz.at

# Generation of structured fields via Spintronic THz emitters

**D. Schulz** [1], **B. Schwager** [1], **J. Berakdar**[*1]
*1. Martin-Luther University, Halle-Wittenberg, 06099 Halle, Germany*

Diffusion of spin currents from magnetically active structures (spintronic THz emitters) into materials with spin-orbit coupling results in the buildup and decay of a directed charge current density, which in turn leads to coherent THz radiation [1]. In this contribution, results [2] of magnetic/electromagnetic simulations will be discussed showing that spintronic THz emitters can be arranged to metastructures that are capable of molding the vectorial distribution and the phase of the emitted THz fields. The simulations evidence the generation of THz fields with tunable magnetic, chiral and topological properties by appropriate material engineering. The properties of cylindrical vector and magnetoelectric beams will be discussed in detail, and it will be shown how these fields couple to matter in general. Some initial applications [3] of the generated fields to superconductors will be presented. The findings point to a new way of generating structured broadband THz fields with possible applications in optoelectronics, ultrafast magnetism, and superconductivity.

Acknowledgements: This work is funded by the DFG through SFB TRR227.

**References**

[1] Th. E. Papaioannou, and R. Beigang, Nanophotonics, 10, 1243-1257, 2021
[2] D. Schulz, B. Schwager, and J. Berakdar, ACS Photonics, 9,1248 (2022)
[3] B. Niedzielski, D. Schulz, and J. Berakdar, Sci. Rep., sub. (2022)

[*]Corresponding author: jamal.berakdar@physik.uni-halle.de

# Non-perturbative, fully quantum formulation of nonlinear optics in 2D media: the holographic principle

**Fabio Biancalana**[*1]
*1. Institute of Photonic and Quantum Sciences, Heriot-Watt University, EH14 4AS, Edinburgh (UK)*

The holographic principle is a conjecture that was first proposed in general terms when studying the unique problems arising from the concept of black hole entropy [1][2], and was formulated in extremely precise terms with the advent of string theory [3]. In essence, the holographic principle relates the classical, perturbative physics of a $d+1$-dimensional spacetime (called anti-de Sitter) with the non-perturbative, fully quantum physics of a $d$-dimensional flat system – connecting two completely different physical systems in an extremely surprising way. Evidence for the correctness of the conjecture has been mounting, and no counterexamples have ever been found in around 25 years of research.

In this talk I will explain the basic features of the holographic principle when applied to condensed matter physics (in a user-friendly way, completely avoiding the unnecessary mathematical abstruseness of string theory!). By constructing an "artificial" spacetime in $d+1$-dimensions (with a special black hole in its interior!), one can achieve a full description of the physics of materials such as graphene, high-temperature superconductors and epsilon-near-zero (ENZ) metamaterials (and potentially many others). The comparison between experiments and theoretical calculations is astounding, for what concerns the linear optical conductivity [4] – but very little has been done in this direction.

More specifically, towards the end of my talk I will focus on the nonlinear optical aspects of the holographic principle. I will show that it is possible to calculate the nonlinear conductivity of graphene, as a function of the probing optical intensity. This method has enormous potential for applications to 2D media, and could open the way for a novel way to study materials that are not subject to perturbation theory, either due to a lack of an energy scale (like in graphene, which has a zero gap) or because the variation of the refractive index are too high even for moderate intensities (like in ENZ materials).

It is my hope that after this talk, the audience will get a flavour of the many possible directions that this concept can take - spanning the study of exotic materials, fluid-dynamics, quantum information theory and the superconductive behaviour of 2D media.

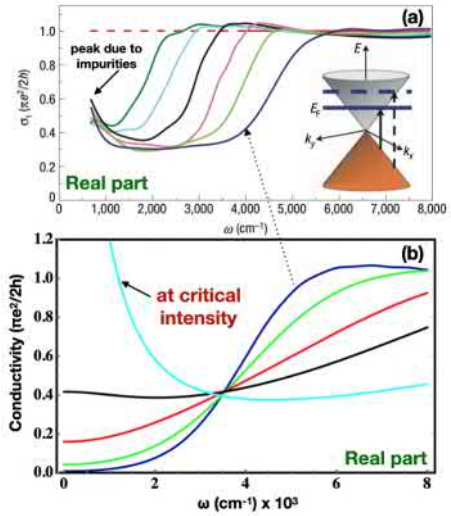


**Fig. 1:** Real part of graphene conductivity when increasing the optical pump intensity, calculated via the holographic principle. A nonlinear electromagnetic field of Born-Infeld type in the AdS spacetime induces a cubic nonlinearity in graphene. The fully quantum nonlinear optical properties of "conformal" (i.e. gapless) 2D materials like graphene can be calculated in a classical theory of gravity in one more spacetime dimension – by using the holographic paradigm.

## References

[1] J.M. Maldacena, Adv. Theor. Math. Phys **2**, 231 (1998).
[2] E. Witten, Adv. Theor. Math. Phys. **2**, 253 (1998).
[3] O. Aharony et al., Phys. Rept. **323**, 183 (2000).
[4] S.A. Hartnoll, Class. Quant. grav. **26**, 224002 (2009).

*Corresponding author: f.biancalana@hw.ac.uk

# Momentum and Angular Momentum of Sound, Water, and Plasma Waves

**Konstantin Y. Bliokh**[*1]
*1. RIKEN, Wako-shi, Saitama 351-0198, Japan*

I will describe the momentum and angular momentum properties of sound [1-3], water-surface [4], and plasma waves [5]. Importantly, the spin angular momentum density plays a crucial role in all of these cases. Even though sound and Langmuir plasma waves are longitudinal, these are vector waves, where the velocity or displacement of the medium particles provides the vector wavefield. In structured wavefields, the local polarization is generally elliptical, i.e., the medium particles move along elliptical trajectories and generate the corresponding local angular momentum, i.e., spin. In addition, the particles experience a slow drift in the wavefield, known in fluid mechanics as the Stokes drift [5]. This drift generates the canonical momentum density in the wavefield. Remarkably, in all cases, the spin and canonical momentum densities satisfy the fieldtheory Belinfante-Rosenfeld relation, involving also the kinetic momentum density (energy flux).

I will present theoretical calculations, as well as recent experimental observations of the above phenomena, including direct observations of the microscopic motion of water particles in structured gravity (water surface) waves [4], Fig. 1. I will also discuss close relations between the canonical wave momentum, Stokes drift, and ponderomotive forces acting on the medium particles [6], as well as their relation to the Abraham-Minkowski controversy.

These results provide a unified picture of the momentum and angular momentum properties for various types of waves.

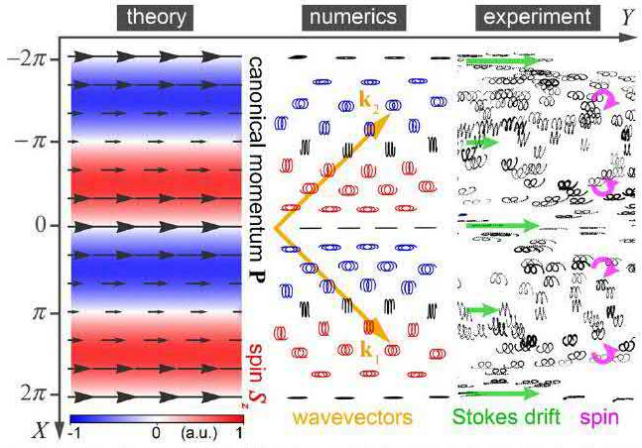


**Fig. 1:** Theoretically calculated surface distributions of the canonical momentum **P** (black arrows) and spin $S_z$ (red-blue) densities in the interference of two plane gravity (water-surface) waves with orthogonal wavevectors $\mathbf{k}_{1,2}$. Numerical and experimental plots show trajectories of microscopic water particles for three wave periods $6\pi/\omega$ [4]. The Stokes drift of the particles and their elliptical motion correspond to the canonical momentum and spin, respectively. The normalized surface coordinates are $X = \sqrt{2}kx$ and $Y = \sqrt{2}ky$.

## References

[1] C. Shi, R. Zhao, Y. Long, S. Yang, Y. Wang, H. Chen, J. Ren, X. Zhang X, Natl. Sci. Rev. 6, 707 (2019).
[2] I.D. Toftul, K.Y. Bliokh, M.I. Petrov, and F. Nori, Phys. Rev. Lett. 123, 183901 (2019).
[3] L. Burns, K.Y. Bliokh, F. Nori, J. Dressel, New J. Phys. 22, 053050(2020).
[4] K.Y. Bliokh, H. Punzmann, H. Xia, F. Nori, M. Shats, Sci. Adv. 8, eabm1295 (2022).
[5] K.Y. Bliokh, Y.P. Bliokh, arXiv:2203.05240 (2022).
[5] T. S. van den Bremer, Ø. Breivik, Philos. Trans. R. Soc. A 376, 20170104 (2017).
[6] K.Y. Bliokh, Y.P. Bliokh, F. Nori, arXiv:2204.07035 (2022).

[*]Corresponding author: kostiantyn.bliokh@riken.jp

# Spin-independent geometric self-focusing of light driven by the photon spin

**Samlan Chandran Thodika** [1] **Etienne Brasselet**[*1]
*1. University of Bordeaux, CNRS, F-33400, France*

Patterning the orientation of liquid crystals is a well-known way to encode arbitrary optical phase profile of a geometric nature within physically flat optical elements, which has led to the advent of liquid crystals spin-orbit photonics technologies. One of the simplest practical example is that of geometric phase lenses, whose convergent or divergent nature can be controlled by the handedness of the incident circularly polarized light.

Recently, such geometric phase lensing met the nonlinear optics of liquid crystals in the framework of so-called 'nematicons', which deal with self-trapping of light as a result of localized optically induced reorientation of a liquid crystal slab [1]. The latter work discusses the experimental observation of self-trapping of light in a particular light-matter interaction geometry interpreted as being the result of propagation dependent spin angular momentum transfer from light to matter. This eventually leads to alternating in-plane twisting of the liquid crystal orientation, thereby realizing a continuum nonlinear version of a previous linear optics, static, discrete one [2].

Still, the direct identification of the basic physical process at play - the nonlinear geometric phase lensing - remains elusive so far. Here we report on its experimental identification quantitatively supported by a model encompassing the structural and optical features associated to such light-matter interaction. This invites considering the nowadays well-established spin-orbit photonics of liquid crystals from a nonlinear perspective.

**References**

[1] C. P. Jisha, A. Alberucci, J. Beeckman, and S. Nolte, Self-Trapping of Light Using the Pancharatnam-Berry Phase, Physical Review X 9, 021051 (2019).
[2] S. Slussarenko, A. Alberucci, C. P. Jisha, B. Piccirillo, E. Santamato, G. Assanto, and L. Marrucci, Guiding Light via Geometric Phases, Nature Photonics 10,571 (2016).

[*]Corresponding author: brasselet@u-bordeaux.fr

# How to knot microwaves

**Robert P Cameron**[*2], **Wolfgang Löffler** [1,2], **Karl D Stephan** [1,2]

1. *SUPA and Department of Physics, University of Strathclyde, Glasgow G4 0NG, United Kingdom*
2. *Huygens-Kamerlingh Onnes Laboratorium, Leiden University, 2333 Leiden, CA, The Netherlands*
3. *Ingram School of Engineering, Texas State University, San Marcos, TX, United States of America*

In this purely theoretical talk we will consider a novel antenna design proposed recently by the authors [1] to generate monochromatic electromagnetic knots and other "unusual electromagnetic disturbances" [2] in the microwave domain. The antenna is a spherical array of radiating dipolar elements configured to approximate the desired electromagnetic field near its centre. Numerical simulations indicate that a specific embodiment of the antenna with a radius of 61.2 cm and only 20 element pairs driven at a frequency of 2.45GHz can yield linked and torus-knotted electric and magnetic field lines approximating those of an "electromagnetic tangle"; a monochromatic electromagnetic knot closely related to the well-known Rañada-Hopf type electromagnetic knots [3] but simpler in its construction. The antenna could be used to locally excite plasmas.

**References**

[1] R. P. Cameron, W. Loeffler, K. D. Stefan, J. Opt. 23, 064006 (2021).
[2] R. P. Cameron, J. Phys. Commun. 2, 015024 (2018).
[3] A. F. Rañada, Lett. Math. Phys. 18, 97 (1989).

[*]Corresponding author: robert.p.cameron@strath.ac.uk

# 3D Structuring of Light with Metaoptics

**Federico Capasso**[*1]
*1. John A. Paulson School of Engineering and Applied Sciences, Harvard University, Cambridge, MA 02138,USA*

Metaoptics offer fresh opportunities for structuring light as well as dark. I will discuss metasurfaces that enable light's spin and OAM to evolve, simultaneously, from one state to another along the propagation direction [1,2], along with nonlocal supercell designs that demonstrate multiple independent optical functions at arbitrary large deflection angles with high efficiency. [2] In one implementation the incident laser is simultaneously diffracted into Gaussian, helical and Bessel beams over a large angular range and in another one a compact wavelength-tunable external cavity laser with arbitrary beam control capabilities including hologram lasing is demonstrated [2]. Finally, the realization of 2D phase and polarization singularities will be discussed [3].

**References**

[1] Ahmed H. Dorrah, Noah A. Rubin, Aun Zaidi, Michele Tamagnone & Federico Capasso Nature Photonics 15, 287 (2021)
[2] Ahmed H Dorrah, Noah A Rubin, Michele Tamagnone, Aun Zaidi, Federico Capasso Nature Communications **12**, 6249 (2021)
[3] Soon Wei Daniel Lim, Joon-Suh Park, Maryna L. Meretska, Ahmed H. Dorrah, Federico Capasso Nature Communications, **12**, 4190 (2021)

[*]Corresponding author: capasso@seas.harvard.edu

# Applications of XUV - OAM beams to image transient dynamics of plasmonic nanostructures and magnetic vortex.

**F. Capotondi*[1], D. De Angelis [1], G. De Ninno [1,2], F. Guzzi [1], G. Kourousias [1], M. Manfredda [1], I.P. Nikolov [1], M. Pancaldi [1], E. Pedersoli [1], P. Rebernik Ribič [1], A. Simoncig [1], C. Spezzani [1], M. Zangrando [1], D. Bresteau [3], M. Luttmann [3], M. Fanciullib [3,9], T. Ruchon [1], M. Vimal [3], M. Sacchi [4,10], I. Bykova [5], C. David [5], B. Rösner [5], C. Bevis [6], C. Grova [6], G. F. Mancini [6], C. R. Sousa [7], I. L. Prejbeanu [7], L. Vila [7], B. Dieny [7], P. Vavassori [8]**

*1. Elettra-Sincrotrone Trieste S.C.p.A., Basovizza, Italy*
*2. Laboratory of Quantum Optics, University of Nova Gorica, Nova Gorica, Slovenia*
*3. Université Paris-Saclay, CEA, CNRS, LIDYL, Gif-sur-Yvette, France*
*4. Sorbonne Université, CNRS, Institut des NanoSciences de Paris, Paris, France*
*5. Paul Scherrer Institut, Villigen-PSI, Switzerland*
*6. Dipartimento di Fisica - Università degli Studi di Pavia, Pavia, Italy*
*7. Université Grenoble Alpes, CNRS, CEA, Grenoble INP, IRIG-SPINTEC, Grenoble, France*
*8. CIC nanoGUNE, San Sebastian, Spain*
*9. Laboratoire de Physique des Matériaux, Cergy Paris Université, Cergy-Pontoise, France*
*10. Synchrotron SOLEIL, L'Orme des Merisiers, Gif-sur-Yvette, France*

The use of light beams possessing orbital angular momentum (OAM) is becoming more frequently a tool for manipulating physical systems and probing their properties in different fields, such as biology, telecommunication, imaging and quantum technologies [1]. The wave-fronts of such beams develop a distinctive corkscrew shape determined by an azimuthal angular dependence of $\exp(i\ell\varphi)$ for the electric field phase, which is associated with an OAM of $\ell\hbar$ per photon. For example, at mesoscopic length scales, due to the twisted wavefront, the OAM can exert a torque, exploited by optical tweezers for manipulating and trapping particles around the phase singularity [2]. Only recently the advent of sophisticated and brighter radiation sources has boosted the generation of OAM modes at shorter wavelengths, allowing to add chemical selectivity and spin sensitivity to dichroic effects. In this talk, I will present the conventional diffractive optics or directly by means of direct source emission [3]. Furthermore, I will present the results of two recent experiments performed at DiProl beamline using XUV-OAM modes taking advantage of the peculiar features of the FERMI source. More specifically:

- we have studied the interaction of phase spiral beams with spin magnetic vortices, showing that the far field scattering profile encodes the vortex symmetries in a way that depends on the sign and value of $l$, giving rise to a new kind of magnetic helicoidal dichroism (MHD) [4].
- we have exploited the possibility of achieve super-resolution imaging using OAM in diffraction-based imaging technique at FEL [5], showing how the speckles forming the diffraction pattern encode information on the light orbital angular momentum.

For both experiments the possibility to extend the developed techniques in the time-domain realm to either study the spin topology dynamics and plasmonic excitation in metallic nanostructures will be addressed with preliminary results.

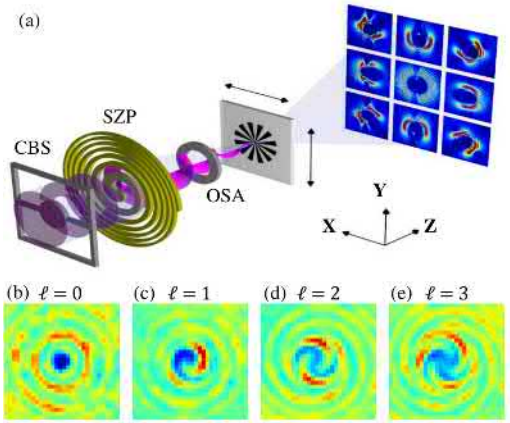


**Fig. 1:** Sketch of the experimental setup to generate OAM beam from spiral Zone Plate. (b) - (e) Far field image of the interference pattern between Laguerre-Gaussian OAM beam and planar wave for different $\ell = 0, 1, 2, 3$.

## References

[1] L. Allen, et al. Phys. Rev. A 45, 8185 (1992). L. Paterson, et al. Science 292, 912 (2001). L. Gong, et al. Light 8,27 (2019). A. M. Yao, et al. Adv. Opt. Photonics 3, 161 (2011).
[2] L. Paterson, et al. Science 292,912 (2001). D. G. Grier, et al. Nature 424,810 (2003).
[3] E. Allaria, et al. Nature Photonics 6 (10), 699-704. P. Rebernik Ribič, et al. Phys. Rev. X 7, 031036 (2017).
[4] M. Fanciulli, et al. Phys. Rev. A 103, 013501 (2021). M. Fanciulli, et al. Phys. Rev. Lett. 128, 077401 (2022).
[5] F. Tamburini, et al. Phys. Rev. Lett. 97, 163903 (2006). M.Pancaldi, et al. In preparation (2022).

*Corresponding author: flavio.capotondi@elettra.eu

# Ultra-long photonic quantum walks via spin-orbit metasurfaces

**Francesco Di Colandrea**[*1], **Amin Babazadeh** [1], **Alexandre Dauphin**[†2], **Pietro Massignan** [3], **Lorenzo Marrucci** [1], **Filippo Cardano**[‡1]

*1. Dipartimento di Fisica, Università degli Studi di Napoli Federico II, Complesso Universitario di Monte Sant'Angelo, Via Cintia, 80126 Napoli, Italy*
*2. ICFO – Institut de Ciencies Fotoniques, The Barcelona Institute of Science and Technology, 08860 Castelldefels (Barcelona), Spain*
*3. Departament de Física, Universitat Politècnica de Catalunya, Campus Nord B4-B5, 08034 Barcelona, Spain*

Processing quantum information encoded into spatial modes of light already proved instrumental for a number of quantum applications. In the context of quantum simulation, dynamical evolutions of particles in complex lattices have been realized in different platforms, where photonic modes are judiciously coupled to let the optical field evolve like the target system. This in turn has led to the observation of many interesting phenomena, like exotic topological phases [1], localization effects [2] or non-Hermitian physics [3]. From a broader perspective, this technology has permitted massive implementations of Boson sampling and its variants [4], that recently lead to the first demonstration of quantum advantage [5]. Here we introduce a photonic setup that allows to generate quantum walks in the space spanned by optical modes carrying quantized transverse momentum [6] [Fig. 1(a)]. The action of the quantum evolution operator is realized via light propagation through patterned devices yielding space-dependent polarization transformations [Figs. 1(b,c)]. Based on the concept of Pancharatnam-Berry phases, these transformations allow to shape the field wavefront and polarization structure, so as to mimic the effect of the target evolution.

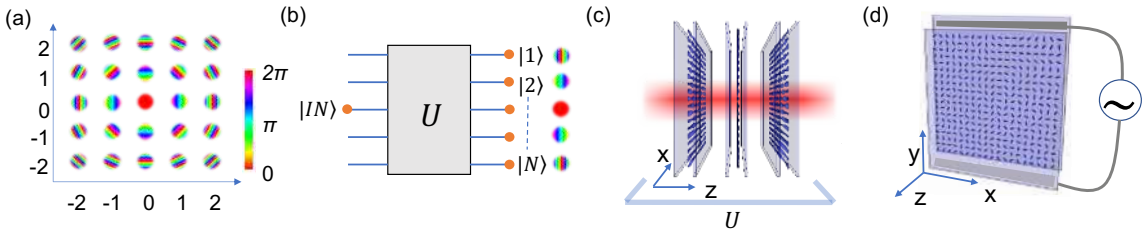


**Fig. 1:** (a) Position states are associated with optical modes carrying quantized transverse momentum, exhibiting periodic phase profiles in the plane transverse to the system optical axis ($z$ axis). (b) The quantum state of particle occupying a single lattice site, or equivalently a single mode, is mapped into the outpute state via a unitary evolution operator $U$, corresponding to a quantum walk. (c) The unitary map $U$ can be realized by propagating light through liquid-crystal metasurfaces, yielding a periodic polarization transformation. (d) These exhibit a thin layer of liquid-crystal material, having a space-dependent optic-axes distribution. An oscillating electric field across the device permits to adjust the optical birefringence of such devices.

This modulation is achieved through birefringent liquid-crystal metasurfaces, essentially made of a micrometric layer of liquid-crystal material having patterned optic axes [Fig. 1(d)]. These provide a generalization of well-known q-plates and are based on the same technology [7]. By engineering metasurfaces having fastly varying optic axes, we are able to generate long evolutions (equivalent to hundreds of time-steps) via a few optical elements, thus keeping optical losses at minimum. In standard setups, indeed, the number of resources scales at least linearly with the number of simulated time-steps, thereby introducing an exponential attenuation of traveling photons. In our experiment, we successfully realize up to 320 time-steps quantum walks, going far beyond state-of-the-art implementations of this dynamics. Optical modes involved in our experiment propagate in a single beam within the setup, yet they are eventually resolved by focusing them on a camera, where optical Fourier transform converts transverse momenta into spatial positions. To demonstrate the potential of our platform, we generate disordered quantum walks to realize maximal entanglement between the two natural partitions of the system, which was earlier investigated theoretically but not achieved experimentally hitherto. Our work is part of a larger effort to leverage structured light and its accurate manipulation for photonic quantum technologies [8,9].

## References

[1] T. Ozawa, et al., Rev. Mod. Phys. **91**, 015006 (2019).
[2] A. Crespi, et al., Nat. Photonics **7**, 322–328 (2013).
[3] L. Xiao, et al., Nat. Phys. **16**, 761–766 (2020).
[4] D. J. Brod, E. F. Galvão, A. Crespi, R. Osellame, and N. Spagnolo, Adv. Photonics **1**, 1 (2019).
[5] H. -S. Zhong, et al. ,Science **3**70, 1460–1463 (2020).
[6] F. Di Colandrea, et al., arXiv:2203.15051 (2022).
[7] A. Rubano, F. Cardano, B. Piccirillo, and L. Marrucci, J. Opt. Soc. Am. B **3**6, D70 (2019).
[8] S. Goel, et al., arXiv:2204.00578 (2022).
[9] S. Z. D, Plachta, M. Hiekkamäki, A. Yakaryılmaz, and R. Fickler, arXiv:2202.04915 (2022).

*Corresponding author: francesco.dicolandrea@unina.it
†Corresponding author: alexandre.dauphin@icfo.eu
‡Corresponding author: filippo.cardano2@unina.it

# Time reversed optical waves by arbitrary vector spatiotemporal field generation

**Mickael Mounaix [1], Nicolas K. Fontaine [2], David T. Neilson [2], Roland Ryf [2], Haoshuo Chen [2], Juan Carlos Alvarado-Zacarias [2], Joel Carpenter*[1]**

*1. School of Information Technology and Electrical Engineering, The University of Queensland, Brisbane QLD 4072, Australia*
*2. Nokia Bell Labs, 600 Mountain Ave, NJ, 07974, USA*

Over the past decade, the field of structured light has developed with the use of programmable displays such as spatial light modulators (SLM)[1]. Full control of light requires the ability to shape all a beam's properties. That is, the amplitude, phase and polarization as a function of space and of time (or frequency).Recent demonstrations showed how to control light either spatially with wavefront shaping techniques, temporally with pulse shaping techniques, or a partial spatial and temporal control, with applications ranging from imaging and communications to micromanipulation and quantum optics[2]. However, no demonstration of full spatiotemporal beam shaping (e.g. independent control of all the spatial and temporal properties of light). An important reason for this is a spatiotemporal beam is three-dimensional in nature (two transverse, one longitudinal), yet wavefront shaping typically employs the 2D surface of an SLM to generate the beam.

In this paper, we demonstrate a new class of spatiotemporal wavefront shaper, a device capable of measuring and generating arbitrary spatiotemporal optical beams[3]. We control the amplitude and phase of 90 spatial and polarization modes, over 4.4 THz of bandwidth and 20ps of delay. We demonstrate arbitrary control of all the degrees of freedom of light (spatial, polarization, spectral, temporal) propagating through a multimode fiber. Such device could find applications in all fields that require full polarization-resolved spatiotemporal field control, such as the delivery of short pulses for non-linear imaging or light matter interactions.

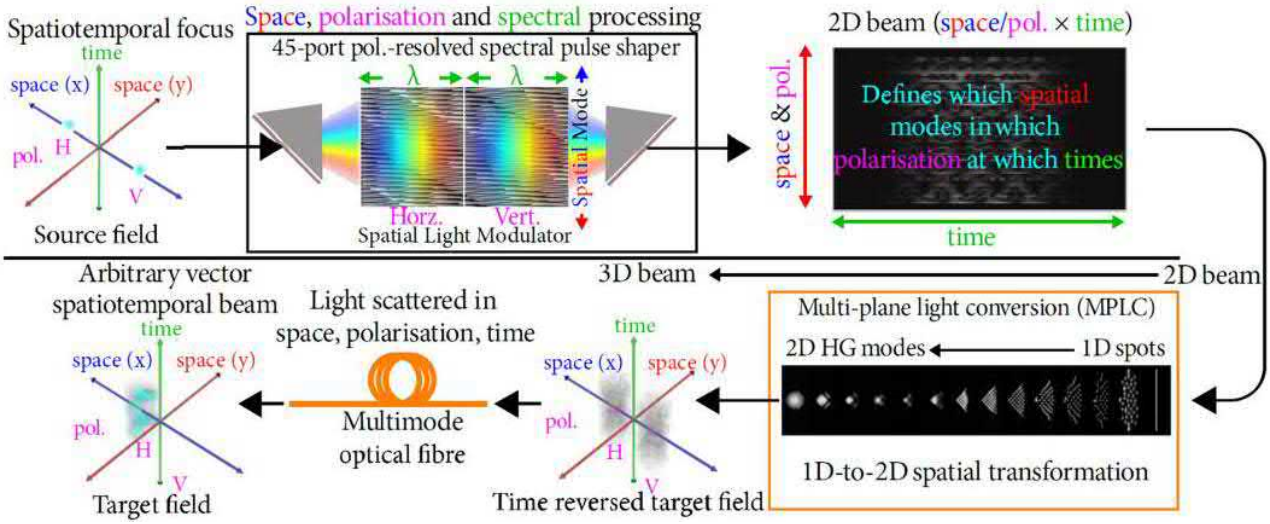


**Fig. 1:** Simplified schematic of our optical time reversal device, capable of mapping an input vector spatiotemporal input field onto an arbitrary vector spatiotemporal output field. Amplitude, phase, spatial mode, polarization and spectral/temporal properties can all be independently addressed simultaneously.

## References

[1] G. Lazarev, P.-J. Chen, J. Strauss, N. Fontaine, and A. Forbes, "Beyond the display: phase-only liquid crystal on Silicon devices and their applications in photonics [Invited]," Opt. Express, vol. 27, no. 11, pp. 16206-16249, 2019, doi: 10.1364/OE.27.016206.
[2] H. Rubinsztein-Dunlop et al., "Roadmap on structured light," J. Opt., vol. 19, no. 1, p. 13001, 2016, doi: 10.1088/2040-8978/19/1/013001.
[3] M. Mounaix et al., "Time reversed optical waves by arbitrary vector spatiotemporal field generation," Nat. Commun., vol. 11, no. 1, p. 5813,2020 , doi: 10.1038/s41467 – 020 – 19601 – 3.

*Corresponding author: j.carpenter@uq.edu.au

# The Radial Momentum of Light

**Lixiang Chen**[*1]
*1. Department of Physics, Xiamen University, Xiamen 361005, China*

As is well known, angular position and orbital angular momentum (OAM) of photons are a conjugate pair of variables that have been extensively explored for quantum information science and technology. In contrast, the radial degrees of freedom remain relatively unexplored. Here we exploit the radial position and radial momentum, to demonstrate Einstein-Podolsky-Rosen correlations between down-converted photons [1]. By using the annular apertures as the radial slits, we also demonstrate a radial version of light's diffraction in the radial momentum state space [2]. Also, we exploit logarithmic radial position and hyperbolic momentum to explore the rigorous uncertainty principle in radial degree of freedom. Based on quantum Mellin transform, we further define and confirm the radial version of intelligent states that satisfy the equality in the uncertainty relation [3]. Our results reveal that these well-defined radial variables are essential for fundamental test of quantum mechanics, and shedding the light on quantum applications.

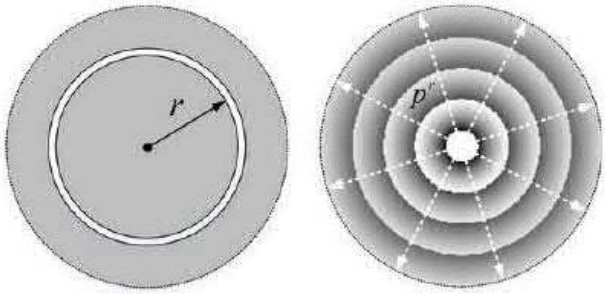


**Fig. 1:** The radial position and radial momentum of light

## References

[1] L. Chen, T. Ma, X. Qiu, D. Zhang, W. Zhang, and R. W. Boyd, "Realization of the Einstein-Podolsky-Rosen paradox using radial position and radial momentum variables," Phys. Rev. Lett. 123, 060403 (2019).
[2] T. Ma, D. Zhang, X. Qiu, Y. Chen, and L. Chen, "Radial diffraction of light in the radial momentum state space," Opt. Lett. 45, 5152 (2020).
[3] Z. Zhang, D. Zhang, X Qiu, Y. Chen, S. Franke-Arnold, and L. Chen, "Experimental investigation of the uncertainty principle for radial degrees of freedom," (submitted, 2022).

[*]Corresponding author: chenlx@xmu.edu.cn

# Tunable Photon-Induced Spatial Modulation of Free Electron Wavepackets

**Shai Tsesses**[*1], **Raphael Dahan**[†1], **Kangpeng Wang** [1], **Ori Reinhardt** [1], **Guy Bartal** [1], **Ido Kaminer** [1]

*1. Andrew and Erna Viterbi Department of Electrical and Computer Engineering, Technion – Israel Institute of Technology, Haifa, Israel*

Spatially shaping electron beams has great importance in industrial and academic applications, such as nanolithography, microscopy, material studies and fabrication inspection. To this end, the frontier of research in recent years has been spatial coherent shaping, achieved via phase and amplitude holograms for electrons [1-3]. Of particular importance is achieving tunable spatial modulation of electron beams, a long-term challenge that has received increased interest in recent years [4]. Recently, a new method to generate such spatial electron modulation was envisioned, based on the ultrafast interaction of electron pulses and near-field electromagnetic waves [5,6]. This idea has attracted increased attention following theoretical predictions for the correction and purification of electron beams [7,8], however it is yet to be performed experimentally with electron-light interactions.

Here, we present active spatial modulation of electrons by engineering their interaction with ultrafast surface plasmon interference patterns. The experiment is performed in an ultrafast transmission electron microscope (UTEM). We generate an electron vortex and vortex lattice, verifying the coherent shaping process via electron diffraction. We follow this by demonstrating active control over the electron distribution, switching between electron Bessel beams of different orders, through the tuning of the plasmonic field via incident laser polarization. Thereafter, by also tuning the laser intensity [9], we control the nonlinear interaction order, showing how filtering electrons that gained different amounts of energy in the interaction possess a different shape. Through this process, the entire electron distribution undergoes 2D spatial Rabi oscillations [10,11]. These results present the first observation of a prediction that the electron angular momentum quanta depends on the interaction order [9]. Our work presents new degrees of freedom to actively shape electron wavefunctions, with possibilities for improving state-of-the-art electron microscopy with tunable and tailored electron beams.

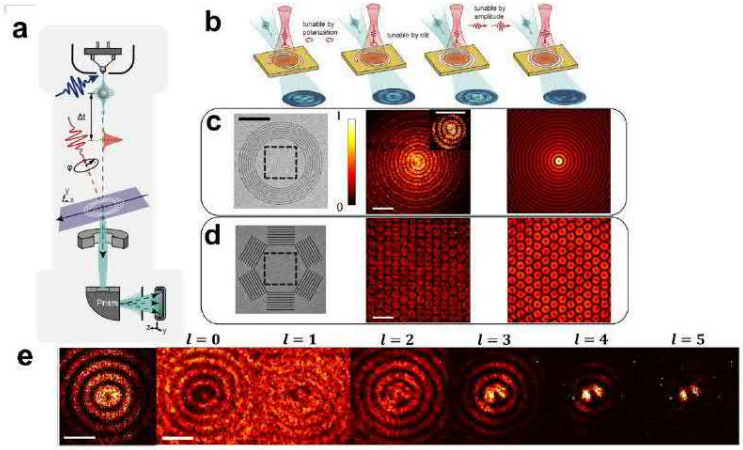


**Fig. 1:** Tunable photon-induced shaping of free electrons. (a) The experimental apparatus (UTEM). (b) Degrees of freedom for manipulating electron beams with light. (c),(d) From left to right: the plasmonic coupling slit used for the shaping (scale bars is $10\mu$m ), the measured distribution of electrons gaining energy after the interaction (scale bars are $2\mu$m ), and the expected shape from calculation. (e) $A1^{st}$ order Bessel plasmonic field generates an electron Bessel vortex beam, with a different shape for each interaction order $l$ (scale bars are 1 um).

## References

[1] J. Verbeeck et al., Nature 467, 301 (2010).
[2] Grillo, V. et al., Phys. Rev. X 4, 011013 (2014).
[3] R. Shiloh et al., Ultramicroscopy 144, 26(2014).
[4] J. Verbeeck et al., Ultramicroscopy 190, 58 (2018).
[5] I. Madan et al., Sci. Adv. 5, 8358 (2019).
[6] G. M. Vanacore et al., Nat. Mater. 18,573 (2019).
[7] A. Konečná and F. J. G. de Abajo, Phys. Rev. Lett. 125, 30801 (2020).
[8] Feist, http://A.etA.et al., Phys. Rev. Res. 2, 043227 (2020).
[9] W. Cai et al., Phys. Rev. B 98, 45424 (2018).
[10] Feist, A. et al., Nature 521, 200-203 (2015).
[11] Wang, K. et al., Nature 582, 50 – 54 (2020)

[*]Corresponding author: tsesses2@gmail.com
[†]Corresponding author: raphaeld@campus.technion.ac.il

# Skyrmionic Hopfions: particle-like twisted topologies in light

**M.R. Dennis**[*1,2], **D. Sugic** [1,3], **R. Droop** [4], **E. Otte** [4], **D. Ehrmanntraut** [4], **C.D. Parmee** [5], **F. Nori** [3,6], **J. Ruostekoski** [5], **C. Denz** [4]

*1. School of Physics and Astronomy, University of Birmingham, Birmingham B15 2TT, UK*
*2. EPSRC Centre for Doctoral Training in Topological Design, University of Birmingham, Birmingham B15 2TT, UK*
*3. Theoretical Quantum Physics Laboratory, RIKEN Cluster for Pioneering Research, Wako- shi, Saitama 351-0198, Japan*
*4. Institute of Applied Physics and Center for Nonlinear Science (CeNoS), University of Muenster, 48149 Muenster, Germany*
*5. Physics Department, Lancaster University, Lancaster LA1 4YB, UK*
*6. Physics Department, University of Michigan, Ann Arbor, Michigan 48109-1040, USA*

Three-dimensional (3D) particle-like topological excitations, such as skyrmions and hopfions, were originally proposed as topological models of fundamental particles and nuclei, and have received much attention in high- energy and condensed matter systems. Rather than being based on special points and lines, the field values wrap around a 2-dimensional or 3D sphere "target space" within a plane or volume. In this sense, a full Poincaré beam, which realises all points on the Poincaré sphere of polarisations in the transverse plane, is a 2D optical "baby skyrmion".

The full state of light, including polarisation and phase, being determined by a normalised 2-dimensional complex Jones vector, determines a point on a 3D hypersphere we call the "optical hypersphere". Loops of varying phase and the Poincaré sphere determine the intricately tangled topological "Hopf fibration" of this 3-sphere, and intricate. We design, experimentally generate and measure an optical beam configuration which realises all polarisations and phases together in a propagation volume, realising a 3D optical skyrmionic hopfion [1]. For sufficiently high topological degree, the 3D polarisation structures are linked and knotted, yet may be understood as being built on a skeleton of C lines of circular polarisation.

This nontrivial optical state can be embedded into nontrivial optical excitations of atoms [2]. In both cases the 3D topology is characterised by a continuous topological charge density, characterised by the helicity density $\mathbf{A}\cdot\mathbf{B} = \mathbf{A}\cdot\nabla\times\mathbf{A}$, where the synthetic magnetic vector potential $\mathbf{A}$ is provided by polarisation density current for atoms, and the orbital current of the light field.

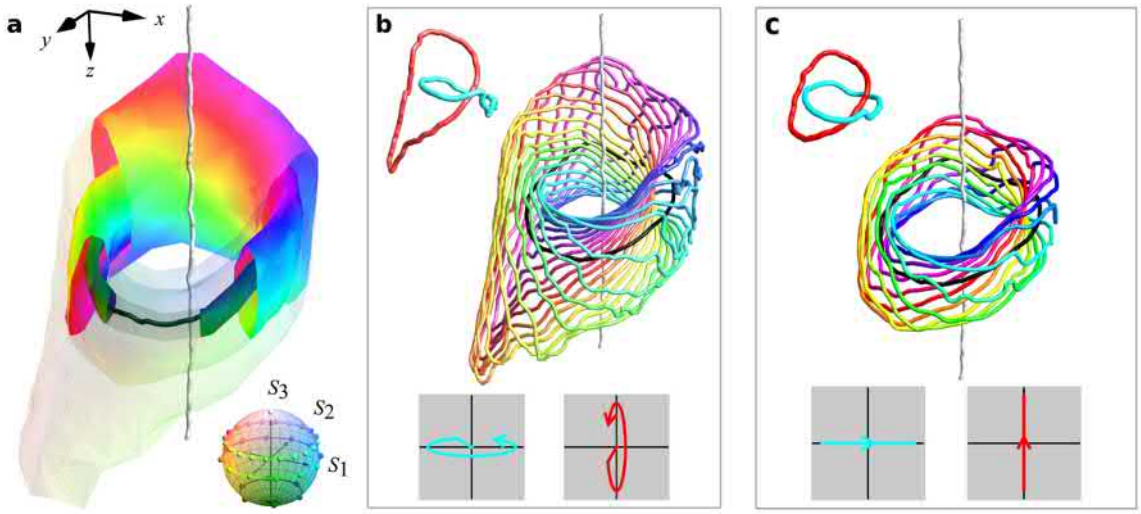


**Fig. 1:** Structure of the skyrmionic hopfion. The optical texture is reconstructed from the polarisation and phase measurements via volumetric full field reconstruction of the optical beam. The measured volume is coloured following the Poincaré sphere (inset) and reveals the topological structure of the Hopf fibration. (a) Two C lines, the black loop and the threading straight white line, organise the texture into nested tori. Each toroidal surface represents points characterised by the same ellipticity. The colours wind nontrivially around each torus, and a few polarisation filaments making up these tori are shown in the insets: in (b), the lighter surface is made of lines characterised by RH elliptic polarisation; in (c), the surface of liner polarisations is made of lines along which the polarisation state is linear.

## References

[1] D. Sugic, R. Droop, E. Otte, D. Ehrmanntraut, F. Nori, J. Ruostekoski, C. Denz, M. R. Dennis, "Particle-like topologies in light," Nature Communications **12** 6785 (2021)
[2] C. D. Parmee, M. R. Dennis, J. Ruostekoski, "Optical excitations of Skyrmions, knotted solitons, and defects in atoms," Communications Physics **5** 54 (2022)

*Corresponding author: m.r.dennis@bham.ac.uk

# Topology in three-dimensionally structured light

**C. Denz**[*1,2], **R. Droop** [1], **E. Asché** [1], **D. Ehrmanntraut** [1], **E. Otte** [1,3]
*1. Institute of Applied Physics, University of Muenster, Germany*
*2. Physikalisch-Technische Bundesanstalt, The German Metrology Institute, Braunschweig, Germany*
*3. Geballe Laboratory for Advanced Materials, Stanford University, USA*

Within the last decades, customized light fields have found applications in various research areas, ranging from nano-scale complexity in three dimensions (3d) over optical micromanipulation to high-resolution imaging and material machining [1]. Besides well-established amplitude and phase modulation, polarization has been rediscovered as a degree of freedom that enriches the diversity of spatial structure, leading to fully structured light.

These advancements require a high stability which can be realized by structures with a topological nature. Well-known topological structures in light are spin and orbital angular momentum that are associated with singularities in polarization or the phase of a light field, respectively. These optical topological structures are characterized by integer invariants and represent "holes" in the light degree of freedom [2]. In our contribution, we combine the methods and tools of structured light with topological constructs giving rise to tailored topological photonics, an emerging field of classical light. It not only paves the way for new kinds of confined light structures, but also to the metrology of related quantities

When these topologies are employed in spatially varying phase distributions, they lead to an orbital flow density (OFD) while spatially structured polarization topologies provide spin flow density (SFD) patterns. Both together define the transverse energy flow (TEF). We introduce an interferometric approach to realize the defined customization of TEF topologies [3]. By applying higher-order Laguerre- as well as Ince-Gaussian modes, we demonstrate a broad spectrum of sophisticated field configurations with complex flow dynamics including saddle points or centers. Depending on the chosen type of higher-order modes and their indices, we are able to control the shape of these flow fields as well as the position, number or order of embedded critical points.

Two-dimensional topological structures in the transverse distribution of light as networks of caustics [4] or skyrmionic polarization structures [5] have been recently demonstrated. When light is in addition spatially confined as e.g. in the focus of a light beam, a non-negligible longitudinal vector field contribution is added, leading to striking volumetric phase or polarization topologies as Moebius polarization bands can occur [6]. Even though this approach enables sophisticated nano-scale non-paraxial light fields, the modulation in the propagation direction is limited to the short Rayleigh length of the tightly focused beam. We developed a paraxial approach that enables the defined customization of extended 3 d light fields without focusing. The spatial topology may vary within a wavelength in propagation direction, and is based on counter propagating transversely extended structured light fields to create complex 3 d light fields at the wavelength scale [7].

Recently, light has also been structured in such a way to tie knots, creating complex, three-dimensional light structures. Knotted structures embedded in optical fields are highly interesting since the topology surrounding the knot defines the stability of such light structures. The knot itself is a field singularity line, therefore structuring the entire electric field. Up to now, these topologic structures have only been considered in phase [8] or polarization [9] separately since the customization and analysis of the full, vectorial field rep-resents a major current challenge. To generate such fully structured knotted light structures in 3 d, we superimpose structured paraxial light of orthogonal polarization and combine beam shaping, digital propagation, spatially resolved 3 d phase decoding and polarimetry. As examples, we realize 3 d light fields in polarization and phase that result in complex topological constructs as the Hopf fibration [10], among others. They resemble truly localized, particle-like objects in space.

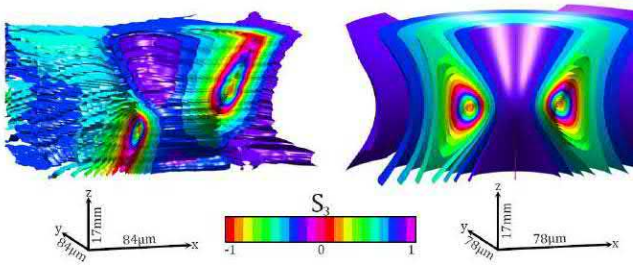


**Fig. 1:** S3 isosurfaces cut along the $x-z$-plane to visualize a Hopf-like fibration. Experimental results on the left and numerical results on the right. Scaling of the spatial dimensions is given by the length of the coordinate axes.

## References

[1] H. Rubinsztein-Dunlop, Journ. Opt. 19, 013001 (2017). [2] E. Otte, C. Denz, Journ. Opt. 23, 073501 (2021).
[3] E. Otte, E. Asché, C. Denz, Journ. Opt. 21, 064001 (2019). [4] A. Zannotti, C. Denz et al., Nat. Commun. 11,3597 (2020).
[5] R. Gutiérrez-Cuevas, E. Pisanty, Journ. Opt. 23, 024004 (2021).
[6] E. Otte, K. Tekce, S. Lamping, B. J. Ravoo, C. Denz, Nat. Comm. 10, 4308(2019).
[7] R. Droop, E. Asché, E. Otte, C. Denz, Sci. Rep. 11, 18019 (2021).
[8] M. R. Dennis, R. P. King, B. Jack, K. O'Holleran, M. J. Padgett, Nat. Phys. 6, 118-121 (2010).
[9] H. Larocque, D. Sugic, D. Mortimer, A. J. Taylor, R. Fickler et al., Nat. Phys. 14, 1079-1082 (2018).
[10] D. Sugic, R. Droop, E. Otte, D. Ehrmanntraut, et al., Nat. Commun. 12, 6785 (2021).

[*]Corresponding author: denz@uni-muenster.de, cornelia.denz@ptb.de

# Chirality and optical activity of twisted light

**Kayn A. Forbes**[*1]
*1. University of East Anglia, Norwich, Norfolk, NR4 7TJ, United Kingdom*

It is well established that circularly polarised light is chiral, and may therefore interact with chiral materials in differential ways depending on the handedness of the material (or light): such phenomena are known as optical activity or chiral light-matter interactions [1]. Irrespective of polarisation, optical vortex modes that possess the phase exp $(i\ell\phi)$ are chiral (see Figure 1). Whether this optical chirality stemming from phase structure could engage in chiral light-matter interactions in an alogous manner to circular polarisation effects has been a topic of debate for two decades. Initial studies were of the believe it did not [2,3]; proliferating recent works continue to prove otherwise [4]. Consequently, the field of structured light and chirality is growing rapidly. The aim of this talk is to survey the field from its genesis to present day, looking at the fundamental concepts that have been discovered along the way.

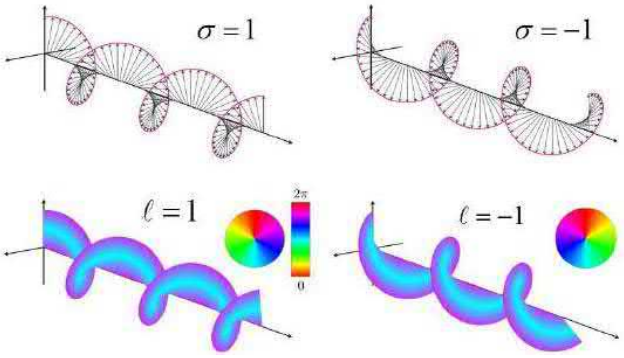


**Fig. 1:** (top row) chiral helical pattern of circularly-polarised electromagnetic fields, the handedness determined by the sign of $\sigma$; (bottom row) chiral helical pattern of the wavefront of an optical vortex mode, the handedness determined by the sign of $\ell$( phase inset).

As an indication of how far the field has progressed, one only needs to read Les Allen's personal memoir in the Theme issue 'Optical orbital angular momentum' [5]. In it he states that in 1993 he and Miles Padgett (unpublished work) showed that unpolarised (paraxial) optical vortices failed to demonstrate optical rotation in glass pipes of sugar solution. Fast forward to 2022 and it has recently been shown [6] that an unpolarized optical vortex if tightly focused produces an optical chirality which can produce optical activity effects with chiral matter (see Figure 2), a remarkable phenomenon when placed in the context of what was previously deemed possible in classical optics. Optical vortex beams and the orbital angular momentum of light continue to yield extraordinary and unique features.

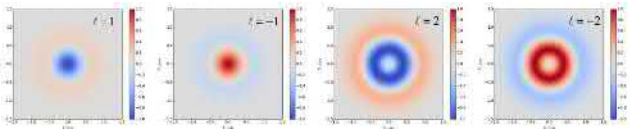

**Fig. 2:** Spatial distributions of the optical chirality density in the focal plane of non-paraxial unpolarized (in the 2D sense) optical vortex beams. $p = 0$ in all.

**References**[1] L. D. Barron, Molecular Light Scattering and Optical Activity (Cambridge University Press, Cambridge, 2009).
[2] D. L. Andrews, L. D. Romero, and M. Babiker, On Optical Vortex Interactions with Chiral Matter, Optics Communications 237, 133 (2004).
[3] F. Araoka, T. Verbiest, K. Clays, and A. Persoons, Interactions of Twisted Light with Chiral Molecules: An Experimental Investigation, Physical Review A 71, 055401 (2005).
[4] K. A. Forbes and D. L. Andrews, Orbital Angular Momentum of Twisted Light: Chirality and Optical Activity, J. Phys. Photonics 3, 022007 (2021).
[5] L. Allen, Orbital Angular Momentum: A Personal Memoir, Philosophical Transactions of the Royal Society A: Mathematical, Physical and Engineering Sciences 375, 20160280 (2017).
[6] K. A. Forbes, Optical Helicity of Unpolarized Light, ArXiv:2112.11555 [Physics] (2021).

*Corresponding author: FIND ME

# Shape-shifting cold atoms with vector light

**Jinwen Wang**[1,2], **Francesco Castellucci** [1], **Thomas W. Clark**[3], **Sphinx J. Svensson**[1], **Sonja-Franke Arnold**[*1]

*1. School of Physics and Astronomy, University of Glasgow, Glasgow, G12 8QQ, Scotland*

*2. Shaanxi Province Key Laboratory of Quantum Information and Quantum Optoelectronic Devices, Xi'an Jiaotong University, Xi'an 710049, China*

*3. Wigner Research Centre for Physics, Budapest H-1525, Hungary*

Over the last decades we have learned how to control the spatial shape of light, granting us unprecedented control over its phase and polarisation structures. Atomic vapours provide an interface that converts optical structures into polariton structures, responsive to electromagnetic and inertial forces.

Most investigations and applications of light-atom interaction are concerned with homogeneously polarized light, or scalar light. Light-atom interaction is however, by its very nature, a vectorial process [1], that depends explicitly on the alignment between an external magnetic field **B** and the optical and atomic polarizations, with the interaction determined by

$$\hat{H} = -\mathbf{D}\cdot\mathbf{E}(r,\phi) + g_F \mu_B \mathbf{F}\cdot\mathbf{B}, \tag{1}$$

where **E** is a complex vector field, which may contain phase and polarisation singularities, and **B** is an external magnetic field. The interplay between the local polarisation direction and magnetic field direction allows us to design atomic spin polarisation patterns in a cloud of cold rubidium atoms with spatially dependent optical activity [2].

We have recently demonstrated how 3D magnetic field alignment can be inferred from single absorption images of a vector vortex beam passing through an atomic cloud. Both azimuthal and tilt angle of **B** can then be deduced from spatial Fourier analysis of the absorption pattern [3].

We are currently exploring vectorial light-atom interaction for a larger variety of vector beams, e.g. for light of varying concurrence or 'vectorness',

$$\mathbf{E}(r,\phi) = E_-(r)\cos(2\chi)e^{-im\phi}\boldsymbol{\sigma}_- + E_+(r)\sin(2\chi)e^{in\phi}\boldsymbol{\sigma}_+. \tag{2}$$

Here the polarisation pattern is determined by the OAM numbers $m$ and $n$ in the circular polarisation components, and $\chi$ which parametrises their balance and the resulting degree of 'vectorness'. The vector nature of the light is mapped onto the spatial alignment of the atomic spin polarisations, and can be deduced from the observed intensity and polarisation profile of the absorption pattern as shown in Fig. 1. Initial results show that the measured Fourier amplitude corresponds to the squared vectorness of the light field.

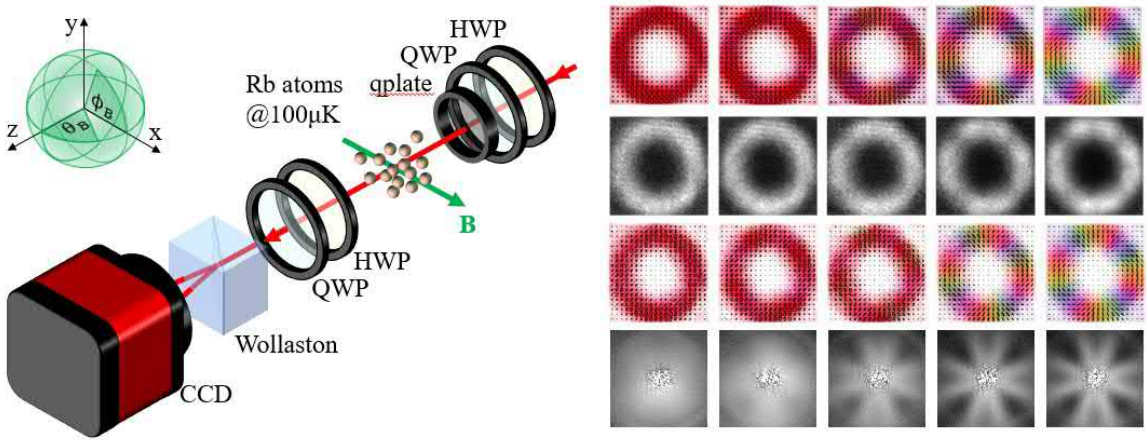


**Fig. 1:** Left: Schematic setup. Testing interaction of vector vortex light with cold Rb87 atoms exposed to external magnetic field. Right: Light with different polarisation patterns (top) generates atomic spin polarisation patterns, as measured by absorption intensity (2nd row) and polarisation profiles (3rd row), with atomic density patterns (4th row).

## References

[1] J. Wang, F. Castellucci, and S. Franke-Arnold, AVS Quantum Science **2**, 031702 (2020). [2] N. Radwell, T.W. Clark, B. Piccirillo, S.M. Barnett, and S. Franke-Arnold, Phys. Rev. Lett. **114** 123603 (2015). [3] F. Castellucci, T.W. Clark, A. Selyem, J. Wang, and S. Franke-Arnold, Phys. Rev. Lett. **127** 233202 (2021).

*Corresponding author: Sonja.Franke-Arnold@glasgow.ac.uk

# Paraxial Skyrmionic Beams

**Amy McWilliam[1], Zhujun Ye[1], Fiona C. Speirits[1], Claire Cisowksi[1], Sonja-Franke Arnold[1], Stephen M. Barnett[1], Jörg B. Götte[*1,2]**

*1. School of Physics and Astronomy, University of Glasgow, Glasgow, G12 8QQ, Scotland*
*2. College of Engineering and Applied Sciences, Nanjing University, Nanjing 210093, China*

We show that a class of vector vortex beams possesses a topological property that derives both from the spatially varying amplitude of the field and its varying polarization. This property arises as a consequence of the inherent skyrmionic nature of such beams and is quantified by the associated skyrmion number. We present a theory of such Skyrmions within paraxial optics, exploiting mathematical analogies with the study of superfluids. We illustrate this idea for some of the simplest vector beams and discuss the physical significance of the skyrmion number in this context.

We consider a superposition of two orthogonally polarized paraxial beams of either light or electrons and express the resulting field in the form of a locally-normalized state vector:

$$|\psi(\boldsymbol{r})\rangle = \frac{|0\rangle + v(\boldsymbol{r})|1\rangle}{\sqrt{1+|v(\boldsymbol{r})|^2}}, \tag{1}$$

where $v(\boldsymbol{r}) = e^{i\theta_0}u_1(\boldsymbol{r})/u_0(\boldsymbol{r})$ and $|0\rangle$ and $|1\rangle$ denote the state vectors of the orthogonally polarised spatial modes. The Skyrmion field is most readily defined in terms of an effective magnetization $\boldsymbol{M}$, which is the local direction of the Poincaré vector for light or the Bloch vector for an electron beam. In terms of our locally normalized state it is

$$\boldsymbol{M} = \langle\psi(\boldsymbol{r})|\boldsymbol{\sigma}|\psi(\boldsymbol{r})\rangle, \tag{2}$$

where $\boldsymbol{\sigma}$ is a vector operator with the Pauli matrices as Cartesian components. For a light beam, the Cartesian components of $\boldsymbol{M}$ correspond to the normalized local Stokes parameters $S_1, S_2$ and $S_3$, and for the electrons to the local directions of the electron spin. The Skyrmion number is then the number of rotations of the magnetisation around the Bloch sphere as we traverse a closed circuit around the centre of the Skyrmion. This Skyrmion number has the mathematical form:

$$n = \frac{1}{4\pi}\int \mathbf{M}\cdot\left(\frac{\partial\mathbf{M}}{\partial x}\times\frac{\partial\mathbf{M}}{\partial y}\right)\mathrm{d}x\,\mathrm{d}y, \tag{3}$$

where the integration takes place over the magnetic surface, taken here to define the plane $z = 0$.

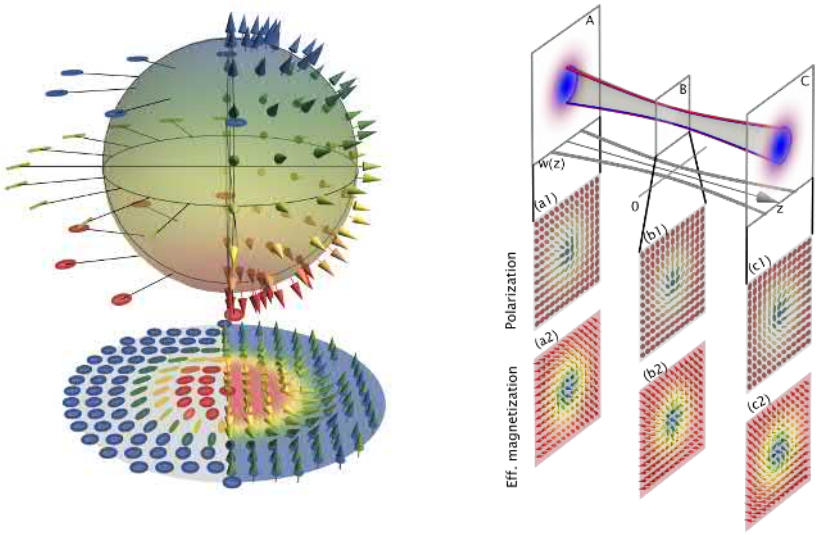


**Fig. 1:** Left: Stereographic projection of the spatially varying polarization or effective magnetization $\boldsymbol{M}$ onto the Poincaré or Bloch sphere. We encode the degree of circular polarization $S_3$ and the $z$ component $M_z$ on the same color scheme. For definiteness we choose in our examples the polarization states $|0\rangle$ and $|1\rangle$ to correspond to left and right handed circular polarization respectively or, for electrons, the eigenstates of the $z$ component of the spin. Right: Polarization structure for a superposition of LG modes with $\ell_1 = 1$ and $\ell_0 = 0$ focussed at $z = 0$. The beam surface separating the regions in which the modes have the larger amplitude, $u_0$ (blue) and $u_1$ (red). A, B, and C are three cross sections of interest, at $z = -z_R/2, 0$ and $z_R/2$ respectively. a1), b1) and c1) are spatially varying polarization patterns corresponding to each plane, while a2), b2) and c2) are the corresponding effective magnetizations, with the classic chiral and hedgehog forms respectively.

## References

[1] S. Gao, F. C. Speirits, F. Castellucci, S. Franke-Arnold, S. M. Barnett, J. B. Götte, Phys. Rev. A. **102**, 053513 (2020)

*Corresponding author: joerg.goette@glasgow.ac.uk

# Electrostatic OAM generation, detection and ghost imaging in electron microscopy

**Vincenzo Grillo**[*1]
*1. CNR-NANO Via G. Campi 213/a, I-41125 Modena, Italy*

Electron Vortex Beams (EVBs) have been an important revolution in electron microscopy. Many of its initial applications regarded the study of dichroism, and symmetries of materials and nanostructures.

There are many ways to generate electron vortex beams nowadays, from holograms to magnetic needle. A particularly appealing method is the use of two parallel electrostatic line of charge that produce a near exact and tunale vortex beam [1]. Using this configuration and special MEMS technology we were able to produce a large vortex with more than 1000 quanta of orbital angular momentum and control also its aberrations [2]. When many of these devices are put together we are able to generate complex wavefunctions. We could demonstrate that these are ideal patterns for computational ghost imaging that we have implemented in electron microscopy for the first time [3].

On the other hand we have now demonstrated the first electrostatic OAM sorter that can be used for a chirality measurement better and more efficiently than any EVB based approach.

One of our results is the use of the OAM sorter to study a newly introduced composite symmetry of nature related to planar chirality that is diagonal after the log-polar conformal mapping introduced by the OAM sorter. We believe this could be of general interest also for light optics and imaging applications [4].

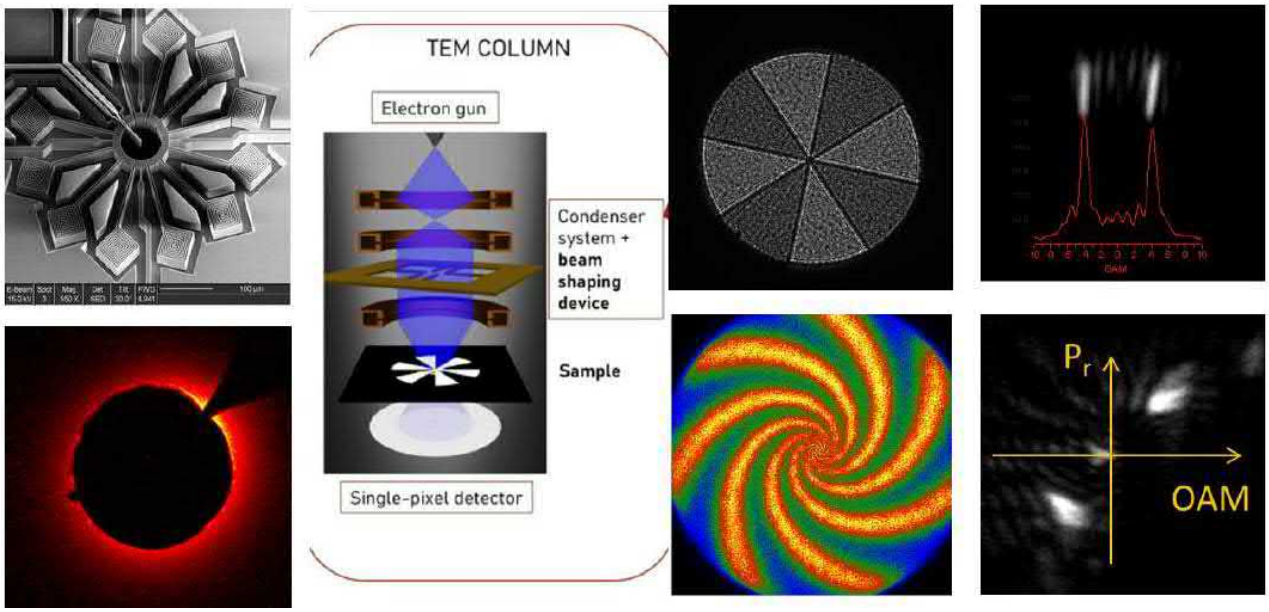


**Fig. 1:** (left) Device for vortex beams generation along with the generated vortex with $1 = 1000$.(center) scheme of computational ghost imaging (right) experimental result of OAM sorter on petal beam and spiral vortex beam.

This work has been carried out with the help of personnel in CNR-NANO,CNR-IMM, Forschungszentrum Juelich, University of Glasgow, University of Ottawa, Thermo Fisher Scientific.

I wish to acknowledge the support from the European Union's Horizon 2020 Research and Innovation Programme (Grant Agreement No. 766970 Project "Q-Sort", No. 964591 "SMART-electron")

## References

[1] AH Tavabi, H Larocque, et al. Physical review research 2, 013185 (2020)
[2] AH Tavabi, P Rosi et al. arXiv:2203.00477 (2022)
[3] A. Kallepalli, L. Viani et al. http://arXiv.org/abs/2204.09997arXiv.org/abs/2204.09997 (2022)
[4] AH Tavabi, P Rosi, et al. arXiv:2110.03391 (2021)

*Corresponding author: presenting.author@email.com

# High-dimensional entanglement for quantum communication

**QUIT Physics group, friends** & **Marcus Huber**[*1,2]
*1. TU Wien, Atominstitut*
*2. IQOQI Vienna, Austrian Academy of Sciences*

Entanglement unlocks many applications in quantum communication, such as the highest possible level of security in quantum key distribution. As photons are inevitably lost or decohered over longer distances, it seems obvious that using the full spectrum of photonic degrees of freedom is desirable. In addition to more encodable bits per photon, entanglement in high dimensions also yields a surprising resistance to noise [1]. This comes at the expense of more complicated measurements that in themselves can contribute to the overall noise in the data, leading to an interesting optimisation. While random, noisy entanglement may not always be useful or need unrealistic control to be harnessed, I will also present a protocol that can be used in high-dimensional systems, even with restricted measurement possibilities [2], which has recently been successfully employed in path [3] and energy-time [4] experiments.

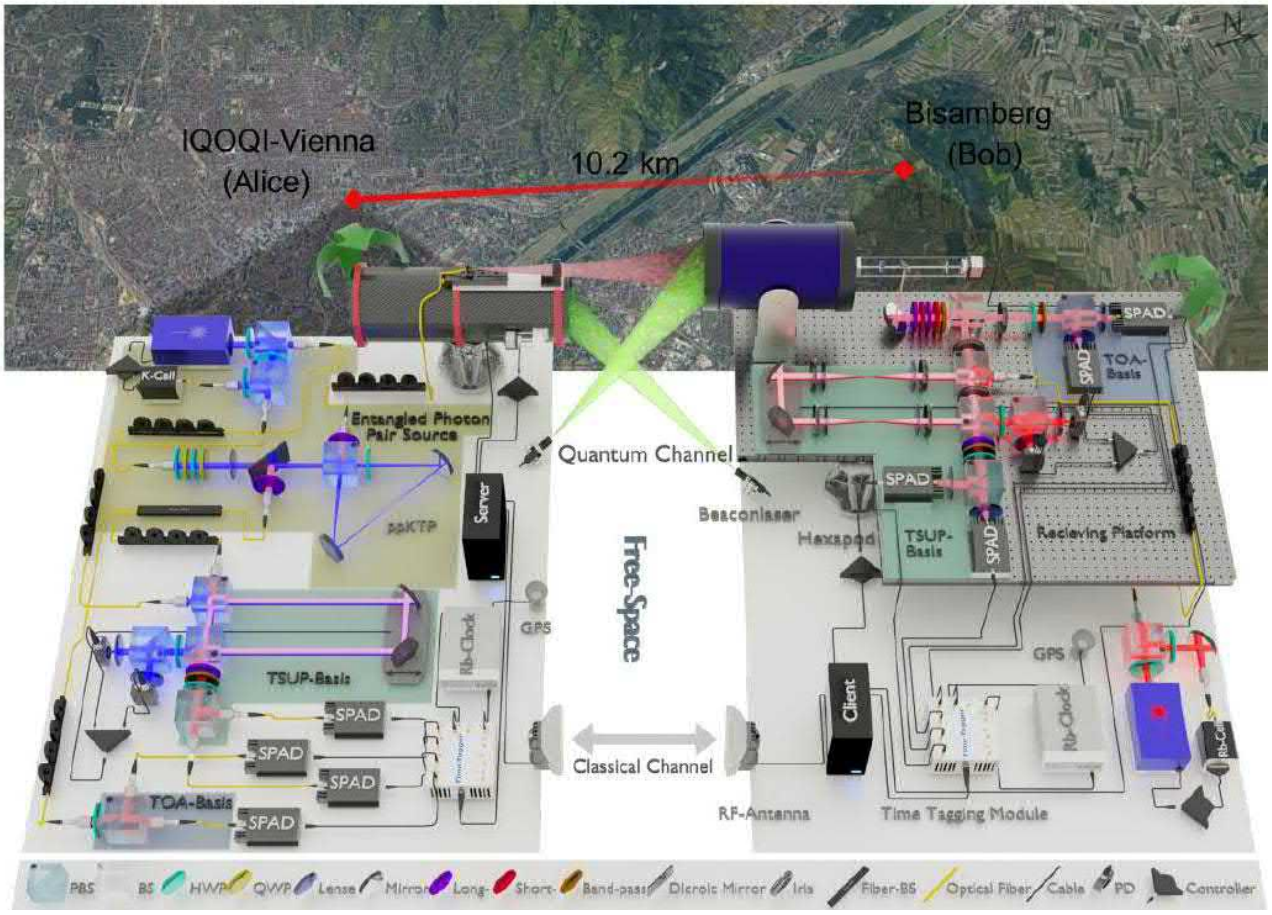


**Fig. 1:** Recent free-space experiment showing the potential for high-dimensional advantages in quantum key distribution (QKD).

## References

[1] S. Ecker, F. Bouchard, L. Bulla, F. Brandt, O. Kohout, F. Steinlechner, R. Fickler, M. Malik, Y. Guryanova, R. Ursin, M. Huber, Phys. Rev. X 9, 041042 (2019)
[2] M. Doda, M. Huber, G. Murta, M. Pivoluska, M. Plesch, Ch. Vlachou, Phys. Rev. Applied 15, 034003, (2021)
[3] http://X.HuX.Hu, C. Zhang, Y. Guo, F. Wang, W. Xing, C. Huang, B. Liu, Y. Huang, C. Li, G. Guo, X. Gao, M. Pivoluska, M. Huber, Phys. Rev. Lett. 127,110505 (2021)
[4] L. Bulla, M. Pivoluska, K. Hjorth, O. Kohout, J. Lang, S. Ecker, S. Neumann, J. Bittermann, R. Kindler, M. Huber, M. Bohmann, R. Ursin, arXiv:2204.07536

*Corresponding author: marcus.huber@tuwien.ac.at

# Structured Photons – Their Application in Quantum Photonics

**Ebrahim Karimi** *[1,2]

*1. Department of Physics, University of Ottawa, Advanced Research Complex, 25 Templeton Street, K1N 6N5, Ottawa, ON, Canada*
*2. National Research Council of Canada, 100 Sussex Drive, K1A 0R6, Ottawa, ON, Canada*

Photons, the quanta of light, possess several different degrees of freedom, e.g., frequency, polarization, spatial and temporal modes, which can be used as platforms for quantum information applications. Polarisation, corresponding to the vectorial nature of light, is bi-dimensional, and thus can represent '0' and '1' in the digital world. Unlike polarisation, transverse and temporal modes would provide an unbonded vector space and could be used to extend the alphabet beyond the '0's and '1's to any arbitrary integer numbers. Photons in superposition states of these different degrees of freedom are known as Structured Photons. In the classical regime, structured light has found tremendous applications, e.g., overcoming the diffraction limit (STED microscopy), for optical spanners, communication multiplexing, and generating non-trivial 3D topologies such as Möbius, ribbons and knots. In the quantum domain, structured photons may be used to realise higher-dimensional states, and thus are employed in quantum communication, computation, and simulation applications.

The recent progress, challenges, and applications of structured photons in modern photonics, such as generation of polychromatic structured photons [1], structured XUV photons [2-3], and their interaction with materials [4-5] be the subject of my talk. Finally, I will discuss their applications in high-dimensional quantum communication [6], e.g., free-space [7], underwater [8-9], fibre [10] and curved spacetime [11] links and their security analysis [12].

**References**

[1] M F Ferrer-Garcia et al., "Polychromatic Electric Field Knots," Physical Review Research 3, 033226 (2021).
[2] F Kong et al., "Vectorizing the spatial structure of high-harmonic radiation from gas," Nature Communications 10, 2020 (2019).
[3] F Kong et al., "Generating few-cycle radially polarized pulses," Optica 6, 160 (2019).
[4] S Sederberg et al., "Vectorized optoelectronic control and metrology in a semiconductor," Nature Photonics 14, 680 (2020)
[5] A D'Errico et al., "Full-mode characterization of correlated photon pairs generated in spontaneous downconversion," Optics Letters 46, 2388 (2021)
[6] A Sit et al., "Quantum cryptography with structured photons," Structured Light for Optical Communication, 139-176 (2021)
[7] A Sit et al., "High-dimensional intracity quantum cryptography with structured photons," Optica 4, 1006-1010 (2017).
[8] F Hufnagel et al., "Characterization of an underwater channel for quantum communications in the Ottawa River," Optics Express 27, 26346 (2019).
[9] F Hufnagel et al., "Investigation of underwater quantum channels in a 30 meter flume tank using structured photons," New Journal of Physics 22, 093074 (2020).
[10] A Sit et al., "Quantum cryptography with structured photons through a vortex fiber," Optics Letters 43, 4108 (2018).
[11] Q Exirifard et al., "Towards Communication in a Curved Spacetime Geometry," Communications Physics 4, 171 (2021).
[12] F Bouchard at al., "Experimental investigation of high-dimensional quantum key distribution protocols with twisted photons," Quantum 2, 111 (2018).

*Corresponding author: ebi.karimi@gmail.com

# Direct Generation of Tunable Orbital Angular Momentum Beams in Microring Lasers with Broadband Exceptional Points

**Mercedeh Khajavikhan**[*1,2]

*1. Ming Hsieh Department of Electrical and Computer Engineering, University of Southern California, Los Angeles 90089,USA*
*2. Department of Physics Astronomy, Dornsife College of Letters, Arts, Sciences, University of Southern California, Los Angeles 90089, USA*

Non-Hermitian exceptional points (EPs) represent a special type of degeneracy where not only the eigenvalues coalesce, but also the eigenstates tend to collapse on each other [1]. Thus far, however, in order to stabilize a system at the vicinity of an exceptional point, its related parameters must be carefully tuned and/or continuously controlled. To overcome this limitation, here we introduce a new family of exceptional points based on unidirectional coupling. This can be readily implemented by incorporating an S-shaped waveguide element in a microring cavity. In active settings, this configuration can be designed such that it operates exclusively in the broken phase (above the exceptional point), resulting in unidirectionality with unprecedented resilience to perturbations, thus providing a robust approach for directly generating beams with distinct and predetermined orbital angular momenta (OAM). By virtue of their geometry and high index contrast, microring resonators support whispering gallery modes (WGMs) that carry orbital angular momentum [2]. However, due to its rotational symmetry, an active microring structure simultaneously supports beams of equal positive and negative topological charges, resulting in a net zero OAM generation. To enforce unidirectional operation in the active microrings, we use an S-shaped waveguide inside the resonator in which the two ends are adiabatically tapered in order to ensure energy dissipation and negligible power reflection. As a result, the S-bend provides asymmetric loss/coupling between the two counter-propagating modes. A schematic of this structure with additional corrugations on the exterior cavity walls is depicted in Fig. 1(a). The asymmetric coupling, caused by the lossy ends of the S-shaped construct, leads to an exceptional point that is inherently chiral.

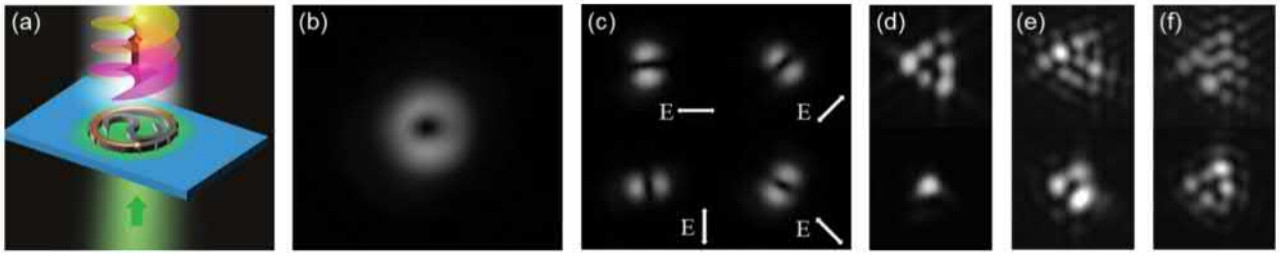


**Fig. 1:** (a) Schematic illustration of an S-microlaser emitting light with a tunable orbital angular momentum. (b) The emitted intensity, showing a doughnut-shaped profile. (c) the emission is azimuthally polarized. (d) Topological charge associated with the R/LHCP emissions, denoting a beam with an OAM of $\ell = 1$ lasing in the $m = 27 WGM$. (e) Temperature tuning to 235 K shifts the resonance to the 28th WGM increasing the OAM to $= 2$. (f) 150 K the resonance shifts to the $m = 29$ WGM, further adjusting the OAM to $\ell = 3$.

To experimentally verify the above-mentioned behavior, an OAM microring laser is fabricated on an InP wafer with InGaAsP quantum wells as the gain material. Square shaped protrusions are incorporated along the outermost sidewall of the ring resonator. These scatterers serve as a second-order grating, generating vertical free-space emission with lower-order twisted beams. We first characterized a device that supports a resonance in the $27^{th}(m = 27)$WGM at a temperature of 295 K. The microring is equipped with $q = 26$ scattering elements on its sidewall. These scatterers lower the orbital angular momentum down to a value of $l = 1$. The intensity profile presented in Fig. 1(b) displays the doughnut shape associated with a vortex beam. As expected, the intensity profile of the emission is predominantly azimuthally polarized (Fig. 1(c)). Moreover, using the triangular aperture technique [3], the OAM characterization indicates a value of $l = 1$ (Fig. 1(d)). At a temperature of 235 K, the $m = 28$ WGM oscillates and the emission has an OAM value of $l = 2$ (Fig. 1(e)). Further tunability is likewise confirmed at a temperature of 150 K (Fig. 1(f)) [4,5].

In conclusion, we demonstrated a new type of exceptional point in microring resonators that are able to directly generate vector vortex beams with a tunable topological charge. Our work features the first realization of exceptional points with robust chirality in microring structures, and may open up new possibilities for studying non-Hermiticity in angular momentum space, vortex beam generation, as well as for sensing.

Acknowledgments. AFOSR (MURI: FA9550-20-1-0322, MURI: FA9550-21-1-0202), DARPA (D18AP00058), ONR (N00014-19-1-2052, N00014-20-12522, MURI: N00014-20-1-2789), ARO (W911NF-17-1-0481), NSF (ECCS CBET 1805200, ECCS 2000538, ECCS 2011171), and US-Israel Binational Science Foundation (BSF; 2016381).

## References

[1] Makris, K. G., El-Ganainy, R., Christodoulides, D. N., & Musslimani, Z. H., Phys. Rev. Lett. 100, 103904 (2008).
[2] X. Cai et al. Science 338, 363-366 (2012).
[3] J. M. Hickmann, J. S. Fonseca, W. C. Soares & S. Chávez-Cerda, Phys. Rev. Lett. 105, 053904 (2010).
[4] W. E. Hayenga et al., ACS Photonics 6,1895 (2019)
[5] Y. N. G. Liu et al., Nature Physics 17, 704-709 (2021)

*Corresponding author: khajavik@usc.edu

# Spin to orbital angular momentum transfer in nonlinear wave mixing

**B. Pinheiro da Silva**[1], **W. T. Buono**[2], **L. J. Pereira**[1], **D. S. Tasca**[1], **K. Dechoum**[1], **A. Z. Khoury**[*1]

*1. Instituto de Física, Universidade Federal Fluminense, 24210-346 Niterói-RJ, Brazil*

*2. School of Physics, University of the Witwatersrand, Private Bag 3, Johannesburg 2050, South Africa*

The interplay between spin and orbital angular momentum in nonlinear wave mixing can be useful for new photonic devices based on the cross control between different optical degrees of freedom. Polarization controlled switching of orbital angular momentum (OAM) operations [1] and radial-angular coupling in type-II second harmonic generation (SHG) [2] have been investigated in our group. This subject has attracted the interest of different groups within a broader scope [3][4]. Beyond second harmonic generation, the nonlinear response to structured light fields has been also investigated in four-wave mixing [5][6]. Novel quantum communication schemes can benefit from the interaction between structured light and nonlinear media [7].

In this work we discuss the spin to orbital angular momentum transfer in type-II second harmonic generation. The concept of spin-orbit non-separable structures plays a central role in this context, with potential applications to novel photonic devices based on the spin-orbit control. The angular momentum transfer is assisted by a vector vortex beam, which is nonlinearly mixed with a circularly polarized Gaussian beam. This effect can be useful for information transfer between photonic degrees of freedom encoded on different wavelengths, and for connecting different physical platforms in quantum information networks.

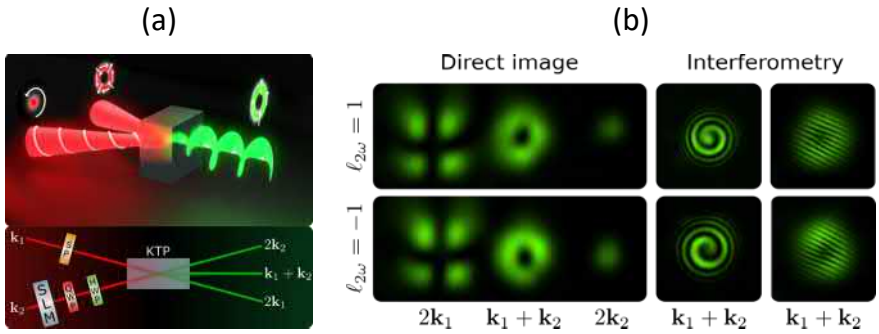


**Fig. 1:** (a) Experimental scheme for spin-orbit angular momentum transfer in second harmonic generation. SP: S-plate for generation of the vector-vortex beam. SLM: Spatial light modulator. QWP: Quarter waveplate. HWP: Half waveplate. KTP: Potassium Titanyl Phosphate (KTiOPO4) crystal. (b) Images produced on the three outputs of the second harmonic field. Laguerre-Gaussian modes with topological charge $\ell_{2\omega} = \pm 1$ are evident in the $\mathbf{k}_1 + \mathbf{k}_2$ beam, as characterized by the spiral and forked intereference fringes shown on the right.

The incoming electric field of frequency $\omega$, which is compounded by two waves with different wave vectors $\mathbf{k}_1$ and $\mathbf{k}_2$, can be written as

$$\mathbf{E}^{(\omega)}_{\mathbf{k}_1} = [\mathscr{A}_{1x}(\mathbf{r})\hat{\mathbf{x}} + \mathscr{A}_{1y}(\mathbf{r})\hat{\mathbf{y}}]e^{i\mathbf{k}_1\cdot\mathbf{r}}, \tag{1}$$

$$\mathbf{E}^{(\omega)}_{\mathbf{k}_2} = (\alpha\hat{\mathbf{x}} + \beta\hat{\mathbf{y}})\mathscr{A}_2(\mathbf{r})e^{i\mathbf{k}_2\cdot\mathbf{r}}, \tag{2}$$

where $\mathscr{A}_{1x}(\mathbf{r})$ and $\mathscr{A}_{1y}(\mathbf{r})$ are the transverse structures carried by polarizations $x$ and $y$, respectively, of the beam $\mathbf{k}_1$, and $\mathscr{A}_2(\mathbf{r})$ is the structure of the beam $\mathbf{k}_2$. The unit vectors $\hat{\mathbf{x}}$ and $\hat{\mathbf{y}}$ are, respectively, the horizontal and vertical polarization states, weighted by the complex numbers $\alpha$ and $\beta$, which obey the normalization relation $|\alpha|^2 + |\beta|^2 = 1$.

The type-II phase matching couples the horizontal and vertical polarization components of the fundamental field ($\omega$) to generate the second harmonic ($2\omega$) with vertical polarization. The resulting electric field amplitudes of the outgoing waves are

$$\mathbf{E}^{(2\omega)}_{2\mathbf{k}_1} = g_1\mathscr{A}_{1x}(\mathbf{r})\mathscr{A}_{1y}(\mathbf{r})e^{i2\mathbf{k}_1\cdot\mathbf{r}}\hat{\mathbf{y}}, \tag{3}$$

$$\mathbf{E}^{(2\omega)}_{2\mathbf{k}_2} = g_2\,\alpha\,\beta\,\mathscr{A}_2^2(\mathbf{r})e^{i2\mathbf{k}_2\cdot\mathbf{r}}\hat{\mathbf{y}}, \tag{4}$$

$$\mathbf{E}^{(2\omega)}_{\mathbf{k}_1+\mathbf{k}_2} = g_{12}[\alpha\mathscr{A}_{1y}(\mathbf{r}) + \beta\mathscr{A}_{1x}(\mathbf{r})]\mathscr{A}_2(\mathbf{r})e^{i(\mathbf{k}_1+\mathbf{k}_2)\cdot\mathbf{r}}\hat{\mathbf{y}}, \tag{5}$$

where $g_1$, $g_2$ and $g_{12}$ are the nonlinear coupling coefficients. The output wave along $\mathbf{k}_1 + \mathbf{k}_2$ carries two contributions. The $y$ ($x$) polarization of the input wave $\mathbf{k}_1$ is coupled to the $x$ ($y$) polarization of the wave $\mathbf{k}_2$. This spin-orbit crosstalk allows for the angular momentum transfer from the spin of the input wave $\mathbf{k}_2$ to the orbital component of the second harmonic output $\mathbf{k}_1 + \mathbf{k}_2$.

## References

[1] Buono, W. T., Santiago, J., Pereira, L. J., Tasca, D. S., Dechoum, K., and Khoury, A. Z., Opt. Lett. **43**, 1439–1442 (2018)

[2] Buono, W. T., Santos, A., Maia, M. R., Pereira, L. J., Tasca, D. S., Dechoum, K., Ruchon, T., and Khoury, A. Z., Phys. Rev. A **101**, 043821 (2020)

[3] Qiu, X., Li, F., Zhang, W., Zhu, Z., and Chen, L., Optica **5**, 208 (2018)

[4] Wu, H.-J., Yang, H.-R., Rosales-Guzman, C., Gao, W., Shi, B.-S., and Zhu, Z.-H., Phys. Rev. A **100**, 053840 (2019)

[5] Mallick, N. S. and Dey, T. N., J. Opt. Soc. Am. B **37**, 1857–1864 (Jun 2020).

[6] Offer, R. F., Daffurn, A., Riis, E., Griffin, P. F., Arnold, A. S., and Franke-Arnold, S., Phys. Rev. A **103**, L021502 (2021)

[7] Cai, C., Ma, L., Li, J., Guo, H., Liu, K., Sun, H., Yang, R., and Gao, J., Photon. Res. **6**, 479 (2018)

[*]Corresponding author: azkhoury@id.uff.br

# A classical model of spontaneous parametric down-conversion

**Girish Kulkarni**[*1], **Jeremy Rioux** [1], **Boris Braverman, Maria V. Chekhova** [2,3], **and Robert W. Boyd** [1,4]

*1. Department of Physics, University of Ottawa, Ontario K1N 6N5, Canada*
*2. Max Planck Institute for the Science of Light, Staudtstr. 2, 91058 Erlangen, Germany*
*3. University of Erlangen-Nuremberg, Staudtstr. 7/B2, 91058 Erlangen, Germany*
*4. The Institute of Optics, University of Rochester, Rochester, New York 14627, USA*

We model spontaneous parametric down-conversion (SPDC) as classical difference frequency generation (DFG) of the pump field and a hypothetical stochastic ”vacuum” seed field. We analyticallyshow that the second-order spatiotemporal correlations of the field generated from the DFG process replicate those of the signal field from SPDC. Specifically, for low gain, the model is consistent with the quantum calculation of the signal photon’s reduced density matrix; and for high gain, the model’s predictions are in good agreement with our experimental measurements of the far-field intensity profile, orbital angular momentum spectrum, and wavelength spectrum of the SPDC field for increasing pump strengths. We further theoretically show that the model successfully captures second-order SU(1,1) interference and induced coherence effects in both gain regimes. Intriguingly, the model also correctly predicts the linear scaling of the interference visibility with object transmittance in the low-gain regime - a feature that is often regarded as a quintessential signature of the nonclassicality of induced coherence. Our model may not only lead to novel fundamental insights into the classical-quantum divide in the context of

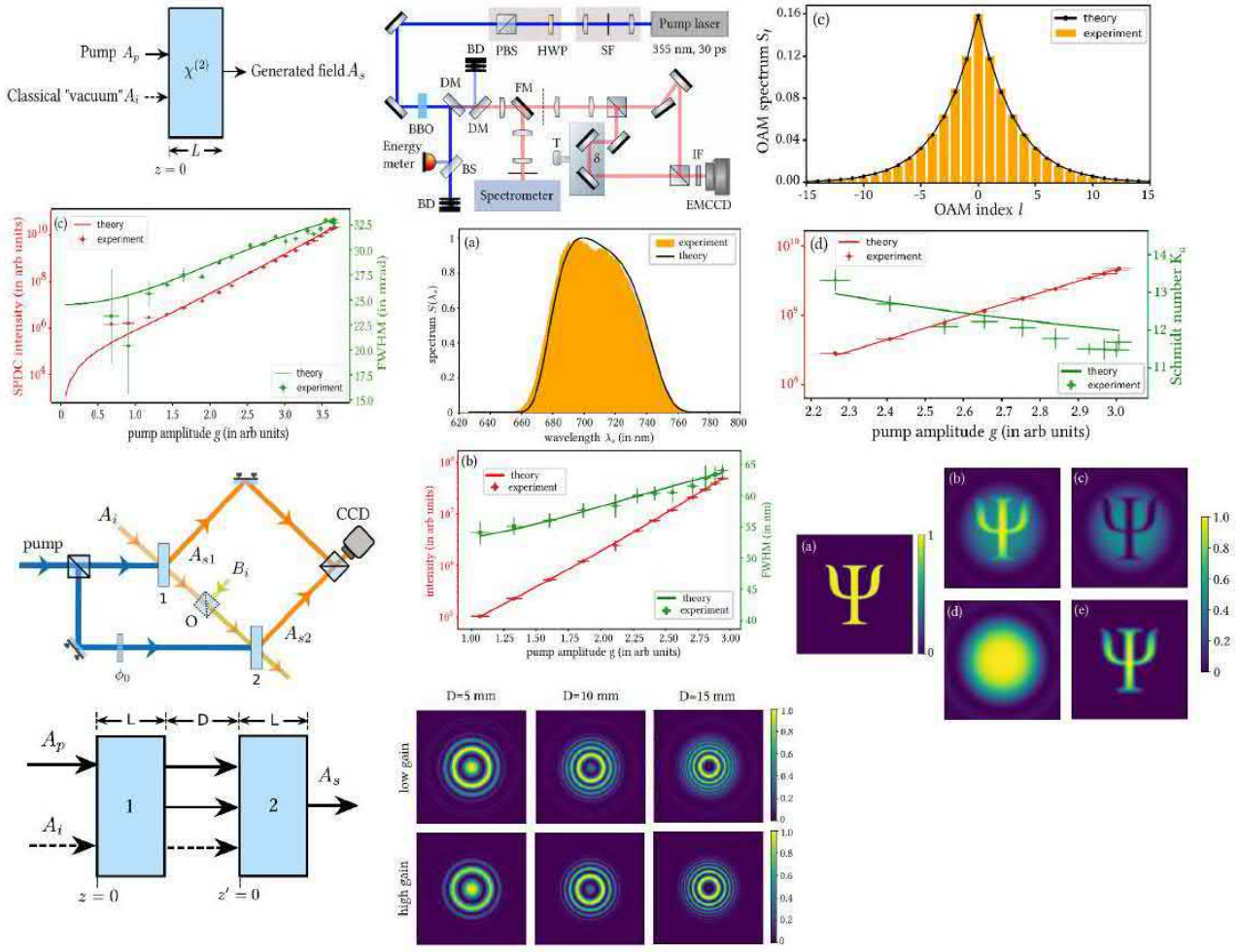


**Fig. 1:** This is the image on the homepage of the ICOAM22 conference.

## References

[1] G. Kulkarni, J. Rioux, B. Braverman, M. V. Chekhova, and R. W. Boyd, arXiv:2201.03842

*Corresponding author: girishvnit@gmail.com

# Engineering high-dimensional quantum entanglement via path identity

**Jaroslav Kysela**[*1], **Manuel Erhard**[†2], **Armin Hochrainer**[1,2], **Mario Krenn**[1,2], **Anton Zeilinger**[‡1,2]

*1. Faculty of Physics, Vienna Center for Quantum Science & Technology, University of Vienna, 1090 Vienna, Austria*
*2. Institute for Quantum Optics and Quantum Information, Austrian Academy of Sciences, 1090 Vienna, Austria*

Quantum entanglement not only lies at the heart of some of the counter-intuitive features of quantum mechanics but has also found applications as computational and communication resource in the nascent quantum technologies. The demand for reliable and efficient sources of entanglement is therefore only expected to rise in the future. Arguably the most common process of entanglement generation for photons is the spontaneous parametric downconversion (SPDC) in non-linear crystals. High-dimensional entangled states can be produced this way with some limited control over the form of the state.

An alternative approach that allows for versatile and modular generation of high-dimensional entanglement is provided by the recently developed concept of entanglement by path identity [1], for a review see [2]. Instead of making use of a single SPDC (or another) process a network of sources is considered where the form of the resulting states is governed by the network geometry. Most notably, none of the sources alone produces entanglement. One can instead incrementally increase the entanglement dimension by incorporating more sources. The framework is inspired by the experiment of Zou, Wang, Mandel [3][4]. In this two-crystal experiment, the photon path of the first crystal is overlapped with the photon's path of the second crystal (an idea suggested by Zhe-Yu Ou), such that there is no information whether the photon has been produced in the first or second crystal. The indistinguishability by path identity leads to an induced coherent superposition of the other photon's origin.

We report the first, proof-of-principle experimental demonstration [5] of the concept of entanglement by path identity. A series of three non-linear crystals is aligned such that no information exists as to which of them produces a pair of photons. This indistinguishability translates into a coherent superposition of three different scenarios, corresponding to three different values of orbital angular momentum. The resulting class of states the setup can produce reads $\alpha_0|0,0\rangle + \alpha_1|2,2\rangle + \alpha_2|-2,-2\rangle$, where the amplitude as well as the phase of each coefficient can be tuned independently.

We further discuss the general framework that allows to build entanglement sources for higher dimensions, more particles as well as other degrees of freedom and some connections to previous approaches are made. The support of the Austrian Academy of Sciences and the University of Vienna via the project QUESS (Quantum Experiments on Space Scale) is acknowledged.

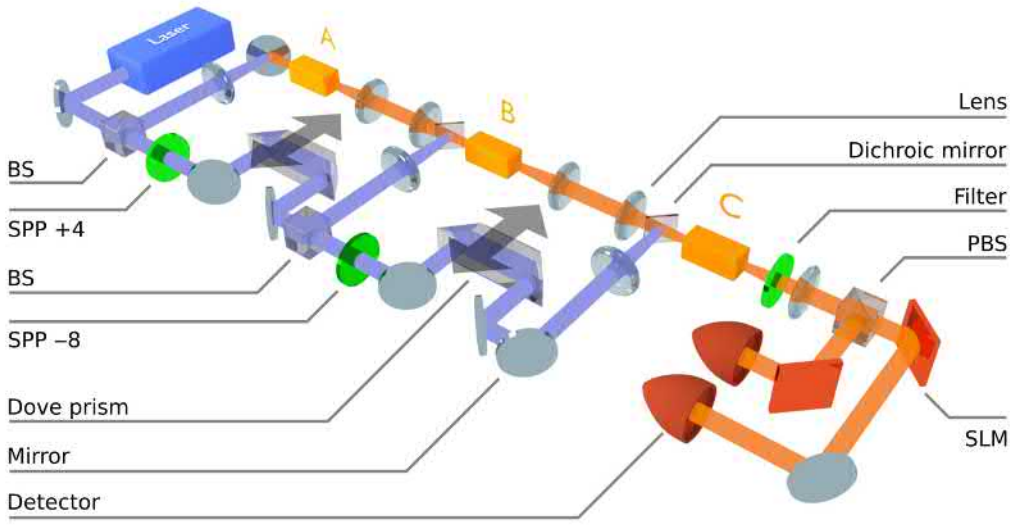


**Fig. 1:** The setup for the generation of photon pairs displaying three-dimensional entanglement in their orbital angular momentum (OAM). Three different non-linear crystals A, B, and C are pumped individually by the same laser source (blue beams, 405 nm), where the intensity of each beam is controlled by variable-splitting-ratio beam splitters (BS). The mutual phases are further set by movable Dove prisms. The resulting quantum state of down-converted photons (orange beams, 810 nm) produced via type II SPDC is a superposition of three OAM terms, each of which originates in one of the crystals: the term $|0,0\rangle$ in crystal A; term $|2,2\rangle$ in crystal B due to a spiral phase plate (SPP) imparting 4 quanta of OAM to the pump beam; and term $|-2,-2\rangle$ in crystal C due to an additional SPP. The pump beam is filtered out by dichroic mirrors and a band-pass filter and the remaining down-converted photons are separated by a polarizing beam splitter (PBS) and subjected to projective measurements implemented by spatial light modulators (SLM) and fiber-coupled single-photon detectors.

## References

[1] M. Krenn, A. Hochrainer, M. Lahiri, A. Zeilinger, Phys. Rev. Lett. **118**, 080401 (2017)
[2] A. Hochrainer, M. Lahiri, M. Erhard, M. Krenn, A. Zeilinger, arXiv:2101.02431 [quant-ph]
[3] X. Y. Zou, L. J. Wang, L. Mandel, Phys. Rev. Lett. **67**, 318 (1991)
[4] L. J. Wang, X. Y. Zou, L. Mandel, Phys. Rev. A **44**, 4614 (1991)
[5] J. Kysela, M. Erhard, A. Hochrainer, M. Krenn, A. Zeilinger, 2020 Proc. Natl Acad. Sci. 117 26118–22

[*]Corresponding author: jaroslav.kysela@univie.ac.at
[†]Corresponding author: manuel.erhard@univie.ac.at
[‡]Corresponding author: anton.zeilinger@univie.ac.at

# Environmental and Fibre Sensing with Structured Light

**Zhaozhong Chen [1], Sara Angelucci [1], Aleksandr Bolding [1], Alasdair Clark [1], Adam Valles [2], and Martin P.J. Lavery*[1]**

*1. James Watt School of Engineering, University of Glasgow, G12 8QQ*

*2. ICFO-Institut de Ciencies Fotoniques, , 08860 Castelldefels (Barcelona), Spain*

The interaction of optical fields with disordered and complex media has been an area of considerable interest for many researchers. Such media commonly induces intensity and phase distortions that can be disruptive for optical communications and imaging systems [1]. However, these optical distortions are directly dependent on the environment that the complex media is situated within and therefore the distortions can be used for optically sensing that environment. Structured beams, such as those that carry Orbital Angular Momentum (OAM), experience unique distortion during propagation. One such notable behaviour is called vortex splitting, where a beam that carries an OAM $\ell = \mathrm{n}$, will break up into $n$ vortices of $\ell = 1$ that are spatially separated [2]. Complex phase aberrations such as vortex splitting is experienced by a beam carrying OAM during propagation through bulk aberrating optical channels such as long distance free-space channels, underwater channels or in multimode fibres [3,4]. Deciphering the origins of changes in specific aberrations observed, could be used to developed enhanced environmental sensing technologies.

We will discuss our recent work utilising mode decomposition assisted machine learning approaches to identify trainable features in the distortions of structured beams for environmental monitoring and shape sensing in optical fibres. Our novel technique revealed features that can be used reliably with regression models to predict temperature variations of 0.6C and wind speed variations of 0.01 m/s over km equivalent turbulent free-space channels with controllable and verifiable temperature and wind speed, fig 1 . We have further extended this ML feature analysis technique for shape sensing in few and multiple mode fibre. With this technique we have identified highly trainable features that allow us to locate the presence of a fibre bends to a precision of better than 1 mm at a remote distance of up to 1 km. These approaches could be used to create low-cost fibre shape sensors or path dependent weather measurement for a wide range environmental monitoring application.

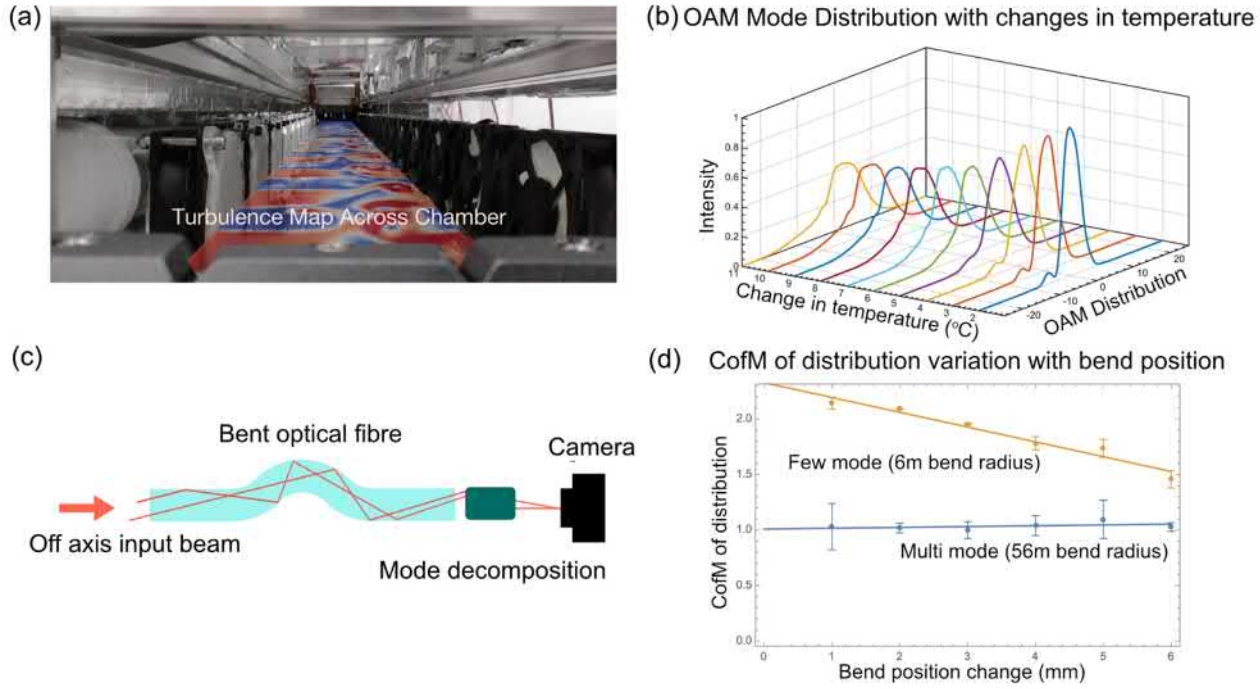


**Fig. 1:** (a) An environmental simulator was developed that has control of wind speed and temperature across the channel. (b) When an optical beam carrying an OAM of $I = 3$ is passed through the channel the power in that mode is spread over several neighbouring spatial modes. The distribution of this power spreading will change depending on the temperature and windspeed, which can be used to determine changes in weather that have occurred over the channel. (c) Bends in optical fibre distort the propagation of light through the waveguide causing modal crosstalk. Changing the position of the bend changes the distortion observed in the optical field. (d) Mode decomposition assisted ML revealed the centre of mass of the modal distributions changes in a near linear way that can be used for accurate fibre shape sing.

## References

[1] H. Rubinsztein-Dunlop et al, J. Opt. 19013001 (2016)
[2] M S Soskin et al., Phys. Rev. A56 4064-75 (1997)
[3] M.P.J. Lavery et al., Science Advances, 3, 10 (2017)
[4] S. Viola et al., Physical Review Letters, 2, 033093 (2020)

*Corresponding author: martin.lavery@glasgow.ac.uk

# Efficiently sorting overlapping quantum states of light

**Max Tyler [1], Suraj Goel [1], Feng Zhu [1], Saroch Leedumrongwatthanakun [1], Mehul Malik [1], Jonathan Leach*[1]**
*1. School of Engineering and Physical Sciences, Heriot-Watt University, Edinburgh, EH14 4AS, UK*

The efficient manipulation, sorting, and subsequent measurement of optical modes and single-photon quantum states is an important challenge in classical and quantum optical science. While methods for sorting orthogonal quantum states of light in high dimensions, such as those carrying orbital angular momentum, have been demonstrated recently, the efficient separation and measurement of non-orthogonal or overlapping states has not yet been achieved. Here we will discuss the simultaneous and efficient sorting of overlapping quantum states of light encoded in the transverse spatial degree of freedom of a photon. Our system realises unambiguous state discrimination within the framework of a multi-plane light converter (MPLC) that can sort a wide range of non-orthogonal states encoded in dimensions ranging from d = 3 to d = 7. These results lay the groundwork for optimal image identification and classification via optical networks, with potential applications ranging from self-driving cars to quantum communication systems.

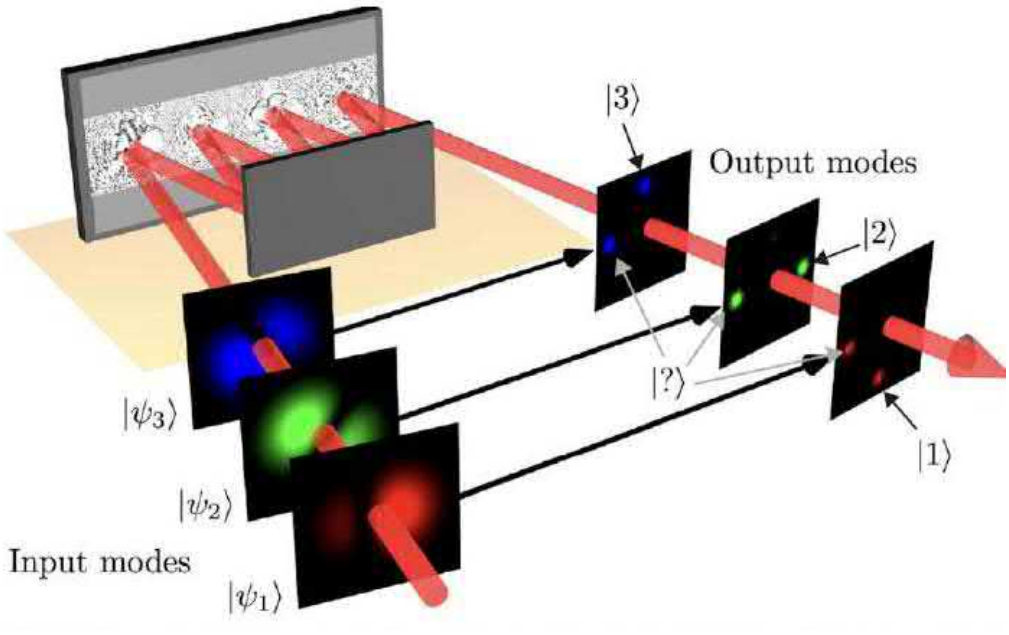


**Fig. 1:** Schematic of the mode sorter for non-orthogonal states with colour used to represent the field amplitude distribution of different modes. The input modes are non-orthogonal states composed of Hermite-Gaussian modes.

*Corresponding author: j.leach@hw.ac.uk

# Singular Optics From a Data Science Perspective

**Daniel Leykam**[*1]

*1. Centre for Quantum Technologies, National University of Singapore, Science Drive 2, 117543, Singapore*

Singular optics - the study of phase and polarization singularities in wave fields - has delivered fruitful insights not just in optics, but also in related branches of physics that deal with structured waves, including electron vortex beams, acoustics, and topological phases of matter [1]. The key idea underlying applications in all these fields is that singularities carry quantised topological charges that make them both robust to perturbations and easily identifiable, e.g. as forks in interference fringes [2]. Complicated phenomena including unidirectional edge modes and bound states in the continuum can be understood by conservation of a topological charge.

While qualitative measures such as topological charges are powerful, it can be challenging to incorporate them into quantitative analysis methods such as machine learning algorithms. For example, how should one define error bars or uncertainties in a noisy measurement of a quantised topological charge? How should one infer the presence of a singularity from a limited set of measurements? Can wave singularities be used to form simplified representations of complex wave fields? Data science techniques, specifically topological data analysis, offer powerful approaches for solving these problems [3,4].

I will provide a physicist-friendly introduction to topological data analysis, focusing on persistent homology. Persistent homology computes topological features of datasets over a range of characteristic length or intensity scales. The scaledependence of different topological features of the data, such as clusters (zero-dimensional features) or cycles (onedimensional features), can be summarised using a persistence diagram, e.g. shown in Fig. 1. Topological features that persist over a broader range of scales are more likely to be real and meaningful features of the data than noise-induced artefacts. Persistent homology hence allows one to reliably assign shapes to noisy datasets such as point clouds. Possible applications to optics and photonics include the detection of phase transitions [5,6] and the machine learning-based identification of dark solitons and other topological defects in experimental images [7,8].

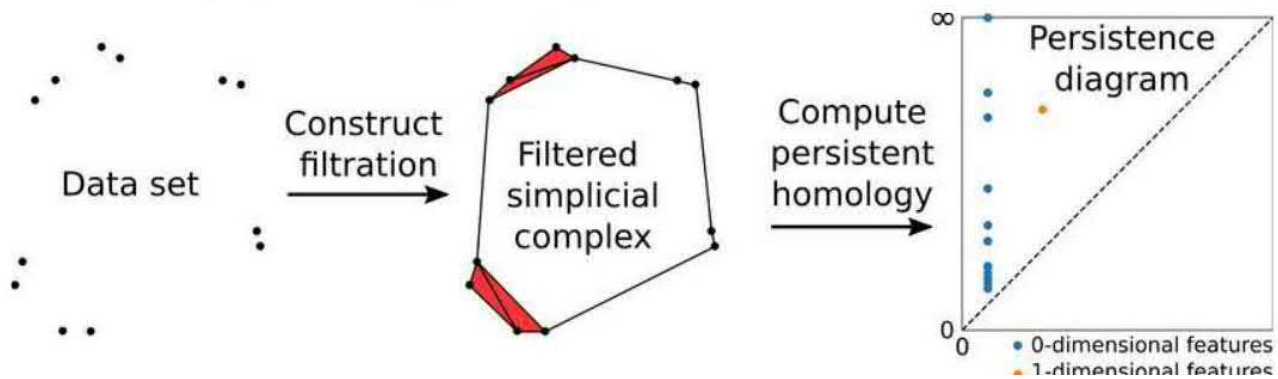


**Fig. 1:** Summary of the persistent homology pipeline. Given data (e.g. a point cloud) and a suitable metric (e.g. Euclidean distance), simplicial complices encoding the connectivity between the data points at various characteristic distance scales are constructed. The robustness of topological properties of the simplicial complices (e.g. number of clusters and holes) is summarised using a persistence diagram; points (features) further from the diagonal (dashed line) are more robust.

## References

[1] M. Soskin, S. V. Boriskina, Y. Chong, M. R. Dennis, and A. Desyatnikov, Singular optics and topological photonics, J. Opt. 19, 010401 (2017).
[2] M. R. Dennis, K. O'Holleran, and M. J. Padgett, Singular Optics: Optical vortices and polarization singularities, Prog. Opt. **53**, 293 (2009).
[3] G. Carlsson, Topological methods for data modelling, Nature Rev. Phys. 2,697 (2020). [4] J. Murugan and D. Robertson, An Introduction to Topological Data Analysis for Physicists: From LGM to FRBs, arXiv: 1904.11044.
[5] D. Leykam and D. G. Angelakis, Photonic band structure design using persistent homology, APL Photon. 6, 030802 (2021).
[6] Y. He, S. Xia, D. G. Angelakis, D. Song, Z. Chen, and D. Leykam, Persistent homology analysis of a generalized AubryAndre-Harper model, arXiv:2204.13276.
[7] D. Leykam, I. Rondon, and D. G. Angelakis, Dark soliton detection using persistent homology, arXiv: 2107.14594.
[8] S. Guo, A. R. Fritsch, C. Greenberg, I. B. Spielman, J. P. Zwolak, Machine-learning enhanced dark soliton detection in Bose-Einstein condensates, Mach. Learn.: Sci. Technol. 2, 035020 (2021).

*Corresponding author: daniel.leykam@gmail.com

# The Geometric Phase of Entanglement for Trapped Optical Vortices and Its Interpretation as an Information Measure

**Mark T. Lusk**[*1], **Mark E. Siemens** [2]
*1. Department of Physics, Colorado School of Mines, Golden, Colorado, U.S.A.*
*2. Department of Physics, University of Denver, Denver, Colorado, U.S.A.*

An entangled two-photon state, $N\left(\cos(\alpha/2)\,|A\rangle\,|B\rangle + \sin(\alpha/2)\,|B\rangle\,|A\rangle\right)$, is constructed so that it propagates within an axisymmetric, multi-mode fiber with a harmonic dielectric profile. Each of the single-photon states, $|A\rangle$ and $|B\rangle$, is an orbiting vortex whose tilt and trajectory can be tailored independently[1]. The two-photon state accumulates a geometric phase that is not equal to the sum of the geometric phases of the associated single-photon states[2],[3]. The difference amounts to a *Geometric Phase of Entanglement (GPE)*. A state operator formalism is constructed in which geometric phase is expressed in terms of state operators, sometimes called density matrices. This reveals that the GPE is the difference between the geometric phase of the reduced state operators and geometric phase in the absence of any entanglement. The decomposition is significant because these are phases that can be measured after physically separating the photons.

The reduced state operators can each be decomposed into a sum of two pure state operators. Interestingly, each of these four pure states corresponds to an orbiting vortex, as illustrated in the left panels of the figure.

While the total state operator is pure, the reduced state operators are mixed and so can have non-zero von Neumann measures of entropy. A functional relationship is derived between the GPE and the reduced state entropies, as shown at right in the figure. This information-based interpretation of the GPE suggests that, if the photons are spatially separated, the geometric phase measured for one photon will exhibit a quantum correlation with that of the other photon. The prospect of measuring a quantum-erasable geometric phase is therefore considered.

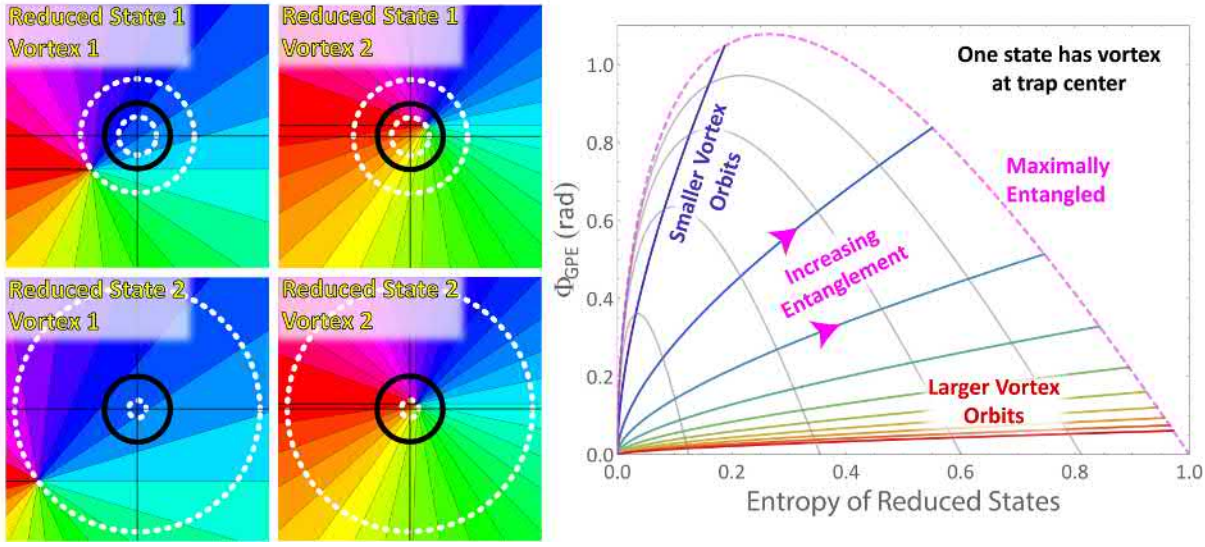


**Fig. 1: Left.** Four plots of phase are shown for a particular position along the trap axis. A two-photon state composed of entangled vortices is constructed so that one vortex orbits at a fixed radius (black circles) while the other vortex is fixed at the trap center. The associated state operator has two reduced state projections that can each be expressed as the sum of two pure states. The four pure states correspond to vortices that orbit on the trajectories shown with dashed white circles. **Right.** The reduced state operators are mixed and have equal, non-zero von Neumann entropies. These have a functional relationship with the GPE. The gray arched curves each give the GPE for a prescribed value of entanglement. The rainbow-colored curves each give the GPE for a prescribed radius of the orbiting vortex in the original two-photon state. As in the left panels, the other vortex is fixed at the trap center. The indigo curve is for a small orbit radius while the red curve is for a large orbit radius.

## References

[1] J. Andersen, D. Voitiv, M. Siemens, M.T. Lusk, Phys. Rev. A **104** 033520 (2021)
[2] D. Voitiv, M.T. Lusk, M. Siemens, Opt. Lett. **47** 1089 (2022)
[3] M.T. Lusk, D. Voitiv, C. Zhu, M. Siemens, ArXiv 2111.07338, Phys. Rev. A (to appear, 2022)

*Corresponding author: mlusk@mines.edu

# Transport and Manipulation of High-Dimensional Entanglement through a Complex Medium

**Suraj Goel [1], Saroch Leedumrongwatthanakun [1], Natalia Herrera Valencia [1], Will McCutcheon [1], Hugo Defienne [2], Pepijn Pinkse [3], Claudio Conti [4], and Mehul Malik*[1]**

*1. Institute of Photonics and Quantum, Sciences, Heriot-Watt University, Edinburgh, UK*
*2. School of Physics and Astronomy, University of Glasgow, Glasgow, UK*
*3. MESA+ Institute for Nanotechnology, University of Twente, Enschede, The Netherlands*
*4. Department of Physics, University Sapienza, Rome, Italy*

Quantum states of light entangled in their spatial and temporal structure offer the potential for noise-robust quantum communication networks that harness the full information carrying capacity of a photon. For example, we have recently demonstrated how high-dimensional entanglement enables one to perform quantum steering under extreme conditions of noise and loss [1], opening a pathway towards practical device-independent quantum communication networks. A central challenge in the realisation of such networks is the ability to precisely control and reliably transport high-dimensional entangled states of light. While qubit-entanglement has been distributed over large distances through free-space and fibre, the transport of highdimensional entanglement is hindered by the complexity of the channel. In addition to transport, methods for the precise control and measurement of high-dimensional quantum states are notoriously difficult to implement, usually requiring a sophisticated mesh of cascaded interferometers constructed with bulk or integrated optics.

Here we show how the platform of a simple complex scattering medium can be used for both the transport and precise control of high-dimensional entangled states of light. First, we demonstrate the transport of six-dimensional spatial-mode entanglement through a two-metre long, commercial multi-mode fibre [2, 3]. We show how entanglement itself can be used to measure the transmission matrix of the complex medium, allowing the recovery of quantum correlations that were initially lost. In contrast to the classical technique of measuring a response function one state at a time, our method exploits the idea of channel-state duality to map the entire transmission matrix of a complex, multi-mode scattering channel onto a single high-dimensional entangled state. By using a property unique to high-dimensional entanglement, the medium is rendered transparent to entanglement by carefully "scrambling" the photon that did not enter it, rather than unscrambling the photon did.

In a second recent experiment, we demonstrate how a complex medium can be used for programming high-dimensional quantum circuits for light by leveraging inverse-design techniques, enabling us to manipulate bipartite entangled states of light in up to seven dimensions [4]. Furthermore, we show how this programmability allows us to turn a multi-mode fibre into a generalised multi-outcome measurement device, allowing us to both transport and certify entanglement within the transmission channel itself. Our work serves as an alternative yet powerful approach for realising precise control over high-dimensional quantum states of light, with clear applications in next-generation quantum communication and computing technologies.

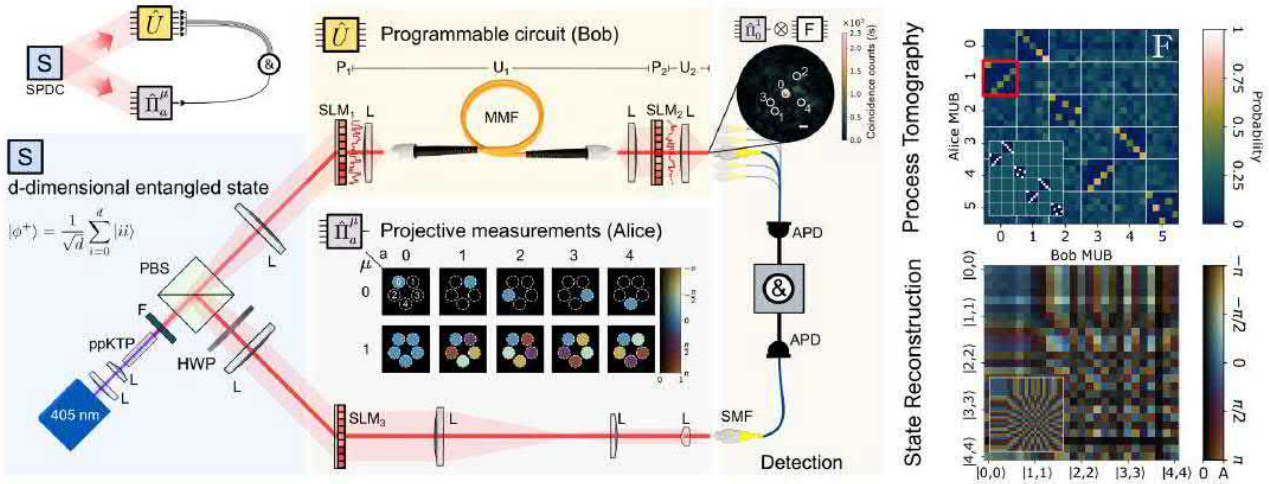


**Fig. 1:** (Left) A high-dimensional spatially entangled state is manipulated using a five-dimensional Fourier gate programmed using a multi-mode fibre (MMF) placed between two spatial light modulators (SLM1 and 2). (Right) Process tomography data and the corresponding reconstructed density matrix of the Fourier gate show good agreement with theoretically predicted values (insets).

## References

[1] V. Srivastav, N. H. Valencia, W. McCutcheon, S. Leedumrongwatthanakun, S. Designolle, R. Uola, N. Brunner, and M. Malik, arXiv:2202.09294 (2022).
[2] N. H. Valencia, S. Goel, W. McCutechon, H. Defienne, and M. Malik, Nature Physics 16, 1112(2020).
[3] N. H. Valencia, V. Srivastav, M. Pivoluska, M. Huber, N. Friis, W. McCutcheon, M. Malik, Quantum 4, 376(2020)
[4] S. Goel, S. Leedumrongwatthanakun, N. H. Valencia, W. McCutcheon, C. Conti, P. Pinkse, and M. Malik, arXiv:2204.00578 (2022).

*Corresponding author: m.malik@hw.ac.uk

# Quantum Interactions with Structured Electrons

**Amy Turner** [1], **Cameron Johnson** [1], **Benjamin J. McMorran**[*1]
*1. Department of Physics, University of Oregon, 1585 E 13th Avenue, Eugene, Oregon 97403, United States of America*

Structured electron beams can be used to probe the coherence and symmetry of inelastic electron scattering as well as demonstrate "interaction-free" measurements. Nanofabricated holographic gratings are used to engineer the phase, amplitude, and momentum distribution of free electron wavefunctions in transmission electron microscopes (TEMs) [1,2] and scanning electron microscopes (SEMs) [3,4]. We have used this technology to efficiently prepare electrons with quantized orbital angular momentum (OAM) [5,6], create arbitrary superpositions of pure spatial modes [2], electron beams that coil in space [7], remove aberrations [8], or serve as efficient beamsplitters for use in electron interferometers [9,10].

Recently, we used two holographic gratings to create a Mach-Zehnder electron interferometer [10]. We utilized Gaussian probes to demonstrate inelastic interferometry. Furthermore, we employed the two-grating interferometer to perform interaction-free measurements with electrons [11]. Plans to extend this research to investigations of chiral interactions with electron OAM states will be discussed.

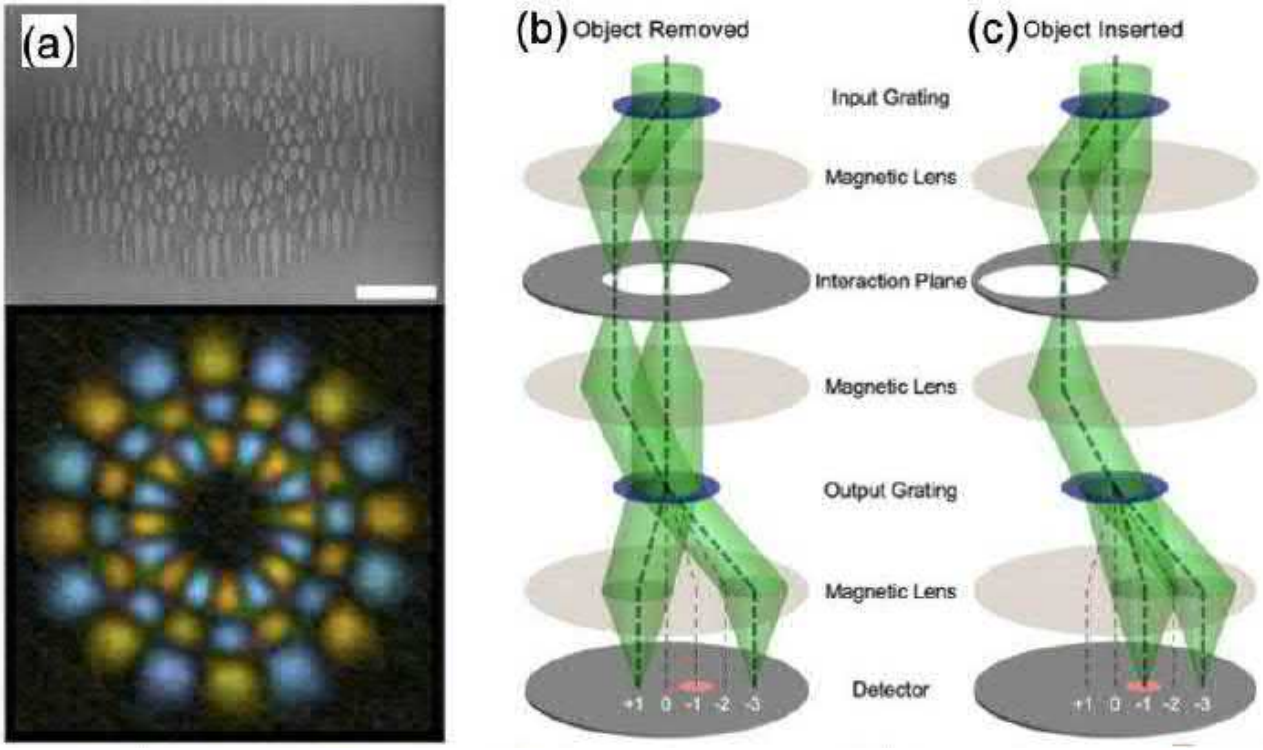


**Fig. 1:** (a) A nanofabricated phase hologram ( 2 micron scale bar at top) used to prepare electron beams in a superposition of pure Laguerre-Gauss modes. (b) Phase gratings can be used to build a Mach-Zehnder interferometer with discrete outputs and beam modes such as OAM states in different paths. (c) When one path undergoes an interaction with a target, such as blockage by an object shown here or OAM-dependent scattering from an object, this disrupts destructive interference in one of the outputs, providing an "interaction-free" measurement.

**References**
[1] T. R. Harvey, J. S. Pierce, A. K. Agrawal, P. Ercius, M. Linck, and B. J. McMorran, New J. Phys. 16, 093039 (2014).
[2] C. W. Johnson, J. S. Pierce, R. C. Moraski, A. E. Turner, A. T. Greenberg, W. S. Parker, and B. J. McMorran, Opt. Express 28, 17334(2020).
[3] B. J. McMorran, J. D. Perreault, T. A. Savas, and A. Cronin, Ultramicroscopy 106, 356 (2006).
[4] T. Řiháček, M. Horák, T. Schachinger, F. Mika, M. Matějka, S. Krátký, T. Fořt, T. Radlička, C. W. Johnson, L. Novák, B. Sed'a, B. J. McMorran, and I. Müllerová, Ultramicroscopy **225**, 113268 (2021).
[5] B. J. McMorran, A. Agrawal, I. M. Anderson, A. A. Herzing, H. J. Lezec, J. J. McClelland, and J. Unguris, Science 331, 192 (2011).
[6] B. J. McMorran, A. Agrawal, P. A. Ercius, V. Grillo, A. A. Herzing, T. R. Harvey, M. Linck, and J. S. Pierce, Philos. Trans. R. Soc. Math. Phys. Eng. Sci. 375, 20150434 (2017).
[7] J. Pierce, J. Webster, H. Larocque, E. Karimi, B. McMorran, and A. Forbes, New J. Phys. 21, 043018 (2019).
[8] M. Linck, P. A. Ercius, J. S. Pierce, and B. J. McMorran, Ultramicroscopy **182**, 36 (2017).
[9] C. W. Johnson, D. H. Bauer, and B. J. McMorran, Appl. Opt. **59**, 1594(2020).
[10] C. W. Johnson, A. E. Turner, and B. J. McMorran, Phys. Rev. Res. 3, 043009 (2021).
[11] A. E. Turner, C. W. Johnson, P. Kruit, and B. J. McMorran, Phys. Rev. Lett. 127, 110401 (2021).

[*]Corresponding author: mcmorran@uoregon.edu

# 3D Time-of-Flight Imaging using Ultra-thin Endoscopy

**Simon Peter Mekhail**[1],**Daan Stellinga**[2], **David Philips**[3], **Tomáš. Čižmár**[4,5], **Miles Padgett**[*1]

*1. School of Physics and Astronomy, University of Glasgow, Glasgow, United Kingdom*
*2. Faculty of Science and Technology, University of Twente, Twente, The Netherlands*
*3. School of Physics and Astronomy, University of Exeter, United Kingdom*
*4. Leibniz Institute of Photonic Technology, Jena, Germany*
*5. Institute of Scientific Instruments of the CAS, Brno, Czech Republic*

Advances in endoscopic technology has enabled imaging in formerly difficult to access areas. Among these, new developments in ultra-thin single fibre imaging has broadened the horizons endoscopy to imaging in areas which exhibit exceptional sensitivity to probe size [1]. Whereas traditional endoscopes may use fibre bundles, where each core in a common cladding works as single pixel, a single multimode fibre (MMF) has the advantage of carrying one to two orders of magnitude more information on the fibre modes for the same probe size [2]. Multimode fibres however do not act as a simple imaging conduit, rather a light field which is launched into a MMF can be expressed as a superposition of the orthogonal fibre modes. In a typical multimode optical fibre, with a 50um core and a numerical aperture (NA) of 0.22, there are in the order of 1000 modes. As these modes propagate down the fibre the input field is transformed due to the differing phase velocities of the modes. The resulting output field, therefore, rarely resembles the input superposition, rather a speckle pattern. This transformation can be regarded as linear and, after characterising the fibre, the input field can be structured such that a desired output field is achieved.

Calibration is performed by scanning 2000 input plane waves oversampling the fibre modes by a factor of two. This is done by varying the grating period on a digital micro-mirror device (DMD). At the distal end of the fibre, images are taken by phase stepping the plane wave relative to a stationary internal reference to give the optimal phase and amplitude for each input wave at each pixel in the field of view of the fibre. To image, input DMD masks are calculated to form a single spot in the far field of the fibre's distal facet. The spot is then scanned by changing the input field to interrogate a scene. Reflected light is be collected through a secondary fibre running concurrently with the excitation fibre. These are both held in a custom made 20 gauge needle as shown in Figure 1 A.

For depth information, imaging is performed with a 700 ps pulsed q-switched laser at a repetition rate of 21 kHz. A reference photodiode on the excitation arm of the setup is used as a trigger to start timing and data are collected with an avalanche photodiode sampled at 2.5 GHz. After interpolating and temporally localising the peak the time of flight is converted into a distance to the reflecting object. Imaging is performed at 5.0 Hz for a circular field of view with a diameter of 75 scanned spots. Spatial resolution was determined to be 1.5 times the diffraction limit and depth accuracy was estimated to within $\pm 5$ mm. An example frame capture is shown in Figure 1 B. Ongoing developments in this work are exploring the effects of bending on image reconstruction without the need for measuring a new transmission matrix.

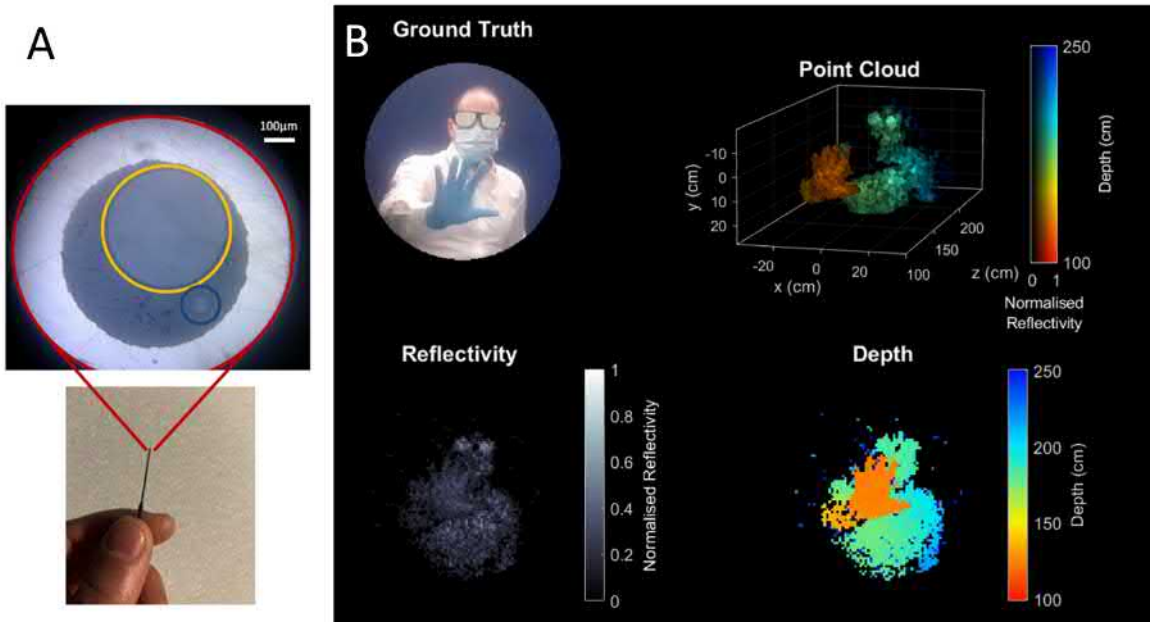


**Fig. 1:** Needle endoscope tip and recording snap shot. (A) Needle endoscope tip emission fibre (small) is highlighted in blue and collection (large) in yellow. (B) Capture from a video recorded with the endoscope at a distance of 2m adapted from [3].

## References

[1] S. Turtaev, I.T. Leite, T. Altwegg-Boussac, J. M. P. Pakan, N. L. Rochefort, T. Čižmár, Light. Sci. Appl. **7** 92 (2018)
[2] Y. Choi, C. Yoon, M. Kim, T. D. Yang, C. Fang-Yen, R. R. Dasari, K. J. Lee, W. Choi, Phys. Rev. Lett. **109** 20 (2012)
[3] D. Stellinga, D. B. Phillips, S. P. Mekhail, A. Selyem, S. Turtaev, T. Čižmár, M. J. Padgett, Science. **374** 6573 (2021)

*Corresponding author: miles.padgett@galsgow.ac.uk

# Spatio-temporal optical vortex (STOV) pulses: propagation and OAM conservation

**S.W. Hancock** [1], **S. Zahedpour** [1], **H.M. Milchberg**[*1],

*1. Institute for Research in Electronics and Applied Physics, Dept. of Electrical Engineering, and Dept. of Physics University of Maryland, College Park, MD 20742 USA*

A spatio-temporal optical vortex (STOV) pulse is a polychromatic electromagnetic structure with orbital angular momentum (OAM) and optical phase circulation defined in spacetime, where in its simplest form, the OAM vector is perpendicular to the direction of propagation. STOVs were originally observed as emergent electromagnetic structures underlying nonlinear selffocusing collapse [1], a universal process including relativistic self-guiding in plasmas and filamentation in transparent media. Here I will review several topics from our experimental and theoretical work over the last several years. We have demonstrated linear generation of STOV-carrying pulses using a $4f$ pulse shaper and studied their free space propagation from near field to far field, capturing their evolving spatiotemporal amplitude and phase [2] using a new single shot diagnostic for singular optical pulses. This work was later verified in experiments observing STOVs in the far field [3].We have also demonstrated STOV OAM conservation in (second) harmonic generation, verifying that STOV OAM applies at the single photon level [4]. Most recently, theories have been developed for STOV-based OAM [5,6]. I will describe our modal theory for STOV propagation in dispersive materials [6], with implications for propagation through various media along with experimental results.

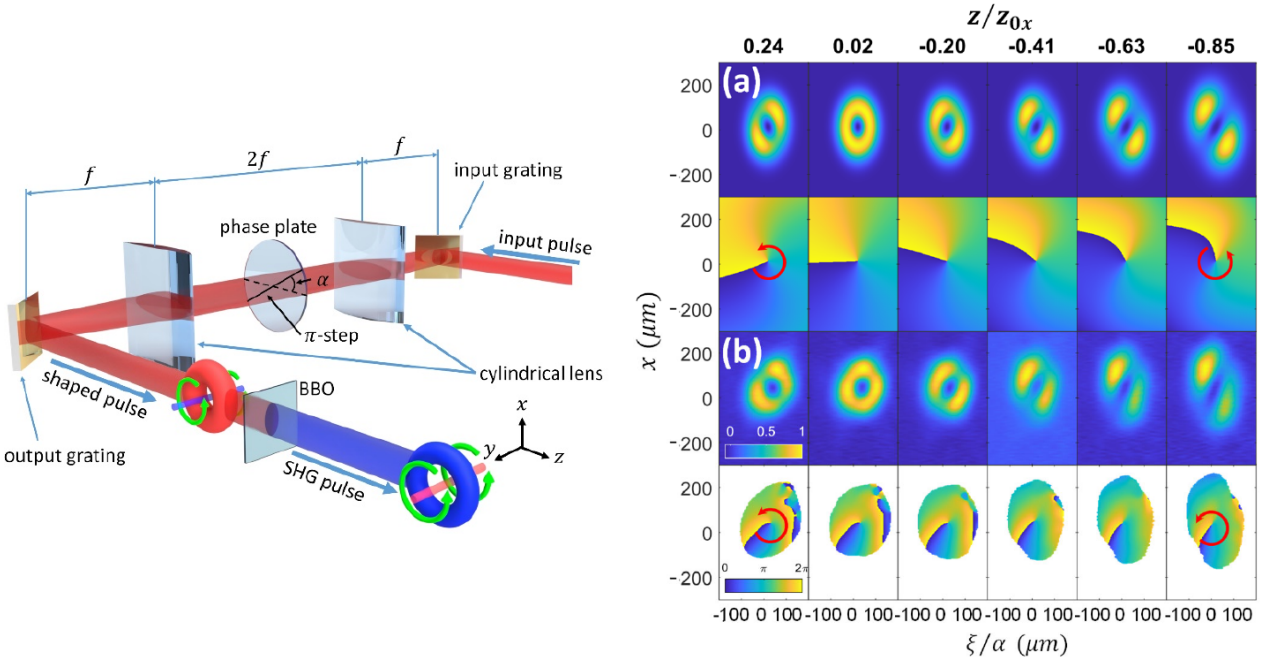


**Fig. 1:** Left panel: Example $4f$ pulse shaper used to generate a $\ell = \pm 1$ STOV –carrying pulse at 800nm, composed of two 1200 groove/mm gratings, two $f = 10$ cm cylindrical lenses and a transmissive $\pi$-step phase plate (for generating an edge-first flying donut STOV in the near field of the shaper). A spiral phase plate is used for generating a donut in the far-field [2]. The fused silica phase plate has a 882 nm step oriented at $\pm 40°$ to the grating dispersion direction. A $100\mu m$ thick BBO crystal for SHG is located 20cm from the output grating. More recent results to be described use an SLM-based shaper. Right panel: Spatiotemporal intensity and phase profiles of a $\ell = 1$ STOV propagating through its beam waist ($z = 0$), as predicted by the modal theory (a) and measured (b). Within each frame, pulse propagation is right-to-left. Symbols: $z_{0x} = \pi w_{0x}^2/\lambda$, and $\alpha = w_{0\xi}/w_{0x}$ is the spacetime eccentricity parameter, where $w_{0x}$ and $w_{0\xi}$ are space-like and time-like modal scale lengths [6].

## References

[1] N. Jhajj, I. Larkin, E.W. Rosenthal, S. Zahedpour, J. K. Wahlstrand, and H. M. Milchberg, Spatiotemporal Optical Vortices, Phys. Rev. X 6, 031037 (2016).
[2] S.W. Hancock, S. Zahedpour, A. Goffin, and H. M. Milchberg, Free-space propagation of spatiotemporal optical vortices, Optica 6, 1547 (2019).
[3] A. Chong, C. Wan, J. Chen, and Q. Zhan, Generation of spatiotemporal optical vortices with controllable transverse orbital angular momentum, Nat. Photonics 14, 350 (2020).
[4] S.W. Hancock, S. Zahedpour, and H. M. Milchberg, Second-harmonic generation of spatiotemporal optical vortices and conservation of orbital angular momentum, Optica 8, 594 (2021)
[5] K. Bliokh, Spatiotemporal Vortex Pulses: Angular Momenta and Spin-Orbit Interaction, Phys. Rev. Lett. 126, 243601 (2021).
[6] S.W. Hancock, S. Zahedpour, and H. M. Milchberg, Mode Structure and Orbital Angular Momentum of Spatiotemporal Optical Vortex Pulses, Phys. Rev. Lett. 127, 193901 (2021).

*Corresponding author: milch@umd.edu

# Classical and Quantum scattering of vortex beams from small particles

**Gabriel Molina-Terriza**[*1,2,3], **Martin Molezuelas** [1], **Jon Lasa** [1], **Álvaro Nodar** [1], **Ruben Esteban** [1], **Javier Aizpurua** [1,2]

*1. Centro de Física de Materiales, Paseo Manuel de Lardizabal 5, 20018 Donostia-San Sebastián, Spain*

*2. Donostia International Physics Center, Paseo Manuel de Lardizabal 4, 20018 Donostia-San Sebastián, Spain*

*3. IKERBASQUE, Basque Foundation for Science, Maria Diaz de Haro 3, 48013 Bilbao, Spain*

Scattering of light from particles is one of the cornerstones in which it is founded many branches of physics and technology. From optical tweezers, to characterization of pollutants in air and liquid, the applications of scattering theory are many and diverse. Classical scattering theory has received a lot of attention in the last decades, as new numerical methods allowed using classical Mie theory in regimes that were typically unattainable without substantial computing power [1].

On the other hand, the last decades have also witnessed an explosion of experimental techniques to generate beams of light that cannot be described with classical electromagnetism. Such quantum sources of light include single photon sources, entangled photon sources and squeezed light, among others. Quantum sources of light allow for an extra degree of freedom in the control of light, the quantum correlations between different modes. This can be used to improve certain metrological schemes and sensing technologies. However, the study of the scattering of quantum sources of light from small particles is still in its infancy.

In this talk, I will review our recent advances in the description and experiments of the scattering of different modes of light from small particles. I will show that a description in terms of the angular momentum and helicity modes of the electromagnetic field is very useful in certain applications. Also, I will show the differences of the classical and quantum description of the scattering of different modes (Figure 1).

We have measured the back/scattering with high refractive index spherical particles of the order of the wavelength and bigger. We have shown that the scattering of these particles is highly dependent on the wavelength of light and present oscillations in the backscattered intensity. These oscillations can be described within Mie theory and they can be used to accurately measure the optical thickness of the particles (Figure 2).

We have also used classical Mie theory to describe the scattering of entangled photon states from spherical particles, demonstrating that the effect of resonances in small particles can greatly affect the purity and the entanglement of certain quantum states [2].

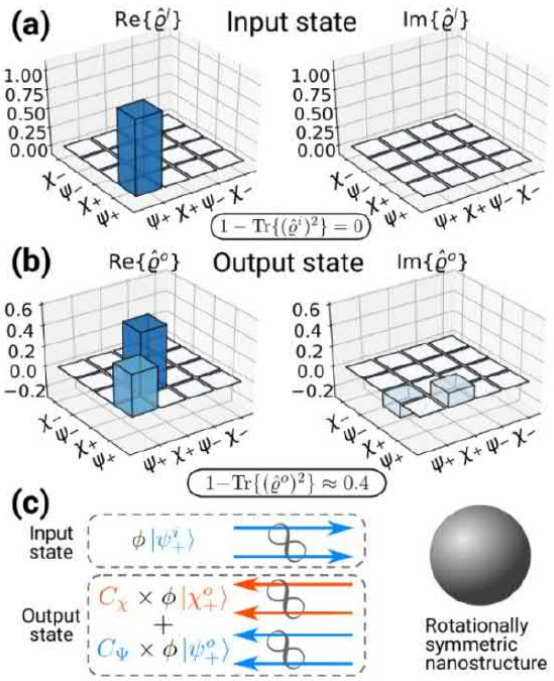


**Fig. 1:** Examples of input and output density matrices from a resonant dielectric sphere

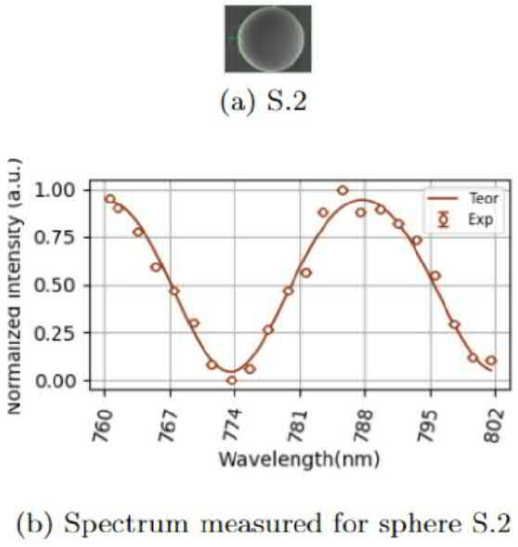


**Fig. 2:**Backscattering spectrum from a dielectric sphere.

## References

[1] Hulst, Hendrik Christoffel, and Hendrik C. van de Hulst. Light scattering by small particles. Courier Corporation, 1981.

[2] Jon Lasa-Alonso et al 2020 New J. Phys. 22123010

*Corresponding author: gabriel.molina@ehu.eus

# DMD-based optical traps for stirring-up and observing Bose-Einstein condensate superfluid dynamics

**S. Simjanovski [1], M. T. Reeves [1,2], G. Gauthier [1], M. J. Davis [1,2], H. Rubinsztein-Dunlop [1], T. W. Neely*[1]**

*1. Australian Research Council Centre of Excellence for Engineering Quantum Systems, School of Mathematics and Physics, University of Queensland, St. Lucia, QLD 4072, Australia*

*2. Australian Research Council Centre of Excellence in Future Low Energy Electronics Technology, School of Mathematics and Physics, University of Queensland, St. Lucia, QLD 4072, Australia*

Optical traps realise powerful means for the creation and manipulation of ultracold atomic Bose-Einstein condensates. I will describe our techniques for using these traps to both confine [1] and stir up [2] quasi 2D disc and ring shaped BECs, through direct stirring with optical barriers. First, I will describe our application of machine learning to optimise the experimental generation of persistent currents in a 2D ring trapped BEC, by allowing the learner to control the motion of an optical stirring barrier. We find that the learner determines optimal solutions under several different constraints, including maximising.

Second, I will describe how we use multiple stirring beams to directly engineer a lattice of vortices into the BEC, by creating and pinning the vortices to each optical beam's location. While these pinned vortices can be arranged in an arbitrary configuration within the BEC, we choose to initialise the system in a hexagonal lattice, close to the ground state configuration of a rotating BEC containing $\sim N\hbar/2$ angular momentum per particle.

We then use these initial configurations for two varying experiments on quantum turbulence. After preparing the optimised persistent current state, we study the dynamics of the system after in-trap interference with a stationary condensate. The interaction between the rotating and stationary superfluids realises a velocity shear layer. We find that the shear layer rapidly results in a ring of quantised vortices [see Fig. 1(i)]. This vortex ring is unstable and decays into vortex clusters, indicative of the superfluid Kelvin-Helmholtz instability. By studying the cluster sizes with increasing hold time, we find analogous behaviour to decaying classical 2D turbulence. We study the final states of the system at long hold times and compare them with the predicted results of the microcanonical ensemble [2].

From the initial vortex lattice configuration, we find the lattice melts in seconds, in response to a finite temperature phonon bath due to the non-zero temperature of the condensate/thermal cloud system, as shown in Fig. 1(ii). These strongly correlated vortex liquid states have gained prominence in the theory of the fractional quantum Hall effect, where the 2D electron gas move analogous to vortices in an incompressible fluid. The vortex analogue of these states has not been previously observed, as generating these low-energy vortex configurations has been experimentally challenging. Our techniques provide a pathway forward for studying these exotic states of vortex matter.

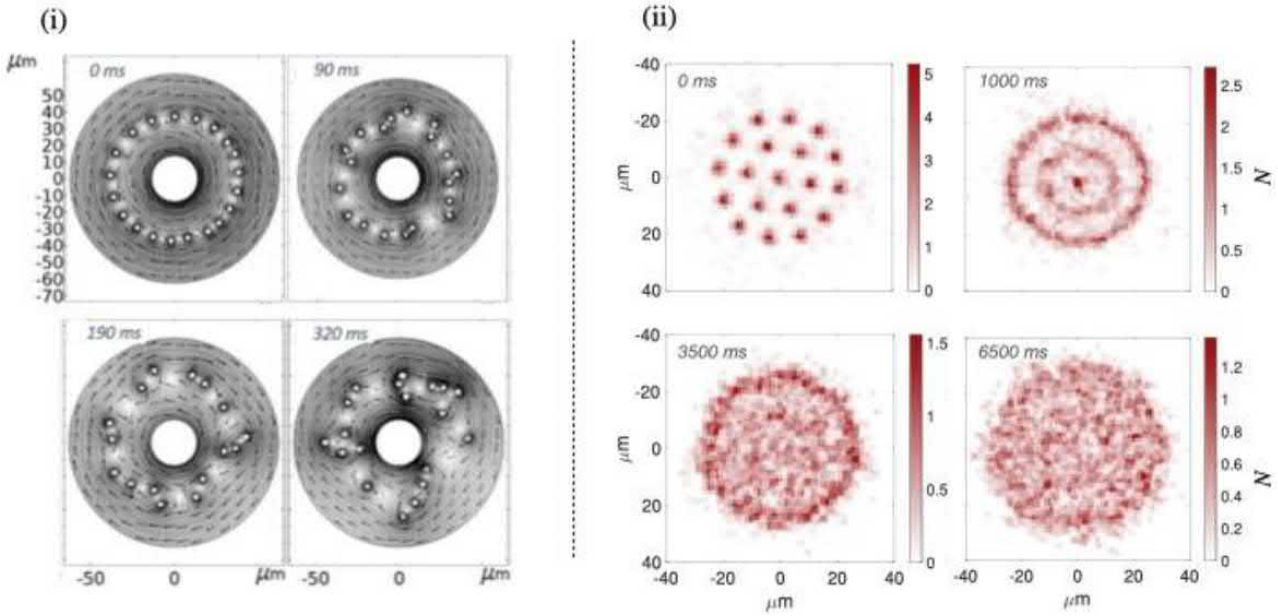


**Fig. 1:** (i) Decaying shear layer in a disc-shaped condensate, visualised by reconstructing the fluid flow field from the experimentally determined vortex positions. (ii) Experimental histograms of vortex positions, demonstrating melting of the initial hexagonal lattice arrangement of the vortices.

## References

[1] G. Gauthier, I. Lenton, N. McKay Parry, M. Baker, M. J. Davis, H. Rubinsztein-Dunlop, and T. W. Neely, Optica 3, 11361143 (2016).

[2] M. T. Reeves, K. Goddard-Lee, G. Gauthier, O. R. Stockdale, H. Salman, T. Edmonds, X. Yu, A. S. Bradley, M. Baker, H. Rubinsztein-Dunlop, M. J. Davis, and T. W. Neely Phys. Rev. X12, 011031 (2022).

*Corresponding author: t.neely@uq.edu.au

# Knots of darkness in turbulent media

**D. G. Pires**[*1], **D. Tsvetkov** [1], **N. Chandra** [1] **and N. M. Litchinitser** [1]
*1. Department of Electrical and Computer Engineering, Duke University, Durham, North Carolina 27708, USA*

Ever since Allen *et. al.* introduced the Laguerre-Gaussian (LG) modes a seminal work published in 1992 [1], the photonics community has been investigating their singular optical properties and using them for various applications. For instance, optical beams carrying orbital angular momentum (OAM) enable new approaches to particle manipulation [2], quantum protocols [3] and improving sensing [4] and imaging systems [5]. Yet another important potential application field where optical vortices could have a significant impact is optical communications [6]. In particular, the infinite subspace spanning the OAM states facilitates the multiple superpositions of orthogonal states of light. In this context, propagation of optical vortices in free-space [6], nonlinear media [7], atmospheric turbulence [8] and underwater environment [9] has been extensively studied. On the other hand, more exotic structured light forms can be designed from optical vortices known as optical knots [10]. Commonly defined as a closed, non-intersecting curve embedded in three dimensions and constructed by superposing multiple LG modes with specific weights, optical knots have been recently considered as an alternative way to the data transmission [11]. Therefore, understanding of the stability properties of optical knots in realistic environmental conditions, such as turbulence, is of paramount importance.

In this study, we have considered three types of structures, as shown in Fig. 1 (a): Trefoil knot, Hopf link, and an unknot. Respectively, these structures possess three, two, and zero crossings. We obtain the LG superposition for each knot by obtaining the associated Milnor polynomial and projecting it into the LG basis [10]. The interaction with turbulence is realized by generating Kolmogorov phase-screens and moving the initial beam across it to capture various phase changes corresponding to different Strehl ratio (SR) values. Physically, turbulence induces a local refractive index change affecting the three-dimensional structure of the knot. Figure 1 (b) shows the histograms for the possible outcomes after a Trefoil knot interacts with turbulence possessing various SR. Upon losing one crossing it transforms into a Hopf link and, after losing another crossing, it it transforms into one (or more) unknot. Naturally, if the local refractive index change is abrupt, the beam will be destroyed and no structure can be recovered. In Fig. 1 (c) we plot the percentage of recovered Trefoils in terms of the SR. We observe that up to $SR = 0.0075$ more than 60% of the trefoils are preserved. Additionally, we have performed the same study for other types of knots and find that under certain conditions they may be more stable than regular optical vortices [12]. It is well-known that higher-order OAM states of light are very sensitive to external perturbations, breaking the singularity into multiple singularities with charges $\pm 1$. However, optical knots are formed by an arrangement of $\pm 1$ singularities, and thus, are more stable to local refractive index changes.

We present a stability analysis of optical knots in turbulent media. By using a phase-screen approach to create a turbulent environment, we observe that optical knots can have a high recovery percentage even after interacting with strongly turbulent media. These results may find further applications in the development of new optical communication protocols. We acknowledge the support from Office of Naval Research MURI (N00014-20-1-2558).

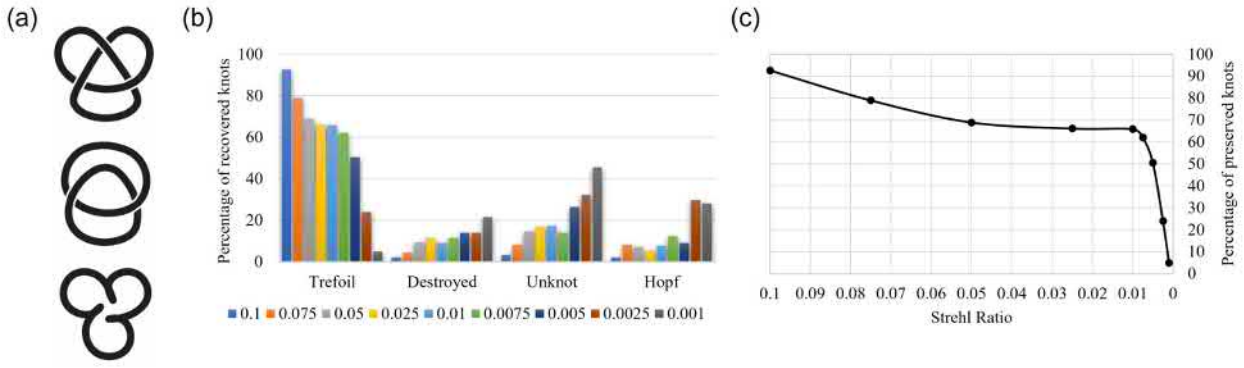


**Fig. 1:** (a) Schematic of the possible knot structures after a trefoil knot interacts with turbulence. From top to bottom: Trefoil knot, Hopf link and unknot. (b) Percentage of recovered knots for different Strehl ratio. (c) Percentages of preserved trefoils for various SR.

## References

[1] L. Allen, M. W. Beijersbergen, R. Spreeuw and J. Woerdman, Phys. Rev. A. **45** 8185 (1992)
[2] M. Padgett and R. Bowman, Nat. Photonics. **5** 343–348 (2011)
[3] L. Aolita and S. Walborn, Phys. Rev. Lett. **98** 100501 (2007)
[4] Y. Fan, G. Arwatz, T. Van Buren, D. Hoffman and M. Hultmark, Exp. Fluids **56** 138 (2015)
[5] J. M. Conan, G. Rousset and P. Y. Madec, JOSA A **12** 1559–1570 (1995)
[6] A. E. Willner, H. Huang, Y. Yan, Y. Ren, N. Ahmed, G. Xie, C. Bao, L. Li, Y. Cao, Z. Zhao, J. Wang, Advances in Optics and Photonics **1** 66-106 (2015)
[7] K. Dholakia, N. Simpson, M. Padgett and L. Allen, Phys. Rev. A. **54** R3742 (1996)
[8] B. Rodenburg, M. P. J. Lavery, M. Malik, M. N. O'Sullivan, M. Mirhosseini, D. J. Robertson, M. Padgett and R. W. Boyd, Opt. Lett. **37** 3735-3737 (2012)
[9] J. Baghdady, K. Miller, K. Morgan, M. Byrd, S. Osler, R. Ragusa, W. Li, B. M. Cochenour, and E. G. Johnson, Opt. Exp. **24** 9794-9805 (2016)
[10] M. R. Dennis, R. P. King, B. Jack, K. O'holleran, and M. J. Padgett, Nat. Photonics. **6** 118-121 (2010)
[11] H. Larocque, A. D'Errico, M. F. Ferrer-Garcia, A. Carmi, E. Cohen and E. Karimi, Nat. Communications **11** 1-8 (2020)
[12] Y. Ren, H. Huang, G. Xie, N. Ahmed, Y. Yan, B. I. Erkmen, N. Chandrasekaran et al., Opt. Lett. **38** 4062-4065 (2013)

[*]Corresponding author: danilo.gomes.pires@duke.edu

# Integrating structured wave techniques into neutron sciences

**Dusan Sarenac [1], Charles W. Clark [2], David G. Cory [1,3], Huseyin Ekinci [1,4], Melissa Henderson [1,4], Michael Huber [5], Connor Kapahi [1,4], Lisa Debeer-Schmitt [6], Dmitry Pushin*[1,4]**

*1. Institute for Quantum Computing, University of Waterloo, Waterloo, ON, Canada, N2L3G1*
*2. Joint Quantum Institute, National Institute of Standards and Technology and University of Maryland, College Park, Maryland 20742, USA*
*3. Department of Chemistry, University of Waterloo, Waterloo, ON, Canada, N2L3G1*
*4. Department of Physics and Astronomy, University of Waterloo, Waterloo, ON, Canada, N2L3G1*
*5. National Institute of Standards and Technology, Gaithersburg, Maryland 20899, USA*
*6. Neutron Scattering Division, Oak Ridge National Laboratory, Oak Ridge, TN 37831, USA*

In this talk I will cover the recent developments related to generating structured neutron waves and their corresponding applications. Neutrons have played an important role is numerous fundamental physics experiments in addition to being a unique probe of materials [1,2]. The uniqueness of neutrons comes from their angstrom sized wavelength, electrical neutrality, and relatively large mass. Hallmark neutron science experiments include the first demonstration of gravity on a quantum particle, probing of dark energy/fifth forces, observing the $4\pi$ symmetry of spinor rotation, observing non-classical correlations and the quantum Cheshire Cat, and precision measurements and imaging of material properties and dynamics.

The integration of structured wave techniques into neutron science has been rather difficult due to low fluence rates, small transverse coherence lengths (nm to $\mu$m ), and poor neutron camera resolutions ( 100$\mu$m to 5 mm ). Our first demonstrations with neutron orbital angular momentum (OAM) were done with interferometric measurements showing the control and manipulation of the average OAM value [3,4]. We had followed this with studies and experiments that consider the coupling between the neutron's spin degree of freedom and OAM [5-7]. The $^3$He neutron spin filters were used in conjunction with specifically oriented triangular coils to prepare neutron beams with lattices of spin-orbit correlations, as demonstrated by their spin-dependent intensity profiles. These correlations can be tailored to particular applications, such as neutron studies of topological materials. Lastly, in this talk I will cover our most recent advances and applications with light and neutron OAM beams.

## References

[1] Willis, B.T.M. and Carlile, C.J., 2017. Experimental neutron scattering. Oxford University Press.
[2] Rauch, H. and Werner, S.A., 2015. Neutron Interferometry: Lessons in Experimental Quantum Mechanics, Wave-Particle Duality, and Entanglement (Vol. 12). Oxford University Press, USA.
[3] Clark CW, Barankov R, Huber MG, Arif M, Cory DG, Pushin DA. Controlling neutron orbital angular momentum. Nature. 2015 Sep;525(7570):504-6.
[4] Sarenac, D., Huber, M.G., Heacock, B., Arif, M., Clark, C.W., Cory, D.G., Shahi, C.B. and Pushin, D.A., 2016. Holography with a neutron interferometer. Optics express, 24(20), pp.22528-22535.
[5] Sarenac, D., Kapahi, C., Chen, W., Clark, C.W., Cory, D.G., Huber, M.G., Taminiau, I., Zhernenkov, K. and Pushin, D.A., 2019. Generation and detection of spin-orbit coupled neutron beams. Proceedings of the National Academy of Sciences, 116(41), pp.20328-20332. [4] F. Author, P. Author, L. Author, Phys. Rev. Lett. 123, 12345 (2021).
[6] Nsofini, J., Sarenac, D., Wood, C.J., Cory, D.G., Arif, M., Clark, C.W., Huber, M.G. and Pushin, D.A., 2016. Spin-orbit states of neutron wave packets. Physical Review A, 94(1), p.013605.
[7] Sarenac, D., Kapahi, C., Chen, W., Clark, C.W., Cory, D.G., Huber, M.G., Taminiau, I., Zhernenkov, K. and Pushin, D.A., 2019. Generation and detection of spin-orbit coupled neutron beams. Proceedings of the National Academy of Sciences, 116(41), pp.20328-20332.

*Corresponding author: dmitry.pushin@uwaterloo.ca

# High Dimensional Quantum Sources with Optical Fibers

**Siddharth Ramachandran**[*1]
*1. Boston University, Boston, MA 02215, USA*

Entangling photons in the orbital angular momentum (OAM) degree of freedom, demonstrated over 20 years ago [1], yields a promising pathway for increasing the dimensionality of quantum sources, of utility in high-dimensional communications [2,3] as well as in efficient quantum computing algorithms in higher-dimensional Hilbert spaces [4]. One of the primary means of generating entangled-photon sources with diversity in OAM has been the use of spontaneous parametric down-conversion in bulk $\chi^{(2)}$ nonlinear crystals. An efficient integrated-optic source that could emit photons in tailorable, on-demand OAM superpositions would help transition the field to more deployable scenarios much as integrated optics has helped in the development of quantum sources that operate in the conventional, fundamental, ground state, Gaussian-shaped mode.

Here, we show that the use of ring-core optical fibers that enable the transport of a large ensemble of OAM carrying modes, yields a versatile platform for engineering quantum sources by exploiting spontaneous four-wave mixing (SFWM) between fiber modes. Fibers stably transmitting OAM modes were developed roughly a decade ago [5], and have now yielded a multimode platform with as many as 60 stable modes [6]. This provides for a plethora of SFWM phase matching possibilities [7] enabling control not only over the wavelengths at which the photon pairs can be generated, but also over the shapes of their joint spectral densities (JSD), ranging from correlated, uncorrelated, to anti-correlated [8]. This allows for a single platform, with only control over the angular momentum content of the pump, to yield desired biphoton correlations of interest in a variety of entanglement as well as heralding applications.

This talk will describe recent experiments aimed at the development of compact, single-aperture devices whose biphoton emissions can be engineered to exploit the spatial dimension of light.

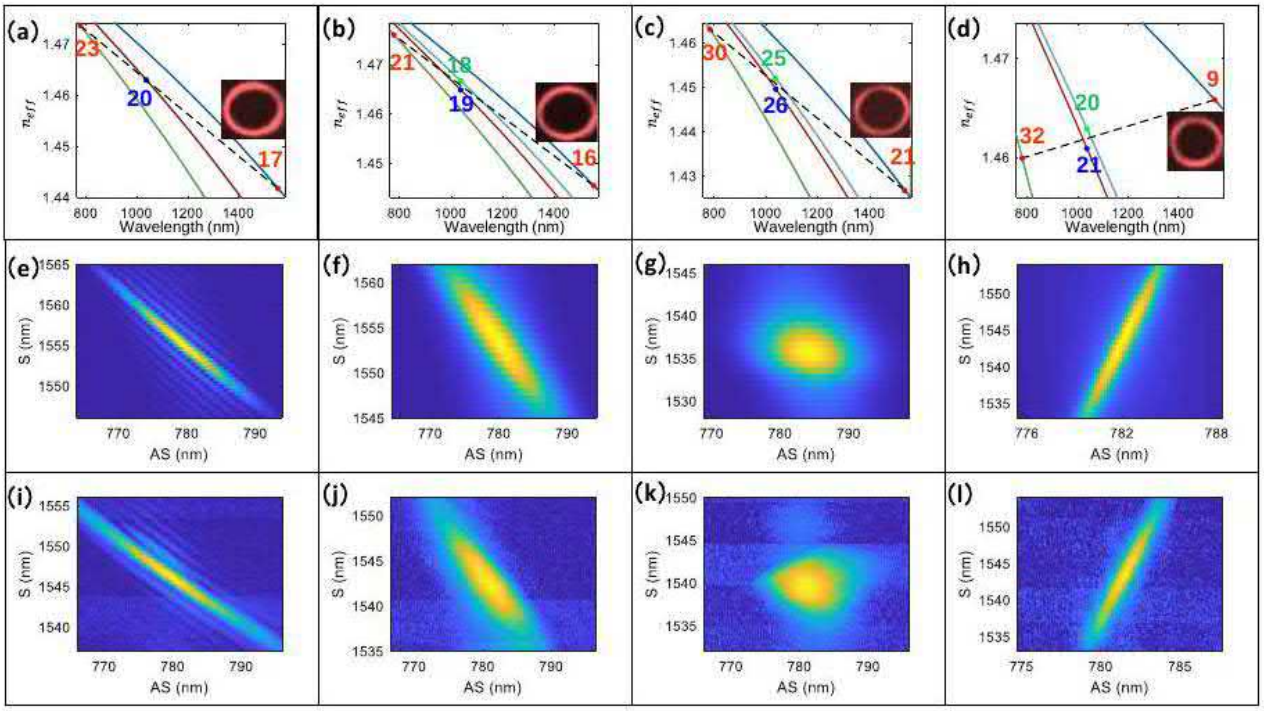


**Fig. 1:** Exemplary experiments of SFWM with OAM fibers showing the ability to generate correlated, uncorrelated and anti-correlated biphoton spectra in a single fiber with control over the angular momentum content of the pump along. Top row: solid curves are show the $n_{eff}$ *vs.* $\lambda$ of different modes in the fiber, with modes numerically identified by their OAM content. Dashed lines represent the mode and wavelength combinations that satisfy phase matching relationship (and hence yield SFWM). Middle row: resultant simulated JSDs with a 1038-nm, 150-fs pump. Bottom row: corresponding experimentally measured JSDs.

## References

[1] A. Mair et al., "Entanglement of the orbital angular momentum states of photons," Nature 412, 313 (2001).
[2] R. Fickler et al., "Quantum entanglement of high angular momenta," Science 338, 640 (2012)
[3] D. Cozzolino et al., "OAM States Enabling Fiber-based High-dim. Quantum Communication," Phys. Rev. Applied 11, 064058 (2019).
[4] M. A. Nielsen, I. L. Chuang, Quantum Computation and Quantum Information (Cambridge Univ. Press, Cambridge, 2010).
[5] S. Ramachandran et al., "Generation and propagation of radially polarized beams in optical fibers," Optics Letters, 34, 2525 (2009).
[6] Z. Ma et al., "Record (60) uncoupled modes in a step-index fiber due to a new light guidance mechanism...," ECOC, TU4A.3. (2021).
[7] X. Liu et al., "Nonlinear FWM with enhanced diversity & selectivity via spin and OAM conservation." APL photonics 5, 010802 (2020).
[8] X. Liu et al., "Shaping Biphoton Spectral Correlations with Orbital Angular Momentum Fiber Modes," Quantum 2.0 (2022).

[*]Corresponding author: sidr@bu.edu

# Hiding Ignorance Using High Dimensions

**Jacquiline Romero**[*1,2], **Michael Kewming**[1,2], **Sally Shrapnel**[1,2], **Andrew G. White** [1,2]

*1. School of Mathematics and Physics, University of Queensland, Brisbane, Queensland 4072, Australia.*
*2. Australian Research Council Centre of Excellence for Engineered Quantum Systems (EQUS)*

The absence of information—entirely or partly—is called ignorance. Naturally, one might ask if some ignorance of a whole system will imply some ignorance of its parts. Our classical intuition tells us yes, however quantum theory tells us no: it is possible to encode information in a quantum system so that despite some ignorance of the whole, it is impossible to identify the unknown part. Experimentally verifying this counterintuitive fact, requires controlling and measuring quantum systems of high dimension $d > 9$. We provide this experimental evidence using the transverse spatial modes of light.

Consider a teacher testing a student who has not studied for an exam about the contents of a two-chapter textbook (Fig. 1) . Each chapter contains $d$ possible questions with an equivalent number of answers. The student is required to know the answers $y_0$ and $y_1$ to two possible questions, uniformly drawn from either chapter, i.e, $y_0 \in Y_0$ and $y_1 \in Y_1$. The combination of answers from both chapters is a single dit string $y{=}y_0y_1$, uniformly drawn from the Cartesian product of the random variables $Y = Y_0 \times Y_1$. Before the test the student is permitted to store only one dit of information in their study notes $\mathscr{P}_y$ which is encoded in a physical system $E$. The ignorance of the whole $Y$—both chapters—is bounded by the dimension of the encoded system $d$. The encoding is only a single dit so one dit of information can be encoded [1].

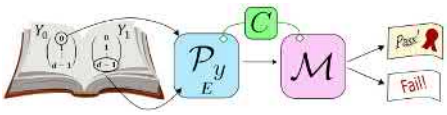


Figure 1: A book contains two chapters with information $Y_0$ and $Y_1$. An ignorant student–who does not know any content—will be asked to answer a question from either chapter. Luckily they are allowed to bring a single answer—1 dit—corresponding to either $y_0{\in}Y_0$ or $y_1{\in}Y_1$ via study notes $\mathscr{P}_y$ which are stored physically in a classical (or quantum) register $E$. In the test, the student can be asked to answer a single question $\mathscr{M}$ about the whole $y = y_0y_1$, or the parts $y_0$ or $y_1$. The teacher has access to a system $C$ that is classically correlated with the student's notes (solid green line). The teacher's goal is to ask questions $\mathscr{M}$ such that she can uncover which chapter the student is ignorant of [2].

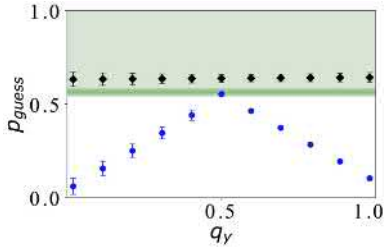


Figure 2: We choose $d{=}13$ to check if the teacher can uncover which the ignorant part. We plot the guessing probability as a function of the question that teacher asks, where $q_y$ indicates the bias. Error bars correspond to 1 standard error.

Consider how the ignorance of the parts—either $Y_0$ or $Y_1$—relates to this ignorance of the whole. If the student prepares their notes such that they always encode the answers from $Y_1$; $E{=}Y_1$. As a result they know $Y_1$ with certainty $P(Y_1|E{=}Y_1){=}1$ but must guess the $Y_0$ randomly $P(Y_0|E{=}Y_1){=}1/d$. For $d{=}2$, the probability of guessing the parts correctly is $p_{\text{guess}}(Y_C|E){=}0.75$, where $C$ is a classical random variable $c{\in}\{0,1\}$ pointing to the part that must be answered. Now assume the teacher has access to $C$—which is classically correlated with the student's notes $E$ such that $P(c{=}0|E){=}1$—then they will always ask a question from $Y_0$, forcing the student to guess randomly. Thus, $C$ points to the source of ignorance.

We show that using a quantum encoding, it is not possible for the teacher to spot the part that the student is ignorant of. We choose $d = 13$ and plot the results in Fig. 2. We plot the guessing probability as a function of the question that teacher asks, where $q_y$ indicates the bias. If $q_y{=}1$ then the teacher always asks the student for the answer to $Y_0$, and vice versa. We observe that using a quantum encoding the student's guessing probability of the parts (black diamonds) is constant and is always greater than the whole (green band). For the optimal classical case (blue) the teacher can always find a the unknown part. Here we plot the guessing probability for $E{=}Y_1$ for $q_y < 0.5$ and $E{=}Y_0$ for for $q_y > 0.5$.

## References

[1] T. Vidick and S. Wehner, "Does Ignorance of the Whole Imply Ignorance of the Parts? Large Violations of Noncontextuality in Quantum Theory", PRL, 107, 030402, 2011
[2] M.Kewming, S. Shrapnel, A.G. White, and J. Romero, "Hiding Ignorance Using High Dimensions", PRL, 124, 250401, 2020

*Corresponding author: m.romero@uq.edu.au

# Control of structured wavefields with conformal transformations

**G. Ruffato**[*1,2], **A. Vogliardi** [1], **M. Ferrari** [1], **E. Rotunno** [3], **V. Grillo** [3], **H. Kobayashi** [4], **and F. Romanato** [† 1,2,5]

*1. University of Padova, via Marzolo 8, 35131 Padova (Italy)*
*2. Quantum Technologies Research Center, University of Padova, via Gradenigo 6, 35127 Padova (Italy)*
*3. CNR-Istituto Nanoscienze, Centro S3, Via G Campi 213/a, I-41125 Modena (Italy)*
*4. Graduate School of Engineering, Kochi University of Technology, 185 Tosayamada-cho, Kochi 782-8502 (Japan)*
*5. CNR-IOM Istituto Officina dei Materiali, S.S. 14 - Km. 163.5 - 34149 Trieste (Italy)*

The necessity to control the spatial degrees of freedom of light and electron beams has inspired a rich portfolio of techniques and devices with different levels of complexity and integration. Among all, conformal mappings provide an effective tool to manipulate wavefields in a compact and versatile way. Besides the well-known log-pol mapping for OAM analysis, a new conformal mapping, the so-called circular-sector transformation, has been recently introduced [1, 2] to perform optical multiplication and division. Regardless the type of mapping, the required optical elements share the property of being harmonic, i.e., solutions of Laplace equation. In a more general approach to propagating structured phases, we present here a general framework where the generation, transmission, and measurement of structured beams are described in terms of conformal mappings implemented by harmonic phases. The general solutions, called multipole phases after their similarity with the integrated potentials of electric/magnetic multipoles, suggest even-unexploited beams for spatial multiplexing [3]. Their generation and measurement, based on circular-sector transformations, inspire new methods to measure aberrations or to inspect electric/magnetic multipoles in electron microscopy [4]. More recently, the generated caustics have been proved to find the correct description in terms of roulette curves, suggesting a method for the controlled generation of cusps configurations [5] and accelerating regular cusp beams [6] for micromanipulation and high-resolution microscopy or lithography. The harmonic phase plates can be realized in the form of continuously-variant Pancharatnam-Berry silicon metasurfaces [7]. In addition, we discuss the limits of this fabrication approach and consider the advantages provided by dual-functional metaoptics. We present an insight into this framework, focusing on the most important implications for the manipulation of OAM and structured wavefields.

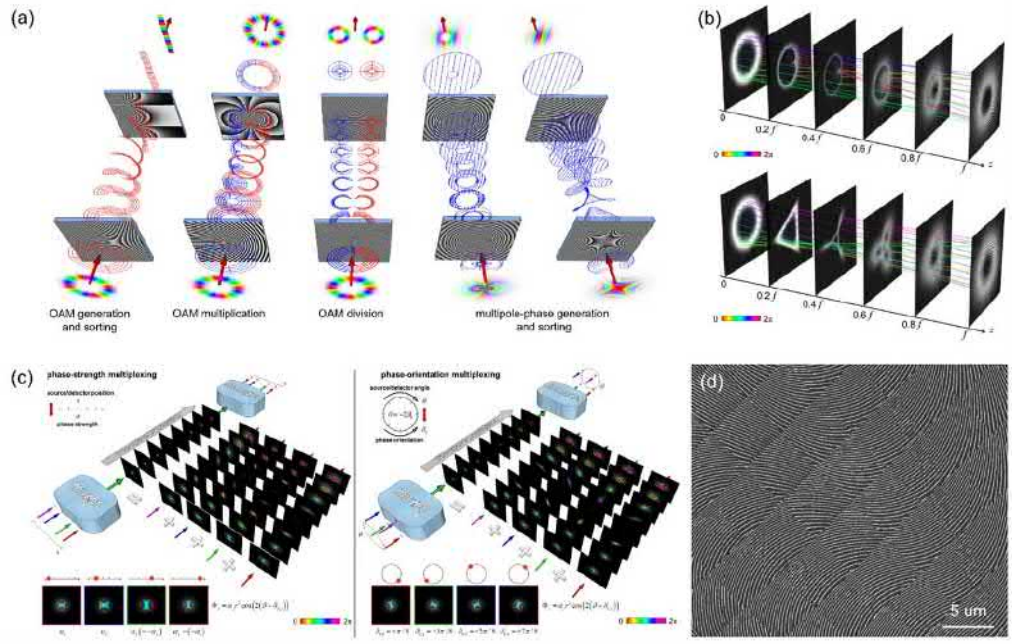


**Fig. 1:** The manifold scenario of harmonic phases for structured beams. (a) Conformal transformations for OAM measurement and algebra [1,2]. Conformal measurement of aberrations and multipole-phases (MPs) in optics and electron microscopy [4]. (b) Generation of roulette caustics and accelerating regular cusp beams [5,6]. (c) Scheme of MP division multiplexing: non-singular beams with two continuous degrees of freedom [3]. (d) Implementation of the optical elements as continuously-variant Pancharatnam-Berry silicon metasurfaces [7].

## References

[1] Ruffato, G., Massari, M., and Romanato, F. Light: Sci. & Appl. 8, 113 (2019).
[2] Takashima, S., Kobayashi, H., and Iwashita, K. Phys. Rev. A 100, 063822 (2019).
[3] Ruffato, G., Grillo, V., and Romanato, F. Opt. Express 29(23), 38095-38108 (2021).
[4] Ruffato, G., Rotunno, E., Giberti, L. M. C., and Grillo, V. Phys. Rev. Appl. 15, 054028 (2021).
[5] Ruffato, G., and Kobayashi, H. Opt. Comm. 490, 126893 (2021).
[6] Ruffato, G., Brunetta, S., and Kobayashi, H. Opt. Comm. **517**, **128325**(**2022**).
[7] Ruffato, G., and Romanato, F. Opt. Express 28(23), 34201-34218 (2020).

[*]Corresponding author: presenting.author@email.com
[†]Corresponding author: filippo.romanato@unipd.it

# Ion wavepackets interacting with vortex laser beams

**Felix Stopp**[1], **Maurizio Verde**[1], **Milton Katz**[2], **Martín Drechsler**[2], **Sebastian Wolf**[1], **Christian Schmiegelow**[2], **Ferdinand Schmidt-Kaler**[*1]

*1. QUANTUM, Institut für Physik, Johannes Gutenberg-Universität Mainz, Staudingerweg 7, 55128 Mainz*

*2. Departamento de Física and IFIBA, FCEN, Universidad de Buenos Aires, Ciudad Universitaria, Pabellón I, 1428 Ciudad de Buenos Aires*

Trapped single ions feature several assets for investigating the interaction with vortex laser beams [1][2][3][4]: The ion internal electronic states and the external states of motion can be prepared and analyzed with the highests precision. Also, the ion wavepacket can be positioned at will, accurately and fast, and its size and shape can be controlled at the nm-scale [5]. Therefore, trapped ions become a near-to-ideal setup for preparing and measuring non-classical quantum states [6].

Here, we report the optical super-resolution sensing of a trapped ion's wave packet. We have been inspired by the ground state depletion microscopy technique. Scanning a vortex beam spatially over a single trapped $^{40}Ca^{+}$ ion, we test the excitation on the $S_{1/2}$ to $D_{5/2}$ transition near 729 nm. With a vortex laser waist size of about 4.2 $\mu$m we sense the wave packet size of about 39 nm for the near-to-ground state cooled ion [7]. We reach a resolution $\sigma \sim 30$ nm, enhanced by a factor of x12 as compared to the non-saturated situation. On the other hand, superresolution techniques may serve as a fast diagnosis tool of the ion motion [8]. We find that the coherent nature of the excitation dynamics of the ion electronic state improves the resolution quantified by the point spread function and investigate the resolution limit. In the future we will take benfit of the few nm resolution limit and aim for imaging Fock states e.g. $|n\rangle$ =1, non-classical matter wave packets.

## References

[1] C. Schmiegelow, F. Schmidt-Kaler, Euro. Jour. of Phys. D 66, 157 (2012)
[2] C. Schmiegelow, et al., Nat. Comm. 7, 12998 (2016)
[3] G. Quinteiro, F. Schmidt-Kaler, C. Schmiegelow, Phys. Rev. Lett. 119, 253203 (2017)
[4] M. Solyanik-Gorgone, A. Afanasev, C. Carlson, C. Schmiegelow, F. Schmidt-Kaler, J. Opt. Soc. Am. B 36(3), 565 (2019)
[5] V. Kaushal, et al., AVS Quantum Sci. 2, 014101 (2020), arXiv:1911.10983
[6] J. Hilder, et al., Phys. Rev. X.12.011032 (2022)
[7] M. Drechsler et al., Phys. Rev. Lett. 127, 143602 (2021)
[8] Z. Qian, et al., Phys. Rev. Lett. 127, 263603 (2021)

*Corresponding author: felstopp@uni-mainz.de

# Teleporting high-dimensional OAM states

**Bereneice Sephton**[1], **Adam Vallés** [1,2,3], **Isaac Nape** [1], **Mitchell A. Cox** [4], **Fabian Steinlechner**[5,6], **Thomas Konrad** [7,8], **Juan P. Torres** [3,9], **Filippus S. Roux** [10], **Andrew Forbes**[*1]

*1. School of Physics, University of the Witwatersrand, Private Bag 3, Wits 2050, South Africa*
*2. Molecular Chirality Research Center, Chiba University, 1-33 Yayoi-cho, Inage-ku, Chiba 263-8522, Japan*
*3. ICFO - Institut de Ciencies Fotoniques, The Barcelona Institute of Science and Technology, Castelldefels (Barcelona) 08860, Spain*
*4. School of Electrical and Information Engineering, University of the Witwatersrand, Johannesburg, South Africa*
*5. Fraunhofer Institute for Applied Optics and Precision Engineering, Albert-Einstein-Str. 7, 07745 Jena, Germany*
*6. Friedrich Schiller University Jena, Abbe Center of Photonics, Albert-Einstein-Str. 6, 07745 Jena, Germany*
*7. School of Chemistry and Physics, University of KwaZulu-Natal, Durban, South Africa*
*8. National Institute of Theoretical and Computational Sciences (NITheCS), KwaZulu-Natal, South Africa*
*9. Department of Signal Theory and Communications, Universitat Politecnica de Catalunya, Campus Nord D3, 08034 Barcelona, Spain*
*10. National Metrology Institute of South Africa, Meiring Naudé Road, Brummeria, Pretoria 0040, South Africa*

Quantum teleportation plays an important part in the progress of quantum information and the development of quantum technologies [1], [2]; making it an active area of research since the seminal paper was published in 1993 [3]. While being demonstrated in both the continuous [4] and discrete [5] variable regimes as well as with multiple degrees of freedom in a single photon [6], high-dimensional teleportation has not been experimentally achieved beyond 3-dimensions [7], [8]. Here we experimentally demonstrate discrete-variable quantum teleportation in the spatial degree of freedom whereby the restrictive linear Bell-measurement is replaced with non-linear detection. This scheme is illustrated in the figure below. With this, our experiment is shown to be fundamentally different from previous linear implementations as it does not rely on ancillary photons to increase the dimensionality. Instead, we show high-dimensional teleportation exceeding 10 dimensions in orbital angular momentum (OAM) as well as other spatial states with fidelities beyond the classical limit. Our results [9] open the way to implementing teleportation in a practically useful way with an encouraging paradigm allowing versatile and high-capacity optical quantum communication protocols for on-demand states.

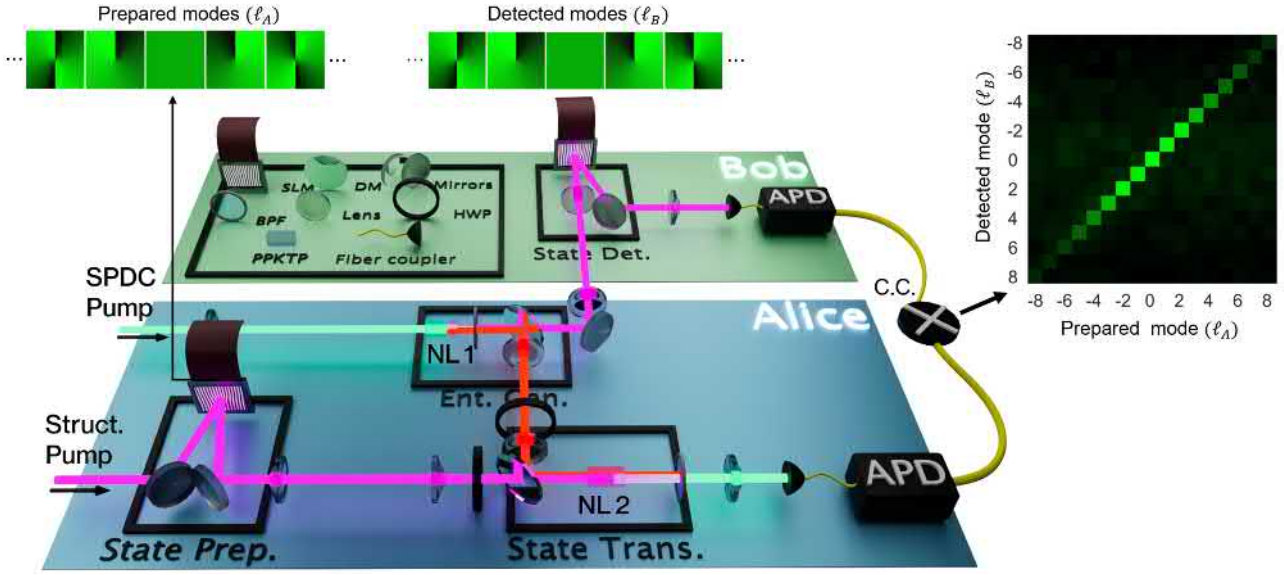


**Fig. 1:** Experimental teleportation system. Two separately pumped $\chi^2$-nonlinear crystals (NL1 and NL2), respectively produce one pair of entangled photons via spontaneous parametric down conversion (SPDC) (which form the entangled channel) and a spatially-structured up-converted photon. Here one of the channel photons is sent to another party (Bob) for communication while the other is overlapped in the second crystal. The second structured pump then up-converts it to generate a third photon where the upconverted photon takes on the shared characteristics and thus is entangled with the Bob's photon while carrying the encoded spatial information. Projection of the upconverted photon then gives the unitary rotation on which to preform on the signal such that the unknown state can be retrieved and successful teleportation achieved. Insets show the OAM structured prepared modes that are then detected by Bob. A clear correlation between the prepared and detected modes are experimentally shown for over 10 OAM modes as an example. SLM: Spatial light modulator; DM: Dichroic mirror; BPF: Bandpass filter; HWP: Half-waveplate, PPKTP: Periodically-poled KTP non-linear (NL) crystal; APD: Avalanche photodiode detector.

## References

[1] M. Nielsen, I. Chuang, *Quantum Computation and Quantum Information*, (Cambridge Univ. Press) (2002)
[2] M. Wilde, *Quantum Information Theory*, (Cambridge Univ. Press) (2013)
[3] C. Bennett, G. Brassard, C. Crépeau, R. Jozsa, A. Peres, W. Wootters, Phys. Rev. Lett. **70** 1895 (1993)
[4] N. Lee, H. Benichi, Y. Takeno, S. Takeda, J. Webb, E. Huntington, A. Furusawa, Akira, Science **332** 6027 (2011)
[5] S. Olmschenk, D. Matsukevich, P. Maunz, D. Hayes, LM Duan, C. Monroe, Science **323** 5913 (2009)
[6] XL. Wang, XD. Cai, ZN. Su, MC. Chen, D. Wu, L. Li, NL. Liu, CY. Lu, JW. Pan, Nature **518** 7540 (2015)
[7] Yi-Han Luo, *et. al.*, Phys. Rev. Lett. **123** 7 (2019)
[8] Xiao-Min Hu, *et. al.*, Phys. Rev. Lett. **125** 23 (2020)
[9] B. Sephton, A. Vallés, I. Nape, M. Cox, F. Steinlechner, T. Konrad, J.P. Torres, F.S. Roux, A. Forbes, arXiv preprint **arXiv:2111.13624** (2021)

[*]Corresponding author: andrew.forbes@wits.ac.za

# Nonlinear Photonic Topological Insulators

**Lukas Maczewsky** [1], **Marco Kirsch** [1], **Matthias Heinrich** [1], **Alexander Szameit**[*1]
*1. Institute for Physics, University of Rostock, Albert-Einstein-Strasse 23, 18059 Rostock, Germany*

In the context of photonics, topology has emerged as an abstract, yet surprisingly powerful, new paradigm for controlling the flow of light. As such, it holds great promise for a wide range of advanced applications, from scatter-free routing and switching of light along arbitrary three-dimensional trajectories to long-distance transmission of slow-light waves. In this talk, a nonlinearity-induced photonic topological insulator is presented. It is shown how nonlinearity can drive an initially topologically trivial system into a transient topological phase, where nonlinearly self-defined chiral edge states exist. In contrast to soliton formation in an arrangement with preexisting topological features, it is the action of nonlinearity itself that establishes nontrivial topology here (see Fig. 1) [1]. Moreover, the implementation of nonlinear dynamics in a second-order photonic topological insulators is demonstrated, where nonlinear topologically protected edge states may form [2]. In the presented experiments, lattices of coupled optical waveguides are employed as a versatile platform to explore nonlinear physics.

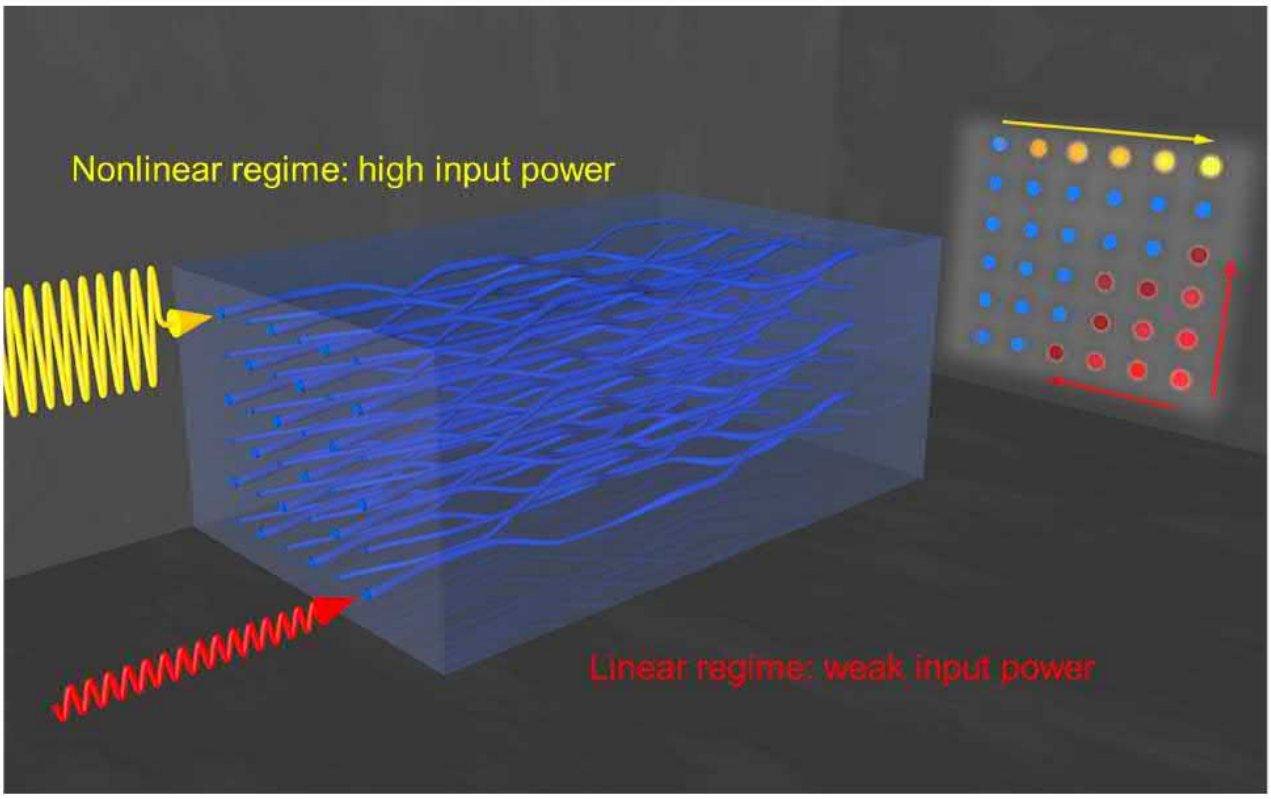


**Fig. 1:** Formation of a nonlinear photonic topological insulator using high-power light.

## References

[1] L. Maczewsky et al., Science 370, 701-704 (2020).
[2] M. Kirsch et al., Nature Phys. 17, 995-1000 (2021).

[*]Corresponding author: alexander.szameit@uni-rostock.de

# Tailoring Optical Angular Momentum with Fibers and Chips: Devices and Applications (Invited Talk)

**Jian Wang**[*1,2]
*1. Wuhan National Laboratory for Optoelectronics, Huazhong University of Science and Technology, Wuhan 430074, China*
*2. Optics Valley Laboratory, Wuhan 430074, China*

Light beams carrying spin angular momentum (SAM) and orbital angular momentum (OAM) have seen wide applications ranging from optical manipulation to optical communications. In this talk, we review recent advances in various devices for tailoring SAM and OAM with fibers and chips [1]: 1) controllable all-fiber OAM mode converter [2] (Fig. 1); 2) generation of OAM beams using fiber-to-fiber butt coupling [3]; 3) meta-facet fiber for twisting ultra-broadband light with high phase purity [4]; 4) spin-orbit mapping of light in a few-mode fiber [5]; 5) ultra-directional high-efficiency chiral silicon photonic circuits [6]; 6) dielectric silicon metasurfaces enabling twisted light generation/detection/(de)multiplexing [7]; 7) silicon-based ultra-compact broadband polarization diversity OAM generator [8-10] (Fig. 2); 8) chip-scale optical vortex lattice generator on silicon platform [11]. Additionally, we also present various applications with SAM and OAM [12-14], such as optical tweezers/spanners, optical metrology, optical interconnects/communications, quantum information processing, etc.

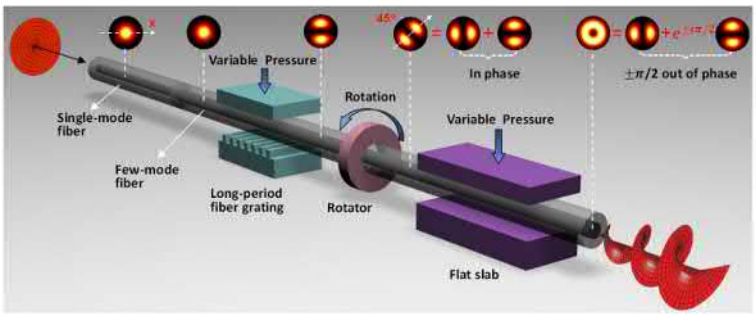


**Fig. 1:** Controllable all-fiber orbital angular momentum (OAM) mode converter [2].

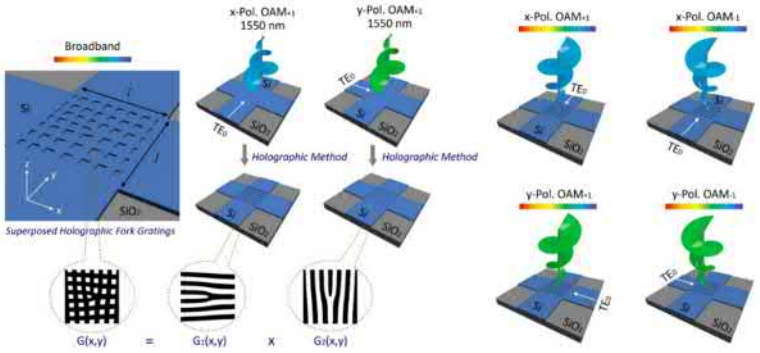


**Fig. 2:** Silicon-based ultra-compact broadband polarization diversity OAM generator [9].

Acknowledgement: This work was supported by the National Natural Science Foundation of China (NSFC) (62125503).

## References

[1] J. Wang, Y. Liang, Front. Phys. 9, 688284 (2021).
[2] S. Li, Q. Mo, X. Hu, C. Du, J. Wang, Opt. Lett. **40**, 4376(2015).
[3] S. Li, Z. Xu, R. Zhao, L. Shen, C. Du, J. Wang, IEEE Photon. J. 10, 6601607 (2018).
[4] J. Du, J. Wang, Appl. Phys. Lett. 113, 061103 (2018).
[5] L. Fang, H. Wang, Y. Liang, H. Cao, J. Wang, Phys. Rev. Lett. 127, 233901 (2021).
[6] L. Fang, H. Luo, X. Cao, S. Zheng, X. Cai, J. Wang, Optica 6, 61 (2019).
[7] J. Du, J. Wang, Opt. Express, 26, 13183 (2018)
[8] N. Zhou, S. Zheng, X. Cao, S. Gao, S. Li, M. He, X. Cai, J. Wang, Opt. Lett. 43, 3140(2018).
[9] N. Zhou, S. Zheng, X. Cao, Y. Zhao, S. Gao, Y. Zhu, M. He, X. Cai, J. Wang, Sci. Adv. 5, eaau9593 (2019).
[10] Y. Zhu, H. Tan, N. Zhou, L. Chen, J. Wang, X. Cai, Opt. Lett. 45, 1607(2020).
[11] J. Du, J. Wang, Opt. Lett. 42, 5054 (2017).
[12] J. Wang, Sci. China Phys. Mech. 62, 034201 (2019).
[13] L. Fang, M. J. Padgett, J. Wang, Laser Photon. Rev. 11, 1700183 (2017).
[14] J. Liu, I. Nape, Q. Wang, A. Vallés, J. Wang, A. Forbes, Sci. Adv. 6, eaay0837 (2020).

*Corresponding author: first.author@email.com

# Advances in Utilizing OAM Multiplexing for Communication Systems in the THz and Mid-IR Frequency Bands

**Alan E. Willner**[*1]
*1. University of Southern California, Los Angeles, CA, USA 90089-2565*

In communication systems, space-division-multiplexing (SDM) represents the ability to transmit multiple independent data channels each on a different electromagnetic beam that occupies a unique part of the spatial domain. A subset of SDM is mode-division-multiplexing (MDM), in which each of the beams is transmitted on a different orthogonal spatial mode from a modal basis set. This orthogonality helps ensure that there is little inherent crosstalk among the different data-carrying beams when multiplexing, transmitting, and demultiplexing them. Such MDM techniques have the potential to significantly increase the overall system data capacity as well as the spectral efficiency (bits/sec/Hz). Orbital-angular-momentum (OAM) modes have been shown to serve as the modal basis set for MDM communication systems, both in free-space and in fiber [1]. Much of the communications research to date has been in optical and millimeter-wave systems. This presentation will deal primarily with OAM communication systems that are based in the terahertz (THz) and mid-infrared (MIR) frequency bands [2-5]. Although OAM-based communication systems are conceptually similar in all these frequency regions, there are important differences in terms of generating, propagating, and recovering such data channels. This presentation will deal with these technical challenges and describe advances in THz and MIR OAM-based communication links (see embedded figure).

Specifically, this presentation will highlight (a) **THz** [2-4]: Optics can play a key role in THz OAM-based communication systems. An example is the mixing of 2 stable lasers such that the "beat" frequency is in the THz region. Moreover, high-speed optical modulators can be used to imprint high-speed data onto one of the optical beams, which is then translated into the THz OAM beam. Links have been demonstrated that combine mode, polarization, and frequency multiplexing to achieve an increase in data capacity at 0.3 THz.
(b) **MIR** [5]: OAM-based communication links in the MIR can use either native MIR optical elements or wavelength-convert beams from the near IR. This wavelength conversion can be relatively inefficient, but it does leverage the existing high-data-rate components in the telecommunications band of 1.55 microns. Links have been demonstrated that combine mode and wavelength multiplexing to achieve higher capacity in the 3.4-micron region. the following advances:

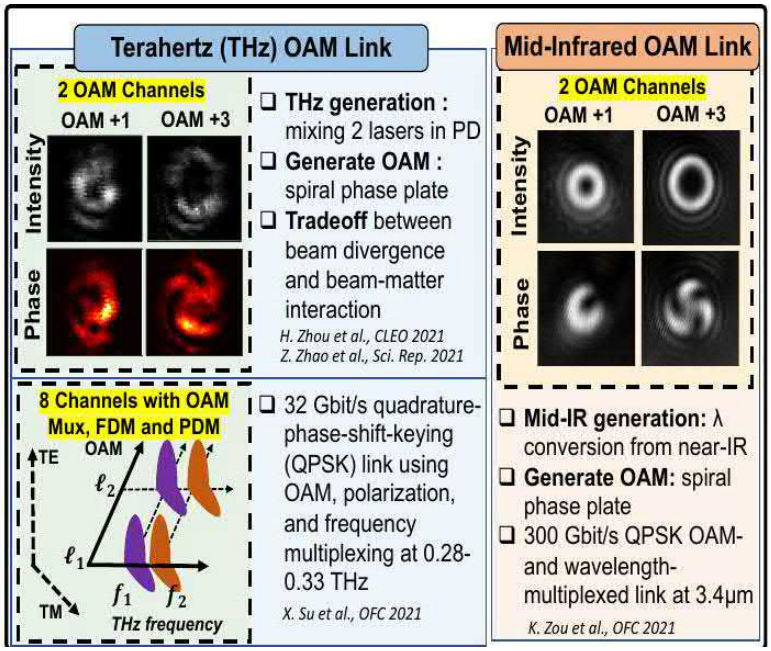


## References

[1] Alan E. Willner, Kai Pang, Hao Song, Kaiheng Zou, and Huibin Zhou, "Orbital Angular Momentum of Light for Communications," Applied Physics Reviews, vol. 8, Article number: 041312, 2021 .
[2] Xinzhou Su, et al., "Demonstration of 8-Channel 32-Gbit/s QPSK Wireless Communications at 0.28 – 0.33 THz Using 2 Frequency, 2 Polarization, and 2 Mode Multiplexing," IEEE/OSA Conf. on Optical Fiber Comm. (OFC), paper M3J.4, 2021 [3] Amir Minoofar, et al., "Experimental Demonstration of Free-Space sub-THz Communications Link Using Multiplexing of Beams Having Two Different LG Modal Indices," European Conf. on Optical Comm. (ECOC), paper Th2B.3, 2021. [4] Xinzhou Su; et al.," THz Integrated Circuit with a Pixel Array to Multiplex Two 10-Gbit/s QPSK Channels Each on a Different OAM Beam for Mode-Division-Multiplexing," Postdeadline Paper Th4B .4, San Diego, CA, March 2022.
[5] Kaiheng Zou, et al., "Demonstration of Free-Space 300-Gbit/s QPSK Communications Using Both Wavelength- and Mode-Division-Multiplexing in the Mid-IR," IEEE/OSA Conf. on Optical Fiber Communications (OFC), paper W7E.5, 2021.

[*]Corresponding author: willner@usc.edu

# Structuring light for controlled propagation of optical and atomic solitons

**Grant Henderson[1], Christopher J. Gibson[1], Gordon R. M. Robb[1], Gian-Luca Oppo[1], Alison M Yao*[1]**
*1. SUPA & Department of Physics, University of Strathclyde, Glasgow, Scotland, UK*

Designing non-trivial light distributions and controlling them during propagation is of interest for modern optical technologies and particle/atom trapping. One approach to maintaining the spatial profile of an optical beam as it propagates is to carefully balance the diffraction of a Gaussian beam with the self-focussing effect of a Kerr nonlinear medium to produce spatial solitons. This approach fails, however, when the optical beam carries orbital angular momentum (OAM). Instead of maintaining its ring-like intensity distribution, the beam fragments into daughter solitons, with the number of solitons formed depending, in general, on the OAM index, $m$ [1]. The onset of fragmentation can be delayed, however, if the optical beam has spatially-varying polarization, for example by using a vector superposition of beams with orthogonal polarizations and equal and opposite OAM, so called fully-structured light (FSL). This has been demonstrated experimentally in hot rubidium gas [2].

In this work we move from hot gases to ultracold atomic gases and consider the propagation of structured optical fields through Bose Einstein Condensates (BECs). Assuming that we are far-detuned, we can model this numerically using the normalised coupled equations:

$$\partial_z F = i\nabla_\perp^2 F + i\left(\frac{-s|\psi|^2}{1+\sigma_{sat}|F|^2}\right)F, \qquad (1); \qquad \partial_z \psi = i\nabla_\perp^2 \psi - i\left(s|F|^2 + \beta_{col}|\psi|^2 - iL_3|\psi|^4\right)\psi. \qquad (2)$$

Equation (1) is a nonlinear Schrödinger equation (NLSE) for the light, $F$, containing terms describing diffraction ($\nabla_\perp^2$) and a saturating self-focusing nonlinearity. This has the same form as the NLSE for the Kerr case, but here the nonlinearity is provided by the BEC instead of the optical field. This is then coupled to equation (2), which is a nonlinear Gross-Pitaevskii equation (GPE) describing the atoms of the BEC, $\psi$ [4]. This contains terms describing the kinetic energy ($\nabla_\perp^2$) and interatomic scattering ($\beta_{col}$), as well as a term describing three-body loss ($L_3$) that accounts for the evolution of the BEC wave-function in high-density regimes. The two fields are coupled by terms proportional to the sign of the light-atom detuning, where $s = \mp 1$ corresponds to red/blue detuning, respectively.

The coupling with the atoms allows additional degrees of freedom w.r.t. the pure Kerr case. In particular, the behaviour of the atoms is fundamentally different depending on the atom-light detuning: if the light is red-detuned, the atoms are attracted to intensity maxima, while if the light is blue-detuned, the atoms are attracted to intensity minima. We can also choose to have weakly attractive or repulsive interactions depending on the interatomic scattering length of interactions of ground-state atoms.

We consider an experimentally realisable BEC with a Thomas-Fermi transverse distribution of diameter $100\mu$m and a longitudinal length of around 2mm and choose to focus on weakly repulsive interactions ($\beta_{col} = 3.5$). The optical beam has wavelength $\lambda = 720$ nm and Gaussian beam waist $w_F = 10\mu$m, giving a Rayleigh range $z_R = \pi w_F^2/\lambda \approx 0.44$ mm. This can be converted to an optical vortex beam carrying OAM of $m\hbar$ per photon using a spatial light modulator (SLM) with an "m"-forked diffraction grating.

We will show that red-detuned light carrying OAM fragments into solitons, suggesting that the BEC is behaving like an effective Kerr medium. As the light is red-detuned, atoms are attracted to intensity peaks and hence "captured" by the daughter optical solitons, resulting in coupled light-atom solitons. We show that both the optical and atomic solitons carry angular momentum and that the number of solitons formed, and their velocities, is dependent on the OAM of the optical field. For blue-detuned light, however, the atoms are attracted to the intensity minima and we will demonstrate how superpositions of optical vortex beams can be used to guide the atoms in the dark, potentially realising stable atomic rings and a single-frequency optical ferris wheel [5].

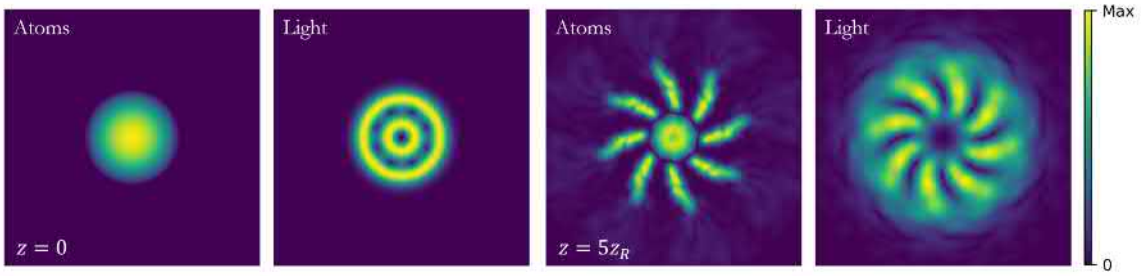


**Fig. 1:** Left: Blue-detuned atomic and optical fields at $z = 0$. Light is a superposition of Laguerre-Gaussian modes with OAM $m = 2$ and $m = -6$; Right: atomic and optical fields at $z = 5z_R$.

## References

[1] W. J. Firth and D. V. Skryabin, Phys. Rev. Lett. **79**, 2450 (1997); A. S. Desyatnikov and Y. S. Kivshar, Phys. Rev. Lett. **87**, 033901 (2001); M. S. Bigelow, P. Zerom, and R. W. Boyd, Phys. Rev. Lett. **92**, 083902 (2004).
[2] F. Bouchard, H. Larocque, A. M. Yao, C. Travis, I. De Leon, A. Rubano, E. Karimi, G.-L. Oppo, and R. W. Boyd, Phys. Rev. Lett. **117**, 233903 (2016).
[3] W. Walasik, S. Z. Silahli, and N. M. Litchinitser, Sci. Rep. **7**, 11709 (2017); J. Sun, S. Z. Silahli, W. Walasik *et al.*, Opt. Express **26**, 5118 (2018).
[4] M. Saffman, Phys. Rev. Lett. **81**, 65 (1998); M. Saffman and D. V. Skryabin, in *Spatial Solitons*, (Springer, 2001) pp. 433–447.
[5] S. Franke-Arnold, J. Leach, M. J. Padgett, V. E. Lembessis, D. Ellinas, A. J. Wright, J. M. Girkin, P. Öhberg and A. S. Arnold, Opt. Express **15**, 8619 (2007).

*Corresponding author: alison.yao@strath.ac.uk

# Spatiotemporal Sculpturing of Ultrashort Pulses

**Qiwen Zhan**[*1]

*1. School of Optical-Electrical and Computer Engineering, University of Shanghai for Science and Technology 516 Jungong Road, Shanghai, China 200093*

With the rapid advances in laser technology, ultrafast lasers are widely available and greatly impact many scientific disciplines and industrial applications. Meanwhile, complementary pulse shaping techniques have been developed to synthesize complex optical waveforms for specific application needs. Traditionally pulse shaping focuses on pulse compression and temporal waveform synthesis. Recently, there have been very strong recent interests in structuring light in the spatiotemporal domain.

In this talk I will present a technique that allows us to directly sculpture ultrafast wavepackets in the spatiotemporal domain. Taking advantage of the relationship between frequency and time of chirped pulses, this spatiotemporal pulse sculpturing technique is experimentally demonstrated through the generation of a variety of spatiotemporally sculptured wavepackets (figure 1), including spatiotemporal optical vortex (STOV) [1], STOV lattice with multiple STOVs multiplexed in space and time [2], wavepackets that contain STOV and spatial optical vortex [3], wavepackets that contain STOV with polarization singularities [4], and so on.

Wavepackets with spatiotemporal optical vortices and many other complicated spatiotemporal structures exhibit many unique properties [5,6] and may find important applications when interact with matters. Such a ultrafast spatiotemporal sculpturing technique opens tremendous potential opportunities for sculptured complex spatiotemporal ultrashort wavepackets.

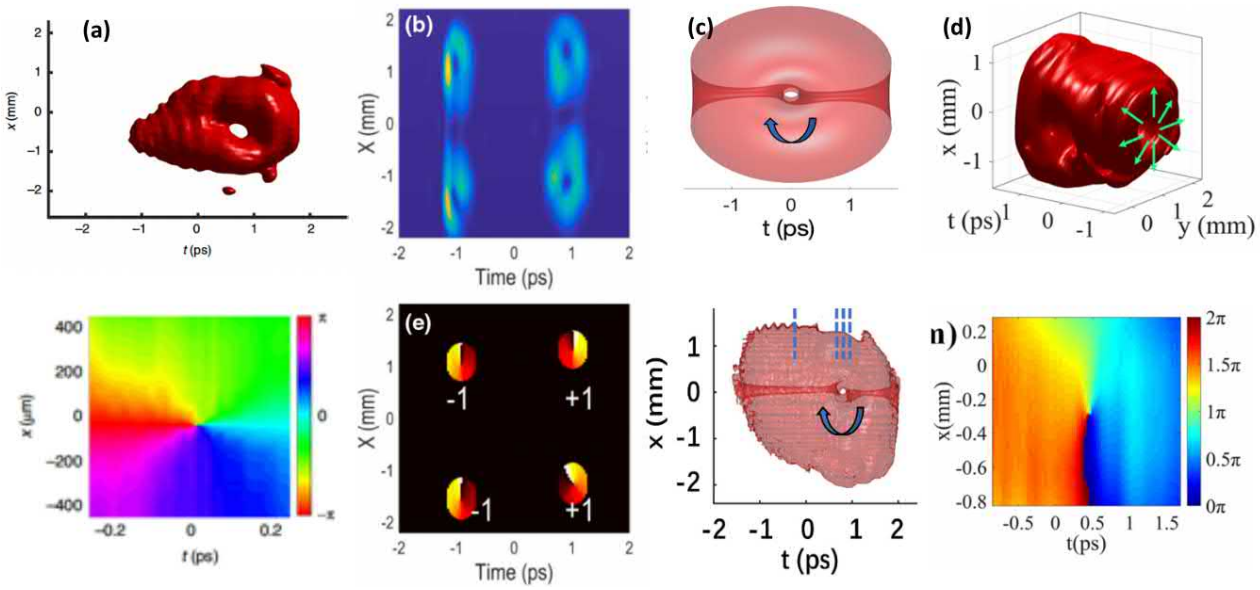


**Fig. 1:** Various examples of spatiotemporal wavepackets with optical singularities. (a) Spatiotemporal optical vortex (STOV) [1]; (b) STOV lattice [2]; (c) STOV with spatial optical vortex [3]; (d) radially polarized STOV [4].

## References

[1] A. Chong, C. Wan, J. Chen, and Q. Zhan, Nature Photon. 14, 350-354 (2020).
[2] Q. Cao, J. Chen, K. Lu, C. Wan, A. Chong, and Q. Zhan, Photonics Research 9, 2261-2264 (2021).
[3] C. Wan, J. Chen, A. Chong, and Q. Zhan, National Science Review, nwab149, (2021).
[4] J. Chen, C. Wan, A. Chong, and Q. Zhan, Nanophotonics 10, 4489-4495 (2022).
[5] J. Chen, L. Yu, C. Wan, and Q. Zhan, ACS Photonics 9, 793-799 (2022).
[6] J. Chen, C. Wan, and Q. Zhan, Advanced Photonics 3, 064001 (2021).

*Corresponding author: qwzhan@usst.edu.cn

# Abstracts

## Contributed Talks

# Angular Momentum and Polarization Transfer from the Twisted Light to Atoms

**Andrei Afanasev**[*1]
*1. The George Washington University, Washington, DC 20052, USA*

Twisted photons, or photons with additional angular momentum along their propagation direction follow novel quantum selection rules for photo-absorption by atoms, as was confirmed experimentally in 729 nm$4^2$ $S_{1/2} \rightarrow 3^2D_{5/2}$ transitions in cold trapped $^{40}Ca^+$ions [1].

Here we consider optical polarization of atoms via absorption of the twisted light. Partially, the effects in question were analyzed in Ref.[2], where a formalism of spin-density matrix for twisted photons was developed and applied for atomic photoabsorption. In addition, recoil momentum effects in quantum processes induced by twisted photons are described in Ref.[3].

Let us consider an atom located at a distance $b$ away from the twisted-photon axis (or a phase singularity) as shown in Figure 1. Twisted-photon electromagnetic fields have both longitudinal and transverse components with respect to the direction of propagation. Treating the photon's spin state as a vector particle, we can expand it in a spherical basis as $|\chi_1\rangle = a^+|\chi_{1+}\rangle + a^0|\chi_{10}\rangle + a^-|\chi_{1-}\rangle$, where $a^{\pm,0}$ are complex amplitudes with normalization $\sum_i |a_i|^2 = 1$. The spin density matrix for a pure state is then $\rho_{ij} = a_i a_j^*$. In general for mixed states it can be presented in terms of eight independent polarization parameters (as opposed to three Stokes parameters for plane waves) that we call vector and quadrupole polarizations $p_i$ and $p_{ik}$, respectively:

$$p_i = i\sum_{ik} \varepsilon_{ijk} a_j a_k^*; p_{ik} = -\frac{3}{2}\left(a_i a_k^* + a_k a_i^* - \frac{2}{3}\delta_{ik}\right)$$

Three anti-symmetric parameters characterize vector polarization - as opposed to only one circular polarization for plane waves; and five symmetric parameters define the quadrupole polarization - as opposed to two Stokes parameters for plane waves' linear polarization.

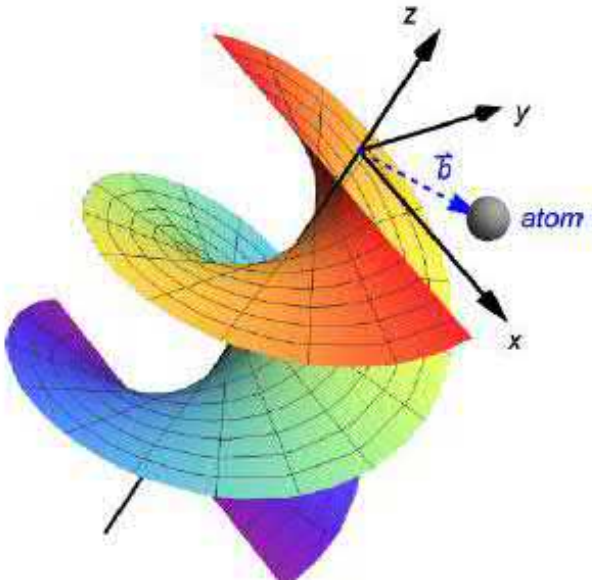


**Fig. 1:** The wavefront of a twisted photon, with atom's position $b$ shown with respect to the optical vortex center.

For an atom exposed to the twisted light, the dominant electric dipole (E1) transition results in one-to-one correspondence - up to signs - between spin-density matrix components of the twisted light field and the excited atom, as derived in Ref.[2]. Transverse spatial dimensions of certain polarization features of the optical vortices appear to be independent on beam's expansion caused by diffraction.

## References

[1] A. Afanasev, C.E. Carlson, C.T. Schmiegelow, J. Schulz, F. Schmidt-Kaler, and M. Solyanik, "Experimental verification of position-dependent angularmomentum selection rules for absorption of twisted light by a bound electron", New J. Phys. 20, 023032 (2018).
[2] A. Afanasev, C.E. Carlson, and H. Wang, "Polarization transfer from the twisted light to an atom", J. Opt. 22, 054001 (2020)
[3] A. Afanasev, C.E. Carlson, A.Mucherjeee, "Recoil momentum effects in quantum processes induced by twisted photons,", Phys.Rev.Res 3,023097.

*Corresponding author: afanas@gwu.edu

# Compressive STED Microscopy with Speckles

**Payvand Arjmand**[*1], **Marc Guillon** [1]
*1. Saints-Pères Paris Institute for the Neurosciences, Université Paris Cité, 75006 Paris, France*

Super-resolution microscopy has been an essential tool for biological imaging since it allows the visualization of the specimen at spatial scales beyond the diffraction limit. However, complex media such as biological tissues scatter light, which makes the observation of deeper layers of tissues very challenging. STED (Stimulated Emission Depletion) microscopy is one of most common implementations of super-resolution techniques, which allows observing the deepest inside tissues, up to 100m. In STED microscopy, a diffraction limited excitation spot is overlaid with a red-shifted beam featuring a zero intensity point at the center. Depletion of the molecular electronic excited state results in a sharp effective point spread function [1]. The center of the donut is usually designed as a phase spiral (or optical vortex) where the intensity vanishes. Beyond 100m deep in tissues, light is scattered and turned into a speckle pattern. Although speckle patterns may be considered as loss of information, it has been demonstrated that they can be used in optical imaging to retrieve the information from the object after complex media [2]. In addition, speckles are ideally suited for performing compressive imaging since they are statistically orthogonal (i.e. strongly incoherent) relatively to the cross-correlation product. It was thus shown that three-dimensional super resolution microscopy could be achieved by saturating the fluorescence excitation [3]. In addition, we showed that subdiffraction confinement of fluorescence can be achieved thanks to the high density of optical vortices in speckle patterns [4].
Here, we implement compressive 3D super-resolution microscopy by saturating the stimulated emission with speckles, so gaining three advantages in comparison with the state of the art [3]. Using red-shifted light beams leads to reduced photo-toxicity, reduced auto-fluorescence background and improved penetration depth.

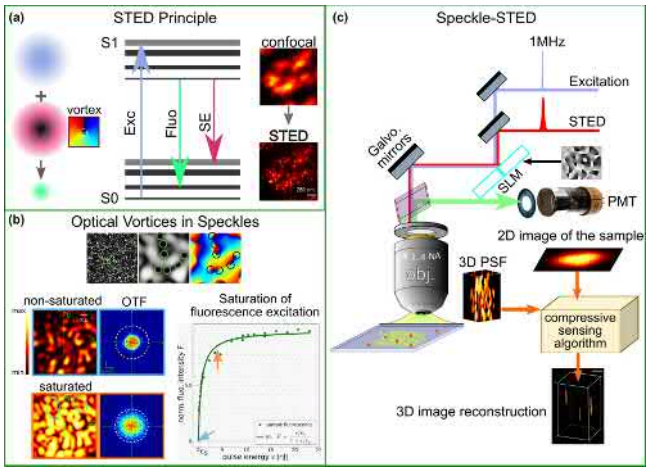


**Fig. 1:** (a) The principle of STED Microscopy, Experimental images by M. Guillon (unpublished data), scale bar: 250 nm (b) The illustration of optical vortices in a speckle pattern. The saturation of fluorescence excitation with a speckle leads to a larger optical transfer function and allows super-resolution microscopy. (c) Scheme of the Speckle-STED microscope

## References

[1] S. Hell, and J. Wichmann, "Breaking The Diffraction Resolution Limit By Stimulated Emission: Stimulated-Emission-Depletion Fluorescence Microscopy," *Optics letters*, vol. 19, pp. 780–782, 1994.

[2] J. Bertolotti *et al.*, "Non-invasive imaging through opaque scattering layers," *Nature*, vol. 491, pp. 232–234, 2012.

[3] M. Pascucci *et al.*, "Superresolution Imaging of Optical Vortices in a Speckle Pattern," *Physical Review Letters*, vol. 116, pp.093904, 2016.

[4] M. Pascucci *et al.*, "Compressive Three-Dimensional Super-Resolution Microscopy with Speckle-Saturated Fluorescence Excitation," *Nature Communications*, vol. 10, pp. 1–8, 2019.

*Corresponding author: payvand.arjmand@u-paris.com

# A condensate of light as a sensor of chirality

**Robert Bennett**[*1], **David Steinbrecht**[2], **Stefan Yoshi Buhmann**[3]
*1. School of Physics & Astronomy, University of Glasgow, Glasgow G12 8QQ, United Kingdom*
*2. Charité — Universitätsmedizin Berlin, Charitéplatz 1, 10116, Berlin, Germany*
*3. Institut für Physik, Universität Kassel, Heinrich-Plett-Straße 40, 34132, Kassel, Germany*

Bose-Einstein condensates (BECs) are a few actualisations of purely quantum phenomena at a macroscopic level. Over the last few years, a new type of condensate has emerged, known as a photon BEC. Such an object can be realised relatively cheaply and easily (compared to atomic BECs) in a dye-filled microcavity. The host dye molecules induce an effective photon-photon interaction that leads to macroscopic ground state occupation once a certain pump threshold has been reached. In this work, we introduce medium-induced symmetry breaking by considering chiral molecules immersed in the dye, lifting the degeneracy between left- and right-circularly polarised modes. Even the tiniest imbalance in the concentration of left and right enantiomers is imprinted on the condensate polarisation [1], which can then be read out. This means that the photon BEC can be used as a precise, room temperature, liquid phase sensor of relative concentrations of chiral molecules in a solute, with accuracy competitive with current state-of-the-art methods.

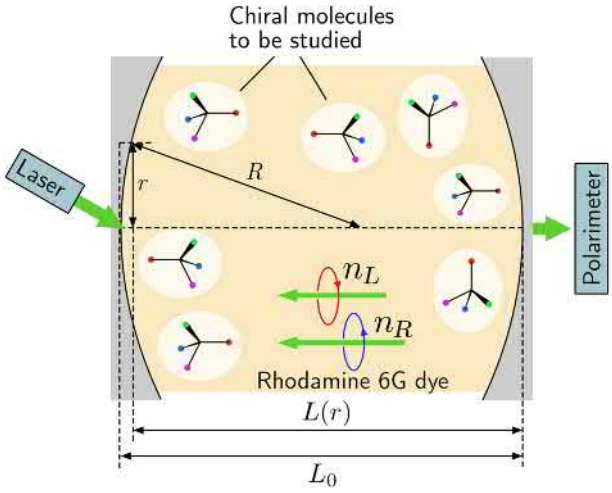


**Fig. 1:** Schematic of the physical system used in the proposed sensor

## References

[1] R. Bennett, David Steinbrecht, Yaroslav Gorbachev, Stefan Yoshi Buhmann Phys. Rev. Applied **13** 044031 (2020)

*Corresponding author: robert.bennett@glasgow.ac.uk

# Ultra-sensitive measurement of transverse displacements with linear photonic gears

**Raouf Barboza**[1], **Amin Babazadeh**[1], **Lorenzo Marrucci**[1], **Filippo Cardano**[*1], **Corrado de Lisio**[1], **Vincenzo D'Ambrosio**[†1]

*1. Dipartimento di Fisica, Università di Napoli Federico II, Complesso Universitario di Monte S. Angelo, Via Cintia, 80126 Napoli, Italy*

Accurately measuring mechanical displacements is essential for a vast portion of current technologies. Several optical techniques accomplish this task, allowing for non-contact sensing even below the diffraction limit. Structured light can be a resource for enhanced sensing purposes as for instance in the "photonic gears". This technique enables a boost of the sensitivity in roll angle measurements thanks to a bidirectional mapping between the polarization state and a properly tailored vectorial mode of a paraxial light beam [1]. Similarly, ultra-sensitive measurements of a transverse displacement can be performed by mapping it into the polarization rotation of a laser beam [2]. By exploiting this technique, dubbed "linear photonic gears", we measured, in ordinary ambient conditions, the relative shift between two objects with a resolution of 400 pm. We argue that a resolution of 50 pm should be achievable with existing state-of-the-art technologies. Our single-optical-path scheme is intrinsically stable and it could be implemented as a compact sensor, using cost effective integrated optics.

## References

[1] V. D'Ambrosio, N. Spagnolo, L. Del Re, S. Slussarenko, Y. Li, L. Chuan Kwek, L. Marrucci, S. P. Walborn, L. Aolita, F. Sciarrino, Nat. Commun. **4**, 2432 (2013)

[2] R. Barboza, A. Babazadeh, L. Marrucci, F. Cardano, C. de Lisio, V. D'Ambrosio, Nat. Commun. **13**, 1080 (2022)

[*]Corresponding author: filippo.cardano2@unina.it

[†]Corresponding author: vincenzo.dambrosio@unina.it

# Nonlinear up-conversion of scalar and vectorial vortices through high harmonic generation

**Alba de las Heras**[*1], **Alok Kumar Pandey**[†2], **Julio San Román** [1], **Tanguy Larrieu** [2], **Javier Serrano** [1], **Elsa Baynard** [2], **Guillaume Dovillaire** [3], **Moana Pittman** [2], **Charles G. Durfee** [4], **Luis Plaja** [1], **Sophie Kazamias** [2], **Olivier Guilbaud** [2], **Carlos Hernández-García** [1]

*1. Grupo de Investigación en Aplicaciones del Láser y Fotónica, Departamento de Física Aplicada, Universidad de Salamanca,Pl. La Merced s/n, Salamanca E-37008, Spain*

*2. Laboratoire Irène Joliot-Curie, Université Paris-Saclay, UMR CNRS,Rue Ampère, Bâtiment 200, Orsay Cedex F-91898, France*

*3. Imagine Optic, rue Charles de Gaulle, 18, Orsay F-91400, France*

*4. Department of Physics, Colorado School of Mines, Golden, Colorado 80401, USA*

The nonlinear process of high harmonic generation (HHG) stands as a highly coherent tool to up-convert the properties of infrared/visible light into the extreme ultraviolet regime (XUV), or even into the soft x-rays. Thanks to HHG, we experimentally and theoretically report the generation of XUV scalar and vectorial vortices with very high topological charges [**??**]. On the one hand, scalar vortex beams present a homogenous polarization and a twisted wavefront along the azimuth, which encodes light's orbital angular momentum (OAM). The total wavefront twist, measured as the peak-to-valley wavefront value in one wavelength, points out the overall topological charge, $\ell$, of the vortex beam. In HHG, the topological charge of scalar vortices scales linearly with the harmonic order i.e., $\ell_q = q\ell_1$[**??**], which allows for the generation of high harmonic vortices with high OAM. On the other hand, vector-vortex beams merge a spatially varying polarization and a twisted wavefront, so their properties of spin angular momentum and OAM are intertwined. We demonstrate that the corresponding conservation law in HHG is ruled by the topological Pancharatnam charge, $\ell_P$, satisfying $\ell_{P,q} = q\ell_{P,1}$[**??**]. Additionally, the up-conversion of vector-vortex beams is far from trivial, since these beams are hybrid modes whose structure evolves during propagation [**??**].

In Fig. 1, we show the characterization of the 25 th harmonic beam resulting from a vortex driver of $\ell_1 = 4$ (left) or from a vector-vortex driver of $\ell_{P,1} = 2$ (right). The experimental XUV beam (top row) is characterized using wavefront sensing metrology, which enables a full measurement of intensity and phase [1]. The theoretical beam (bottom row) is computed in the full quantum strong-field approximation and considers propagation effects in the transverse plane [**??**]. Our results demonstrate the up-conversion of scalar and vectorial phase singularities leading to very high topological charges in the XUV, up to $\ell_{25} = 100$. Such structured XUV beams may encourage advances in high-resolution imaging, attochemistry, or the fundamentals of intense laser-matter interactions.

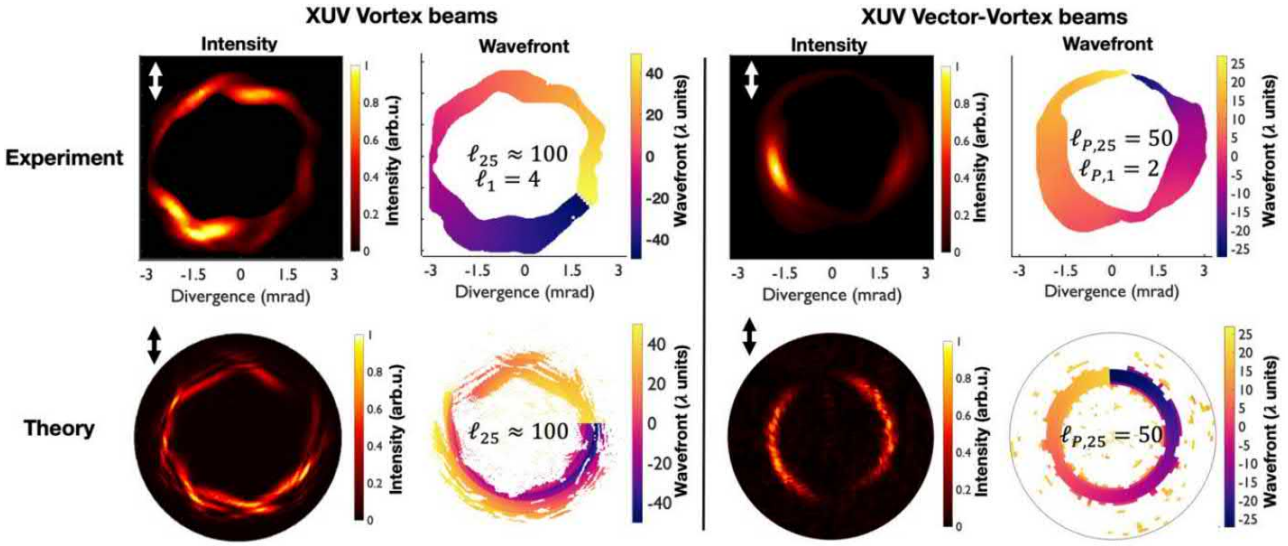


**Fig. 1:** Characterization of XUV vortex and vector-vortex beams. We show the experimental (top row) and theoretical (bottom row) intensity of the vertical polarization projection and wavefront of the $25^{th}$ harmonic beam. In the left panel, the HHG driver is a vortex of $\ell_1 = 4$, whereas in the right panel the driver is a vectorial vortex of $\ell_{P,1} = 2$. In both cases, the overall topological charge of the wavefront agrees with the expected conservation law.

## References

[1] A. K. Pandey, A. de las Heras, T. Larrieu, J. San Román, J. Serrano, L. Plaja, E. Baynard, M. Pittman, G. Dovillaire, S. Kazamias, C. Hernández-García, and O. Guilbaud, ACS Photonics **9**, 944-951 (2022)

[2] A. de las Heras, A. K. Pandey, J. San Román, J. Serrano, E. Baynard, G. Dovillaire, M. Pittman, C. G. Durfee, L. Plaja, S. Kazamias, O. Guilbaud, and C. Hernández-García, Optica **9**, 71-79 (2022)

[3] C. Hernández-García, A. Picón, J. San Román, and L. Plaja, Phys. Rev. Lett. **111**, 083602 (2013).

[*]Corresponding author: albadelasheras@usal.es

[†]Corresponding author: alok- kumar.pandey@etu.univ-amu.fr

# Einstein Beams: Light beams following gravitationally-lensed trajectories

**Enrique J. Galvez***, **Thao P. Nguyen, Valeria Rodriguez-Fajardo, Jacob M. Freedman**
*1. Department of Physics and Astronomy, Colgate University, Hamilton, New York 13346, U.S.A.*

The deflection of light rays due to gravity occurs over a relatively short distance relative to the distances from the lensing object to source and observer. Thus, gravitational deflections can be reproduced in the laboratory by a planar optical element. The versatility of spatial light modulators (SLM) makes them suitable for reproducing the observations of gravitational lensing in the laboratory. Light rays traveling near an object of mass $M$ will acquire a net deflection that depends inversely on impact parameter $r$ [1]:

$$\alpha = \frac{2r_S}{r}, \tag{1}$$

as shown in Fig. 1a, and where $r_S = 2GM/c^2$ is the Schwarzchild radius, with $G$ being the gravitational constant and $c$ the speed of light. Reproduction of this deflection in the laboratory is easily accomplished by programming of the SLM with a phase [2]

$$\phi = -4kr_S \ln\frac{r}{r_0}, \tag{2}$$

where $r_0$ is a constant.

We report here on experimental and theoretical work on this problem. We find that recreation of the gravitational lensing of light beams reproduces the astrophysical observations of Einstein rings and arcs, which are angular patterns of light received at a point (e.g., Earth). Because we can image the entire wavefront, this work opens the investigation of optical beams, which modified by gravity, propagate through space but which are never seen by observations from Earth. Our studies are limited to monochromatic beams, yet we find that the optical beams that arise from gravitationally-lensed trajectories are a new class of singular beams rich in caustics. They do not conform with previously well known types of beams, such as Gaussian or non-diffracting, and so constitute a class on its own, for which we call them "Einstein beams."

The experiments use an expanded monochromatic laser beam to illuminate the SLM, which is programmed with a corresponding phase encoding given above. With this arrangement we have been able to reproduce astrophysical observations: Einstein rings and arcs. However, with the versatility of the SLM we can add asymmetry, azimuthal phases (i.e. topological charges), and multiple lensing masses. The most interesting aspect of this work has been the study of the resulting Einstein beams. The radially-dependent deflection of light rays off a symmetric lensing object produces a beam pattern that closely resembles a Bessel beam, as shown in Fig. 1b, but which is more accurately described by a confluent hypergeometric function. We have verified the observations with a theoretical evaluation of the corresponding Fresnel diffraction integral. The distinctive feature of the beam is its propagation. The beam pattern retains its shape without distortion while expanding non-monotonically with the propagation distance $z$. This expansion depends on $\sqrt{z}$, which becomes a nearly linear for most of the imaging positions in the laboratory. The addition of an azimuthal vortex phase results in a high-order Bessel-like pattern. The zeros of the patterns match the Bessel-function zeros.

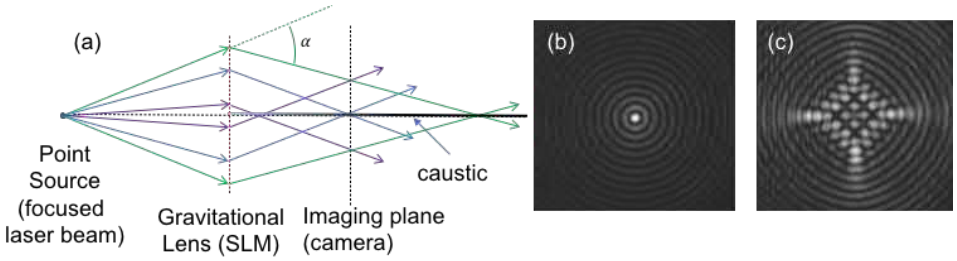


**Fig. 1:** (a) Ray picture of gravitational lensing deflections of light rays, and Einstein-beam patterns for symmetric (b) and asymmetric (c) lensing objects.

For no vortex phase the central axis is the location of a linear caustic. The addition of a vortex phase creates a circular caustic that is typical of beams carrying orbital angular momentum. As soon as the symmetry of the lensing object is broken, either with the addition of ellipticity or with the splitting of the lensing object into a pair, the caustic pattern changes to feature 4 caustic cusps forming an astroid shape, as shown in Fig. 1c, and which were foreseen in the study of asymmetric lensing [3]. The details of number maxima within the main astroid caustic connecting the cusps depend on the strength (mass) of the lensing object and on the degree of asymmetry or ellipticity. The corresponding astrophysical pattern observed from Earth is an Einstein cross. The addition of orbital angular momentum to the gravitational deflection creates an asymmetry in the Astroid patterns and in the astrophysical-like observations.

This work was funded by the National Science Foundation grant PHY-2011937.

## References

[1] P . Schneider, J. Ehlers, E.E. Falco, *Gravitational Lenses* (Springer-Verlag, Berlin 1992).
[2] E.J. Galvez, J.M. Freedman, Proc. SPIE **11701** 117010U (2021)
[3] R .D. Blandford, I. Kovner, Phys. Rev. A **38** 4028 (1988).

*Corresponding author: egalvez@colgate.edu

# OAM multiplexed quantum entanglement and quantum teleportation

**Shengshuai Liu** [1], **Kai Zhang**[1] **Jietai Jing**[*1]
*1. State Key Laboratory of Precision Spectroscopy, East China Normal University, Shanghai 200062, China*

Multiplexing is a very important concept in optical communication technology. By combining multiple channels into a single channel, multiplexing can largely enhance the data-carrying capacity of the optical carrier. Different types of multiplexing can be realized by using different degrees of freedom (DOFs) of light. Recently, the orbital angular momentum (OAM) of light [1], one of the most fundamental physical quantities, has been used to realize multiplexing [**??**] due to the infinite range of possibly achievable OAM modes. Because of this advantage, OAM has found many applications in quantum information processing. In discrete variable (DV) regime, OAM has been utilized to generate high-dimensional quantum entanglement [4]. DV and continuous variable (CV) quantum systems are two equally important platforms for quantum information processing. In CV regime, OAM multiplexing is an effective way to boost the scale of entanglement. The scale of quantum entanglement determines its quantum information carrying and processing capability. Therefore, it is essential to generate large-scale quantum entanglement by utilizing OAM multiplexing. In this report, we will introduce our recent experimental works about the deterministic generation of 13 pairs OAM multiplexed bipartite quantum entanglement [5], the implementation of 9 sets of OAM multiplexed tripartite quantum entanglement [6], and the realization of a large-scale quantum network over 66 OAM optical modes [7] based on the four-wave mixing processes. Based on these OAM multiplexed quantum entanglement, we also developed OAM multiplexed all-optical quantum teleportation [8], in which 9 orbital angular momentum multiplexed channels of parallel all-optical quantum teleportation are deterministically established.

## References

[1] L. Allen, M. W. Beijersbergen, R. J. C. Spreeuw, and J. P. Woerdman, Phys. Rev. A 45, 8185 (1992).
[2] J. Wang, J. Yang, I. M. Fazal, N. Ahmed, Y. Yan, H. Huang, Y. Ren, Y. Yue, S. Dolinar, M. Tur, and A. E. Willner, Nat. Photonics 6, 488 (2012).
[3] N. Bozinovic, Y. Yue, Y. Ren, M. Tur, P. Kristensen, H. Huang, A. E. Willner, and S. Ramachandran, Science 340, 1545 (2013).
[4] R. Fickler, R. Lapkiewicz, W. N. Plick, M. Krenn, C. Schaeff, S. Ramelow, and A. Zeilinger, Science 338, 640 (2012).
[5] X. Pan, S. Yu, Y. Zhou, K. Zhang, K. Zhang, S. Lv, S. Li, W. Wang, and J. Jing, Phys. Rev. Lett. 123, 070506 (2019).
[6] S. Li, X. Pan, Y. Ren, H. Liu, S. Yu, and J. Jing, Phys. Rev. Lett. 124, 083605 (2020).
[7] W. Wang, K. Zhang, and J. Jing, Phys. Rev. Lett. 125, 140501 (2020).
[8] S. Liu, Y. Lou, and J. Jing, Nat. Commun. 11, 3875 (2020).

[*]Corresponding author: jtjing@phy.ecnu.edu.cn

# Orbital Angular Momentum for Biomedical Diagnosis and Tissues Characterization

**Ivan Lopushenko** [1], **Anton Sdobnov** [1], **Alexander Bykov** [1], **Igor Meglinski**[*2,1]

*1. Optoelectronics and Measurement Techniques, University of Oulu, Oulu, Finland*

*2. College of Engineering and Physical Sciences, Aston University, Birmingham, UK*

We explore the potential of using shaped light with angular momentum in diagnosis of cells and biological tissues. The angular momentum of light contains a spin contribution, conditioned by the polarization of the electromagnetic fields and an orbital contribution, related to their spatial structure [1]. While the spin angular momentum has been extensively employed in diagnostic studies (see for example [2],[3],[4]), the orbital angular momentum (OAM) has been added to the practical toolkit very recently [5]. When the shaped light propagates in a homogeneous transparent medium, both spin and orbital angular momenta are conserved. In the medium with complex structure and anisotropic scattering the spin and orbital angular momenta are changed significantly that leads to spin-orbit interaction. Such a spin-orbit interaction leads to the mutual influence of the polarization and the trajectories of twisted photons propagating in the medium. Significant increase of the visibility contrast and penetration depth when imaging through the homogeneous scattering media with OAM light beams was demonstrated [6],[7]. Nevertheless, the potential of OAM for biomedical diagnosis and characterization of cells and tissues is far from being fully explored. In this report we present the results of our most recent studies of how the spin-orbit interaction leads to the mutual influence of trajectories of the shaped light beam propagated in tissue-like medium, and how sensitive OAM to subtle alterations in biological tissues and cells cultures. We show that when the Laguerre-Gaussian (LG) beam propagates through normal and abnormal tissue samples the OAM is preserved with the noticeably different phase shift - twist of light (Fig.1). The results suggest that shaped light with the OAM is preserved with the noticeably different phase shift - twist of light (Fig.1). The results suggest that shaped light with OAM could be up to $\sim 0^3$ times more sensitive to the refractive indices changes within the tissue samples and, therefore, has a potential to revolutionize the current practices of tissue diagnosis, e.g. histology examination. Thus, the application of OAM in applications.

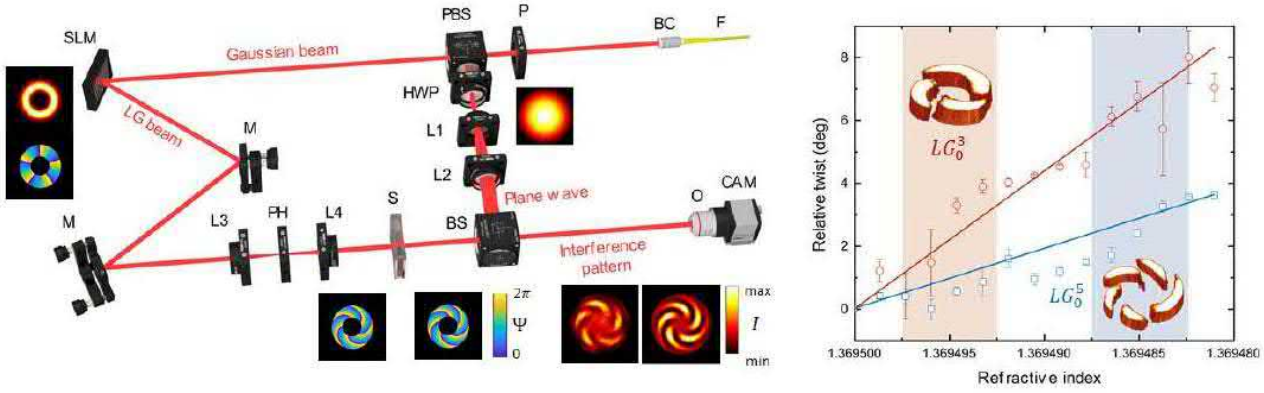


**Fig. 1:** Schematic presentation of the experimental setup used in the study of LG beams propagation through tissue samples (left). Relative twist of light observed for the $LG_0^3$ and $LG_0^5$ beams propagated through the sample with the gradient of refractive index (right).

This work received funding from the Academy of Finland (grant project 325097 ), INFOTECH, the Leverhulme Trust and The Royal Society (Ref. no.: APX111232 APEX Awards 2021).

## References

[1] G. Molina-Terriza, J. Torres, L. Torner, Nature Physics. 3, 305-310 (2007)
[2] B. Kunnen, C. Macdonald, A. Doronin, S. Jacques, M. Eccles, and I. Meglinski, J. Biophoton. 8, 317 – 323(2015).
[3] M. Borovkova, A. Popov, A. Bykov, and I. Meglinski, J. Biomed. Opt. 25, 057001 (2020).
[4] M. Borovkova, O. Sieryi, I. Lapushenko, N. Kartashkina, J. Pahnke, A. Bykov and I. Meglinski, IEEE Trans. Med. Imaging. 41, 977 – 982(2022)
[5] A. Forbes, Structured light: Tailored for Purpose. OPN OSA, 26-31 June (2020)
[6] A. Doronin, N. Vera, J.P. Staforelli, P. Coelho, and I. Meglinski, Photonics. 6, 56 (2019).
[7] W. B. Wang, R. Gozali, T. A. Nguyen, and R. R. Alfano, Proc. SPIE, 9318, 931805 (2015).

*Corresponding author: igor.meglinski@oulu.fi and/or i.meglinski@aston.ac.uk

# Spin structures in random three-dimensional polarization states

**Andreas Norrman**[*1], **José J. Gil** [2], **Yahong Chen** [3], **Ari T. Friberg** [3], **Tero Setälä** [3]
*1. Institute of Photonics, University of Eastern Finland, P.O. Box 111, FI-80101 Joensuu, Finland*
*2. Department of Applied Physics, University of Zaragoza, Pedro Cerbuna 12, 50009 Zaragoza, Spain*
*3. School of Physical Science and Technology, Soochow University, Suzhou 215006, China*

The emergence of diverse complex structured light fields in modern photonics has evoked the need for a full three-dimensional (3D) and statistical assessment of light's polarization character [1]. In particular, while for light exhibiting two-dimensional (2D) polarization states, as in the case of paraxial beams, the evolution of the electric field is always restricted locally to a fixed plane in space, random optical near fields [2] and tightly focused waves [3] can encompass genuinely 3D polarization states for which the local electric field fluctuates in three orthogonal spatial directions in any coordinate system. At the same time the spin angular momentum (henceforth briefly "spin") of light has gained wide interest in photonics, especially due to its remarkable transverse nature in structured light contexts [4] and its appearance through spin-orbit interactions [5] and chiral light-matter couplings [6]. Nevertheless, even though the spin is intimately connected to the polarization state of the light field, to date most research on the spin of light has concerned exclusively monochromatic (deterministic) and, consequently, completely polarized 2D optical fields. A proper quantification and understanding of the spin structure associated with arbitrary random light of general 3D polarization character is therefore necessary.

A fundamental quality of random 2D light is that its polarization matrix is unambiguously expressible as a sum of a completely polarized state and a totally 2D unpolarized state (i.e., an equiprobable mixture of two orthogonal, fully polarized states whose polarization ellipses lie in the same plane). Since the spin of a 2D unpolarized state is obviously zero, the spin of an arbitrary 2D light field is thus specified solely by the spin associated with the pure (fully polarized) term. For general 3D light, however, such a decomposition does not exist, but instead the 3D polarization matrix turns into an incoherent superposition of a pure state $\mathbf{R}_p$, a so-called discriminating state $\mathbf{R}_m$, and a 3D unpolarized state $\mathbf{R}_u$ (proportional to the $3 \times 3$ identity matrix) [1]. An intriguing consequence of this characteristic representation is that $\mathbf{R}_m$ enables the division of any 3D polarization state $\mathbf{R}$ into two categories: regular states and nonregular states [7]. In the former case $\mathbf{R}_m$ is a real matrix and describes a 2D unpolarized state, while in the latter scenario $\mathbf{R}_m$ is a complex matrix and corresponds to an equiprobable mixture of two mutually orthogonal, fully polarized states with their polarization ellipses lying in different planes. Hence, although the discriminating term $\mathbf{R}_m$ has two equal eigenvalues and the third eigenvalue is zero [1,7], for nonregular states it does not represent 2D unpolarized light but genuine 3D light.

A distinguishing physical feature of a nonregular state is that it always carries a nonzero spin [8], even when the pure component $\mathbf{R}_p$ is not present in the characteristic decomposition. As an example, any evanescent wave generated by a partially polarized or 2D unpolarized plane-wave field in total internal reflection possesses a nonzero spin owing to its truly nonregular 3D nature [9]. This was recently demonstrated experimentally with a partially polarized evanescent wave having a purely transverse spin [10]. Here we establish a general framework for the spin structure of an arbitrary, statistically stationary 3D light field in terms of the characteristic decomposition and the notion of nonregularity [11]. We show how nonregularity of a random 3D polarization state inevitably adds a spin component that affects the orientation and magnitude of the total spin through the degree of nonregularity. Accordingly, in striking contrast to 2D polarization states and regular 3D polarization states whose spin is determined exclusively by that of the pure component (since the spin of a 2D unpolarized state and a 3D unpolarized state is zero), the spin of a nonregular state is generally given as a vector sum of those of the pure term and the discriminating term. Furthermore, we demonstrate how the overall polarimetric purity (or the degree of polarization) of a random 3D light field depends, in a complementary spirit, on the amount of spin anisotropy and intensity anisotropy contained in the field [12]. Our results provide novel fundamental insights into the spin and polarization structures of general 3D optical fields and their nonregularity properties, with potential applications in statistical nanophotonics harnessing random evanescent wave fields and tightly focused vectorial beams [13].

## References

[1] J. J. Gil, R. Ossikovski, Polarized Light and the Mueller Matrix Approach (CRC Press, 2016)
[2] Y. Chen, A. Norrman, S. A. Ponomarenko, A. T. Friberg, Prog. Optics **65**, 105(2020)
[3] Y. Chen, F. Wang, Z. Dong, Y. Cai, A. Norrman, J. J. Gil, A. T. Friberg, T. Setälä, Phys. Rev. A **101**, 053825 (2020)
[4] K. Y. Bliokh, F. Nori, Phys. Rep. 592, 1 (2015)
[5] K. Y. Bliokh, F. J. Rodríguez-Fortuño, F. Nori, A. V. Zayats, Nat. Photonics **9**, 796(2015)
[6] P. Lodahl, S. Mahmoodian, S. Stobbe, A. Rauschenbeutel, P. Schneeweiss, J. Volz, H. Pichler, P. Zoller, Nature 541 , 473 (2017)
[7] J. J. Gil, A. T. Friberg, T. Setälä, I. San José, Phys. Rev. A **95**, 053856 (2017)
[8] J. J. Gil, A. Norrman, A. T. Friberg, T. Setälä, Opt. Lett. 43, 4611 (2018)
[9] A. Norrman, J. J. Gil, A. T. Friberg, T. Setälä, Opt. Lett. 44, 215 (2019)
[10] J. S. Eismann, L. H. Nicholls, D. J. Roth, M. A. Alonso, P. Banzer, F. J. Rodríguez-Fortuño, A. V. Zayats, F. Nori, K. Y. Bliokh, Nat. Photonics **15**, 156 (2021)
[11] J. J. Gil, A. T. Friberg, A. Norrman, T. Setälä, New J. Phys. 23, 063059 (2021)
[12] J. J. Gil, A. Norrman, A. T. Friberg, T. Setälä, Opt. Lett. 44, 3578 (2019)
[13] Y. Chen, F. Wang, Z. Dong, Y. Cai, A. Norrman, J. J. Gil, A. T. Friberg, T. Setälä, Phys. Rev. A 104, 013516 (2021)

*Corresponding author: andreas.norrman@uef.fi

# Optical vortex induced forward transfer for printed electronics and photonics

**Takashige Omatsu**[*1,2]

*1. Graduate School of Engineering, Chiba University, 1-33, Yayoi-cho, Inage-ku, Chiba, 263-8522 JAPAN*
*2. Molecular Chirality Research Center, Chiba University, 1-33, Yayoi-cho, Inage-ku, Chiba, 263-8522 JAPAN*

Laser induced forward transfer technologies allow the non-contact and cost/energy-saving 2-or 3-dimensional print of a variety of donor materials on a receiver substrate without any nozzle clogging, and they have been intensely studied in applications, such as printed photonics/electronics fabrication technology and bioprinting technology involving biological tissues, organs and cells [1,2]. Importantly, most studies of laser induced forward transfer have still been performed by employing a conventional Gaussian beam with a planar wavefront.

Optical vortex, that is a helical light field, possesses an annular spatial form and an orbital angular momentum (OAM) $\ell$ (OAM), associated with its spiral wavefront with an on-axis phase singularity characterized by an integer $\ell$ termed a topological charge [3]. Also, circularly polarized light field carries a spin angular momentum s (SAM), associated with its helical electric field. Thus, circularly polarized optical vortex exhibits a total angular momentum J$(=\ell+$s, TAM), defined as the sum of the OAM and SAM [4]. We are currently proposing an entirely exotic direct print technology, that is optical vortex laser induced forward transfer, in which the optical vortex twists the irradiated materials, such as even solids and high viscosity liquids, to eject and propel a pico-litre (pL)-scale spinning droplet with a long flight distance through the interaction between OAM and irradiated materials. Going beyond the conventional ink-jet printing and laser induced forward transfer technologies, the optical vortex laser induced forward transfer enables the direct print of ultrahigh viscosity donor materials with ultrahigh spatial resolution [5], and it also provides us a new value, that is the exotic fabrication of ring-shaped structures composed of hexagonal close-packed multi-layered nanoparticles with structural colours in the printed dots, without any additional processes [6]. We believe that the optical vortex laser induced forward transfer will pave the way towards the development of advanced photonic/plasmonic devices and next generation bio-printing technologies.

In this presentation, we report here on the 2-dimensional print of micron-scale well-aligned fine dots formed of close-packed and sintered gold nanoparticles by employing the OV-LIFT with the aid of SAM.

A high-density gold nanoparticles (diameter: $\sim 130 \pm 70$ nm ) water/glycerol suspension (viscosity: $10 \sim 20$mPa$\cdot$s ) was used as a donor. The donor was dropped on a glass substrate to form a liquid film (thickness: $\sim 50\mu$m ). A nanosecond green first-order optical vortex pulse ( $\ell = 1$, wavelength: 532 nm, pulse duration: $\sim 2$ ns ) was focused onto the donor film, so as to eject a single donor droplet. The focused optical vortex pulse then exhibited an annular spot with a diameter of $35\mu$m and an energy of 0.4 $\mu$J. The ejected donor droplet was forwarded and printed on a glass receiver substrate placed 0.5 mm away from the film.

Intriguingly, optical vortex pulse enabled the print of close-packed dots with a diameter of $< 50\mu$m, whereas Gaussian beam produced only nonuniform dots (diameter: $80\mu$m ) with aggregations of gold nanoparticles and undesired satellite debris.

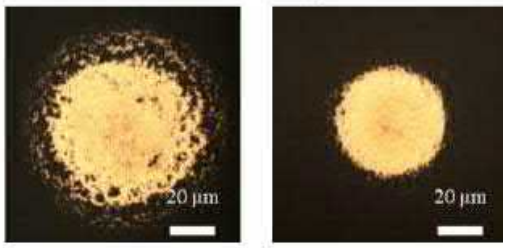


Figure 1: Printed dots by (left) Gaussian and (right) optical vortex $(\mathrm{J}=2)$ beams.

Furthermore, circularly polarized optical vortex pulse with $\mathrm{J}=2(\ell=1,\ \mathrm{s}=1)$ was capable of printing ultrafine dots with better close-packed gold nanoparticles, manifesting that OAM of optical vortex forces the droplet to spin, thereby yielding the close-packing and sintered of gold nanoparticles. Surprisingly, the printed dots were also slightly sintered, as evidenced by low electric resistance $\left(\sim 10^{-7}\Omega\cdot\mathrm{m}\right)$. It is noteworthy that optical vortex pulse with $J=0(\ell=1, s=-1)$ generated only worse close-packed dots without sintering effects. Figure 1 shows the printed dots by the irradiation of Gaussian and optical vortex $(\mathrm{J}=2)$ beams.

To understand fully the mechanism of this exotic phenomenon, the numerical analysis of the ejection of the spinning microdroplet based on hydrodynamics will be further required.

We have discovered that the optical vortex enables the direct print of ultrafine dots with close-packed and sintered gold nanoparticles owing to OAM transfer effects with the aid of SAM. The optical vortex laser-induced forward transfer technique will open the door towards next-generation printed photonics/electronics.

**References**

[1] J. M. Fernández-Pradas, P. Sopeña, S. González-Torres, A. Arrese, J. Cirera, P. Serra, "Laser-induced forward transfer for printed electronics applications," Appl. Phys. A Mater. Sci. Process. 124, 1-8 (2018).
[2] Y. S. Rim, S. H. Bae, H. Chen, H. De Marco, Y. Yang, "Recent Progress in Materials and Devices toward Printable and Flexible Sensors," Adv. Mater. 28, 4415-4440 (2016).
[3] R. Nakamura, H. Kawaguchi, M. Iwata, A. Kaneko, R. Nagura, S. Kawano, K. Toyoda, K. Miyamoto, T. Omatsu, "Optical vortex-induced forward mass transfer: manifestation of helical trajectory of optical vortex," Opt. Express 27,38019 (2019).
[4] H. Kawaguchi, K. Umesato, K. Takahashi, K. Yamane, R. Morita, K. Yuyama, S. Kawano, K. Miyamoto, M. Kohri, T. Omatsu, "Generation of hexagonal close-packed ring- shaped structures using an optical vortex," Nanophotonics https://doi.org/10.1515/nanoph-2021-0437 https://doi.org/10.1515/nanoph-2021-0437 (2021).

*Corresponding author: omatsu@faculty.chiba-u.jp

# Three-dimensional polychromatic knots and skyrmionic textures via tightly-focused beams

**Emilio Pisanty** * [1,2,3], **Rodrigo Gutiérrez-Cuevas** [4]

*1. ICFO – The Insitute of Photonic Sciences, 08860 Castelldefels (Barcelona), Spain*
*2. Max Born Institute for Nonlinear Optics and Short Pulse Spectroscopy, 12489 Berlin, Germany*
*3. Department of Physics, King's College London, WC2R 2LS London, UK*
*4. Institut Fresnel, Aix-Marseille Université, 13397 Marseille, France*

The past two decades have uncovered a wide variety of paraxial and nonparaxial light beams that exhibit exotic and nontrivial topologies, from Möbius strips and ribbons to knotted structures in field lines and optical vortices. In particular, in recent work we showed that expanding the reach of topological optics to include polychromatic beams, for which the electric-field vector traces a complex curve in space over an optical cycle, allows for novel symmetries and novel topologies. For counter-rotating circular polarizations at frequencies $\omega$ and $2\omega$, this Lissajous figure forms a trefoil, and if the individual beams contain phase singularities, this trefoil folds into itself with a novel symmetry (invariance under coordinated rotations) and a novel topology (equivalent to a torus knot) [1]. However, due to the use of paraxial beams, this torus-knot topology was only observed in a synthetic space that lifted the paraxial polarization components into a separate, synthetic dimension.

In this work, we show how this restriction can be lifted by combining counter-propagating tightly-focused optical vector vortices of frequencies $\omega$ and $2\omega$. When suitably tuned, a radially-polarized nonparaxial vector vortex becomes fully circularly polarized in the radial-longitudinal plane. The combination of two such forward-circular polarizations at different frequencies, and with different azimuthal phase gradients, then produces a fully three-dimensional trefoil polarization field with the explicit topology of a torus knot or a torus link [2].

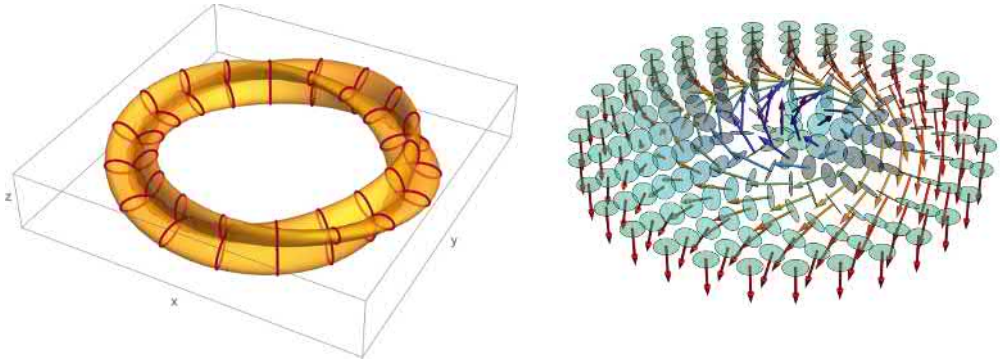


**Fig. 1:** (left) Trefoil Lissajous figures following the electric field of a tightly-focused bichromatic vector vortex beam, with the trefoil tips forming a nontrivial torus link. (right) Each individual tightly-focused vector vortex forms an optical skyrmionic spin texture: at every point the field is circularly polarized, and all orientations of the polarization circle are represented.

In addition to this nontrivial topology in the combined bichromatic field, each tightly-focused radial vector vortex also presents a nontrivial topology of its own. Indeed, the creation of a fully-circular polarization in the radial-longitudinal plane carries an additional consequence: the field is fully circularly polarized (or very close to that) at all points in space. The vortex nature of the field manifests itself in the orientation of this circular polarization, which – as the position ranges over the focal plane – covers all the possible directions. In other words, the tight focusing of a suitable vector vortex beam produces a skyrmionic spin texture [3], analogous to recent achievements in evanescent waves near plasmonic surfaces, but with the added advantage that it occurs in free space, opening further avenues for the use of topological optics as an interface for topological physical phenomena in solid-state and cold-atom systems.

## References

[1] E. Pisanty et al. Nat. Photon. **13** 569 (2019)
[2] E. Pisanty et al. In preparation (2022).
[3] R. Gutiérrez-Cuevas and E. Pisanty. J. Opt. **23** 024004 (2021)

*Corresponding author: emilio.pisanty@kcl.ac.uk

# Magnetic Helicoidal Dichroism with XUV Light Carrying Orbital Angular Momentum

**M. Fanciulli**[*1,2], **M. Pancaldi** [3], **E. Pedersoli** [3], **M. Vimal** [1], **D. Bresteau** [1], **M. Luttmann** [1], **D. De Angelis** [3], **P. R. Ribic** [3], **B.Rösner** [4], **C. David** [4], **C. Spezzani** [3], **M. Manfredda** [3], **R. Sousa** [5], **I.-L. Prejbeanu** [5], **L. Vila** [5], **B. Dieny** [5], **G. De Ninno** [3,6], **F. Capotondi** [3], **M. Sacchi** [7,8], **T. Ruchon**[†1]

*1. LIDYL, Université Paris-Saclay, CEA, CNRS, 91191 Gif-sur-Yvette, France*
*2. Laboratoire de Physique des Matériaux et Surfaces, CY Cergy Paris Université, 95031 Cergy-Pontoise, France*
*3. Elettra-Sincrotrone Trieste S.C.p.A., 34149 Basovizza, Trieste, Italy*
*4. Paul Scherrer Institut, 5232 Villigen, Switzerland*
*5. IRIG-SPINTEC, Université Grenoble Alpes, CNRS, CEA, Grenoble INP, 38000 Grenoble, France*
*6. Laboratory of Quantum Optics, University of Nova Gorica, 5001 Nova Gorica, Slovenia*
*7. Institut des NanoSciences de Paris, CNRS, Sorbonne Université, 75005 Paris, France*
*8. Synchrotron SOLEIL, L'Orme des Merisiers, Saint-Aubin, B.P.48, 91192 Gif-sur-Yvette, France*

After finding many applications in the visible range, OAM beams with XUV wavelengths and ultra-short pulse duration, in the femtosecond to attosecond ranges, became available recently at high-harmonic generation (HHG) and free-electron laser (FEL) sources [1-3], widening considerably their application range. However, it has thus far found very scarce applications for magnetooptics, which rather harnesses the spin angular momentum of light to investigate and control magnetization, through the Faraday and Kerr effects.

Recently, we analysed theoretically the interaction of OAM beams with magnetic structures featuring non-uniform magnetization, in particular of XUV beams with magnetic vortices consisting of a curling in-plane magnetization [4]. We predicted that the far field intensity profile encodes the vortex symmetry in a way that depends on the sign and value of the topological charge $\ell$, an effect deriving from the inhomogeneous modification of the regular reflectivity coefficients by the local magnetization. We named this effect Magnetic Helicoidal Dichroism (MHD). As for magnetic circular dichroism, MHD can be observed by inverting the sign of either the orbital momentum or of the magnetization, i.e. by switching the handedness of either the light helicoidal wavefront, or of the magnetic vortex.

In this contribution we report on the first experimental evidence of MHD (Fig. 1) obtained at the DiProI station of the FERMI free-electron laser source by measuring the scattered intensity from an Fe-Ni-alloy dot forming a magnetic vortex. The photon energy of the $\sim 100$ fs long pulses was set to 52.8eV($\sim 23$ nm wavelength ) in order to match the Fe $3p \rightarrow 3$ d core resonance, enhancing magnetooptical effects at XUV wavelengths and providing element selectivity. The scattered intensity data, collected as a function of $\ell$ and of the magnetic vortex winding sense, compared well to theoretical model predictions [5]. We show also how the short pulses of the free-electron laser OAM beam make it possible to follow the evolution of the magnetization topology at the sub-ps timescale after an optical excitation.

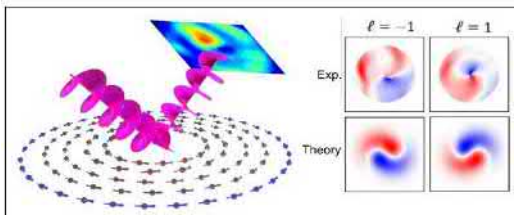


Figure 1: Left) Experimental sketch for the observation of magnetic helicoidal dichroism. (Right panel) Differences between the images acquired for two opposite curling senses of the magnetic vortex, showing a typical 2*D* chiral structure, which depends on the incoming orbital angular momentum (top). Theoretical result (bottom).

The match between theory and experiments confirms the potential of the new toolset provided by MHD for studying complex magnetic structures and, in particular, for addressing their laser-triggered ultrafast dynamics. Understanding the interaction of OAM-light with a magnetic vortex has many potential interests. At the fundamental level, it allows to observe a new kind of dichroism, to study the role of photon spin-orbit coupling mediated by magnetization, as well as to explore new possibilities of angular momentum transfer between light and matter. In terms of applications, MHD in reflection can be exploited as a new spectroscopic tool joining the family of magnetic dichroism techniques. For their symmetry and size, magnetic vortices can be considered as an ideal benchmark sample to explore the interaction with OAM beams; moreover, given their rich dynamical response in the ultrafast domain, they are promising structure for light manipulation of the magnetization topology.

## References

[1] R. Géneaux, et al., Nat. Comm., 7, 12583 (2016).
[2] D. Gauthier, et al., Nat. Comm., 8, 14971 (2017).
[3] P. R. Ribič, et al, Phys. Rev. X 7, 031036 (2017).
[4] M. Fanciulli et al., Phys. Rev. A, 103, 013501 (2021)
[5] M. Fanciulli et al., accepted in Phys. Rev. Lett. (https://arxiv.org/abs/2103.13697 https://arxiv.org/abs/2103.13697)

[*]Corresponding author: mauro.fanciulli@u-cergy.fr
[†]Corresponding author: thierry.ruchon@cea.fr

# Transfer of optical orbital angular momentum to the transverse motion of the center of mass of a single trapped ion

**Felix Stopp[1], Maurizio Verde[1], Milton Katz[2], Martín Drechsler[2], Sebastian Wolf[1], Ferdinand Schmidt-Kaler[1], Christian T. Schmiegelow[*2]**

*1. QUANTUM, Institut für Physik, Johannes Gutenberg-Universität Mainz, Staudingerweg 7, 55128 Mainz*
*2. Departamento de Física and IFIBA, FCEN, Universidad de Buenos Aires, Ciudad Universitaria, Pabellon I, 1428 Ciudad de Buenos Aires*

We show how light carrying orbital angular momentum can excite the motion of a single trapped ion in a plane transverse beam's propagation direction. We use a singly charged $^{40}$Ca ion confined in the 3D harmonic potential of a Paul trap. The narrow $S_{1/2}$ to $D_{5/2}$ transition near 729 nm splits in resolved Zeeman sub-levels under an external magnetic field. Also, due to the 3D confining, motional sidebands occur in the spectrum. By tuning the laser frequency over these resonances we verify that the orbital angular momentum of the beam can either be transferred to the center of mass motion of the ion or to the internal/relative motion of the electron with respect to the core. Indeed, we observe the appearance of transitions in which the atom's center of mass motion can increment or reduce its vibrational motion in a direction which is forbidden for a plane or Gaussian beam. We use a Laguerre-Gauss beam containing a total of two quanta of angular momentum, one from the polarization and one from its topological structure. As we demonstrated previously, such beams can excite transitions with a change of two units in the atomic magnetic number. In that case, the two units of angular momentum from the beam are transferred to the relative motion of the valence electron with respect to the core [1,2]. Here we show that the orbital angular momentum content of the beam can also be transferred to the movement of the center of mass of the trapped ion. Moreover, we show that if we cool this motional mode close to the ground state, the red and blue sidebands show coherent oscillations governed by a new kind of Lamb-Dicke parameter which now depends on the ratio of the ion's wave packet size with respect to the spatial extension of the transverse gradient in the vortex light field.

## References

[1] Schmiegelow, C. T.; Schulz, J.; Kaufmann, H.; Ruster, T.; Poschinger, U. G. and Schmidt-Kaler, F.; Nature communications, 7, 12998 (2016)
[2] Schmiegelow, C.T. and Schmidt-Kaler, F.; The European Physical Journal D 66, 157 (2012)

[*]Corresponding author: presenting.author@email.com

# Recent development of OAM mode generation for quantum communication

**Mujtaba Zahidy**[*1], **Yaoxin Liu** [1], **Daniele Cozzolino** [1], **Hamid Tebyanian** [3], **Yunhong Ding**[1], **Toshio Morioka**[1], **Leif K. Oxenløwe**[1], **Davide Bacco**[1,2]

*1. Center for Silicon Photonics for Optical Communication (SPOC), Department of Photonics Engineering, Technical University of Denmark, Kgs. Lyngby, Denmark*

*2. QTI S.r.l., largo Enrico Fermi 6, 50125, Firenze, Italy*

*3. Department of Mathematics, University of York, Heslington, York, YO10 5DD, United Kingdom*

Orbital angular momentum (OAM) degree of freedom of light constitutes an important resource for both classical and quantum information technologies. OAM mode multiplexing significantly increases data transmission capacity in classical and quantum communications while OAM unbounded nature allows for generating high-dimensional quantum states that are useful to increase the secret key rate or resilience against errors in quantum key distribution (QKD) [1]. QKD employing OAM modes of light has been already demonstrated [2], however, the most significant obstacle on the way of fully exploiting its potential is the fast generation of these modes and manipulating them at high rate in an scalable fashion. We here present a silcion based photonic integrated chip, Fig. 1, able to excite orbital angular momentum modes in a ring-core fiber. The chip is proved to perform parallel quantum key distribution using 2 and 3 different OAM modes simultaneously. A ring-core fiber of 800m length was used as the quantum channel. We achieved a crosstalk in the range of -10 to -18 dB between modes which allowed us to perform QKD with a quantum bit error rate of 1-4%.

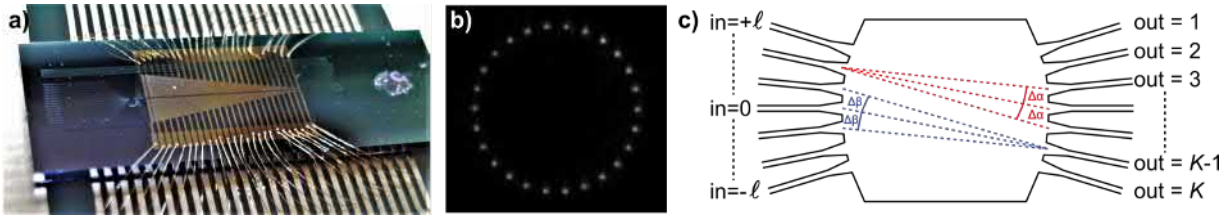


**Fig. 1:** a) Picture shows the photonic integrated device used in the experiment. b) Infrared image of the grating couplers output. The 26 output are arranged on a ring of 325.5$\mu m$ c) Schematic of the star-coupler structure.

In addition, by using the same device, we introduced a new method to generate genuine random numbers exploiting an undesirable drawback of the channel, thus OAM mode crosstalk. Random numbers are an invaluable resource with many applications in science, cryptography, etc. In particular, quantum key distribution requires that generation of states is completely random, hence, a true random number generator is necessary to guarantee successful transmission of a secure key.

Measurement result in quantum mechanics is intrinsically random. Many degrees of freedom have been investigated for generation of randomness. However, not adequate attention has been paid to the orbital angular momentum of light. In [4], we present a quantum random number generator based on the intrinsic randomness inherited from the superposition of orbital angular momentum modes caused by the crosstalk inside a ring-core fiber. By introducing a partially controlled crosstalk, a superposition of OAM modes is generated upon coupling light in the ring-core fiber. The modes undergo a mode-to-time bin transformation which helps us to separately detect them. Performing time-of-arrival measurement in single-photon regime allows us to generate random numbers with a rate of higher than 10 Mbit/s after privacy amplification. To summarize, we exploit a silicon photonic chip coupled to a ring-core fiber, for generating parallel quantum keys in a space-division-multiplexing approach and for demonstrating a new method for high-key-rate throughput quantum random number generator.

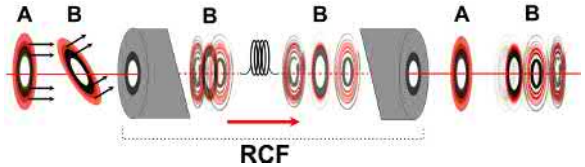


**Fig. 2:** A superposition of OAM modes is generated by entering the RCF with a tilted input. Above, input mode 'A' will not experience distortion as its wavefront is aligned to the RCF, however, input mode 'B' is transformed to a superposition of different modes due to the coupling angle. Various modes are separated along the fiber due to their different group velocities.

These experiment sets the first steps towards quantum orbital angular momentum division multiplexing enabled by a compact and light-weight silicon chip, and further pushes the development of integrated scalable devices supporting orbital angular momentum modes.

## References

[1] Daniele Cozzolino, Beatrice Da Lio, Davide Bacco, Leif Katsuo Oxenløwe, Adv.Quantum Technol. **2019**, 2, 1900038

[2] Daniele Cozzolino, Davide Bacco, Beatrice Da Lio, Kasper Ingerslev, Yunhong Ding, Kjeld Dalgaard, Poul Kristensen, Michael Galili, Karsten Rottwitt, Siddharth Ramachandran, Leif Katsuo Oxenløwe, Phys. Rev. Applied **11**, 064058 (2019)

[3] Mujtaba Zahidy, Yaoxin Liu, Daniele Cozzolino, Yunhong Ding, Toshio Morioka, Leif K. Oxenløwe and Davide Bacco, nanoph **2021** 0500 (2021)

[4] Mujtaba Zahidy, Hamid Tebyanian, Daniele Cozzolino, Yaoxin Liu, Yunhong Ding, Toshio Morioka, Leif K Oxenløwe, Davide Bacco, AVS Quantum Sci. **4** 011402 (2022)

[*]Corresponding author: muzah@fotonik.dtu.dk

# Abstracts

## Posters

# Generating Twisted Light using Archimedean Spirals: A Real-Space Real-Time Study

**Esra Ilke Albar**[*1], **Valeriia P. Kosheleva**[†1], **Franco Bonafe** [1], **Michael Ruggenthaler**[1], **Angel Rubio**[1,2], **Heiko Appel** [1]
*1. Max Planck Institute for the Structure and Dynamics of Matter, Hamburg, Germany*
*2. Center for Computational Quantum Physics (CCQ), Flatiron Institute, 162 Fifth Avenue, New York NY 10010, USA*

The fact that light can carry not only energy and momentum but also orbital angular momentum (OAM) was predicted theoretically more than 30 years ago [1], [2]. The light beams with nonzero projection OAM onto the propagation direction are called twisted (vortex) light. These beams are being studied extensively in various fields of physics (see reviews [3], [4] and references therein). Nowadays, the twisted light beams in optical range can be routinely produced by various methods [5], [6], however, their on-chip generation remains an open question. In this sense, metallic Archimedean spirals are good candidates to produce light with nonzero OAM [7]. Henceforth, we consider the scattering of plane wave light by Archimedean spirals with the objective of twisted light production. Special emphasis is put on analyzing the "twisted" properties of the scattered radiation.

We perform numerical simulations of the process under consideration using the Maxwell solver of the real-time real-space Octopus code [8]. The circularly polarized plane-wave light is sent into a simulation box that contains an Archimedean spiral. We theoretically develop an approach within Riemann-Silberstein formalism [9] to investigate the scattered field in terms of total and orbital angular momentum. The generation of twisted light within this setup is based on the helical structure of the spiral which causes the transfer of orbital angular momentum to the electromagnetic field through light-matter interaction.

### References

[1] Boris Ya. Zel'dovich, N. F. Pilipetskiĭ, and V. V. Shkunov, Sov. Phys. Usp. **25**, 713 (1982).

[2] L. Allen, M. W. Beijersbergen, R. J. C. Spreeuw, and J. P. Woerdman, Phys. Rev. A **45**, 8185 (1992).

[3] B. A. Knyazev and V. G. Serbo, Physics-Uspekhi **61**, 449-479 (2018) .

[4] M. Babiker, D. L. Andrews, and V. E. Lembessis, J. Opt. **21**, 013001 (2019).

[5] R. Chen, H. Zhou, M. Moretti, X. Wang, and J. Li, IEEE Commun. Surv. Tutor. **22**, 840 (2020).

[6] X. Fang, H. Ren, K. Li, H. Luan, Y. Hua, Q. Zhang, X. Chen, and M. Gu, Adv. Opt. Photon. **13**, 772 (2021).

[7] R. M. Kerber, J. M. Fitzgerald, X. Xiao, S. S. Oh, S. A. Maier, V. Giannini, and D. E. Reiter, New Journal of Physics **20**, 095005 (2018).

[8] N. Tancogne-Dejean *et al*., J. Chem. Physics **152**, 124119 (2020).

[9] L. Silberstein, Annalen der Physik **327**, 579 (1907).

[*]Corresponding author: esra-ilke.albar@mpsd.mpg.de
[†]Corresponding author: valeriia.kosheleva@mpsd.mpg.de

# The Gouy Phase in Parametric Downconversion: Decoupling of Spatial and Spectral Degrees of Freedom

**Baghdasar Baghdasaryan**[*1,2], **Carlos Sevilla** [3], **Fabian Steinlechner**[†3,4], **Stephan Fritzsche**[1,2,4]

*1. Theoretisch-Physikalisches Institut, Friedrich-Schiller-Universität Jena, 07743 Jena, Germany*
*2. Helmholtz-Institut Jena, 07743 Jena, Germany*
*3. Fraunhofer Institute for Applied Optics and Precision Engineering IOF, 07745 Jena, Germany*
*4. Abbe Center of Photonics, Friedrich-Schiller-University Jena, 07745 Jena, Germany*

Spontaneous parametric down-conversion (SPDC) is a widely used source for studying and applying photonic entanglement [2]. Years of focused research have led to a solid understanding of the process, but a cohesive description of the paraxial two-photon state has yet to be achieved. In particular, SPDC is usually described in the narrowband or thin-crystal approximations at degenerate frequencies. Taking the full spectral dependence into account is an important step towards describing realistic experimental settings and engineering quantum states with high purity and efficiency. We derived a general expression for the spatio-temporal two-photon state that applies universally across common experimental settings and correctly describes the non-separability of spatial- and spectral modes. In particular, we find that higher-order spatial modes generated in SPDC have different spectral properties. This fact must be taken into account in the development of pure spatial entanglement. We formulate a criterion, how to decouple the spatial from the spectral degree of freedom by taking into account the Gouy Phase of interacting beams. This work provides new insights into the role of the Gouy phase in nonlinear processes and also into the preparation of engineered entangled states for multidimensional quantum information processing.

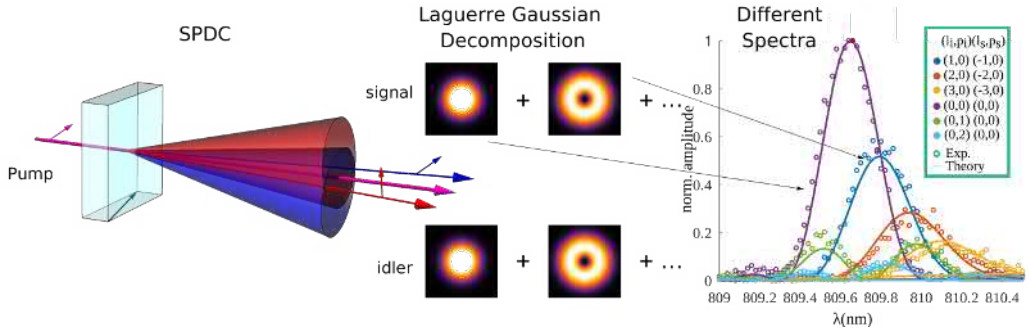


**Fig. 1:** In spontaneous parametric down-conversion (SPDC), a coherent laser interacts with a nonlinear crystal to convert high-energy photons into entangled photon pairs, also called signal and idler. The spatial degree of freedom (DoF) of generated photons can be investigated by performing a mode decomposition of the joint two-photon state in an appropriate basis. Since, under quasi-collinear geometries, orbital angular momentum (OAM) is conserved in SPDC, Laguerre Gaussian (LG) modes, which are eigenfunctions of OAM [1], are very often used to describe the spatial DoF of the two-photon state [3]. We have found theoretically and confirmed experimentally that the LG modes of the decomposed the two-photon state possess different spectra.

[1] R. Fickler, R. Lapkiewicz, W. N. Plick, M. Krenn, C. Schaeff, S. Ramelow, and A. Zeilinger, Science **338**, 640 (2012)
[2] M. Erhard, R. Fickler, M. Krenn, and A. Zeilinger, Light: Science & Applications **7**, 17146 (2018).
[3] M. Krenn, M. Huber, R. Fickler, R. Lapkiewicz, S. Ramelow, and A. Zeilinger, Proc. Natl. Acad. Sci. USA **111**, 6243 (2014).

[*]Corresponding author: baghdasar.baghdasaryan@uni-jena.de
[†]Corresponding author: fabian.steinlechner@uni-jena.de

# Detection of Singular Beams on Higher Order Poincare Sphere

**Sarvesh Bansal**[*1], **P. Senthilkumaran** [1,2]
*1. Department of Physics, Indian Institute of Technology Delhi, Hauz Khas, New Delhi, 110016, India*
*2. Optics and Photonic Centre, Indian Institute of Technology Delhi, Hauz Khas, New Delhi, 110016, India*

A novel and elegant method to find the coordinates of the points used to represent polarization singular beams [1] on Higher Order Poincare Sphere (HOPS)[2] is presented. Polarization singularities are the points where anyone of polarization parameters is undefined. Every point (except poles) on a HOPS represents a structured beam with constant ellipticity but varying azimuth across the beam cross-section. HOPS beams have shown applications in many field like tight focusing, imaging, particle acceleration etc. Due to immense potential of HOPS beams it is desired to have simple detection methods. Currently existing methods include Stokes polarimetry and diffraction. Complex Stokes field ($S_{12} = S_1 + iS_2$), constructed using normalized Stokes parameters, is mostly used for the identification of HOPS beams. In the Stokes field the polarization singularities appear as phase vortices of different topological charges. But all the beams represented by same HOPS have similar Stokes phase distribution and same Stokes index. Due to the degeneracy in Stokes index it cannot be used to differentiate two beams on same HOPS. Similarly, HOPS beams have degenerate diffraction pattern and to find the location of beams on HOPS diffraction is required to combined with polarimetry which require multiple measurements [3]. Here, we present simple method to detect the HOPS beams based on the single intensity measurement.

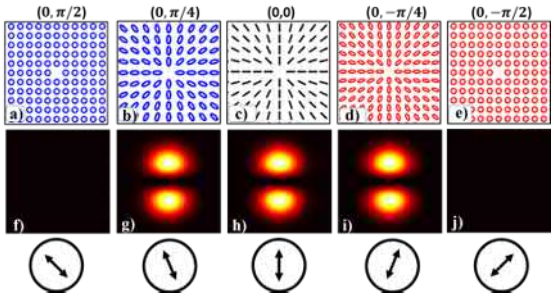


**Fig. 1:** First row depicts the polarization distribution of five incident beams represented by point on constant longitude (0°) of HOPS of index +1. Longitude and latitude of the beam on HOPS is given above each image. Second row depict the transmitted intensity distribution from QWP and polarizer combination. Polarizer orientation is given in last row for each case.

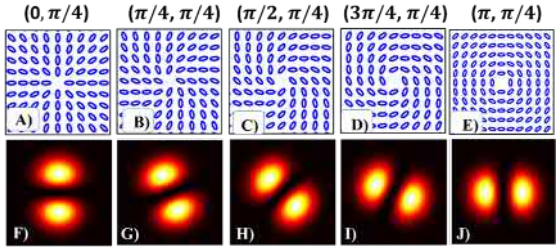


**Fig. 2:** First row depicts the polarization distribution of five incident beams represented by point on constant latitude ($\pi/4$) of HOPS of index +1. Longitude and latitude of the beam on HOPS is given above each image. Second row depict the transmitted intensity distribution from QWP and polarizer combination. Polarizer is fixed at $\pi/8$ with respect to vertical.

A combination of quarter wave plate (QWP) and polarizer (P) is used to detect the coordinates of HOPS beams. When HOPS beam is passed through a combination of QWP-P, intensity lobs are observed in the transmitted beam as shown in Fig 1. These intensity lobs can be observed for particular angle of polarizer. At other orientation of polarizer clear intensity lobs are not observed. Orientation of intensity lobs and polarizer provides the longitude and latitude of the beams on HOPS respectively. Simulated results for HOPS beams with polarization index $+1$ is shown in Fig. 1 and Fig. 2. Figure 1(a-e) depicts the polarization distribution of incident beam on constant longitude (0°) of HOPS. Transmitted intensity from QWP-P arrangement is shown in Fig. 1(f-j) respectively. Polarizer orientation for each case is shown in the bottom row of Fig 1. It can be observed from the Fig. 1 that orientation of intensity lobs in the transmitted beam is same as all the beam are represented on the constant longitude. Polarizer orientation in each case is different which provides the information of different latitude point. Similarly, Fig. 2 (A-E) depict the polarization distribution of beams represented by constant latitude ($\pi/4$). Transmitted intensity from QWP-P combination is shown in Fig. 2(F-J) respectively. For Fig. 2 polarizer is oriented at fixed angle of $\pi/8$ with respect to vertical. It can be seen from Fig. 2 that as the longitude of the beam is changed, the intensity lobs rotate anticlockwise. So, using this method one can find the exact location of beams on HOPS.

## References

[1] I. Freund, Opt. Commun. **201**, 251-270 (2002).
[2] Giovanni Milione, H. I. Sztul, D. A. Nolan, and R. R. Alfano, PRL 107, 053601 (2011).
[3] Gauri Arora, S. Deepa, Saba N. Khan and P. Senthilkumaran, Sci Rep 10, 20759 (2020)

*Corresponding author: bansalsarvesh.s@gmail.com

# Observation of the quantum Gouy phase

**Markus Hiekkamäki**[*1], **Rafael Barros**[†1], **Marco Ornigotti** [1], **Robert Fickler** [1]
*1. Photonics Laboratory, Physics Unit, Tampere University, Tampere, FI-33720, Finland*

When a laser beam propagates through its focus, it experiences a phase delay proportional to the order of its spatial mode, a phenomenon known as the Gouy phase anomaly. Such a phase delay originates from the transverse spatial confinement, or equivalently, the spread in the transverse momentum of the propagating wave, and it is not limited to light waves. Gouy phase analogs have been observed in different quantum systems such as surface plasmon-polaritons, electron waves and matter waves. In optics, the Gouy phase plays an important role in optical cavities, optical tweezers, spatial mode sorters, and metrology [1].

In this work, we present the first observation of the phase delay experienced by spatially structured photon number states propagating through a focus, which we call the quantum Gouy phase. We show experimentally that the quantum Gouy phase of N-photon states is N times that of the mode the photons occupy. We show that the aforementioned speedup of the quantum Gouy phase enables quantum-enhanced metrology of longitudinal displacements, which we demonstrate experimentally using two-photon N00N states.

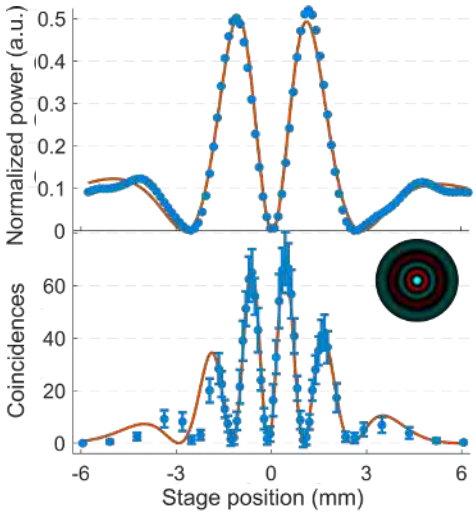


Figure 1: Measured classical (top) and quantum (bottom) interference fringes.

In our experiment, two photons from a pair are spatially structured in orthogonal superpositions of two radial Laguerre-Gaussian modes, and brought onto the same path to form a two-photon radial N00N state [2]. As the two occupied modes have different radial orders, they interfere in propagation due to the difference in their Gouy phases. For the N00N state, the interference manifests in the biphoton spatial probability distribution, and it occurs due to the difference between the quantum Gouy phases. We measure the quantum interference by counting coincidence clicks after coupling the photons to a single-mode fiber moving longitudinally through the focus.

We show in Fig.1 one example measurement, where the interference signal is shown for a superposition of coherent LG beams with $\ell = 0$ and $p = 0,4$ (top) and a 2-photon N00N state occupying the same spatial modes (bottom). The halved period of the 2-photon interference shows the speedup of the two-photon Gouy phase and reveals the quantum advantage of radial N00N states for longitudinal displacement measurements. We certify the quantum advantage by showing that the quantum Fisher information for the longitudinal propagation of radial N00N states features Heisenberg scaling. Lastly, we show that the interference observed with the quantum Gouy phase cannot be retrieved by classical light with half the wavelength, contradicting the standard rule of thumb of N00N state phenomena.

## References

[1] Simin Feng and Herbert G Winful, "Physical origin of the gouy phase shift," Optics letters 26, 485–487 (2001).
[2] Markus Hiekkamäki, Frédéric Bouchard, and Robert Fickler, "Photonic angular superresolution using twisted N00N states" Physical review letters 127.26 (2021): 263601.

[*]Corresponding author: markus.hiekkamaki@tuni.fi
[†]Corresponding author: rafael.barros@tuni.fi

# Misalignment of spin densities in helicity lattices

**Ben W. Butler**[*1], **Jörg B. Götte** [1]
*1. School of Physics and Astronomy, University of Glasgow, Glasgow, G12 8QQ, Scotland*

In this work we reveal that the electric and magnetic parts of the optical spin density are generally misaligned in helicity lattices, which are optical fields in which the intensity of the electric field is homogeneous but the optical helicity varies spatially. Based on this we conclude that the correct form for the electromagnetic (EM) spin density is dual symmetric, that is, invariant under duality transformations.

Optical spin angular momentum is closely related to the polarisation of the field. It is unsurprising then that the spin is intimately connected to the optical helicity, a measure of the handedness of the EM field. Indeed, the helicity density $h$ and spin density $\mathbf{s}$ obey a continuity equation of the form

$$\frac{\partial h}{\partial t} + c\nabla \cdot \mathbf{s} = 0, \tag{1}$$

identical in form to the one obeyed by the EM energy and momentum.

It is well-known that a force proportional to the gradient of the electric field intensity can be used to trap atoms and molecules using laser light. When several lasers are used in conjunction the light may form periodic structures, leading to so-called optical lattices. Less-well-known are optical helicity lattices, in which the electric energy density is constant—and thus the gradient force vanishes—whilst the optical helicity density varies periodically in space. Such lattices therefore offer exciting opportunities for the separation of chiral enantiomers via the chirally discriminating helicity force proposed by Cameron et al [1]. A variety of helicity structures have been proposed which often exhibit interesting and novel physics in their own right, such as regions of bright superchirality. By this we mean regions which display greater enantioselectivity than circularly polarised light, without attenuation in electric field intensity [2] [3]. An example of a helicity lattice is given in Figure 1.

The helicity and spin densities are not unique (again this mirrors the situation with the EM energy and momentum). Two simple and potentially natural expressions for the spin density are what we term the electric spin density, $\mathbf{s}_e$, and the magnetic spin density, $\mathbf{s}_m$. However, neither of these forms is invariant under duality transformations, and thus they are quite unsatisfactory on symmetry grounds [4]. We can form a dual-symmetric expression simply as $\mathbf{s} = (\mathbf{s}_e + \mathbf{s}_m)/2$. It has been suggested that a dual-symmetric helicity density plays a role in chiral-light matter interactions [1], and given the spin-helicity connection noted above, we would expect the spin density to be physically significant as well. The question of which spin density to choose therefore becomes pertinent. The choice is perhaps of no consequence in plane waves and collimated laser beams, in which $\mathbf{s}_e$ and $\mathbf{s}_m$ are generally aligned. However, we demonstrate in this work that this is not the case in helicity lattices. Their misalignment suggests they cannot be used interchangeably when considering interactions with matter. Given the form of the physically-relevant helicity density is dual-symmetric, and the relationship in Eq. (1), we conclude that the correct choice for the spin density should also be the one invariant under duality transformation, thus supporting the conclusion based on electric-magnetic symmetry.

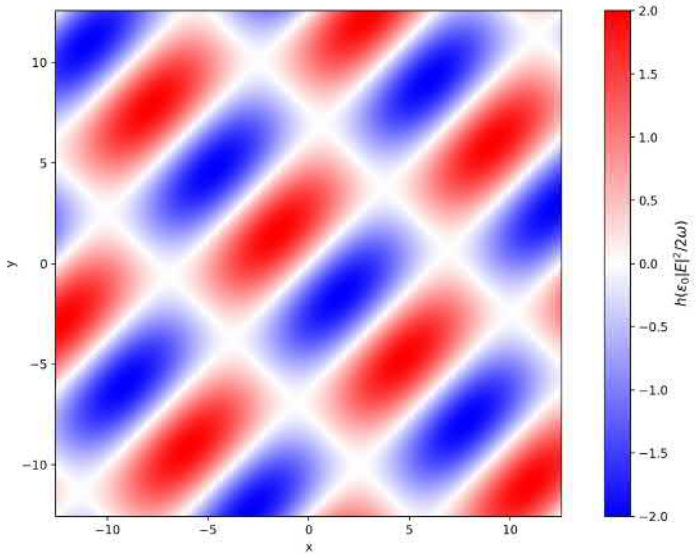


**Fig. 1:** A helicity lattice formed from the superposition of three monochromatic plane waves.

## References

[1] R. P. Cameron, S. M. Barnett, A. M. Yao, New J. Phys. **16** 013020 (2014)
[2] K. C. van Kruining, R. P. Cameron, J. B. Götte, Optica, **5** 1091-1098 (2018)
[3] Y. Tang, E. Cohen, Phys. Rev. Lett. **104** 163901 (2010)
[4] S. M. Barnett, J. Mod. Opt. **57** 1339-1343 (2010)

*Corresponding author: B.Butler.1@research.gla.ac.uk

# Micromanipulation using twisted photons to test superkicks and momentum densities

**Andrei Afanasev**[*1], **Carl E. Carlson**[†2], **Asmita Mukherjee** [3]
*1. Department of Physics, The George Washington University, Washington, DC 20052, USA*
*2. Physics Department, William & Mary, Williamsburg, Virginia 23187, USA*
*3. Department of Physics, Indian Institute of Technology Bombay, Powai, Mumbai 400076, India*

Localized manipulation of small objects using twisted photons can be instrumental in observing large transverse kicks—superkicks—and for finding which expressions for the local momentum and angular momentum densities are correct.

Canonical expressions for the energy-momentum tensor are obtained from symmetry transformations on the Lagrangian using the Noether construction. The result is not generally symmetric in its two indices, but can be symmetrized by adding a total derivative. The subsequent expressions for the momentum and angular momentum are the same when integrated over all space but are not in general locally the same. In particular, the canonical and symmetrized momentum density expressions are not the same for structured light, for example, for twisted photons. Hence they predict different results for forces and angular momenta induced on small test objects.

We will show, with numerical estimates of the size of the effects, testable situations where the canonical and symmetrized forms predict very different torques or very different superkicks on small objects, over a broad range of circumstances. We will also comment on cases where the predicted radiation forces on small objects are very different based on momentum densities obtained from the canonical and symmetrized cases.

[*]Corresponding author: afanas@gwu.edu
[†]Corresponding author: carlson@physics.wm.edu

# Angular momentum redirection phases of vector beams

**A. McWilliam**[*1], **C. M. Cisowski**[†1], **R. Bennett** [1], **S. Franke-Arnold** [1]
*1. School of Physics and Astronomy, University of Glasgow, Glasgow G128QQ, UK.*

We study experimentally and theoretically the transformation of scalar and vectorial fields of light along a closed non-planar trajectory. The intensity, polarization, and vector field profiles undergo a rotation proportional to the solid angle formed on the sphere of angular momentum directions as illustrated in Fig. 1 for a vector field [1]. We interpret these rotations in terms of geometric phases. For homogeneously polarized beams, the rotation can be understood using spin-redirection phases [2, 3] whereas the rotation of the intensity profile can be attributed to orbital redirection phases. Vector beams acquire a geometric phase proportional to the total angular momentum of the beam $j = l + \sigma$ where $l$ is the topological charge and $\sigma$ is the helicity. In the case of vector beams with $j = 0$ such as radial and azimuthal vector beams, the polarization profile appears unrotated and the beams can be considered as eigenmodes of the system. Angular redirection phases can affect optical communications channels based on optical fibres due to twisting and bending effects [4], they can also be witnessed in twisted optical cavities and mirror-based resonators [5, 6].

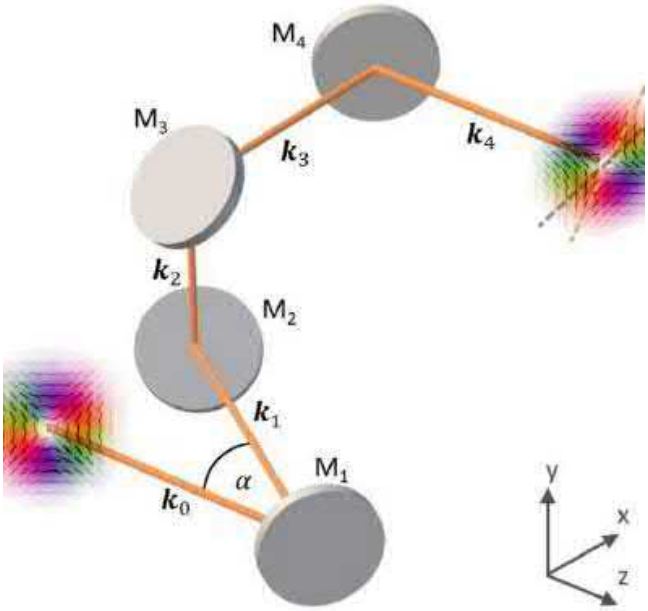


**Fig. 1:** $AnLG_0^1\sigma_{LCP} + LG_0^{-1}\sigma_{RCP}$ vector beam $(j \neq 0)$ taken along a non-planar trajectory using a series of mirror reflections presents a rotated polarization profile as the beam recovers its initial orientation.

## References

[1] A. McWilliam, C. M. Cisowski, R. Bennet1, S. Franke-Arnold, Nanophotonics (2021).
[2] S. M. Rytov, Dokl. Akad. Nauk SSSR, 18, 2, 263-266 (1938).
[3] V. V. Vladimirsky, Dokl. Akad. Nauk SSSR, 31, 222 (1941).
[4] Z. Ma and S. Ramachandran, Nanophotonics, 10, 1, 209-224 (2021).
[5] S. J. M. Habraken and G. Nienhuis, Phys. Rev. A, 75, 033819 (2007).
[6] A. Forbes, Laser Photon. Rev. 13, 11, 1900140 (2019).

[*]Corresponding author: a.mcwilliam.1@research.gla.ac.uk
[†]Corresponding author: clairemarie.cisowski@glasgow.ac.uk

# Measuring the phase and polarization of structured vector beams with quadriwave lateral shearing interferometry

**Timothé Denys**[*1], **Miguel Alonso**[†1,2], **Guillaume Baffou**[‡1], **Rodrigo Gutierrez Cuevas**[§3]

*1. Fresnel Institute, CNRS, Aix Marseille University, Centrale Marseille, Marseille, France*
*2. The Institute of Optics, University or Rochester, Rochester NY 14627, USA*
*3. Langevin Institute, ESPCI Paris, PSL University, CNRS, 1 rue Jussieu, 75005 Paris, France*

A structured vector beam is characterized by its complex phase map and polarization distribution (as in Fig.1), even in the 2D (paraxial) case. Such beam properties are not directly accessible through standard intensity-imaging cameras, and require more elaborate devices to be recovered. The issue of converting phase information into measurable intensity variations has been addressed in several ways during recent years. Guillon et al. [1] list a few of the available solutions, such as common-path interferometers, point-diffraction interferometry, curvature sensing, or Shack-Hartmann wavefront sensing for example, with the latter being the most popular. At the heart of this technique lies the so-called Hartmann mask which imprints intensity variations on the beam to be imaged, so that interferogram patterns are obtained from which the phase can be retrieved.

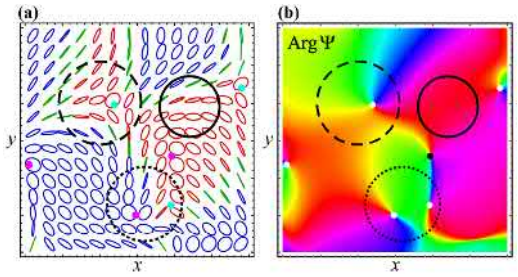


**Fig. 1:** Polarization distribution (a) and Phase map (b) of a structured vector beam, adapted from [2]

Quadriwave lateral shearing interferometry (QLSI) technique uses a similar principle, with a modified Hartmann mask (or grating, pictured in Fig.2.c) that allows for more resolution while still being easy to use and robust against instabilities [3]. From the obtained interferogram, both the intensity and phase can be recovered by looking respectively at the first and higher orders of the Fourier frequency spectrum, containing phase gradients information. This general quantitative phase microscopy (QPM) technique has been widely used for regular wavefront characterization, mostly for bio-imaging and more recently in nanophotonics. Following the work by Guillon et al. [1], we propose to adapt the method to complex wavefront characterization, with a simple modification of the post-processing step, when the image involves a rotational part in the gradient maps.

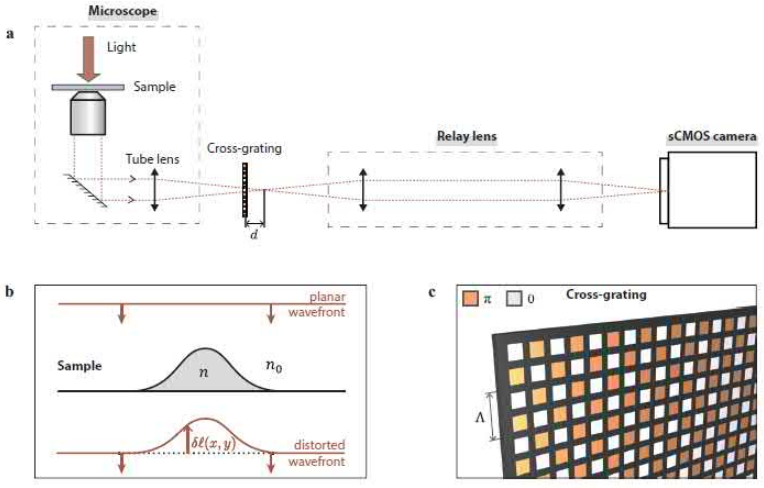


**Fig. 2:** Details of a QLSI camera, adapted from [4]

This project is funded under the **Excellence Initiative of Aix-Marseille University - A*MIDEX**, a French "Investissements d'Avenir" programme, and Agence Nationale de Recherche (ANR) through project ANR-21-CE24-0014-01.

## References

[1] Tengfei Wu, Pascal Berto, Marc Guillon, *Appl. Phys. Lett.* **118** 251102 (2021)
[2] Konstantin Y Bliokh, Miguel A Alonso, Mark R Dennis, *Rep. Prog. Phys.* **82** 122401 (2019)
[3] Guillaume Baffou, *J. Phys. D: Appl. Phys.* **54** 294002 (2021)
[4] Baptiste Marthy, Guillaume Baffou, arXiv:2203.06719v2 (15 Mar 2022)

[*]Corresponding author: timothe.denys@etu.univ-amu.fr
[†]Corresponding author: miguel.alonso@fresnel.fr
[‡]Corresponding author: guillaume.baffou@fresnel.fr
[§]Corresponding author: rodrigo.gutierrez-cuevas@espci.fr

# Ultra-long photonic quantum walks via liquid-crystal metasurfaces

**Francesco Di Colandrea**[*1], **Amin Babazadeh** [1,2], **Alexandre Dauphin** [3], **Pietro Massignan** [3,4], **Lorenzo Marrucci** [1], **Filippo Cardano**[†] [1]

*1. Dipartimento di Fisica, Università degli Studi di Napoli Federico II, Complesso Universitario di Monte Sant'Angelo, Via Cintia, 80126 Napoli, Italy*
*2. Faculty of Physics, University of Vienna, Boltzmanngasse 5, 1090, Vienna, Austria*
*3. ICFO – Institut de Ciencies Fotoniques, The Barcelona Institute of Science and Technology, 08860 Castelldefels, Spain*
*4. Departament de Fisica, Universitat Politècnica de Catalunya, Campus Nord B4-B5, E-08034 Barcelona, Spain*

Efficient photonic simulators rely on the possibility to fine-tune the couplings between optical modes. Engineering particle evolutions across large lattices is a challenging task, which requires sophisticated setups that are often bulky and intrinsically lossy. Here we demonstrate a radically new approach to the generation of quantum walk evolutions containing hundreds of discrete steps, obtained by means of only three liquid-crystal metasurfaces (see Fig. 1(a)). These are periodically-patterned optical elements made of a thin layer of liquid-crystal molecules whose local orientation is changing point-by-point (see Fig. 1(b)), allowing us to implement arbitrary position-dependent polarization transformations. The diffractive action of our periodic metasurfaces maps into a quantum walk on optical modes carrying a quantized amount of transverse momentum [1]. With this platform, we engineer quantum walks up to 320 discrete steps, far beyond state-of-the-art experiments [2]. As an interesting application, we demonstrate that in the long-time limit a dynamically-disordered quantum walk generates maximal entanglement between the system partitions [3]. Our setup is very compact, efficient, and it overcomes crucial limitations of standard photonic simulators of quantum walks, which require a number of optical operations increasing linearly with the number of steps. The reduced optical losses and the large number of optical modes that can be simultaneously manipulated make our setup ideal for engineering sophisticated multi-photon evolutions [4].

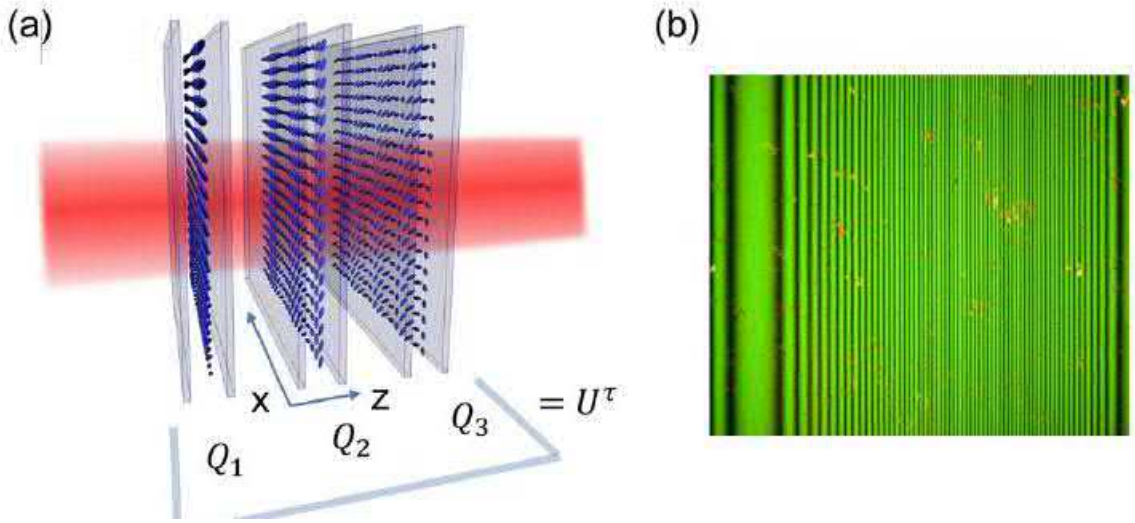


**Fig. 1:** (a) In our setup, only three liquid-crystal metasurfaces implement an entire quantum walk of hundreds of timesteps. (b) A liquidcrystal metasurface, realizing a quantum walk of 240 steps, is observed between crossed polarizers, unveiling its birefringent structure.

## References

[1] A. D'Errico et al., Optica 7, 108 (2020).
[2] F. Flamini, N. Spagnolo, F. Sciarrino, Reports Prog. Phys. 82, 016001 (2018)
[3] R. Vieira, E. P. M. Amorim, G. Rigolin, Phys. Rev. Lett. 111, 180503 (2013).
[4] F. Di Colandrea et al., to be submitted

[*]Corresponding author: francesco.dicolandrea@unina.it
[†]Corresponding author: filippo.cardano2@unina.it

# Generation and measurement of volume-filling structures in paraxial light

**Daniel Ehrmanntraut**[*1], **Ramon Droop** [1], **Danica Sugic** [2], **Eileen Otte** [1], **Mark R. Dennis** [2], **Cornelia Denz** [1]
*1. Institute of Applied Physics, University of Münster, Corrensstraße 2/4, 48149 Münster*
*2. School of Physics and Astronomy, University of Birmingham, Birmingham B15 2TT, UK*

The ongoing interest in structured light has been facilitated in part due to fundamental research, but also due to numerous possible applications in different areas [1]. With its three degrees of freedom-amplitude, phase and polarization applications and interactions can be tailored to fit specific ne eds. Associated with each degree of freedom are singularities in the transverse plane: caustics for amplitude, phase vortices for phase and C-/V-points and L-lines for polarization. These structure the light field around them and must therefore always be considered when the fine structure of light is important. Especially phase vortices and C-points are known for their topological properties, meaning that associated to them is a quantity which is preserved under continuous transformation, e.g. perturbation. Upon propagation they extend to lines, which are regarded as the skeleton of the light field around which the rest of the light field is organized [2]. original physical system may prove difficult. electric field (see Fig 2). deep imaging in tissue.

Shaping the phase vortex and C-line skeleton represents one way of designing paraxial light fields. This was utilized in creating light fields inspired by topological objects. For example, C-lines were shaped in such a way, that they closed on themselves in the shape of mathematical links and knots [3]. Topology has also entered the field of structured light in a different way, where the electromagnetic field in itself expresses a topological nature. Of topical interest are fields inspired by magnetic skyrmions: beams exhibiting a skyrmionic nature have been increasingly studied in recent years [4]. This class of beams exhibits a spin structure similar to the orientation of field lines of magnetic skyrmions. Although both physical systems differ in some ways, research is moving forward in using light to model magnetic skyrmions. Furthermore, structured light can be modelled after other structures in all fields of physics, making it a toolset for studying complex constructs where a direct experimental observation in their

Recently, we reported on generating an optical skyrmionic Hopfion [5], which can be considered as a 3D skyrmion in polarization and phase of light. It combines the aforementioned design via the *C*-line skeleton and the topological nature of the light field itself. In short, it is a volume filling structure, where all states of polarization build disjoint line filaments which link exactly once (see Fig. 1). The phase of the polarization state along a filament cycles by $2\pi$. Thus, both phase and polarization contribute to the topological structure of the light field. Since it is a 3D structure, a setup combining sophisticated methods in beam shaping and Stokes polarimetry was built, enabling generation and both transverse and longitudinal measurement of the full

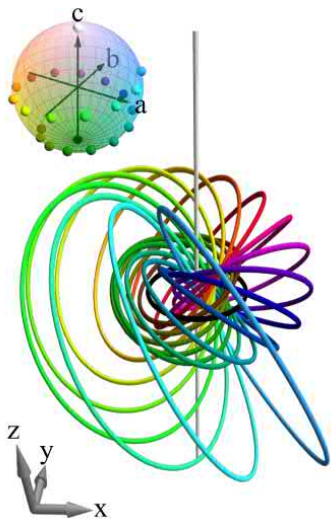


Figure 1: Hopf vibration projected into real space

Structured light will be an important factor in different areas of research going forward. We present advancements towards the full 3D structuring of light. The confined volume, in which these structures are expressed, would also lead to a confined volume of light-matter interaction. This could be useful for e.g. arranging particles in a desired three-dimensional shape. Furthermore, understanding the propagation properties of light fields may also be helpful for optical data communication and

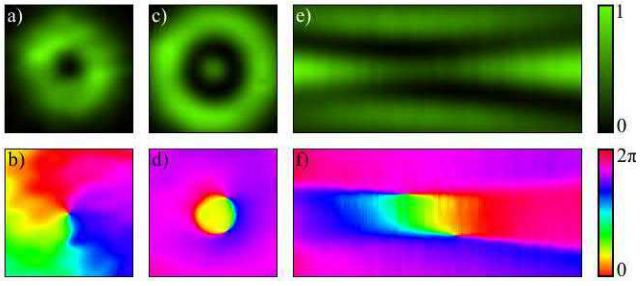


**Fig. 1:** Measured intensity $(a,c)$ and phase $(b,d)$ of two beams with orthogonal, circular polarization in the focal plane. e) and f) show intensity and phase of c) and d) in an $x-z$ cut. These beams build the skyrmionic Hopfion.

## References

[1] H. Rubinsztein-Dunlop et al., "Roadmap on structured light", J. Opt. 19, 013001 (2016)
[2] E. Otte, C. Denz, "Customization and analysis of structured singular light fields", J. Opt. 23, 073501 (2021)
[3] H. Larocque et al., "Reconstructing the topology of optical polarization knots", Nat. Phys. 14, 1079-1082 (2018)
[4] S. Gao et al., "Paraxial skyrmionic beams", Phys. Rev. A 102, 053513 (2020)
[5] D. Sugic et al., "Particle-like topologies in light", Nat. Comm. 12, 6785 (2021)

*Corresponding author: d.ehrmanntraut@wwu.de

# Talbot self-imaging and two-photon interference in ring-core fibers

**Matias Eriksson**[*1], **Benjamin A. Stickler**[2,3], **Lea Kopf**[1], **Markus Hiekkamäki**[1], **Regina Gumenyuk**[1], **Yuri Chamorovskiy**[4], **Sven Ramelow** [5,6], **Robert Fickler**[1]

*1. Physics Unit, Photonics Laboratory, Tampere University, 33720 Tampere, Finland*
*2. Faculty of Physics, University of Duisburg-Essen, 47048 Duisburg, Germany*
*3. QOLS, Blackett Laboratory, Imperial College London, London SW7 2AZ, United Kingdom*
*4. Kotel'nikov Institute of Radio Engineering and Electronics (Fryazino Branch) Russian Academy of Science, 141190 Fryazino, Russia*
*5. Institut für Physik, Humboldt-Universität zu Berlin, 12489 Berlin, Germany*
*6. IRIS Adlershof, Humboldt-Universität zu Berlin, 12489 Berlin, Germany*

Wave propagation on the surface of cylinders exhibits interferometric self imaging, much like the Talbot effect in the near-field diffraction at periodic gratings [1]. We investigate the cylindrical Talbot effect with both classical and quantum light fields. At first, we report the experimental observation of the cylindrical Talbot carpet in weakly-guiding ring-core fibers for classical light fields, corresponding well with the performed simulations (see Fig. 1).

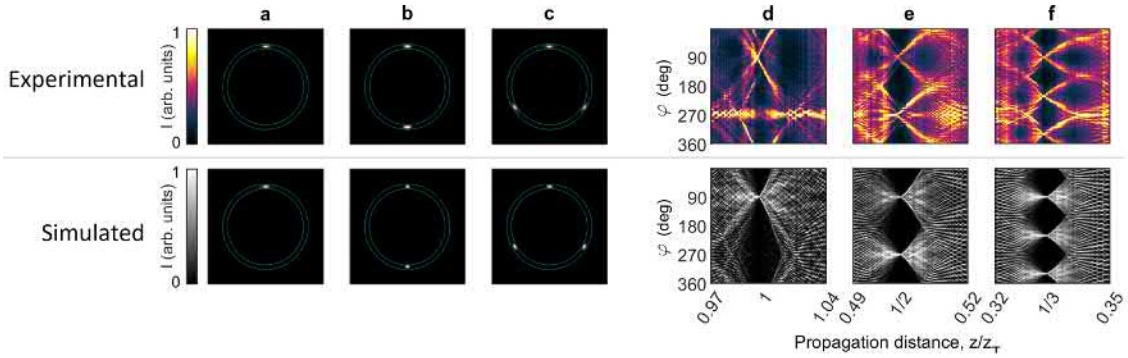


**Fig. 1:** Intensity distributions of output light fields of ring-core fibers illuminated with a single Gaussian input light field. (a-c) Full and fractional self-imaging using ring-core fibers with lengths $z_T$ (a), $z_T/2$ (b), and $z_T/3$ (c), where $z_T$ is the Talbot length. (d-f) Parts of the cylindrical Talbot carpet near $z_T$ (d), $z_T/2$ (e), and $z_T/3$ (f), generated from camera pictures taken while scanning the wavelength and from simulations.

Extending the work to the quantum domain, we show that the ring-core fiber acts as a higher-order optical beamsplitter for single photons, whose output can be controlled by the relative phase between the input light fields [2]. By also demonstrating high-quality two-photon interference between indistinguishable photons sent into the ring-core fiber, our findings open the door to applications in optical telecommunications as a compact beam multiplexer as well as in quantum information processing tasks as a scalable realization of a linear optical network.

## References

[1] H. F. Talbot, Lond. Edinb. Dublin Philos. Mag. J. Sci. **9** 401 (1836)
[2] M. Eriksson, B. A. Stickler, L. Kopf, M. Hiekkamäki, R. Gumenyuk, Y. Chamorovskiy, S. Ramelow, R. Fickler, Phys. Rev. A **104**, 063512 (2021)

*Corresponding author: matias.eriksson@tuni.fi

# Boosted Topological Domain Walls in 1D Photonic Waveguide Arrays

**Angelina Frank**[*1], **Daniel Leykam** [1], **Daria A. Smirnova** [2,3], **Dimitris G. Angelakis** [1,4], **Alexander Ling** [1,5]

*1. Centre for Quantum Technologies, National University of Singapore, 3 Science Drive 2, Singapore 117543*
*2. Nonlinear Physics Centre, Research School of Physics, Australian National University, Canberra ACT 2601, Australia*
*3. Institute of Applied Physics, Russian Academy of Science, Nizhny Novgorod 603950, Russia*
*4. School of Electrical and Computer Engineering, Technical University of Crete, Chania, Greece 73100*
*5. Department of Physics, National University of Singapore, 2 Science Drive 3, Singapore 117551*

The study of topological phenomena in photonic systems offers a route towards robust integrated photonic circuits, based on topological defect modes that are resistant against certain classes of perturbations. For example, one-dimensional wave media can host mid-gap topological defect modes protected by chiral symmetries involving spin-like degrees of freedom, such as sublattice pseudospin, which are closely related to Majorana zero modes [1]. However, most prior experimental studies have been limited to the study of static topological defects. More advanced functionalities, including mode converters and schemes for topological quantum computation, require mobile topological defects moving at a finite velocity, which exhibit intriguing relativistic effects including spin rotation and length contraction [2].

Here, we designed and experimentally observe relativistic topological zero modes in one-dimensional photonic waveguide arrays. The experimental observations can be explained by a tight binding model including nearest neighbour and next-nearest neighbour coupling terms. We studied the properties of the zero modes as a function of their speed, observing their abrupt delocalization when they exceed the effective speed of light in the array, as shown in Fig. 1 (c). The experimentally measured transmission profiles show good agreement with the predicted behaviour such as the defect-dependent centre of mass, inverse participation ratio, and the intensity delocalization upon transitioning from sub- to super-luminal defect speeds.

The employed experimental platform is a novel polymer waveguide made of two heat-curing polymers (GelestOE 50 and Sylgard 184) written by direct laser lithography with single-mode guiding in the UV-Vis range [Figure 1 (a) and (b)]. The platform features a fast fabrication cycle as well as flexibility in device geometry [3]. A 633 nm light source couples to the initial defect mode from where it propagates across an array of $\sim 20$ mm length. Full-wave simulations of the coupling coefficient that take into account next-nearest-neighbour coupling serve as the basis for theoretical predictions.

This work demonstrates a viable platform for the study of fundamental effects in topological photonics and illustrates the potential of topological methods for the design of photonic systems.

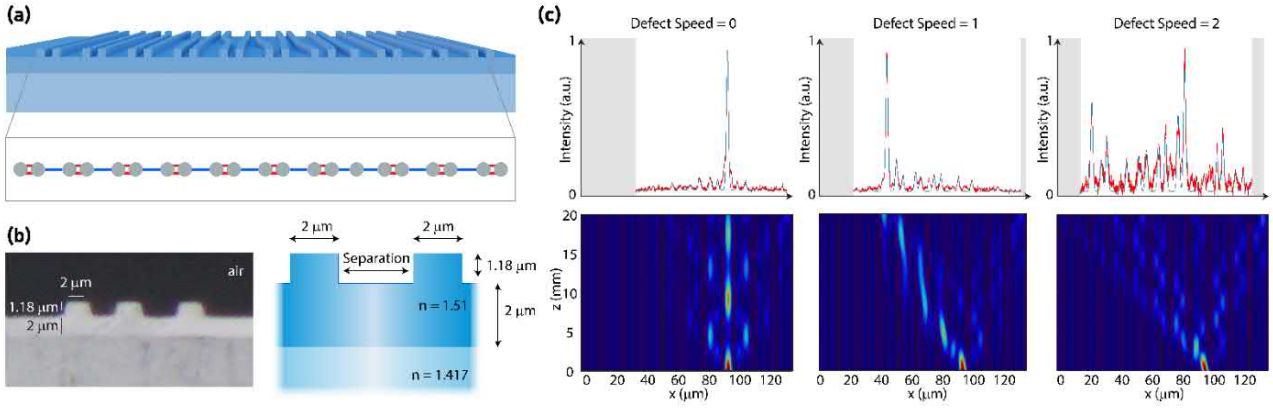


**Fig. 1:** (a) Schematic depiction of a waveguide array with a mobile defect. The waveguide spacing i.e. spacing between sites is either 2 $\mu$m (red bonds) or 5.8$\mu$m (blue bonds) with variation upon modulation of the topological domain wall. (b) Waveguide dimensions and cross section. (c) Top: Experimentally measured transmission profile and delocalization for arrays with increasing defect speeds. The blue trace depicts Gaussian fits of the experimental data (red trace). Bottom: Top-down view of tight-binding-model based simulations of lightpropagation. Light is injected at the initial defect side ($z = 0$) and propagates across 20 mm.

## References

[1] T. Ozawa et al., Rev. Mod. Phys. 91, 015006 (2019).
[2] T. Karzig, G. Refael, and F. von Oppen, Phys. Rev. X 3, 041017 (2013).
[3] K. F. Ng, M. J. L. F. Rodrigues, J. Viana-Gomes, A. Ling, and J. A. Grieve, Opt. Lett. 45, 288(2020).

*Corresponding author: Angelina.frank@u.nus.edu

# Polarization Singularity Array Generation Using Dammann Grating

**Kapil K. Gangwar**[*1], **Sarvesh Bansal** [1], **Jawahar Desai** [1], **P. Senthilkumaran** [1,2]

*1. Department of Physics, Indian Institute of Technology Delhi, Hauz Khas, New Delhi 110016, India*
*2. Optics and Photonics centre, Indian Institute of Technology Delhi, Hauz Khas, New Delhi 110016, India*

A novel method to generate a two-dimensional array of polarization singular beams using a designed Dammann grating is presented. Polarization singularity is a point azimuth defect at which the azimuth ($\gamma$) of a polarization ellipse or linear polarization becomes indeterminate [1]. In the immediate neighborhood of a polarization singularity, the azimuth undergoes rotation and thus the gradient of the azimuth has non-zero curl around a polarization singularity: $\nabla \times \nabla\gamma \neq 0$. Light beams containing polarization singularities can be generated by superposition of two orbital angular momentum (OAM) states in orthogonal polarization states. These beams have spatially varying distribution of polarization states and have shown applications in many fields such as microscopy, particle acceleration, imaging etc. There are three types of polarization singularities- C-points, V-points and L -lines. C-points and L-lines are found in inhomogeneous distribution of ellipse fields, whereas V-points occur in spatially varying distribution of vector fields. The L-lines separate the regions of right and left handedness in an ellipse field distribution. The C-points and V-points are respectively characterized by indices, $I_c$ and $\eta$, defined

$$I_c = \frac{1}{2\pi}\oint_C \nabla\gamma \cdot dl, \qquad \eta = \frac{1}{2\pi}\oint_C \nabla\gamma \cdot dl. \tag{1}$$

Dammann grating is used to generate equal intensity spots [2]. The number of equal intensity spots depends on the grating period and design. It is interesting to note that the action of Dammann grating is independent of polarization and phase profile of the incident beam as it aims to produce equal intensity light spot. Albeit, suprisingly it can replicate polarization distribution in individual diffraction orders. We used electron beam lithography to fabricate the grating. An Indium tin oxide (ITO) coated glass plate was taken as a substrate. Polymethyl methacrylate (PMMA) was spin-coated on to the substrate as e-beam resist. The fabricated Dammann grating has binary phase structure, where phase takes either 0 or $\pi$ value. The fabricated Dammann grating illuminated it with a C-point polarization singularity and produces spots of equal intensity each of which carry C-point singularity of polarization index $I_c$. C-point polarization singularity of desired polarization index $I_c$ is generated using a S-wave plate followed by spiral phase plate [3]. When S-wave plate is illuminated with linearly polarized light, the transmitted beam is embedded with V-point. Then a Spiral phase plate is used to convert V-point into C-point. The polarization distribution of each of the multiple beam-lets in the diffraction order is identical to that of the incident C-point. The element is intended to produce an array of spots of equal intensity. Surprisingly, the topological features of the input beam are preserved at each of the intensity spots.

We present some of the results obtained by our proposed method. Figure 1 depicts the $2 \times 2$ array of a C-point polarization singularities with index $I_c = \pm 1/2$ . Figure 1(a) and 1(d) shows the total intensity distribution of array of bright and dark C-point polarization singularity respectively and figure 1(b) and 1(e) the respective Stokes phases which is defined as $\phi = 2\gamma$. The polarization distribution at each of the bright/doughnut intensity spots are shown in figure (c) and (f) respectively.

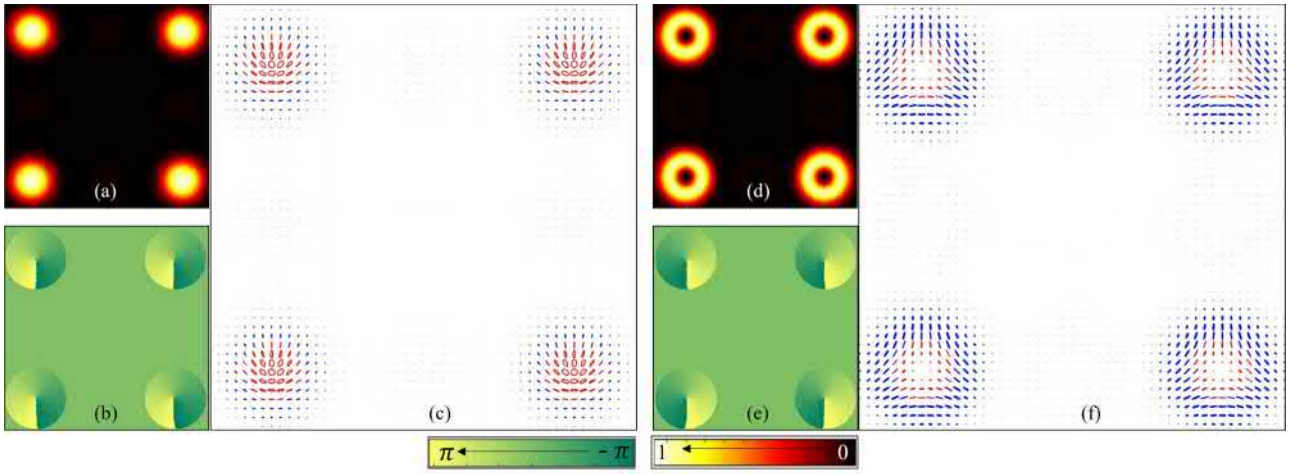


**Fig. 1:** Simulated $2 \times 2$ spots of equal intensity each having polarization distribution of lemon (left side) and star (right side) of index $I_c = \pm 1/2$ respectively. (a),(d) Total intensity; (b),(e) Stokes phase and (c),(f) polarization distribution of lemon(bright) and star(dark) C-point.

The proposed method can be used to generate an array of $2 \times 2$ C-points of different index. The generated array has same polarization distribution and equal intensity in the desired diffraction orders.

## References

[1] I. Freund, Opt. Commun. **201** 251-270 (2002)
[2] H. Dammann and E. Klotz, Opt. Acta **24** 505 (1977)
[3] Gauri Arora, S. Deepa, Saba N. Khan, P. Senthilkumaran, Scientific Reports **10** 20759 (2020)

*Corresponding author: kapil1205gangwar@gmail.com

# Multi-vortex high-harmonic beams from graphene's anisotropy

**Ana García-Cabrera**[*1], **Roberto Boyero-García** [1], **Óscar Zurrón-Cifuentes** [1], **Julio San Román** [1], **Luis Plaja** [1]
**Carlos Hernández-García** [1]

*1. Grupo de Investigación en Aplicaciones del Láser y Fotónica, Departamento de Física Aplicada, Universidad de Salamanca, E-37008 Salamanca, Spain*

High-order harmonic generation (HHG) has emerged as a unique tool to produce ultrafast structured laser beams in the extreme ultraviolet/soft x-rays spectral regime. The deep understanding of this process when driven in gaseous media has triggered the emergence of a wide variety of interaction schemes to control the spatiotemporal properties of the emitted beams, resulting from both spin and orbital angular momentum conservation (SAM, and OAM, respectively) [1]. For example, ultrafast time-dependent OAM pulses were created in HHG driven in Ar [2]. By contrast, HHG in solids has begun to attract the interest of the community more recently. Crystalline targets offer extraordinary rich scenarios in HHG, where the coupling of the electromagnetic field with the target's periodic structure introduces new phenomena, such as the matter-Talbot effect [3] or the recently observed anisotropic HHG from single-layer graphene [4].

In this work, we study HHG in single-layer graphene driven by a mid-infrared vector beam (VB) at normal incidence (see Fig.1, left panel). The exploration of the coupling of graphene's symmetries with the SAM and OAM of the driving beam requires to develop a macroscopic picture of the interaction. In unstructured media, like gases, HHG preserves the geometry of a cylindrical VB driver [5], which can be understood as composed by two OAM modes, $\ell = \pm 1$. In such case, the simultaneous conservation of SAM and parity leads to the photon composition rules for the qth-order harmonic: $q = n_1 + n_2$ odd and $|n_2 - n_1| = 1$, where $n_1$ and $n_2$ are the number of photons of the two OAM modes. Hence, the OAM of the harmonic beam is restricted to $\ell = \pm 1$ components, thus constituting the cylindrical harmonic VB. In contrast, our theoretical simulations show that graphene's periodic azimuthal anisotropy [6] imprints two distinct properties into the generated harmonics: (1) a spin-dependent angular diffraction pattern and, (2) high OAM components. Strikingly, the fundamental symmetry associated with simultaneous spin-orbit conservation forces the splitting of the harmonic beam into a set of spatially resolved EUV vortices with $\ell = |1|$ and well-defined helicity. As an example, the right panel of Fig. 1 shows the intensity and phase distribution of the multi-vortex formation for the 9th harmonic, for the left circular (a and b) and right circular (c and d) components.

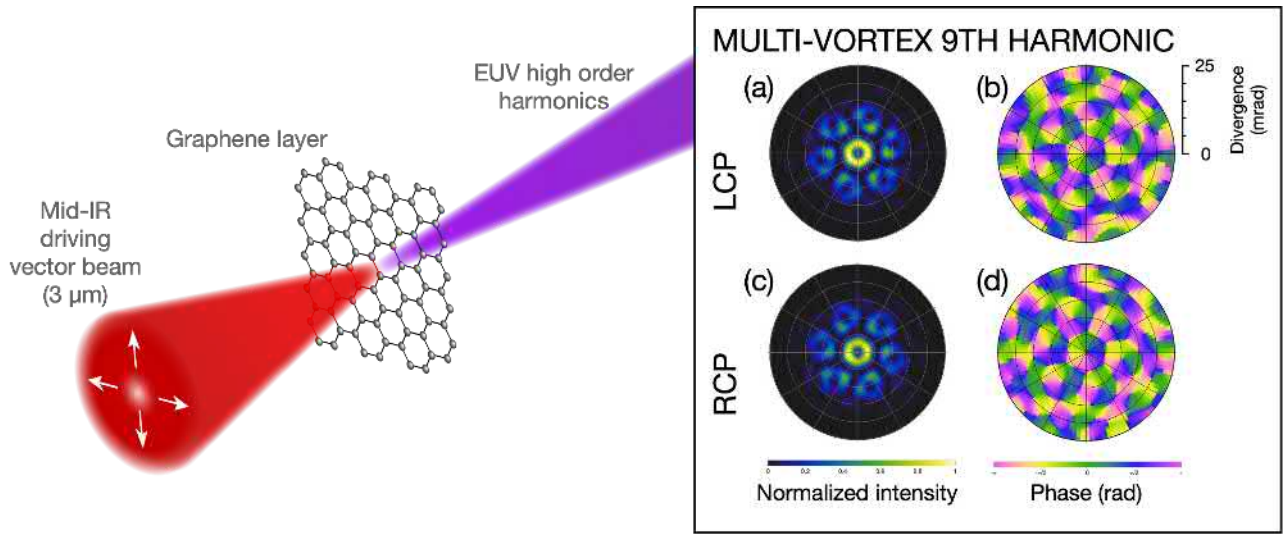


**Fig. 1:** Multi-vortex high-order harmonics in single-layer graphene from a mid-infrared vector beam. The right panel shows the intensity and phase distribution of the 9th harmonic (33 nm), for the left circular (a and b) and right circular (c and d) components.

Our study highlights the non-trivial interplay between the structural symmetries of the target and the driving beam in HHG, as well as its understanding in terms of both spin-dependent diffraction and the fundamental law of simultaneous conservation of SAM and parity. We believe that HHG using structured light and crystalline targets opens exciting new routes not only for the generation of spatially-complex EUV/soft x-ray structured beams, but for a deeper understanding of the ultrafast electron dynamics in structured solid systems.

## References

[1] K. Dorney et al., Nat. Photonics **13** 123-130 (2019)
[2] L. Rego, K. Dorney et al., Science **364** eaaw9486 (2019)
[3] A. García-Cabrera, C. Hernández-García, L. Plaja New J. Phys. **23** 093011 (2021)
[4] N. Yoshikawa, T. Tamaya, K. Tanaka, Science **356** 736-738 (2017)
[5] C. Hernández-García, A. Turpin, J. San Román, A. Picón, R. Drevinskas, A. Cerkauskaite, P. G. Kazansky, C. G. Durfee, I. J. Sola, Optica **4**, 520-526 (2017)
[6] Ó. Zurrón-Cifuentes, R. Boyero-García, C. Hernández-García, Antonio Picón, L. Plaja, Opt. Express **27** 7776 (2019)

*Corresponding author: anagarciacabrera@usal.es

# Learning from the disorder in multimode fibers

**Rodrigo Gutiérrez-Cuevas**[*1], **Maxime W. Mattheès**[1], **Yaron Bromberg**[2], **Julien de Rosny**[1], **Dorian Bouchet**[3], **Sébastien M. Popoff**[1]

*1. Institut Langevin, ESPCI Paris, Université PSL, CNRS, 75005 Paris, France*
*2. Racah Institute of Physics, The Hebrew University of Jerusalem, Israel*
*3. Universiteé Grenoble Alpes, CNRS, LIPhy, 38000 Grenoble, France*

We are steadily reaching the limits of data transmission offered by single mode fibers, where all the available degrees of freedom are being exploited. Multimode fibers (MMF) offer a natural and attractive way forward since they allow exploiting the spatial degree of freedom to support various separate transmission channels at once. However, when coherent light is injected into an MMF, the output is a random distribution of bright and dark spots known as a speckle pattern. This situation is similar to what is seen in scattering media, but the "randomness" in MMF comes from intermodal dispersion which scrambles the information carried in the spatial degree of freedom. This effect is exacerbated when the fiber is bent or deformed in some way, which introduces supplementary intermodal coupling. Therefore, in practice, it is quite difficult to predict the behavior of a given MMF since the slightest imperfection will affect the output field.

One way to overcome this problem is to apply the same techniques used to study scattering media. By leveraging the linearity of the system, light's propagation through MMF can be modeled by a transmission matrix (TM) $\mathbf{H}$ where the output field $\mathbf{Y}_j$ is related to the input $\mathbf{X}_j$ via $\mathbf{Y}_j = \mathbf{H} \cdot \mathbf{X}_j$. The input and output fields can theoretically be represented in terms of any basis set, but the pixel basis is the most commonly used due to the pixelization of spatial light modulators and cameras. As shown in Fig. 1(a), we can deduce the TM by sending random patterns composed of 0 and $\pm 1$ values and measuring their outputs [1]. For MMFs, however, the TM should be given in the representation of the guided modes in order to assess the degree of intermodal coupling and the effect of perturbations. This is achieved by projecting the TM measured in the pixel basis onto the mode basis via $\mathbf{H}_m = \mathbf{M}_o^\dagger \cdot \mathbf{H}_p \cdot \mathbf{M}_i$, where $\mathbf{M}_i$ and $\mathbf{M}_o$ represent the change of basis matrices. By performing this projection directly, one obtains a seemingly random TM (see Fig. 1(b)) in the modal basis even when the fiber is held straight. This is not a signature of disorder, but it is rather due to the aberrations and misalignment present in the optical system. Using the fact that most of the light that reaches the camera comes from the guided mode, we can numerically compensate for these optical imperfections by running an optimization routine that maximizes the energy transfer through the MMF in the mode basis [2]. For a straight fiber, the resulting TM is almost diagonal, with only marginal coupling restricted to the degenerate blocks.

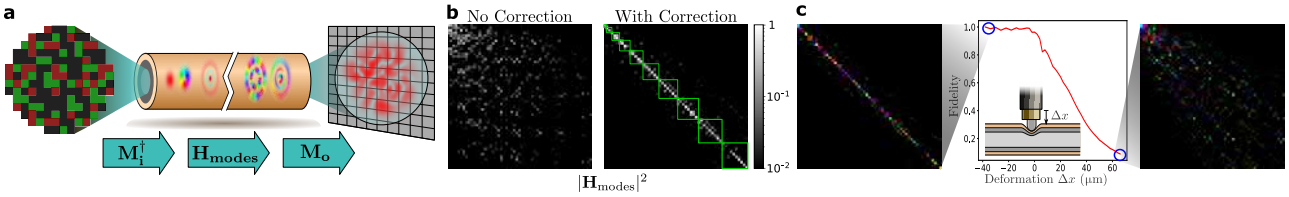


**Fig. 1:** (a) Sketch of the experiment: a random input field couples to the propagating modes and the output is measured by the camera. (b) TM on the modal basis before and after the correction of the aberrations. (c) Effect of local deformation on the modal basis.

The technique of measuring the TM for MMF is highly versatile. It can be applied to any fiber, and is robust to optical misalignment by design. Moreover, since there is no assumption about the resulting TM in the modal basis, e.g. that it must be diagonal, our method works even in heavily deformed fibers. This is in contrast to other approaches that have been taken over the years [4,5]. Figure 1(c) shows the example of a local deformation where we clearly see how the TM goes from being diagonal to seemingly random. Additionally, having the TM for various deformation values makes it is possible to find channels that are insensitive to large deformations. These channels are given by the deformation principal modes which are the eigenmodes of the generalized Wigner-Smith operator $\mathbf{Q} = -i[\mathbf{H}_m^{-1} \cdot \partial_\alpha \mathbf{H}_m - (\mathbf{H}_m^{-1} \cdot \partial_\alpha \mathbf{H}_m)^\dagger]$, where alpha quantifies the amount of the deformation [6]. These modes are also the maximum information states for estimating the deformation parameter $\alpha$ [3] and thus can be used to implement highly accurate sensors with MMF. We also discuss the best strategy to perform this parameter estimation task for intensity-only measurements when a reference arm is not available and/or a more robust setup is desired. In this case, phase retrieval algorithms become necessary to obtain the TM which can subsequently be used to determine the best modes to estimate the parameter. These modes will no longer be the principal modes, which only suffer a global phase shift from the deformation, but rather those whose intensity profile is the most sensitive to the perturbation.

## References

[1] S. M. Popoff, G. Lerosey, R. Carminati, M. Fink, A. C. Boccara, and S. Gigan, Phys. Rev. Lett. **104** 100601 (2010)
[2] M. W. Matthès, Y. Bromberg, J. de Rosny, and S. M. Popoff, Phys. Rev. X **11** 021060 (2021)
[3] D. Bouchet, S. Rotter and A. P. Mosk, Nat. Physics **17** 564 (2021)
[4] J. Carpenter, B. J. Eggleton, and J. Schröder, Opt. Exp. **22** 94 (2014)
[5] M. Plöschner, T. Tyc, and T. Čižmár, Nat. Photonics **9** 529 (2015)
[6] S. Rotter, P. Ambichl, and F. Libisch, Phys. Rev. Lett. **106**, 120602 (2011)

*Corresponding author: rodrigo.gutierrez-cuevas@espci.fr

# Hyperspectral optical vortex modulation

**Vagharshak Hakobyan*** **and Etienne Brasselet†**

*1. Université de Bordeaux, CNRS, Laboratoire Ondes et Matière d'Aquitaine, F-33400 Talence France*

The programmable manipulation of light, both in space and time provides for a very large set of prospective applications, from continuous-wave light wave to ultrashort optical pulses. Recently, the independent control of the optical orbital angular momentum on a discrete set of spectral channels has been reported [1] using micro-arrays of electrically-controlled self-engineered topological defects [3], each of them operating as a microscopic wavelength-tunable 'q-plate' [2]. The latter experimental demonstration of spectral optical vortex modulation is however restricted to a multispectral operation and a given orbital angular momentum state. Extension to a discrete set of orbital angular momentum state has also been achieved, though at the expense of spectral tunability [4].

Here, using macroscopic liquid crystal defects, we address the case of hyperspectral optical vortex generation, where the wavelength spectrum in continuous as opposed to the multispectral situation explored so far. Following a simulation work illustrated by Fig.1, an experimental implementation in the visible domain is reported and discussed in the framework of its envisioned use for 3D topological shaping of ultrashort optical pulses.

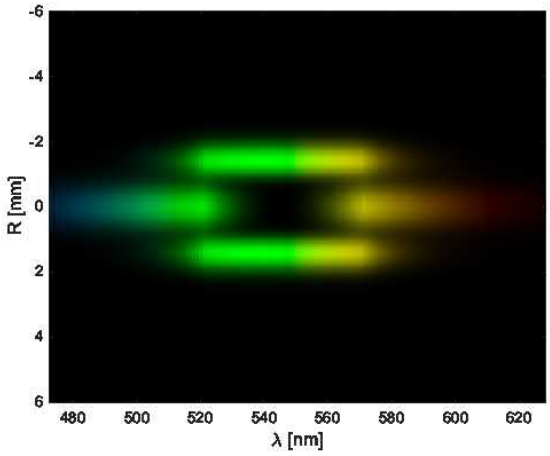


**Fig. 1:** Simulated spatio-spectral meridional cross section in the plane of parameters ($R$, $\lambda$) where $R$ is the radial coordinate of the output modulated field for a broadband polychromatic incident field ($\Delta\lambda \sim 100$ nm).

## References

[1] M. Ghadimi Nassiri and E. Brasselet, Phys. Rev. Lett. **121**, 213901 (2018)
[2] L. Marrucci and C. Manzo and D. Paparo, Phys. Rev. Lett. **96**, 163905 (2006)
[3] E. Brasselet, Book chapter in *Liquid Crystal: New Perspectives*, pp. 1-79, John Wiley and Sons (2021)
[4] M. Ghadimi Nassiri, G. Seniutinas, C. David, S. Juodkazis, and E. Brasselet Appl. Phys. Lett. **118**, 201104 (2021)

*Corresponding author: vagharshak.hakobyan@u-bordeaux.fr
†Corresponding author: etienne.brasselet@u-bordeaux.fr

# Propagation of coupled atom-light solitons carrying angular momentum in a Bose-Einstein Condensate

**Grant Henderson**[*1], **Gordon R. M. Robb**[1], **Gian-Luca Oppo**[1], **Alison M. Yao**[1]
*1. SUPA & Department of Physics, University of Strathclyde, Glasgow, Scotland, UK*

Solitons are localized fields that maintain their spatial profile as they propagate. In nonlinear optics, spatial optical solitons arise when the diffraction of a Gaussian beam is carefully balanced by self-focusing due to a Kerr nonlinear medium. However, when the optical field carries orbital angular momentum (OAM), it fragments into solitons, with the number of solitons formed depending, in general, on the OAM index, $m$ [1]. This has been confirmed experimentally using sodium [2] and hot rubidium vapours [3] as the Kerr medium. Similar fragmentation behaviour has been seen in nonlinear colloidal suspensions [4].

Here, we investigate the propagation of optical fields ($F$) through a Bose-Einstein Condensate (BEC) ($\psi$). We consider an experimentally realisable BEC with a transverse diameter of 100$\mu$m, a longitudinal length of around 2mm, and an optical beam of wavelength $\lambda = 720$ nm and beam waist $w_F = 10\mu$m, giving a Rayleigh range $z_R = \pi w_F^2/\lambda \approx 0.44$ mm. We use a model of coupled normalised nonlinear Gross-Pitaevskii and nonlinear Schrödinger equations similar to [5]:

$$\partial_\zeta \psi = i\nabla_\perp^2 \psi - i\left(s|F|^2 + \beta_{col}|\psi|^2 - iL_3|\psi|^4\right)\psi, \qquad (1)\ ; \qquad \partial_\zeta F = i\nabla_\perp^2 F + i\left(\frac{-s|\psi|^2}{1+\sigma_{sat}|F|^2}\right)F. \qquad (2)$$

Eqn. (1) includes terms relating to kinetic energy ($\nabla_\perp^2$) and interatomic scattering ($\beta_{col}$). We also include a term describing three-body loss ($L_3$) to give an accurate description of the evolution of the BEC wave-function in high-density regimes. The first term on the right in Eqn. (2) describes diffraction and the second describes a saturating focusing or defocusing effect. The two fields are coupled by terms proportional to $s$, the sign of the light-atom detuning: $s = \pm 1$ corresponds to blue (+) / red (-) detuning.

After confirming that this model captures the formation of transverse patterns for weakly repulsive interactions ($\beta_{col} = 3.5$) for both red- and blue-detuned light as described in [5], we then investigate the effect of adding OAM to the optical field. We show that red-detuned light carrying OAM fragments into solitons, suggesting that the BEC is behaving like an effective Kerr medium. As the light is red-detuned, atoms are attracted to intensity peaks and hence "captured" by the daughter optical solitons, resulting in coupled light-atom solitons. We show that both the optical and atomic solitons carry angular momentum and that the number of solitons formed, and their velocities, is dependent on the OAM of the optical field.

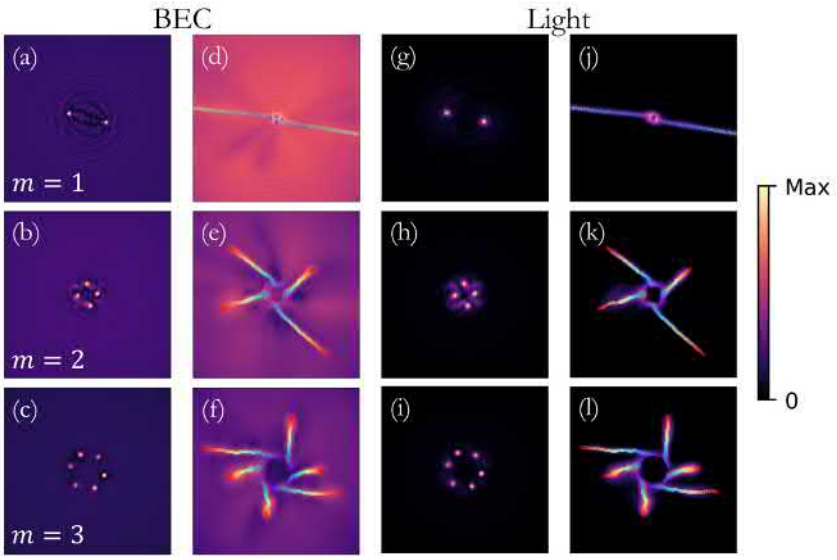


**Fig. 1:** Panels (a)-(c) & (g)-(i): Transverse intensity cross-section of BEC and optical fields, respectively, for $m = 1, 2, 3$ at $\zeta = z_R$ (0.42mm). Panels (d)-(f) & (j)-(l): superimposed images of transverse BEC and optical amplitude distributions $\zeta = 0.5 \rightarrow 4z_R$. Colour scale: zero to maximum amplitude for each field.

Finally, we demonstrate significant slowing down of the transverse motion of the daughter solitons by using a Bessel-Gauss input optical field. When moving to weakly attractive interactions ($\beta_{col} = -2.0$) the radial motion can be almost completely suppressed so that the solitons continue to rotate azimuthally along the length of the atomic medium effectively forming a controllable persistent current.

## References

[1] W. J. Firth and D. V. Skryabin, Phys. Rev. Lett. **79**, 2450 (1997); A. S. Desyatnikov and Y. S. Kivshar, Phys. Rev. Lett. **87**, 033901 (2001).
[2] M. S. Bigelow, P. Zerom, and R. W. Boyd, Phys. Rev. Lett. **92**, 083902 (2004).
[3] F. Bouchard, H. Larocque, A. M. Yao, C. Travis, I. De Leon, A. Rubano, E. Karimi, G.-L. Oppo, and R. W. Boyd, Phys. Rev. Lett. **117**, 233903 (2016).
[4] W. Walasik, S. Z. Silahli, and N. M. Litchinitser, Sci. Rep. **7**, 11709 (2017); J. Sun, S. Z. Silahli, W. Walasik *et al.*, Opt. Express **26**, 5118 (2018).
[5] M. Saffman, Phys. Rev. Lett. **81**, 65 (1998); M. Saffman and D. V. Skryabin, in *Spatial Solitons*, (Springer, 2001) pp. 433–447.

[*]Corresponding author: grant.henderson@strath.ac.uk

# Role of supercritical angle fluorescence in CHIDO microscopy.

**I. A. Herrera-Hernández**[*1], **Luis A. Alemán-Castañeda** [1,2], **Sophie Brasselet** [1], **Miguel A. Alonso**[†1,2]
*1. Aix Marseille Univ, CNRS, Centrale Marseille, Institut Fresnel, UMR 7249, 13397 Marseille CEDEX 20, France*
*2. The Institute of Optics, University of Rochester, Rochester NY 14627, USA*

Super-resolution microscopy (SRM) techniques have allowed overcoming the Rayleigh limit for the 2D localization of fluorescent molecules (fluorophores) that are widely used to label biological systems. In recent years there has been great interest in improving the performance of SRM by measuring the 3D position and 3D orientation of fluorophores, giving rise to several techniques that are based on structuring the fluorescence at the pupil plane of the optical system to encode the spatial information of the fluorophores in their Point Spread Function (PSF). A method proposed recently at the Fresnel Institute, named CHIDO (Coordinate and Height super-resolution Imaging with Dithering and Orientation), has been shown to allow the simultaneous measurement of the position, orientation, and the amount of wobbling of the fluorophores [1]. The 3D spatial and 3D orientation information of the fluorophores is contained in the polarization state, the amplitude and the phase of the field distribution at the pupil plane. CHIDO is based on a vectorial pupil modulation by means of a stressed-engineered birefringent optical element (SEO). This element has been shown to efficiently encode polarization information in the PSFs shape while causing the smallest possible increase of the PSF [2].

In situations where the fluorophores are close (less than a wavelength) to a dielectric interface between media with indices of refraction $n_1$ and $n_2$, such that $n_1 < n_2$ (where $n_1$ corresponds to medium embedding the fluorophores and $n_2$ conrresponds to glass), it is possible to observe contributions at the pupil and image planes (see figure 1) originating from the evanescent components emitted by the fluorophores, which couple onto propagating components in the second medium. These contributions (called supercritical angle fluorescence, SAF) are often ignored in PSF engineering because their amplitude strongly depends on the axial position of the fluorophore. In this work we study the performance of CHIDO in situations where the SAF is present by computing the Cramer-Rao lower bounds [3] on the uncertainties of the spatial and orientation parameters, which are the standard metric for quantifying the performance of different PSF engineering methods [4].

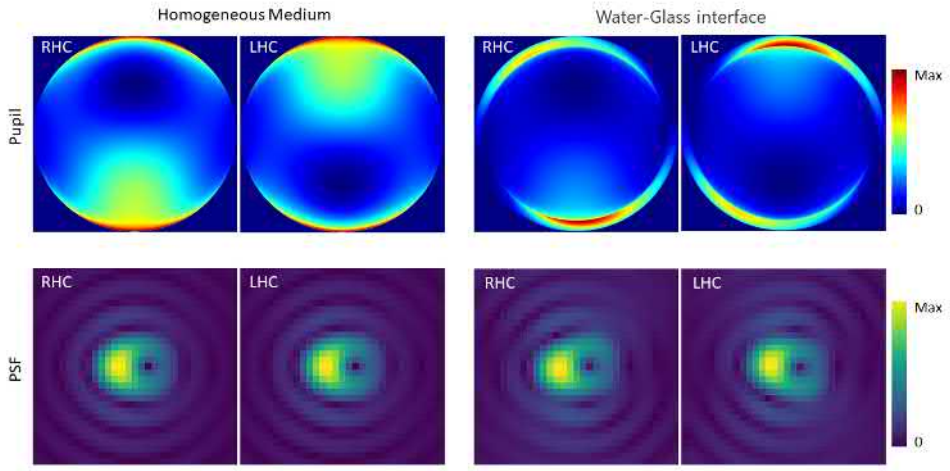


**Fig. 1: Comparison between the two orthogonal circular polarization components (right-hand and left-hand circular) over the pupil plane (intensity) and the corresponding PSFs (amplitude) for the case of a single fluorophore with a given direction, for the cases where it is immersed in a homogeneous medium (no SAF contributions, left), or located near a water-glass interface (with SAF contributions, right).**

## References

[1] V. Curcio, L. A. Alemán-Castañeda, T. G. Brown, S. Brasselet, M. A. Alonso. Nat Commun **11**, 5307 (2020).
[2] A. J. Vella M.A. Alonso. Opt. Express **27**, 36799–36814 (2019).
[3] A. J. Vella M.A. Alonso. Prog. Opt. **65**, 231–311 (2020).
[4] O. Zhang M. D. Lew. J. Opt. Soc. Am. A **38**, 288-297 (2021).

[*]Corresponding author: herrera@fresnel.fr
[†]Corresponding author: miguel.alonso@fresnel.fr

# Entangled ripples and twists of light: Radial and azimuthal Laguerre-Gaussian mode entanglement

**Natalia Herrera Valencia**[*1], **Vatshal Srivastav** [1], **Saroch Leedumrongwatthanakun** [1], **Will McCutcheon** [1], **and Mehul Malik** [1]

*1. Institute of Photonics and Quantum, Sciences, Heriot-Watt University, Edinburgh, UK*

Control over the azimuthal (twisted) and radial (rippled) components of photons has been key for enhancing classical communications protocols and controlling the propagation of light through complex media. In the quantum domain, access to the complete transverse spatial degree-of-freedom is necessary for harnessing the advantages of high-dimensional encoding. In this context, precise measurement of the radial photonic degree-of-freedom has proven to be experimentally challenging primarily due to its transverse amplitude structure. Here we demonstrate the generation and certification of full-field LaguerreGaussian (LG) entanglement between photons pairs generated by spontaneous parametric down-conversion in the telecom regime, certifying entanglement dimensionalities up to 26 in a 43 -dimensional radial and azimuthal LG mode space [1]. Employing a method to characterize the correlations of the two-photon wavefunction [2], we use this information to tune the optical system parameters and optimise the correlations in the azimuthal and radial modes. Accurate spatial state projections of states in the LG basis (and any superposition of these) are implemented with an "intensity-flattening" technique that we have recently demonstrated in both the classical and quantum regime [ 3,4]. Additionally, we study two-photon quantum correlations between 9 LG mode groups, demonstrating a correlation structure related to mode group order and inter-modal cross-talk. Our work demonstrates the potential offered by the full spatial structure of the two-photon field for enhancing technologies for quantum information processing and communication.

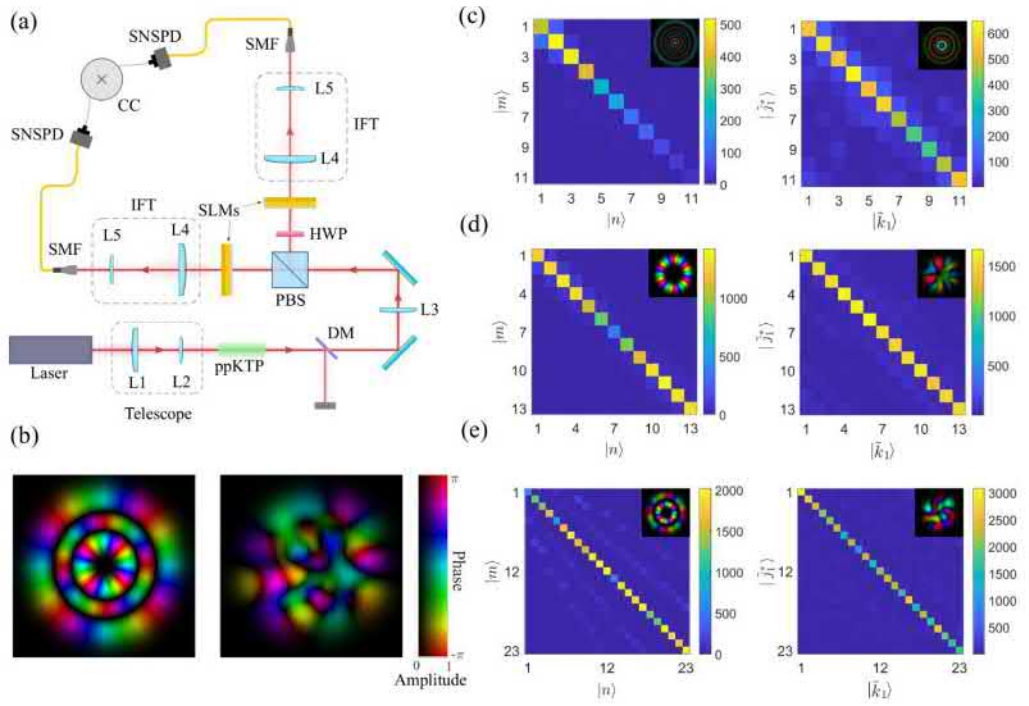


**Fig. 1:** Full-field Laguerre-Gaussian mode entanglement. (a) Pairs of entangled photons at 1550 nm are generated through Type-II spontaneous-parametric-down-conversion. Accurate projective measurements in the LG basis and any superposition are permed with spatial-light-modulators (SLMs), intensity-flattening-telescopes (IFT), and single-mode fibres (SMF). Correlations in the radial and azimuthal LG mode components of the transverse spatial field are obtained by measuring coincidences counts between pairs of (b) Representation of the complex amplitude describing the full-field mode $LG^4$ (left) and a mode from the mutually unbiased basis w.r.t the LG basis composed of a coherent superposition of 43 LG modes (right). (c-e) Two-photon coincidence counts showing in radial, azimuthal, and full-field correlations in the standard *LG* basis of each defined subspace (left), and its second mutually unbiased basis (right).

## References

[1] Natalia Herrera Valencia, et al. Journal of Optics **23**, 104001 (2021).
[2] Vatshal Srivastav, Natalia Herrera Valencia, et al, arXiv:2110.03462 (2021).
[3] Frédéric Bouchard, Natalia Herrera Valencia, et al, Optics Express 26, 31925 (2018).
[4] Natalia Herrera Valencia, et al. Quantum 4, 376(2020)

*Corresponding author: nah2@hw.ac.uk

# Photonic angular super-resolution using twisted N00N states

**Markus Hiekkamäki**[*1], **Frédéric Bouchard**[2], **Robert Fickler**[† 1]
*1. Photonics Laboratory, Physics Unit, Tampere University, Tampere, FI-33720, Finland*
*2. National Research Council of Canada, 100 Sussex Drive, Ottawa, Ontario K1A 0R6, Canada*

Photonic N00N states, i.e., states of light where N photons are in an extremal superposition between two orthogonal states $\frac{1}{\sqrt{2}}(|N,0\rangle + |0,N\rangle)$, have an increased phase-sensitivity in comparison to their classical counterparts. This phase sensitivity has been harnessed in multiple proof-of-principle experiments with one implementation already surpassing the shot-noise limit [1]. By using the increased phase sensitivity offered by N00N states, in conjunction with the increased angular sensitivity of states with large orbital angular momentum (OAM) [2], the angular sensitivity and resolution can be scaled to levels not achievable for classical light [3]. This scaling has been studied theoretically and experimentally, but it has not been demonstrated without additionally invoking other degrees of freedom such as path and polarization. Recently, we demonstrated a reliable way of generating these two-photon twisted N00N states, in a single beam-line, for arbitrary OAM values. In this work we adapt the method demonstrated in [4] to generate high-OAM twisted N00N states, in a simple and flexible system, and show that these states can be used to resolve rotations of the transverse beam-structure better than with a classical beam of light [5].

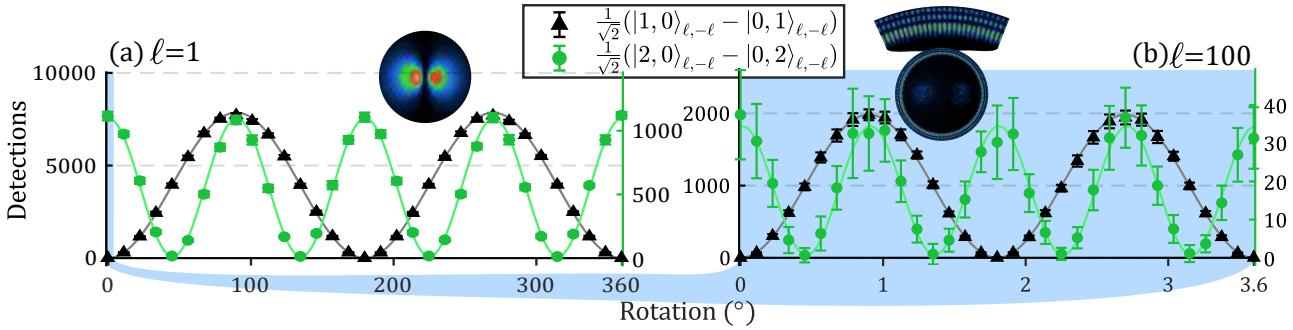


Figure 1: Super-resolution rotation measurements with the OAM values 1, shown in a), and 100, shown in b). The single photon measurements are shown in black, while the two-photon measurements are shown in green. The single photon superpositions form petal beams that are symmetric under a specific physical rotation (see images in insets captured using a laser and camera). Using a two-photon N00N state results in twice the periodicity, hence improving the resolution by a factor of 2. Accidentals have been removed from the two-photon data.

The twisted N00N states are created through two-photon bunching into transverse-spatial modes after independent structuring of the spatial structure of both photons. To demonstrate the systems capabilities, we measured rotation sensitivities of heralded single photons and two-photon N00N states with OAM values ranging from 1 to 100. Two examples of these measurements can be seen in Figure 1. From our measurement data we estimated the Fisher information and angular uncertainty. Our results showed that the angular uncertainty for twisted N00N states scales as $|\Delta\varphi| \propto \frac{1}{N\ell}$ when $N$ is the N00N state photon number and $\ell$ the amount of OAM. Due to the simplicity of the scheme, current tools and methods could be used to overcome the shot-noise limit with a similar experimental system. Additionally, the flexibility of the experimental scheme opens up new possibilities for studying N00N states between arbitrary spatial structures.

## References

[1] S. Slussarenko, M. M. Weston, H. M. Chrzanowski, L. K. Shalm, V. B. Verma, S. W. Nam, G. J. Pryde, Nat. Photon. **11**, 700–703 (2017)
[2] S. M. Barnett, R. Zambrini, J. Mod. Opt. **53**(5-6), 613–625 (2006)
[3] V. D'ambrosio, N. Spagnolo, L. Del Re, S. Slussarenko, Y. Li, L. C. Kwek, L. Marrucci, S. P. Walborn, L. Aolita, F. Sciarrino, Nat. Commun. **4** 2432 (2013)
[4] M. Hiekkamäki, R. Fickler, Phys. Rev. Lett. **126(12)** 123601 (2021)
[5] M. Hiekkamäki, F. Bouchard, R. Fickler, Phys. Rev. Lett. **127(26)** 263601 (2021)

[*]Corresponding author: markus.hiekkamaki@tuni.fi
[†]Corresponding author: robert.fickler@tuni.fi

# Non Circular Conical Diffraction with Fractional Optical Angular Momentum

**Muhammad Waqar Iqbal*** [1,2], **Nicolas Marsal** [1,2] **Germano Montemezzani** [1,2]

*1. Université de Lorraine, CentraleSupélec, LMOPS, 57000 Metz, France*
*2. Chair in Photonics, CentraleSupélec, LMOPS, 57000 Metz, France*

Structured light beams have rapidly developed over the two last decades, starting from possible intrinsic spatial transverse/longitudinal structures to specifically tailored manipulation of the transverse beam profile. Generally, any tailored beam is associated with inhomogeneities in the spatial distributions of one or several of the main field parameters, amplitude, phase and polarization [1]. Such beams may also possess a non-zero orbital angular momentum (OAM). Among such structured beams, one may find vector beams which have a spatially varying polarization. The conical diffraction (CD) phenomenon happening in anisotropic biaxial crystals (BCs) can naturally generate such vector beams if a tightly focused wave is incident with its $\vec{k}$-vector along one of the two optical axes of the crystal. This singular $\vec{k}$-direction leads to degenerated Poynting vectors lying on a slanted cone surface. After the crystal the beam propagates as a diffracting hollow cylinder, which is sharpest at the incident beam waist position (focal image plane FIP). At this plane one observes two closely spaced circularly shaped rings separated by a dark ring (Poggendorff ring). Any two diametrically opposite points on these rings possess orthogonal linear polarizations, leading to the vector character of such waves [2].

CD has recently seen major developments via the exploration of cascaded configurations, whereby two or more crystals are placed in a cascade with their optical axes aligned. Such a cascade of $N$ crystals leads to $2^{N-1}$ double rings in the FIP [3]. As discussed recently [4], such waves possess in general a fractional OAM. Cascaded configurations can be further modified by placing quarter-, half-wave plates, or other polarization scrambling elements between the pairs of BCs, leading to a tailored strongly inhomogeneous azimuthal intensity distribution [5]. Furthermore, the intercalation of a spherical lens was shown to allow the continuous tuning of the actual cascade parameters largely increasing the versatility of the approach [6]. However, in all the reported results so far, the circular shape of CD patterns (rings) is always preserved, both for single crystal and cascaded configurations. Here, we present a wave-vector space manipulation technique allowing to break this circular symmetry [7] and discuss the influence of the parameter underlying the manipulation on the fractional OAM of the resulting waves.

The key aspect of our approach is to split the 2D wave-vector space ($\vec{k}$-space) between two BC's into two 1D spaces. This manipulation is achieved by inserting two cylindrical lenses (CLs) with their axes perpendicular to each other. The two CLs are arranged in such a way as to provide a common image plane of the first FIP (FIP1 corresponding to the focal plane of the focused incident wave) into a second plane placed near the second BC (FIP2). This imaging is, however, associated to different magnification factors $M_x$ and $M_y$ along the $x$ and $y$ transverse directions. The above transformation leads to cascaded CD patterns (observed at FIP2) with strongly broken circular symmetry possessing complex distribution of intensity and polarization [7]. An example is shown in Fig. 1(a)-theory and Fig. 1(b)-experiment, which shows that the resulting pattern is much more complex than a simple anisotropic stretching of concentric circles, what would give rise to ellipses. Indeed, none of the structures in the cascaded CD pattern is elliptical and in the specific case shown here the internal one has a reversed curvature (convex rather than concave if looked from inside). The theoretical model is based on Fourier optics and takes into account the transfer function of the BCs in paraxial approximation and the performed wave-vector space manipulation by the CLs . The approach can be easily extended to three or more crystals in cascade. A calculated example for 3 BCs and a specific $\vec{k}$-space manipulation between each pair of them is shown in Fig. 1(c). The obtained patterns are associated to an overall fractional OAM. The OAM value is influenced by the $\vec{k}$-space manipulation induced by the CLs. The way how the final OAM depends on the parameters describing the imaging between the two focal image planes will be discussed at the meeting.

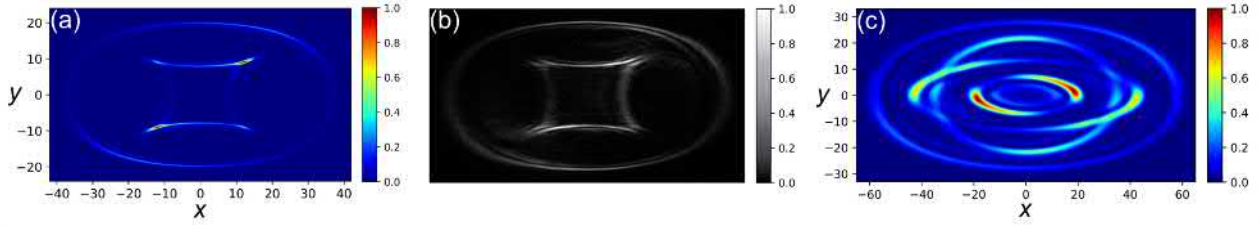


**Fig. 1:** Non-circular CD patterns generated via $\vec{k}$-space manipulation between a cascade of two or three BC's. (a) corresponds to theory and (b) corresponds to experiment for one particular case of a cascade of two BC's. An extension of the technique to 3 crystals is shown in (c). The variables $x$ and $y$ in the theoretical images (a) and (c) are proportional to the coordinates in the observation plane.

## References

[1] A. Forbes, M. Oliveira, M. R. Dennis, Nat. Photon. **15** 253–262 (2021)
[2] A. Turpin, Y. V. Loiko, T. K. Kalkandjiev, J. Mompart, Laser Photonics Rev. **10** 750-771 (2016)
[3] M. V. Berry, J. Opt. **12** 075704 (2010)
[4] A. Brenier, Opt. Mater. **110** 110504 (2020)
[5] S. Mohammadou, B. Mohamadou, G. Montemezzani, Opt. Express **25** 25392–25406 (2017)
[6] V. Peet, Opt. Lett. **40** 750-771 (2016)
[7] M. W. Iqbal, N. Marsal, G. Montemezzani, Sci. Rep. (submitted).

*Corresponding author: muhammad-waqar.iqbal@univ-lorraine.fr

# Quantum phases of bosonic chiral molecules in helicity lattices

**Felipe Isaule**[*1], **Robert Bennett** [1], **Jörg B. Götte** [1]

*1. School of Physics and Astronomy, University of Glasgow, Glasgow G12 8QQ, United Kingdom*

Chiral molecules have attracted significant multidisciplinary attention for many decades, from pharmaceuticals and the life sciences to quantum chemistry and optics. Of particular importance is the ability to identify and separate molecules of different chirality (known as enantiomers of each other), a process usually referred to as chiral discrimination [1].

Recently, the progress on laser cooling [2] has opened the possibility of cooling chiral molecules to the ultracold regime in the following years [3]. This will possibly open exciting new directions in the study of chiral molecules, much in analogy to the already well-established cold atom gases.

Anticipating these developments, in this work we theoretically study the phase diagram of cold and interacting chiral molecules immersed in recently proposed *helicity lattices* [4]. The lattices have homogeneous mean squared values of the electric field, but spatially varying helicity, and thus, they exert a discriminatory force on chiral molecules with different handedness [5]. We model these lattices with an extended Bose-Hubbard model [6], where the chiral molecules are represented as structureless bosonic particles which interact through repulsive on-site and dipolar long-range interactions.

We provide a detailed presentation of the different quantum phases shown by the helicity lattices. In particular, we find that a strong dipole-dipole repulsion between molecules results in the polarization of left/right enantiomers. In an experiment, this would produce a phase separation of enantiomers, acting as an alternative route towards chiral discrimination.

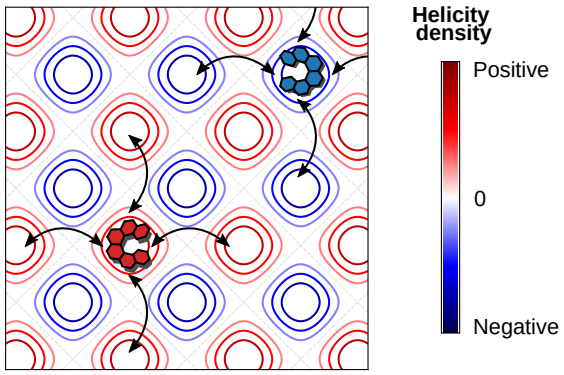


**Fig. 1:** Illustration of a square helicity lattice. Red and blue regions correspond to sites with opposite helicity densities. We assume that left (right) enantiomers can only move within red (blue) sites.

## References

[1] D . Patterson and M. Schnell, Physical Chemistry Chemical Physics **16**, 11114 (2014).
[2] D . McCarron, Journal of Physics B **51**, 212001 (2018).
[3] B . L. Augenbraun *et al.*, Physical Review X **10**, 031022 (2020).
[4] K . C. van Kruining, R. P. Cameron, and J. B. Götte, Optica **5**, 1091 (2018).
[5] A . Canaguier-Durand *et al.*, New Journal of Physics **15**, 123037 (2013).
[6] O . Dutta *et al.*, Reports on Progress in Physics **78**, 066001 (2015).

*Corresponding author: felipe.isaulerodriguez@glasgow.ac.uk

# Controlled generation of high-dimensional OAM entangled state without postselection

**Suman Karan**[*1], **Radhika Prasad** [1], **and Anand K. Jha** [1]
*1. Department of Physics, Indian Institute of Technology Kanpur, Kanpur, UP 208016, India*

The high-dimensional entangled state in orbital angular momentum (OAM) basis offers several advantages in terms of security in entanglement enabled quantum cryptographic protocols, noise robustness in quantum communications, strong generalized Bell's violations, quantum teleportation, and quantum sensing. Spontaneous parametric down-conversion (SPDC) is the most widely utilized method for generating entangled photon pairs in OAM basis, where a pump photon breaks into a signal(s), and an idler(i) photon. The two-photon state generated by SPDC can be expressed in Schmidt decomposed form as $\left|\Psi_{tp}\right\rangle = \sum_l S_l |l\rangle_s |-l\rangle_i$ for pump's OAM index $l_p = 0$, where $S_l$ is the two-photon OAM spectrum[1]. In order to harness the advantages of high-dimensional entangled states, one requires control over $S_l$. This is because some quantum information applications demand a specific form of the state for optimum performance. Furthermore, the generation of the state must be postelection-free, as it compromises the protocols' security benefits. So far, attempts to control $S_l$ without postselection have relied on either adjusting phase matching or pump shaping by changing the beam waist, both of which can only widen the spectrum[2]. Another pump shaping-based strategy by modifying the pump profile has recently been reported, which generates upto 24 -dimensional state with extremely limited control[3]. Here, we propose and demonstrate a method that combines pump-shaping with non-collinear phase matching to generate upto very high dimensional state with the desired shape of $S_l$ in a post-selection-free manner. We use coherent superposition of the radial modes $p$ with $l_p = 0$ in Laguerre-Gaussian (LG) basis as pump field and manipulate the superposition coefficients via active feedbacking to generate the desired spectrum. We generate upto 200-dimensional OAM entangled states of three different shapes: Gaussian, rectangular, and triangular. Control over the generation of such a high dimensional entangled state opens up a new avenue in quantum key distribution and quantum metrology.

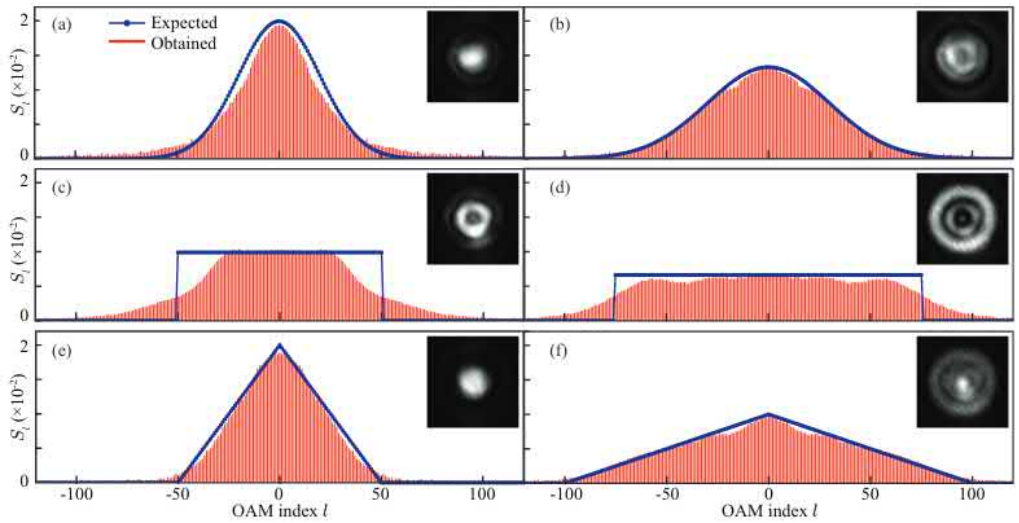


**Fig. 1:** Experimentally generated two-photon entangled OAM spectrum. Expected versus experimentally obtained (a)-(b) Gaussian, (c)-(d) rectangular, and (e)-(f) triangular spectrum of two distinct sizes in each. The associated pump intensity profiles are shown in the inset of each spectrum plot.

In the experiment, we use lab synthesized superposition state of five radial modes $p = 0$ to $p = 4$ of wavelength 405 nm and beam waist $w = 320\mu$m as a pump for SPDC. A $\beta$ - barium borate(BBO) crystal of thickness $L = 15$ mm is placed at noncollinear phase matching angle $\theta_p = 28.71^\circ$ for down-conversion. The two-photon spectrum is measured in the way described in Ref.[4]. Experimentally obtained spectra are shown in Fig.1, together with the corresponding pump superposition intensity profiles (see inset figure). Fig 1 (a), (b) display experimentally generated Gaussian spectrum with a standard deviation of 20 and 30 respectively. Fig.1 (c),(d) shows the rectangular spectrum of width 100 and 150 dimensions. The triangular shapes of base width 100 and 200 dimensions are shown in Fig.1 (e),(f) respectively.

## References

[1] C. K. Law and J. H. Eberly, Phys. Rev. Lett. 92127903 (2004)
[2] Girish Kulkarni, Lavanya Taneja, Shaurya Aarav, and Anand K. Jha, Phys. Rev. A 97063846 (2018)
[3] Shilong Liu, Yingwen Zhang, Chen Yang, Shikai Liu, Zheng Ge, Yinhai Li, Yan Li, Zhiyuan Zhou, Guangcan Guo, and Baosen Shi, Phys. Rev. A101052324(2020)
[4] Girish Kulkarni, Rishabh Sahu, Omar S. Magaña-Loaiza, Robert W. Boyd, and Anand K. Jha, Nat. Comm. 8 1054 (2017)

*Corresponding author: sumankaran2@gmail.com

# Self-focusing vortex beams in turbulence

**Meilan Luo** [1,2], **Matias Koivurova**[*3,4], **Marco Ornigotti** [3], **Chaoliang Ding** [5]

*1. Department of Physics and Synergetic Innovation Center for Quantum Effects and Applications, Hunan Normal University, Changsha, Hunan 410081, China*

*2. Institute of Photonics, University of Eastern Finland, P.O. Box 111, FI-80101 Joensuu, Finland*

*3. Tampere Institute for Advanced Study, Tampere University, 33100 Tampere, Finland*

*4. Faculty of Engineering and Natural Sciences, Tampere University, 33720 Tampere, Finland*

*5. Department of Physics and Henan Key Laboratory of Electromagnetic Transformation and Detection, Luoyang Normal University, Luoyang 471934, China*

A significant limiting factor for orbital angular momentum (OAM) based free-space optical communication is the signal degradation caused by atmospheric turbulence. Turbulence is known to cause loss of power due to defocusing, scintillation, as well as crosstalk between the various OAM states. These effects together render the detection of different OAM states quite challenging in noisy environments.

We have theoretically shown [1] that recently introduced self-focusing fields which carry orbital angular momentum [2], feature remarkable robustness against turbulence induced degradation when compared to a completely coherent beam. In moderately strong oceanic turbulence, the self-focusing OAM beam produces over five orders of magnitude higher peak intensities at the receiver plane, an 80% detection probability for the signal mode, as well as an energy transmission efficiency in excess of 70% over a link of $\sim 100$ m. Counter-intuitively, the focusing properties of such fields may be enhanced with increasing turbulence, causing the mean squared waist to become smaller with greater turbulence strength. Moreover, the focal plane position is only weakly affected by the strength of the turbulence.

These properties offer promise for beams with unprecedented sturdiness against turbulence. The propagation of such a beam is depicted in Fig. 1 below, in varying turbulence conditions. Our results demonstrate that certain types of partial coherence may be highly desirable for optical telecommunication employing OAM.

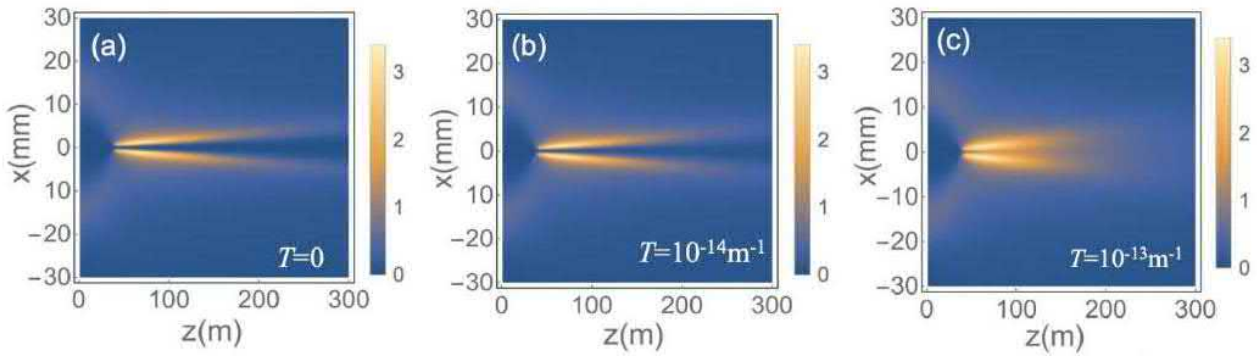


**Fig. 1:** Spectral density distribution of the self-focusing vortex beam propagating in free space (a) and turbulent ocean (b, c) in the $x-z$ plane with OAM index $m=2$. The turbulence parameter $T$ corresponds to $(b)$ moderate and (c) strong oceanic turbulence.

## References

[1] M. Luo, M. Koivurova, M. Ornigotti, and C. Ding, "Turbulence-resistant self-focusing vortex beams," arXiv:2203.01724

[2] Z. Mei, O. Korotkova, D. Zhao, and Y. Mao, "Self-focusing vortex beams," Opt. Lett. 46, 2384–2387 (2021).

*Corresponding author: presenting.author@email.com

# Complete self-healing of V-point singularities

**Baby Komal**[*1], **Gauri Arora** [1], **Sunil Kumar** [1], **P. Senthilkumaran** [2]
*1. Indian Institute of Technology Delhi, Hauz Khas, New Delhi-110016, India*
*2. Optics and Photonics Centre, Indian Institute of Technology Delhi, Hauz Khas, New Delhi 110016, India*

Self-healing of an optical beam is a remarkable property that makes it capable of regenerating its lost information after getting obstructed by any obstacle. Several beams like Bessel [1], Airy [2], and conical beams [3] have been reported earlier of showing intensity self-healing characteristics. We report here the complete self-healing of structured beams that contain V-point singularities.

V-point singularities are polarization singularities with predominant states of polarization as linear [4]. The singularity has null intensity, and the azimuths of the states of polarization (SOP) around the singularity vary in an orderly fashion. These singularities are characterized by indices, defined by the amount of azimuth rotation of the SOPs around it. The generic V-point singularities are radial, azimuthal, anti-radial and anti-azimuthal. They can be directly produced from the laser cavity and are also known to be stable for communication in atmospheric turbulence. V-point singularities being the superposition of spin and orbital angular momentum, increase the degree of freedom in optical communication.

The Poynting vector of a scalar vortex is helical, winding around the vortex core and advancing in the general beam propagation direction. The direction of energy flow is indicated by the direction of the Poynting vector [5], [6] and its transverse component helps in reconstructing the vortex beam. The vector field singularities are superpositions of scalar vortices with charges of equal magnitude and opposite polarity. The Poynting vectors of each component vortex rotate in the opposite sense and help in healing the singular beam faster than a scalar vortex. The polarization healing requires healing of relative phases and amplitudes of the component scalar vortices. The healing of component phases helps in achieving desired azimuth variation and an equal amplitude ratio between the components helps to achieve linear SOPs for V-points.

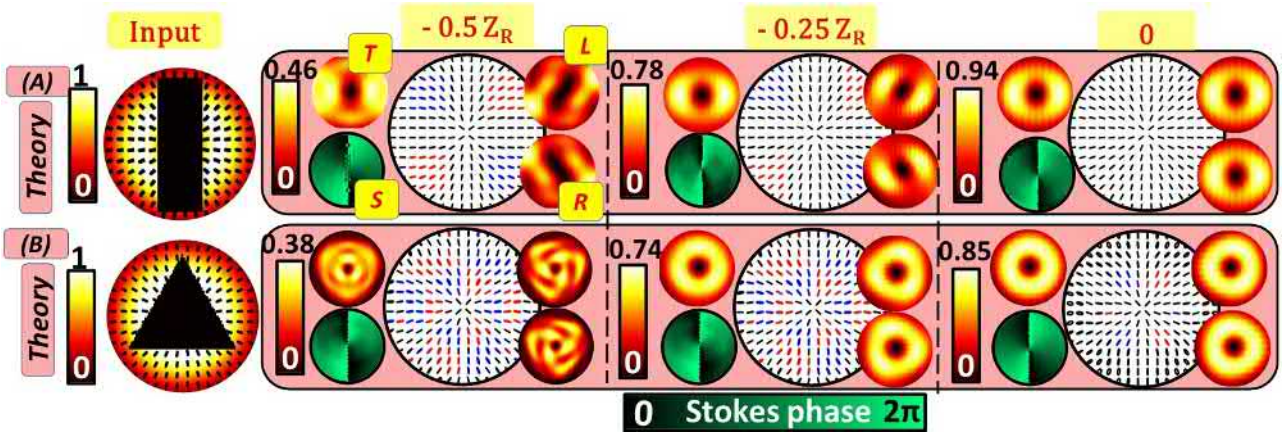


**Fig. 1:** Self-healing of radially polarized beams when symmetrically blocked at the center by a (A) rectangular and (B) triangular obstruction. The polarization patterns of the obstructed beam are observed at different distances. The respective total intensity distributions (T), Stokes phases (S), LCP component (L), and RCP component (R) are represented for each SOP.

It is interestingly observed that the V-points heals its intensity pattern as well as polarization distribution on facing different types of obstruction. The healing is observed in the far-field and is dependent on the shape, size, and symmetry of the obstruction. In Fig.1, V-point healing is observed for a radially polarized beam centrally obstructed by a rectangular and a triangular obstacle. It is observed that the beam heals its do-nut intensity structure with propagation. The Stokes $(S_{12})$ phase also regains its pattern in the far-field. Therefore, the polarization distribution can be visualized to reconstruct at the far-field.

In conclusion, the vector vortex beams are shown to self-heal both intensity and their polarization distribution. The recovery of relative phases and amplitudes of the polarization component fields guides the healing of the polarization distribution. The Poynting vector flow in the transverse plane of these beams plays an important role in the healing process. This self-reconstruction property of vector vortex beams can be of immense use, especially in optical communication.

## References

[1] V. Garc es-Ch avez , McGloin, H. Melville, W. Sibbett, K. Dholakia, Nature **419** 6903 (2002)
[2] J. Broky, G. A. Siviloglou, A. Dogariu, D. N. Christodoulides, Opt. Express **16** 17 (2008).
[3] B. K. Singh, D. S. Mehta, P. Senthilkumaran, Opt. Lett. **39** 7 (2014).
[4] P. Senthilkumaran, Singularities in Physics and Engineering, IOP Publish- ing, (2018).
[5] A. Bekshaev, K. Y. Bliokh, M. Soskin, J. Opt. **13** 5 (2011).
[6] B. K. Singh, M. Bahl, D. S. Mehta, P. Senthilkumaran, Opt. Commun. **293** (2013).

*Corresponding author: bkomal2015@gmail.com

# Spectral vector beams for high-speed spectroscopic measurements

**Lea Kopf**[*1], **Juan Deop Ruano**[1] **Markus Hiekkamäki**[1] **Timo Stolt**[1] **Mikko J. Huttunen**[1] **Frédéric Bouchard**[2] **Robert Fickler**[1]

*1. Photonics Laboratory, Physics Unit, Tampere University, Tampere, FI-33720, Finland*
*2. National Research Council of Canada, 100 Sussex Drive, Ottawa, Ontario K1A 0R6, Canada*

Spectroscopic measurements are amongst the most important optical experimental methods with applications ranging from physics to chemistry, material science, and biology [1]. Conventionally, spectroscopy is performed by measuring wavelength-dependent changes in the transmitted light. In one recent study, it was shown that a strong correlation between a transverse position and the polarization in spatial vector beams can be beneficially applied in high-speed kinematic sensing [2]. We extend this idea to the spectral domain and generate states of light, in which beams have a varying polarization vector across their frequency spectrum. We term such states of light *spectral vector beams* and use them for spectroscopic measurements [3].

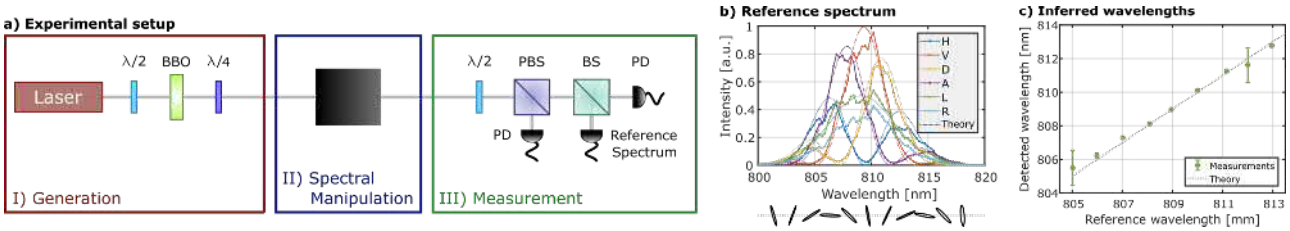


**Fig. 1:** Fig. 1: a) Sketch of the experimental setup. b) Measured spectra of a spectral vector beams with its corresponding polarization patterns. c) Inferred wavelengths from measurements with an adjustable bandpass filter.

We generate a spectral vector beam by superposing a left and right circularly polarized femtosecond pulse with a time delay. The pulse generated with an 80 MHz repetition rate has a duration of 220 fs and is centered around 808 nm. The time delay is realized by using a birefringent crystal and wave plates as shown in Fig. 1 a). Since a time delay translates into a linear phase shift in the frequency domain, coherently superposing the circularly polarized pulses generates a wavelength-dependent polarization pattern across the spectrum. Fig. 1 b) shows a recorded spectrum with its corresponding polarization ellipses. We use this correlation between frequency and polarization to link a polarization measurement outcome to a change in the spectrum, e.g. through absorption.

To demonstrate the capabilities of spectral vector beams as a spectroscopic method, we analyze the effect of a tunable bandpass filter on the spectrum. The measured polarization state is compared to a calibration measurement, which is obtained with a spectrometer of the unperturbed spectrum, e.g. as displayed in Fig. 1 b). As shown in Fig. 1 c), the center wavelength of the filter can be inferred with a standard deviation of 0.30 nm averaged over all reconstructed wavelengths and an averaged discrepancy of 0.20 nm with the expected reference wavelength. Similarly, a tunable absorption line is tracked with an averaged standard deviation of 1.84 nm and an averaged mean discrepancy of 0.34 nm. We show the high-speed capabilities of this technique by tracking a time-varying long-pass filter. Changes in the spectrum down to 166.5 ns are resolved within the bounds of the errors. The read-out speed can be further increased with a faster varying spectrum.

In summary, we demonstrate a simple method to generate spectral vector beams, i.e. light with strong correlation between polarization and its frequency components. Benefiting from this direct correlation, we show that high-speed spectroscopic experiments such as narrow line absorption or transmission measurements are possible using only polarization measurements. As such measurements can be done with fast photodetectors, the method is capable of tracking changes of the frequency spectrum with read-out rates that are only limited by the repetition rate of the laser and the response time of the detectors, i.e. in the GHz regime.

## References

[1] N. V. Tkachenko, "Optical spectroscopy: methods and instrumentations," Elsevier, (2006).
[2] S. Berg-Johansen, F. Töppel, B, Stiller, P. Banzer, M. Ornigotti, E. Giacobino, G. Leuchs, A. Aiello, C. Marquardt, "Classically entangled optical beams for high-speed kinematic sensing," Optica **2(10)**, 864-868 (2015).
[3] L. Kopf, J. Deop Ruano, T. Stolt, M. J. Huttunen, F. Bouchard, R. Fickler, "Spectral vector beams for high-speed spectroscopic measurements," Optica **8**, 930-935 (2021).

*Corresponding author: lea.kopf@tuni.fi

# High efficiency interface between multi-mode and single-mode fibers

**Oussama Korichi**[*1], **Markus Hiekkamäki** [1], **Robert Fickler** [1]
*1. Photonics Laboratory, Physics Unit, Tampere University, Tampere FI-33720, Finland*

Multi-mode fibers (MMFs) and Single-mode fibers (SMFs) are widely used in communication networks. Many factors need to be considered when choosing to utilize either MMFs or SMFs. For example, in applications that require distances of up to 500 m – 600 m, MMFs are the practical choice in terms of cost. Beyond that, SMFs are necessary due to the modal dispersion in MMFs [1]. Hence, a device for efficiently interfacing an MMF with an SMF would be beneficial to optical telecommunication.

In this work, we present a method capable of achieving this interfacing between an MMF and SMF using a multi-plane light conversion scheme (MPLC) [2]. With this method we demonstrate that only 3 phase modulations, realized with a single spatial light modulator (SLM), are enough to achieve MMF to SMF coupling efficiencies of $80\%, 60\%, 50\%$, and $40\%$, using MMFs with core diameters of $8.2\mu$m$, 25\mu$m$, 50\mu$m, and $200\mu$m, respectively.

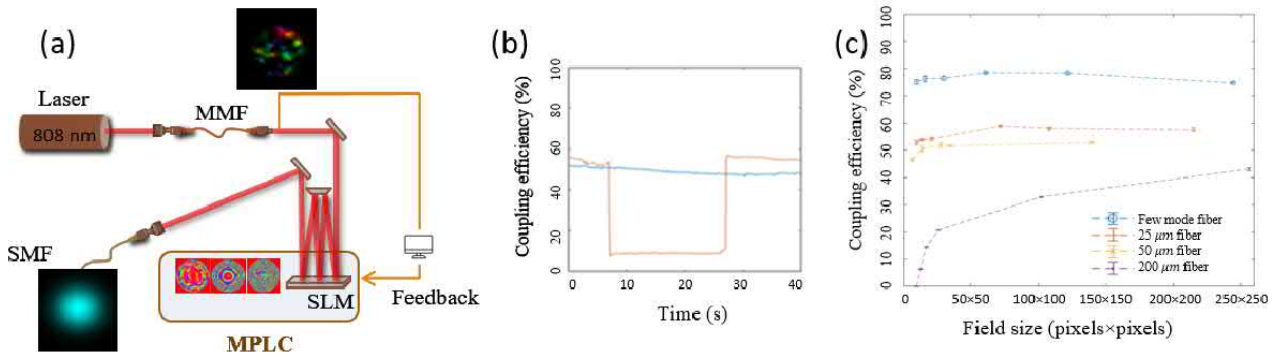


**Fig. 1:** This is the image on the homepage of the ICOAM22 conference.

In the experiment, we sent an 808 nm laser into an MMF and reconstructed the complex transverse amplitude of the output field from an interferogram [3]. We then used the obtained full field information to calculate the 3 phase modulation screens with wavefront matching [4]. The phase screens were optimized to transform the multi-mode field into the Eigenmode of the SMF, i.e., a Gaussian beam profile. The phase screens were used in an MPLC after which the transformed field was coupled into the SMF (see Fig. 1a). Because the field reconstruction as well as the mode transformation was updated in real-time, the obtained coupling efficiency remains stable even if the output field of the MMF changes entirely, for example through strong deformation of the fiber (see Fig. 1b). We additionally tested the influence of device resolution (both in the field reconstruction and MPLC) on coupling efficiencies (see Fig. 1c). For both, we found that commercially available devices with increased speed and efficiency, such as wavefront sensors and deformable mirrors, would be enough to establish an MMF to SMF interface working in the kHz-regime.

The presented method might find applications in optical telecommunication and could also be adapted to correct for very strong atmospheric disturbances in long distance free space communication

## References

[1] Peng, G. D. (Ed.). (2019). Handbook of Optical Fibers. Berlin/Heidelberg, Germany: Springer.
[2] Labroille, Denolle, Jian, Genevaux, Treps, Morizur. (2014). Efficient and mode selective spatial mode multiplexer based on multi-plane light conversion. Optics express, 22(13), 15599-15607.
[3] Takeda, Ina, Kobayashi. (1982). Fourier-transform method of fringe-pattern analysis for computer-based topography and interferometry. JOSA, 72(1), 156-160.
[4] Fontaine, Ryf, Chen, Neilson, Kim, Carpenter (2019). Laguerre-Gaussian mode sorter. Nature communications, 10(1), 1-7.

*Corresponding author: oussama.korichi@tuni.fi

# On the Differences between Helicity and Chirality

**Neel Mackinnon**[*1]
*1. School of Physics and Astronomy, University of Glasgow, Glasgow, G12 8QQ, United Kingdom*

Optical helicity [1] and optical chirality [2] are two quantities that are used to describe chiral electromagnetic fields. The former is defined in terms of the electric and magnetic vector potentials

$$h = \frac{1}{2}\left(\sqrt{\frac{\varepsilon_0}{\mu_0}}A\cdot\nabla\times A + \sqrt{\frac{\mu_0}{\varepsilon_0}}C\cdot\nabla\times C\right)$$

where $A$ and $C$ are defined such that $\nabla\times A = B$ and $\nabla\times C = -D$. The optical chirality, by contrast, is defined in terms of the fields directly. It is given by

$$\chi = \frac{\varepsilon_0}{2}\left(E\cdot\nabla\times E + c^2 B\cdot\nabla\times B\right)$$

In a monochromatic field the two quantities differ only by a constant factor, and the distinction between the two is therefore largely unimportant. However, in a polychromatic field no such proportionality holds, and the two quantities can show very different behaviour. This work explicitly examines the densities of optical helicity and chirality in some simple polychromatic fields: a superposition of two circularly polarised plane waves of different frequencies, a chirped pulse of circularly polarised light, and finally an "optical centrifuge" [3] - the superposition of two co-propagating pulses of circularly polarised light, of opposite handedness, chirped in opposite directions. Even in the simplest case, the polychromaticity can give rise to significant qualitative differences between the two quantities - they may have opposite signs, or one may be zero while the other is not. The origin of these differences lies in the different frequency scaling of the two quantities, which is made relevant by the presence of multiple frequency components in the fields.

**References**

[1] A. F. Rañada and J. L. Tureba, European Journal of Physics, 17, 141, (1996)
[2] Y. Tang and A. E. Cohen, Physical Review Letters, 104, 163901 (2010)
[3] J. Karczmarek, J. Wright, P. Corkum and M. Ivanov Physical Review Letters, 82,3420 (1998)
(This work) N. Mackinnon, Journal of Optics, 21, 125402 (2019)

[*]Corresponding author: first.author@email.com

# A Unifying Approach to Spin and Orbital Angular Momentum for Vector Spherical Harmonics

**Lewis Madden**[*1], **Mark R. Dennis** [1]
*1. School of Physics and Astronomy, University of Birmingham, United Kingdom, B15 2TT*

We present the description for a unifying approach for vector spherical harmonics as non-paraxial, electromagnetic vector fields carrying spin and orbital angular momentum through the familiar magnetic and electric multipole fields, most naturally suited for the case of circular polarisation. These Chandrasekhar-Kendall multipole fields [1] express intrinsic spin and orbital angular momentum in a manner to allow for their intuitive understanding for any field constructed from a scalar potential. We demonstrate this intuitive understanding through the analysis of the spin and orbital angular momentum densities, the quantities resulting from the familiar decomposition of the real part of the complex Poynting vector [2] [3]. We also present the Fourier dual description of such fields through the spin weighted spherical harmonics of Gel'fand, Minlos and Shapiro [4] and the spin raising and lowering operator of Newman and Penrose [5].

One may describe transverse electromagnetic waves through the "vectorisation" of scalar fields, $f_{l,m}$ [6]. Conventions differ between the use of the vector spherical harmonics (VSHs) and the vector multipole fields (VMFs). Here we use a convention outlined by Jackson [7] which closely aligns with the VMF definition,

$$\mathbf{CK}^{\pm}_{l,m}(\mathbf{r}) = \mathbf{M}_{l,m}(\mathbf{r}) \pm i\mathbf{N}_{l,m}(\mathbf{r}) := (\hat{\mathbf{L}} f_{l,m}) \pm \frac{1}{k}\nabla \times (\hat{\mathbf{L}} f_{l,m}).$$

These CK fields can be viewed as spin weighted spherical harmonics, the functions generated from the repeated action of Newman and Penrose's spin ladder operator, $\overset{\pm}{\eth} := -(\sin(\theta))^{\pm s}(\partial_\theta \pm i\csc(\theta)\partial_\phi)(\sin(\theta))^{\mp s}$ on the scalar spherical harmonics, paired with a spherical basis vector, $\mathbf{CK}^{\pm}_{l,m} \leftrightarrow \hat{\mathbf{e}}_{\pm\mp} Y_{l,m}$.

This connection is seen as natural by their Fourier duality, being the Fourier transform of the surface harmonics lying on the surface of a sphere with radius $k_0$. The CK fields form a convenient basis for Taylor expanding the focal field about the focal point and is consistent with the formalism of Richards & Wolf.

The CK fields encompass both the magnetic and electric multipole fields into a single object and so the usual OAM and SAM behaviour (FIG. 1 can be understood by considering a single CK as opposed to the separate E and H fields.

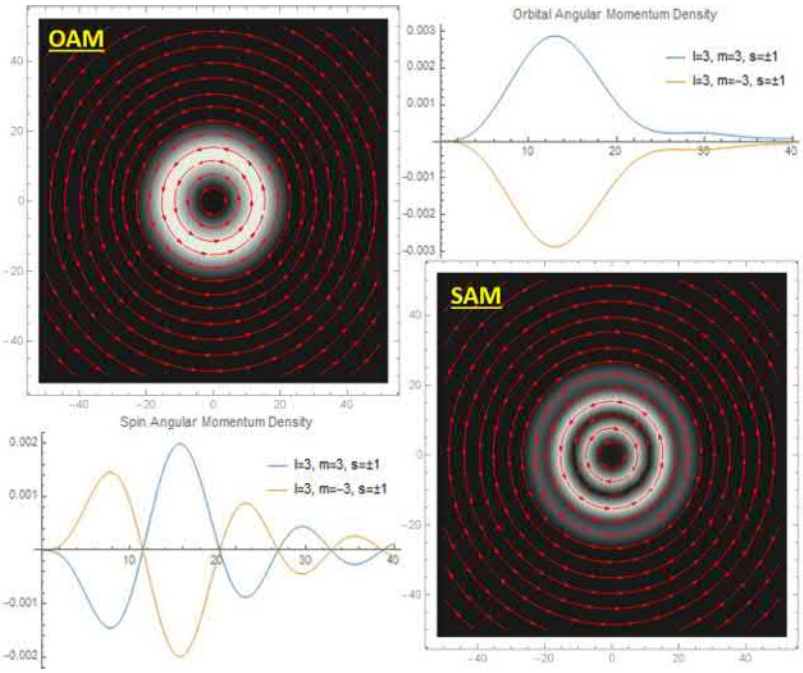


**Fig. 1:** Orbital and Spin angular momentum densities of spin 1 and -1 CK fields, generated from various scalar fields with $l = 3, m = \pm l$. The direction of circulation of the vector fields is determined by the sign, positive angular momentum density corresponds to anti clockwise circulation and negative, with clockwise circulation

## References

[1] S. Chandrasekhar, P. C. Kendall, *On Force-Free Magentic Fields*, The Astrophysical Journal **126**, 457, (1957)
[2] M. V. Berry, Journal of Optics A: Pure and Applied Optics **11**, 9 (2009)
[3] K. Y. Bliokh, F. Nori, *Transverse and Longitudinal Angular Momentum of Light*, Physics Reports, **592**, 1, (2015)
[4] I.M. Gel'fand, R.A. Minlos, Z.Y. Shapiro, *Representations of the Rotation and Lorentz Groups and Their Applications*(Dover Publications, New York, 2018)
[5] R. Penrose, E.T. Newman, Journal of Mathematical Physics, **7**, 863 (1966)
[6] L. C. Biedenharn, J. D. Louck, P. A. Carruthers, *Angular Momentum in Quantum Physics, 8*, Addison-Wesley Reading, MA (1981)
[7] J. D. Jackson *Classical Electrodynamics 2nd ed.* (Wiley, New York, 1975)

*Corresponding author: lxm039@student.bham.ac.uk

# Detection of Non-isotropic Partially Coherent Vector Vortex Beams

**Manisha**[*1], **Stuti Joshi** [1,2], **Saba N Khan** [1,3] **Bhaskar Kanseri** [1,4] **P Senthilkumaran** [1,5]

*1. Singular Optics lab, Department of physics, Indian Institute of Technology Delhi, Hauz Khas, New Delhi-110016, India*

*2. Palacky University, Olomouc, Czech Republic (77900)*

*3. SUPA, School of Physics and Astronomy, University of St Andrews, North Haugh, St Andrews KY16 9SS, UK*

*4. Experimental Quantum Interferometery and Polarization (EQUI), Department of physics, Indian Institute of Technology Delhi, Hauz Khas, New Delhi-110016, India*

*5. Optics and Photonics Canter, Indian Institute of Technology Delhi, Hauz Khas, New Delhi-110016, India*

We presented a method for detecting the polarization singularity index (PSI) of the non-isotropic partially coherent vector vortex beams (n-PCVVBs). Non-isotropicity signifies the distinguishability of the spatial correlations between the two orthogonal electric field components and their mutual correlations. Here we have used the advantage of the non-isotropic nature of n-PCVVBs to obtain the information of PSI. The present study foresees potential application in free-space optical communication, beam shaping, detecting and imaging the atmospheric lidar, and so on.

Polarization and coherence, beingtwo fundamental properties of light, were regarded as mutually independent entities until Wolf's unified theory came into picture [1]. This thought-provoking theory then provided ways to study the statistical properties of electromagnetic (EM) beams in both scalar and vector domain [1][2]. Recently these coherence-induced polarization properties of Em fields attracted lots of attention, when explored in singular fields (for example: phase and polarization singularities). The orbital angular momentum (OAM) and spin angular momentum (SAM) contents of these fields provide an extra degree of freedom, which finds application in free-space communication, robust beam generation , and so on [3]. Vector vortex beams (VVBs) are the special class of polarization singularities, where the predominant SOPs are linear with intensity null at the center [3]. These VVBs are characterized by PSI ($\eta = \frac{1}{2\pi}\oint \Delta\varphi$), $\varphi$ being azimuth and the line integral gives the gradient of azimuth around the singularity. More recently, the generation and detection of isotropic $\delta_{xx} = \delta_{yy}$ vector vortex beams are explored[5]. For these beams the intensity profile is circularly symmetric (see Fig. 1 column(b)) but for non-isotropic$\delta_{xx} \neq \delta_{yy} \neq \delta_{xy}$ PCVVBs, the intensity distribution is azimuthaly asymmetric, which found to be useful in the detection of such beams.

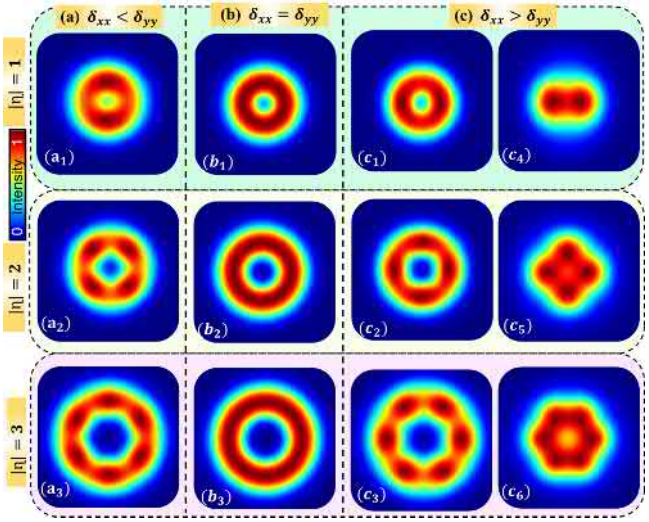


**Fig. 1:** The far-field intensity distribution for various index n-PCVVBs at columns (a). $\delta_{xx} < \delta_{yy}$, (b). $\delta_{xx} = \delta_{yy}$, (c). $\delta_{xx} > \delta_{yy}$

The n-PCVVBs, in the space-frequency domain are characterized by a $2 \times 2$ cross-spectral density (CSD) matrix (**W**), whose elements are of the form $W_{ij}, (i, j = x, y)$ [1]. Using these elements, one can deduce the CSD elements at the observation plane and the intensity distribution at the observation plane can be given as [1]

$$I = W_{xx} + W_{yy} \tag{1}$$

Fig. 1 shows the intensity distributions for various index n-PCVVBs. Three cases are shown here. Column (a) and (c) are the cases, where the non-isotropic nature coming into picture. Due to the non-isotopicity, a no. of high intensity lobes (N) appearing in the azimuthal direction, which are twice of the PSI ($|\eta| = \frac{N}{2}$) of the input beam. The appearance of these lobes depict the higher correlation parameter as one can compare the cases of columns (a) and (C). The distribution of lobes are rotated by $\frac{\pi}{2|\eta|}$ with respect to each other on either cases. Whenever non-isotropicity is there, the PSI can be depicted for very low values of correlations also see $(c_4 - c_6)$. Such detection are useful in communication, detecting and imaging, and so on.

## References

[1] Emil Wolf, Introduction to the Theory of Coherence and Polarization of Light, Cambridge University Press (2007)

[2] Olga Korotkova and Emil Wolf, Optics Communications **246** 35 (2005)

[3] Paramasivam Senthilkumaran, Singularities in Physics and Engineering, IOP Publishing (2018)

[4] Stuti Joshi, Saba NKhan, Bhaskar Kanseri and P Senthilkumaran, Physical Review A **103** 053502 (2021)

[5] Kedar Khare, Priyanka Lochab and Paramasivam Senthilkumaran, Orbital Angular Momentum States of Light, coordinates (2020)

[*]Corresponding author: manisha12101994@gmail.com

# Nonparaxial optical fields containing all possible polarization ellipses in a 4D physical space-time

**David Marco**[*1], **Miguel A. Alonso**[†1,2]
*1. Aix Marseille Univ, CNRS, Centrale Marseille, Institut Fresnel, F-13013 Marseille, France.*
*2. The Institute of Optics, University of Rochester, Rochester, NY 14627, USA.*

Paraxial optical fields containing all transverse polarization ellipses have been widely studied. In particular, the so-called full Poincaré beams [1] map the entire Poincaré sphere surface onto each transverse plane according to stereographical mapping. Recently, 2D skyrmionic structures (also known as baby skyrmions) have been found in the orientation of the spatially variant Stokes vectors in a family of full Poincaré beams [2] since they map a 2D physical space to an entire 2D parameter sphere wrapping around it. More recently, a 3D skyrmionic hopfion has been found in the propagating volume of a beam containing all possible transverse polarization and phase states [3]. Analogously to paraxial fields spanning all transverse polarization ellipses, we present an optical field containing all possible non-paraxial polarization states.

For paraxial fields only two parameters are required to describe the normalized polarization state at each point, since the ellipses are essentially constrained to the plane normal to the main propagation direction (Fig. 1(a)). Therefore, a 2D section of the physical space is sufficient to perform a mapping that spans such a 2D parameter space. On the other hand, the plane containing each polarization ellipse can change for a nonparaxial field having a position-dependent polarization pattern (Fig. 1(b)). Four parameters are thus needed to describe a normalized ellipse oriented in a 3D space. Three of these parameters can be chosen as the components of the normalized spin density vector **S**, which is a vector in 3D real space normal to the plane containing the ellipse. In the paraxial case, this plane does not change, so the direction of **S** remains constant (Fig. 1 (a)), but it does change in the non-paraxial case (Fig. 1 (b)). The length and sense of **S** encode the ellipticity and helicity (that matches $S_3$ in the paraxial case). The fourth parameter would then correspond to the orientation of its semi-major axis on the plane normal to **S**. Alternatively, the four parameters can be encoded in terms of two indistinguishable points over a unit sphere, such that their coordinates are bisected by **S** and their separation is parallel to the ellipse's major axes. At least two ways to define these points have been proposed [4] [5], each with its own desirable properties.

A nonparaxial optical field with all possible polarization ellipses has to be defined over a fourth-dimensional space in order to map the complete 4D parameter polarization space. Here, we present experimentally realizable mathematical solutions describing a spatially- and temporally-varying periodic optical field containing all possible nonparaxial polarization ellipses in a unit cell in the 4D physical space-time. The temporal variation is implemented by slowly varying in time the amplitude ratio between two groups of plane waves with non-coplanar linear polarizations. Some of the solutions presented have the property of presenting uniform intensity, both spatially and temporally. Techniques for their experimental implementation are discussed.

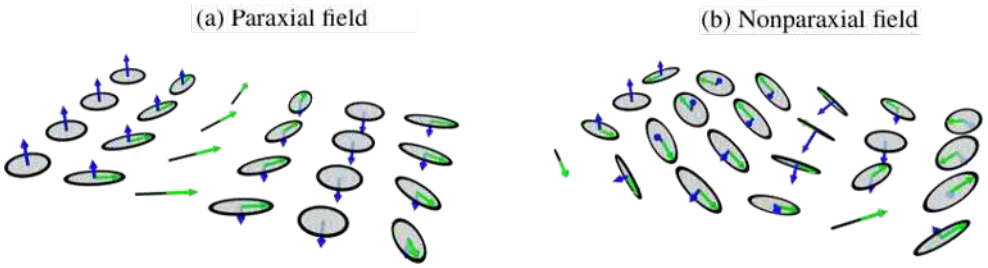


**Fig. 1:** Polarization ellipses of a planar section for two polarization spatially-variant optical fields corresponding to discrete superpositions of plane waves. (a) paraxial field. (b) Nonparaxial field. The normalized spin density vector **S** and the vector defining the orientation of the semi-major axis are depicted in blue and green, respectively.

## References

[1] A. M. Beckley, T. G. Brown, M. A. Alonso, Opt. Express **18** (10) 10777-10785 (2010)
[2] S. Gao, F. C. Speirits, F. Castellucci, S. Franke-Arnold, S. M. Barnett, J. B. Götte, Phys. Rev. A **102** (5) 053513 (2020)
[3] D. Sugic, R. Droop, E. Otte, D. Ehrmanntraut, F. Nori, J. Ruostekoski, C. Denz, M. R. Dennis, Nat. Commun. **12** (1) 1-10 (2021)
[4] J. H. Hannay, J. Mod. Opt. **45** (5) 1001-1008 (1998)
[5] K. Y. Bliokh, M. A. Alonso, M. R. Dennis, Rep. Prog. Phys. **82** (12) 122401 (2019)

[*]Corresponding author: david.marco@fresnel.fr
[†]Corresponding author: miguel.alonso@fresnel.fr

# Semiclassical approximation of Zernike amplitudes via the Higgs oscillator

**Kerr Maxwell**[*1,2] **Mark R Dennis**[1,2]

*1. EPSRC Centre for Doctoral Training in Topological Design, University of Birmingham, Birmingham B15 2TT, UK*

*2. School of Physics and Astronomy, University of Birmingham, Birmingham B15 2TT, UK*

The Poincaré parametrisation, historically used to describe polarisation, has recently been used to describe general structured Gaussian beams via a semiclassical Hamiltonian (ray) optics picture (*1*). In this work we attempt to extended this analysis of the underlying ray structure of paraxial beams to the *complex Zernike modes* (*2*) described by $Z_n^m(r,\phi) = R_n^{|m|}(r)e^{in\phi}$. Higgs showed that these modes are related to the spherical dynamics of repulsive potentials (*3*), the seperability of such solutions to the "Higgs oscillator" has been extensively studied (*4*). This repulsive spherical dynamics can be mapped, via the Gnomonic projection (projection through the centerpoint, see Figure 1a) onto the "repulsive" harmonic oscillator, described by $H_- = \frac{1}{2}(p_i p_i - q_i q_i)$. The isotropic harmonic oscillator $H_+$ and repulsive oscillator $H_-$ both admit decompositions into constants of the motion

$$H_+ = L^2 + M_+^2 + \overline{M_+}^2 \quad \text{and} \quad H_- = -L^2 + {M_-}^2 + \overline{M_-}^2$$

where for $H_-$ the constants are

$$\begin{aligned} L &= xp_y - yp_x, \\ M_- &= \frac{1}{2}(px^2 - py^2 - qx^2 + qy^2), \\ \overline{M_-} &= p_x p_y + q_x q_y. \end{aligned}$$

The allowed combinations of the constants of the motion for $H_-$ trace out a hyperboloid of one sheet (see Figure 1b). These constants are consistent with those described by Higgs and Fradkin (*5*) if one takes $\omega^2$ to be negative.

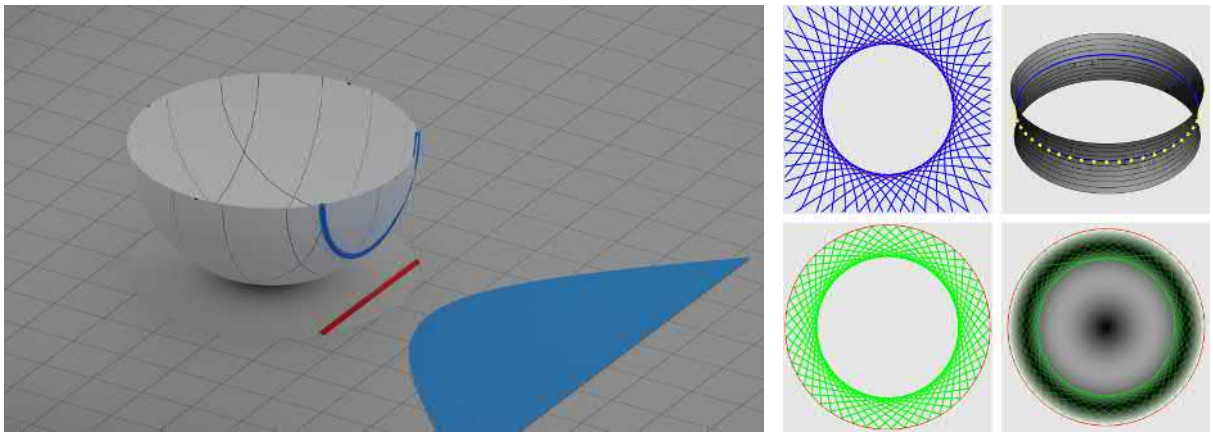

(a) (b)

Figure 1: (a): A ray from the semiclassical Zernike approximation is mapped onto a hemisphere, the Gnomonic projection of the enclosed solid angle is shown by the (truncated) blue area. (b): Eigenrays of the repulsive oscillator (blue) are hyperbolas in the plane (UL), Each hyperbole corresponds to a point on the hyperboloid (UR), each path described here lies on the $L = 1$ contour, each of these are mapped to a straight line (green) under the inverse Gnomonic projection (LL), semiclassical approximations can then be used to build the Zernike mode, whos exact function form is plotted with the rays in LR (work in-progress).

By solving this tractable dynamical system and mapping the resulting hyperbolic paths back into the unit disk via orthogonal projection of the Higgs oscillator, we can use the procedure outlined by Dennis and Alonso (*1*) to dress the rays with a Gaussian profile or phase and thus construct a semiclassical approximation of a complex Zernike mode. From this we hope to derive a geometric quantisation condition for the complex Zernike modes.

## References

1. M. R. Dennis, M. A. Alonso, *Journal of Physics: Photonics* **1**, 025003 (2019).
2. M. Born, E. Wolf, *Principles of optics: electromagnetic theory of propagation, interference and diffraction of light* (Elsevier, 2013).
3. P. W. Higgs, *Journal of Physics A: Mathematical and General* **12**, 309–323 (Mar. 1979).
4. N. M. Atakishiyev, G. S. Pogosyan, K. B. Wolf, A. Yakhno, *Physica Scripta* **94**, 045202 (2019).
5. D. Fradkin, *Progress of Theoretical Physics* **37**, 798–812 (1967).

*Corresponding author: kxm149@student.bham.ac.uk

# A practical approach to measuring paraxial optical Skyrmions

**Amy McWilliam**[*1], **Claire M. Cisowski**[1], **Jörg B. Götte**[1], **Fiona C. Speirits**[1], **Zhujun Ye**[1], **Stephen M. Barnett**[1], **Sonja Franke-Arnold**[1]

*1. School of Physics and Astronomy, University of Glasgow, Glasgow, G12 8QQ, UK*

Skyrmions and their topological properties have been a topic of interest in a wide range of physics, including the study of mesons [1], quantum liquids [2] and magnetic materials [3]. In optics, Skyrmions can be found in propagating paraxial beams, arising when we have superpositions of orthogonally polarised spatial modes [4]. Thanks to recent advances in the design of polarisation-structured light beams via digital holograms, many first experiments have reported the generation of optical Skyrmions [5, 6, 7].

The experimental measurement of Skyrmion numbers, however, is not straight-forward. Previous experimental work has relied either on showing the qualitative similarity between measured polarisation profiles and the theoretical Skyrmions, or by evaluating the Skyrmion number numerically. Skyrmion number is, by definition, a global property of a light beam, that relies on integrating polarisation gradients over the entire transverse beam profile. Gradients are notoriously sensitive to noise, especially in beam areas with very limited intensities, where a fluctuating noise level may overwhelm the signal. Here, we will present an alternative method to calculate Skyrmion numbers, based on contour integration, which removes the need for polarisation gradients. We compare and evaluate both measurement techniques for a variety of experimentally generated optical Skyrmions as well as Skyrmion lattices, demonstrating that our contour method is indeed more robust to noise and hence advantageous when dealing with experimental data.

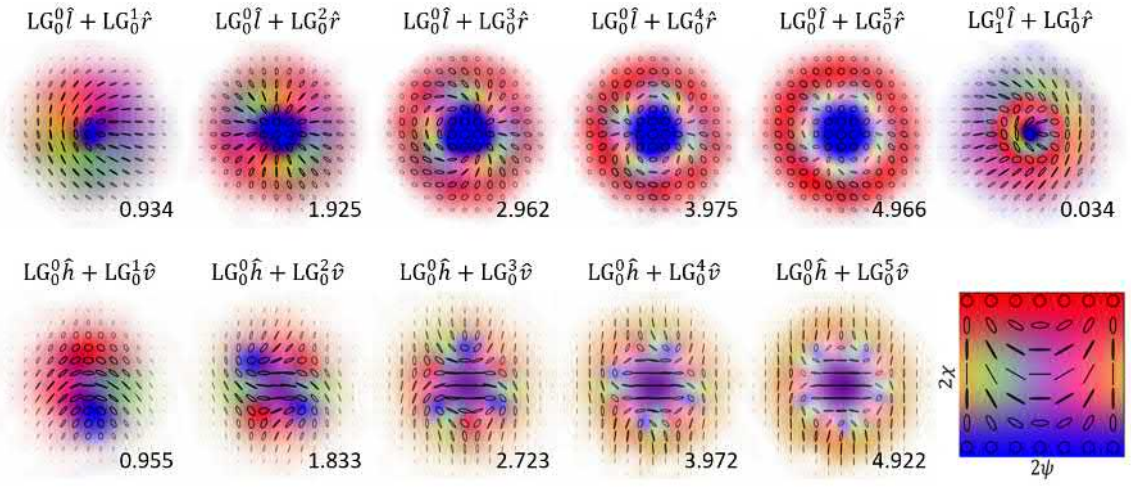


**Fig. 1:** Experimentally measured polarisation structures for vector beams with Skyrmion numbers 1 - 5, and a Poincaré beam with Skyrmion number 0. The top row shows beams of the form $\Psi = \left(\mathrm{LG}_p^\ell|0\rangle + \mathrm{e}^{i\theta}\mathrm{LG}_p^\ell|1\rangle\right)/\sqrt{2}$, with $\theta = 0$, for $|0\rangle = \hat{l}, |1\rangle = \hat{r}$. The bottom row shows beams of the same form but in the horizontal, vertical polarisation basis, $|0\rangle = \hat{h}, |1\rangle = \hat{v}$. The experimentally measured Skyrmion numbers for each beam are indicated. The colour scheme used is shown, where $\chi$ and $\psi$ represent the polarisation ellipticity and orientation, or the azimuthal and polar angles on the Poincaré sphere, respectively, and the intensity is indicated by opacity.

## References

[1] T. H. R. Skyrme, Proc. R. Soc. Lond. Ser. A **260**, 127 (1961).
[2] D. Vollhardt, and P. Wolfle, The Superfluid Phases of Helium 3 (Dover Publications, 2013)
[3] A. Bogdanov and C. Panagopoulos, Nat. Rev. Phys. **2**, 9, (2020)
[4] S. Gao, F. C. Speirits, F. Castellucci, S. Franke-Arnold, S. M. Barnett and J. B. Götte, Phys. Rev. A **102**, 053513 (2020)
[5] D. Sugic, R. Droop, E. Otte, D. Ehrmanntraut, F. Nori, J. Ruostekoski, C. Denz, and M. R. Dennis. Nat. Commun. **12**, 1, (2021)
[6] Y. Shen, E. C. Martínez, and C. Rosales-Guzmán, ACS Photonics **9** (2022)
[7] J. Zhu, S. Liu and Y. Zhang arXiv:2103.11293v2 [quant-ph]

*Corresponding author: a.mcwilliam.1@research.gla.ac.uk

# Orbital angular momentum-based pseudospin coupling in photonic lattices with higher-order conical intersections

**Philip Menz**[*1], **Haissam Hanafi** [1], **Cornelia Denz** [1]

*1. Institute of Applied Physics, University of Münster, Corrensstr. 2/4, 49149 Münster, Germany*

Conical diffraction is a signature of wave propagation governed by a spectral conical intersection. The phenomenon was first studied in biaxial crystals, where the propagation constants of two polarizations of light display a "diabolical" point degeneracy, i.e. a singularity of the spectrum, at a conical intersection. Conical diffraction was thus one of the starting phenomena in singular polarization optics and perhaps the first example of a geometric phase in physics [1].

Recently, conical intersections have also come to the forefront in the electronic band structure of graphene, where the so-called Dirac cones also exhibit diabolical points [2]. Inspired by their electronic counterparts, conical intersections have been studied and realized in the spatial band structure of photonic lattices, emulating their electronic counterparts. Like in the biaxial crystal case, light propagation near the conical intersections of such lattices also exhibits conical diffraction. This in turn mimics the evolution of relativistic spin- $1/2$ Dirac fermions for conical intersections of two bands, as demonstrated in photonic graphene [3], and relativistic spin-1 bosons for three bands, like in the Lieb lattice [4].

In analogy with these particles' real half-integer or integer spin, an additional degree of freedom called pseudospin can be defined for the quasiparticles of such a conical intersection. In photonic lattices, the pseudospin defines how the wavefunction's amplitude and phase are distributed in the substructure of space given by the lattice. Since in photonic lattices a conical intersection is excited by a structured light field carrying orbital angular momentum, conical diffraction and generation of optical phase vortices with topological charge conversion can be observed during propagation (see Fig 1 (b) and (c)). This is due to the interaction of pseudospin with OAM, which maps the spectral singularity into real space [5].

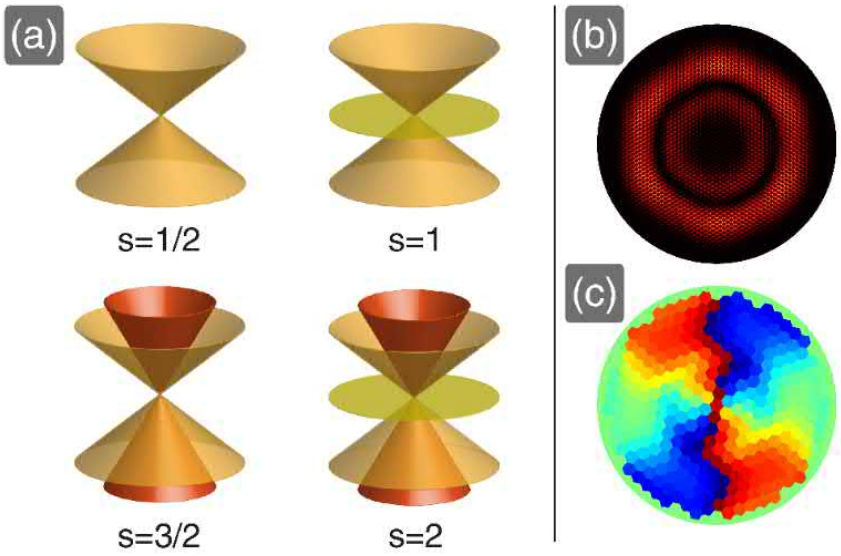


**Fig. 1:** (a) Conical intersections of different pseudospin order s. (b) Conical diffraction intensity in a photonic lattice. (c) Formation of optical phase vortices in a conical diffraction pattern.

Till now, conical diffraction and its topological charge conversion have been shown only for pseudospin $1/2$ and $1$ . In our contribution, we advance the understanding of pseudospin and its action on orbital angular momentum extending it to higher conical intersections in the spatial spectrum of periodic refractive index potentials. We investigate a fivefold spectral degeneracy in the band structures of a novel photonic lattice structure. We present an intuitive approach to explain the connection between spectral and phase singularities, i.e., pseudospin and orbital angular momentum. We show how structured light fields addressing the pseudospin eigenstates diffract conically during propagation in the photonic lattice, and how topological charge conversion leads to the formation of optical phase vortices in the conical diffraction output pattern. Our results pave the way to photonic realizations of conical intersections with higher pseudospin, which mimic relativistic particles with spin values beyond the standard model.

## References

[1] M. Berry, M. Jeffrey, Prog. Opt. 50, 13-50 (2007).
[2] A. K. Geim, K. S. Novoselov, Nat. Mater. 6, 183-191 (2007).
[3] D. Song, V. Paltoglou, et. al., Nat. Commun. 66272(2015).
[4] F. Diebel, D. Leykam, et. al., Phys. Rev. Lett. 116183902 (2016).
[5] X. Liu, S. Xia, et. al., Nat. Commun. 111586 (2020).

*Corresponding author: philip.menz@uni-muenster.de

# A geometric approach to torus-knot angular momentum in high harmonic radiation

**Björn Minneker**[*1,2,3], **Birger Böning**[2,3], **Anne Weber**[1], **Stephan Fritzsche** [1,2,3]

*1. Theoretisch Physikalisches Institut, Friedrich-Schiller-Universität, Jena, Germany*
*2. GSI Helmholtzzentrum für Schwerionenforschung GmbH, Darmstadt, Germany*
*3. Helmholtz Institut, Jena, Germany*

In recent years, strong-field processes like above-threshold ionization, and high harmonic generation (HHG) have gained in importance. In particular, high-energetic radiation emitted in the HHG process can nowadays be tailored quite precisely by utilizing the driving beam properties. Recent investigations [2,3] imply that bicircular twisted Laguerre-Gaussian beams possess a definite torus knot angular momentum (TKAM) $\hat{J}_\gamma = \hat{L} + \gamma\hat{S}$ as a new form of angular momentum. TKAM is conserved in nonlinear atomic processes such as high harmonic generation and can be classified by a time delay parameter $\tau$ and a coordination parameter $\gamma$. These parameters are defined by the respective projected orbital angular momentum $\ell_i$ and the energy $\hbar p_i \omega_0$ of the two superimposed Laguerre-Gaussian beams. We derive a consistent geometric method to determine $\tau$ and $\gamma$ from the driving beam as well as from the high harmonic radiation. The method relates both invariance parameters ($\tau$ and $\gamma$) to a torus knot which can be constructed from the emitted high harmonic radiation. These knots are constructed from the spatio-temporal evolution of the electric field of the respective high harmonic radiation or the driving beam. We demonstrate the classification of the invariance parameters for a planar atomic gas target irradiated by bicircular Laguerre-Gaussian beams explicitly. In addition, we demonstrate that the respective torus knots determined by $\tau$ and $\gamma$ can be mapped onto each other within minor modifications. The numerical calculations are done within the strong-field approximation and the associated quantum orbit approach. Therefore, we also briefly review high harmonic generation by bicircular twisted light beams. This introduced geometric method denotes a different approach to interpret the invariance parameters $\tau$ and $\gamma$, as well as their underlying relations, compared to a purely formal derivation. The investigations presented in this work are in good agreement with previous findings and provide insight into the dynamical symmetry of TKAM in the context of high harmonic generation induced by bicircular twisted Laguerre-Gaussian beams.

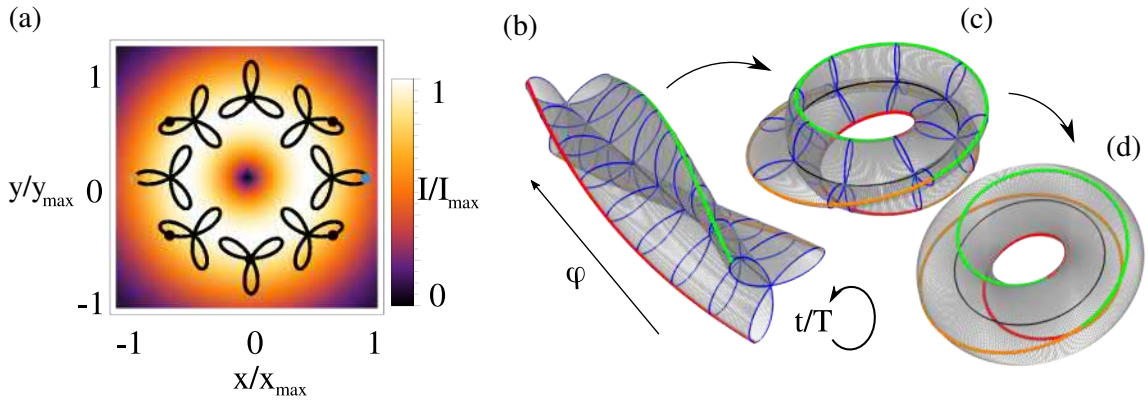


**Fig. 1:** The basic concept to visualize torus-knot angular momentum: (a) Intensity distribution of the driving beam ($\ell_1 = \ell_2 = 1$, $\omega_1 = \omega_2/2 = \omega$) in the target plane. Lissajous figures indicate the polarization of the superimposed LG beams for fixed azimuthal angles $\varphi$. The black dots indicate the electric field vector for a fixed time $t$ and azimuthal angle $\varphi$. The colored dots display the electric field maxima for fixed $\varphi$ and $t$. (b) The blue Lissajous figures are identical to the one in subfigure (a), where $\varphi = 0$ denotes the position at which the electric field vector is maximized (blue dot). The green, red, and orange lines denote the positions of the field maxima. (c) If the open ends in (b) are connected, the green, red, and orange lines form a torus knot. (d) Projection of the torus knot constructed in (c) onto a torus [3].

## References

[1] E.Pisanty et.al. Nat.Photon. 13, 569 (2019)
[2] E.Pisanty et.al. Phys. Rev. Lett. 122, 203201 (2019)
[3] B.Minneker et.al. Phys. Rev. A 104, 053116 (2021)

*Corresponding author: bjoern.minneker@uni-jena.de

# Anisotropic Spatial Entanglement

**Satyajeet Patil**[*1,2], **Shashi Prabhakar**[1], **R. P. Singh** [1]

*1. Quantum Science and Technology Laboratory, Physical Research Laboratory, Ahmedabad 380009, India*
*2. Indian Institute of Technology, Gandhinagar, India 382355.*

Spontaneous parametric down-converted (SPDC) photon pairs violate the EPR-like correlations in the measurement of transverse position and momentum. Due to their strong spatial correlations, SPDC photons find applications in quantum imaging [1] [2]. For the SPDC photons, transverse position correlation length depends on the crystal thickness, whereas transverse momentum correlation length depends on the beam-waist and spatial coherence length of the pump [3]. By controlling these parameters, it is possible to engineer the output spatial entangled state.

Here, we utilize circular asymmetry of the pump by using elliptical-Gaussian beam (EGB), which can carry arbitrary orbital angular momentum (OAM) as high as $1000\hbar$ per photon [4], to change the degree of entanglement in orthogonal transverse directions for down converted photons generated through type-I parametric process in a BBO crystal. The schematic is shown in Fig. 1(a). We applied the method described in [3] to find spatial correlations. Using an EGB, the same nonlinear crystal can generate entangled states of different strengths. We plan to explore the effect of anisotropy of position-momentum entanglement on OAM entanglement.

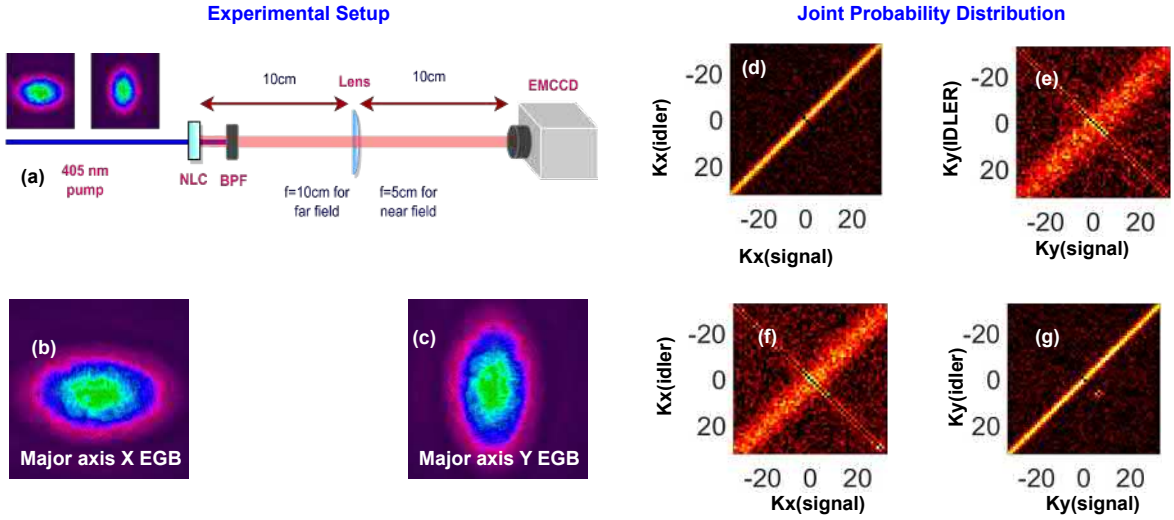


**Fig. 1:** (a) Experimental setup to find near and far field correlations. NLC: Nonlinear crystal, EMCCD: Electron multiplying CCD Camera, BPF: bandpass filter. (b) & (c) EGB with major axis along $x$ and $y$ respectively. (d) & (e) Joint probability distribution along $x$-axis and $y$-axis for EGB with major axis along $x$. (f) & (g) Joint probability distribution along $x$-axis and $y$-axis for EGB with major axis along $y$.

Table 1 shows the variation in measurement of conditional uncertainty ($\Delta(P_{x_s}|P_{x_i})$ & $\Delta(P_{y_s}|P_{y_i})$) of transverse momentum for different orientations of the EGB. Since position correlation length depends only on the crystal length, it does not change with the orientation of EGB. Such anisotropic correlations may find applications in quantum communication through anisotropic media and the imaging fields where the different correlation strengths are required along different directions.

**Table 1:** Variation in momentum correlation length with respect to rotation of the EGB.

| Rotation EGB | $\Delta(P_{x_s}\|P_{x_i})$ | $\Delta(P_{y_s}\|P_{y_i})$ |
|---|---|---|
| 0 | $2.0292\times10^{-3}\pm0.04\ \hbar/\mu$m | $4.2829\times10^{-3}\pm0.17\ \hbar/\mu$m |
| $\pi/2$ | $4.0387\times10^{-3}\pm0.15\ \hbar/\mu$m | $2.1538\times10^{-3}\pm0.05\ \hbar/\mu$m |

## References

[1] H. Defienne, M. Reichert, J. W. Fleischer, et al. Sci. Adv. **5**, eaax0307, (2021)
[2] H. Defienne, J. Zhao, E. Charbon, et al. Phys. Rev. A **103**, 042608 (2021)
[3] M. Edgar, D. Tasca, F. Izdebski, et al. Nat Commun **3**, 984 (2012)
[4] J. Courtial, K. Dholakia, L. Allen, et al. Opt. Commun. **144**, 210 (1997)

*Corresponding author: satyajeetpatil1992@gmail.com

# Observation of triangular-lattice pattern in nonlinear wave mixing with optical vortices

**B. Pinheiro da Silva**[*1], **G. H. dos Santos** [2], **A. G. de Oliveira** [2], **N. Rubiano da Silva** [2], **W. T. Buono** [3], **R. M. Gomes** [4], **W. C. Soares** [5], **A. J. Jesus-Silva** [6], **E. J. S. Fonseca** [6], **P. H. Souto Ribeiro** [2], **A. Z. Khoury** [1]

*1. Instituto de Física, Universidade Federal Fluminense, 24210-346 Niterói, RJ, Brazil*
*2. Departamento de Física, Universidade Federal de Santa Catarina, CEP 88040-900, Florianóplis, SC, Brazil*
*3. School of Physics, University of the Witwatersrand, Private Bag 3, Johannesburg 2050, South Africa*
*4. Instituto de Física, Universidade Federal de Goiás, CEP 74690-900, Goiânia, GO, Brazil*
*5. Núcleo de Ciências Exatas – NCEx, Universidade Federal de Alagoas, CEP 57309-005, Arapiraca, AL, Brazil*
*6. Instituto de Física, Universidade Federal de Alagoas, CEP 57072-970, Maceió, AL, Brazil*

We investigated the cross spatial modulation in nonlinear wave mixing in both frequency up and down conversion schemes, as illustrated in Fig 1. The cross modulation effect was evinced by the demonstration of a striking triangular lattice pattern formed when an optical vortex is mixed with a triangular shaped beam through parametric interaction. This intriguing effect is related to the triangular lattice formed when an optical vortex is diffracted through a triangular aperture, conform was demonstrated in Ref. [1]. However, the spatial cross talk through nonlinear interaction encompasses a richer behaviour, specially regarding the phase conjugation effect that results from the stimulated down-conversion process as compared to the up-conversion scheme. Besides their intrinsic interest from the fundamental point of view, our findings can be useful for a broad audience in optics and photonics, specially for generating structured light fields at wavelengths where spatial modulators are not available.

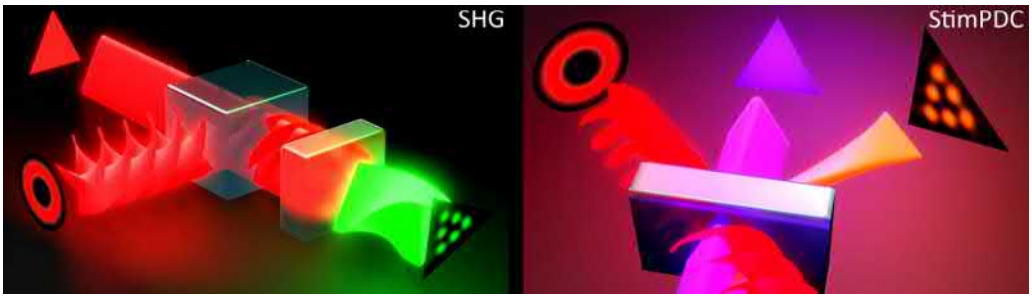


**Fig. 1:** Cross modulation of light fields in nonlinear wave mixing. Left panel: input fields (in red) of same frequency and different spatial structures in second-harmonic generation (SHG). Right panel: input fields of different frequencies and spatial structures (in red and purple) in stimulated parametric down-conversion (StimPDC).

## References

[1] Hickmann, J. M. and Fonseca, E. J. S. and Soares, W. C. and Chávez-Cerda, S., Phys. Rev. Lett. **105** 053904 (2010)

*Corresponding author: braianps@gmail.com

# Photo-excitation of atoms by vector Laguerre-Gaussian beams

**Shreyas Ramakrishna**[*123], **Jiri Hofbrucker**[1,2], **Stephan Fritzsche** [1,2,3]

*1. Helmholtz-Institut Jena, Fröbelstieg 3, D-07743 Jena, Germany*

*2. GSI Helmholtzzentrum für Schwerionenforschung GmbH, Planckstrasse 1, D-64291 Darmstadt, Germany*

*3. Theoretisch-Physikalisches Institut, Friedrich-Schiller-Universität Jena, Max-Wien-Platz 1, D-07743, Jena, Germany*

Laguerre-Gaussian beam [1] can have cylindrical polarization in addition to circular, linear or elliptical polarization. A cylindrically polarized Laguerre-Gaussian beam is also known as a vector Laguerre-Gaussian beam ([2],[3]). In this work, we present a theoretical model to analyze the interaction of atoms with cylindrically polarized Laguerre-Gaussian beams. In particular, we analyze the excitation process of atoms with a single valence electron by cylindrically polarized Laguerre-Gaussian beams. Theoretical analysis is performed within the framework of first-order perturbation theory and by expanding the vector potential of the Laguerre-Gaussian beam in terms of its multipole components. For cylindrically polarized Laguerre-Gaussian beams, we show that the (magnetic) sub-components of electric-quadrupole field vary significantly in the beam cross-section with beam waist and radial distance from the beam axis. In addition, we calculate the total excitation rate of electric quadrupole transition ($4s\,^2S_{1/2} \rightarrow 3d\,^2D_{5/2}$) in a mesoscopic target of $Ca^+$ ion. These calculations shows that the total rate of excitation is sensitive to the beam waist and the distance between center of the target and the beam axis. Our results [4] explicitly show that the cylindrically polarized Laguerre-Gaussian beam is more efficient in driving electric quadrupole transition in the mesoscopic target than the circularly polarized beams.

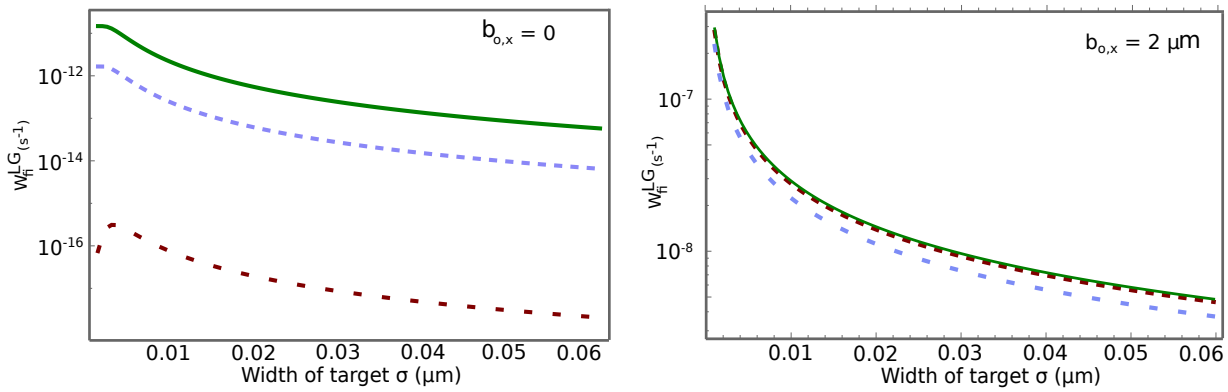


**Fig. 1:** Log plot of the total rate of excitation $W_{fi}^{LG}(s^{-1})$ for electric quadrupole transition between 4s $^2S_{1/2} \rightarrow$ 3d $^2D_{5/2}$ levels of $Ca^+$ ion driven by LG beam is plotted as a function of width of the target $\sigma$ for azimuthal (green solid line), radial (brown dashed line) and circular polarization (blue dotted line). In the top figure the target is placed on the beam axis $b_{o,x} = 0$ and in the bottom figure the target is displaced from the beam axis by $b_{o,x} = 2\ \mu m$. In both the plots, the radial index $p$ and beam waist $w_o$ is kept fixed at 0 and $2.7\mu m$ respectively.

## References

[1] S. M. Barnett, M. Babiker, and M. J. Padgett, Philos. Trans. R. Soc. A, **375**, 20150444 (2017)
[2] J. Wang, F. Castellucci, and S. Franke-Arnold, AVS Quantum Sci. **2**, 031702 (2020)
[3] G. F. Quinteiro, D. E. Reiter, and T. Kuhn, Phys. Rev. A, **95**, 012106 (2017)
[4] S. Ramakrishna, J. Hofbrucker, S. Fritzsche, Phys. Rev. A. **Accepted** (2022)

*Corresponding author: shreyas.ramakrishna@uni-jena.de

# Swinging and Rotating Pendulum Beams: 3D modal wavepackets that simulate the quantum-pendulum

**Valeria Rodríguez-Fajardo***, **Thao Nguyen, Jacob M. Freedman, Enrique J. Galvez†,**
*Department of Physics and Astronomy, Colgate University, Hamilton NY 13346, United States of America*

In nature, there are distinct physical phenomena that are described by the same mathematical framework. This opens the possibility of studying a system by analogy to another, a strategy that is particularly useful in cases where observation of the first one is somehow strenuous or not possible. This is the case of the quantum pendulum and the Mathieu beams: for a matter wave confined to a circle under the influence of a restoring force, the time-independent Schrödinger equation is reduced to the Mathieu equation [1]; correspondingly, for electromagnetic waves assuming an harmonic dependence in time, the two-dimensional Helmholtz equation in elliptical coordinates results in the angular and radial Mathieu equations [2], with the former being identical to the one obtained for the pendulum. As such, Mathieu beams whose Fourier spectrum intensity share the same form with the probability density distribution of the pendulum's position are now known as pendulum beams [3,4].

The energy levels of the quantum pendulum are quantized and are represented by the index $n$, which, due the pendulum's $2\pi$-periodicity requirement, must be even. The behaviour of the pendulum depends on how the energy of the state $n$ compares to the energy of the potential barrier $q$. Since we can access arbitrary values of $q$ for Mathieu beams, we can study different scenarios of the quantum pendulum [4]. Mathieu beams as found directly from the Helmholtz equation are adiffractional and carry an infinite amount of energy, which is not physically feasible. Thus, in the laboratory we generate Mathieu-Gauss beams, which are non-diffracting only over a finite propagation range. Mathematically, they are expressed as

$$\mathrm{MG}_n^{e,o}(\xi,\eta,z;q) = \exp\left(-\frac{ik_t^2}{2k}\frac{z}{\mu(z)}\right)\mathrm{GB}(\mathbf{r})\,\mathrm{M}_n^{e,o}(\xi,\eta;q), \tag{1}$$

where the superscripts $e,o$ stand for even and odd, respectively, and determine their symmetry with respect to the origin, $(\xi,\eta)$ represent the elliptical coordinates (related to Cartesian coordinates by $x = f\cosh\xi\cos\eta$ and $y = f\sinh\xi\sin\eta$, with f the semi-focal distance of the elliptical system), $z$ is the propagation distance, $k_t$ and $k$ are the transverse and total wave numbers, respectively, $\mathrm{GB}(\mathbf{r}) = \exp\left(\frac{-r^2}{\mu(z)w_0^2}\right)\frac{\exp(ikz)}{\mu(z)}$ is the Gaussian beam, with $w_0$ the Gaussian beam width, and $\mathrm{M}_n^{e,o}$ are the adiffractional Mathieu beams given by $\mathrm{M}_n^e(\xi,\eta;q) = C_n\,\mathrm{Je}_n(\xi;q)\,\mathrm{ce}_n(\eta;q)$ and $\mathrm{M}_n^o(\xi,\eta;q) = S_n\,\mathrm{Jo}_n(\xi;q)\,\mathrm{se}_n(\eta;q)$ with $C_n$, $S_n$ normalization constants and $\mathrm{Je}_n$ ($\mathrm{ce}_n$) and $\mathrm{Jo}_n$ ($\mathrm{se}_n$ ) the even and odd radial (angular) Mathieu functions, respectively.

Here, we are interested in observing the evolution of the pendulum rather than its stationary state. Specifically, we want the propagation distance $z$ of the light beam to play the role of time in the pendulum. It is then necessary to make $w_0$ sufficiently large so that $\mu(z) = 1 + i2z/(kw_0^2) \approx 1$ in the observation range, making the field of the form $\mathrm{f}(\mathbf{r_t})e^{k_z z}$ in analogy to the pendulum $\mathrm{g}(\mathbf{r})e^{-\varepsilon t}$. In the laboratory, we generated suitable superpositions of Mathieu beams and studied their progression upon propagation (Fig. 1a). We observed cases analogous to an unbounded pendulum (a rotor) for energies much larger than $q$, where the intensity pattern rotates about its center (Fig. 1b), to a bounded pendulum, where the intensity is confined to a specific angular ($\eta$) range and the energy rearranges itself or "swings" on propagation, when the energies are much smaller than $q$ (Fig. 1c), as well as cases with features of both regimes when the energies are comparable to $q$ (not shown here for the sake of brevity). In the future, we expect to further investigate other superpositions and extend our analogy to pendulums with more complex dynamics.

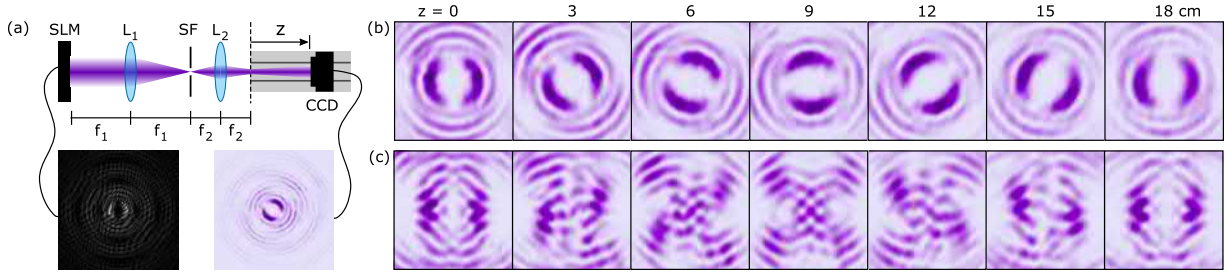


**Fig. 1:** (a) Schematic sketch of the experimental setup. Light from a He-Ne laser is expanded and collimated to overfill a SLM (liquid crystal Spatial Light Modulator). We display a suitable hologram onto the SLM and image it using two lenses ($L_1$ and $L_2$) in a 4f configuration, such that we obtain the desired superposition at the back focal plane of the second lens. Images for different propagation distances ($z$) are acquired by means of CCD camera mounted on a motorized rail. Unwanted diffraction orders are blocked by a spatial filter (SF) located at the focal plane between the two lenses. Example images of the computer generated hologram (using complex amplitude modulation) and light beam are shown for reference. Sequence of example images for superpositions generating (b) an unbounded pendulum (a rotor) and (c) a bounded pendulum.

This work was funded by the National Science Foundation grant PHY-2011937.

## References

[1] E. U. Condon, Phys. Rev. **31** 891 (1928)
[2] J. C. Gutiérrez-Vega, M. D. Iturbe-Castillo, S. Chávez-Cerda, Opt. Lett. **25(20)** 1493 (2000)
[3] M. R. Dennis, J. D. Ring, Opt. Lett. **38(17)** 3325 (2013)
[4] E. J. Galvez, F. J. Auccapuclla, Y. Qin, K. L. Wittler, J. Freedman, J. Opt. **23(2)** 024001 (2021)

*Corresponding author: vrodriguezfajardo@colgate.edu
†Corresponding author: egalvez@colgate.edu

# Design and fabrication of silicon metasurfaces for control of structured light beams.

**F. Romanato** [1,2,4], **A. Vogliardi** [1], **M. Ferrari** [1], **A. Sabatti** [1], **V. Grillo** [3], **and G. Ruffato** [1,2],

*1. Department of Physics and Astronomy, University of Padova, via Marzolo 8, 35131 Padova (Italy)*
*2. Quantum Technologies Research Center, University of Padova, via Gradenigo 6, 35127 Padova (Italy)*
*3. CNR-Istituto Nanoscienze, Centro S3, Via G Campi 213/a, I-41125 Modena (Italy)*
*4. CNR-IOM Istituto Officina dei Materiali, S.S. 14 - Km. 163.5 - 34149 Trieste (Italy)*

Metalenses have shown the possibilities to generate very complex optical layouts and structured light. We consider a general framework where the generation, transmission, and measurement of structured beams are described in terms of conformal mappings implemented by harmonic phases. The general solutions, called 'multipole phases' after their similarity with the integrated potentials of electric/magnetic multipoles, suggest even-unexploited solutions for spatial multiplexing [1] that overcome the limitations of previous techniques based on OAM beams. Also algebra of OAM modes can be managed and controlled, performing multiplication and division of beams embedding different OAM values $[2, 3]$.

We also show the capability to generate multiple high-resolution focused OAM modes at different points in space by exploiting by exploiting the polarization of the incident beam as a degree of freedom. In particular, dual-functional transmission dielectric metalenses based on a set of meta-atoms manipulating both the dynamic and geometric phases, can generate completely different optical layouts simply changing the incoming polarization. More generally, exploiting illumination control in term a of polarization helicity and structured phase- amplitude space distribution it is possible to generate independent and/or interacting combination of multi foci/multi vector beams (VVBs), in order to obtain dynamic control of a multi beams structure. Simulation and experiments based on nanofabricated metalenses will be presented. The results offer a robust techno-logical foundation for exploiting spatial degrees of freedom of structured light in the miniaturization and integration of photonics devices for applications in the fields of high-resolution microscopy, optical manipulation, and optical communications, both in the classical and single-photon regimes.

## References

[1] G. Ruffato, V. Grillo, F. Romanato, Opt. Express 29(23), 38095-38108 (2021)
[2] G. Ruffato, M. Massari, F. Romanato, Light: Sci. & Appl. 8, 113 (2019).
[3] G. Ruffato, F. Romanato, Opt. Express 28(23), 34201-34218 (2020).

# Towards digital, self-contained structured light tools for research and industry

**Keshaan Singh**[*1], **Wagner Tavares Buono** [1], **Sabino Chavez-Cerda** [2], **Manuel Fernandes** [3], **Angela Dudley** [1], **Andrew Forbes** [1]

*1. School of Physics, University of the Witwatersrand, Private Bag 3, Johannesburg 2050, South Africa*
*2. Optics Department, Instituto Nacional de Astrofísica, Óptica y Electrónica, Apartado Postal 51/216, Puebla 72000, Mexico*
*3. School of Chemistry, University of the Witwatersrand, Private Bag 3, Johannesburg 2050, South Africa*

Light, when appropriately structured in its various degrees of freedom, presents interesting physical properties which have proven beneficial for various academic and industrial applications. For instance, the orthonormality of common spatial mode bases is useful for communication, while the non-diffracting structures as well as optical singularities provide advantages when applied to microscopy [1][2]. In order for the benefits of structured light to be readily transferred to fields outside of photonics, easily accessible and affordable solutions need to be provided. We present a series of digital tools for the generation, manipulation and detection of structured light beams, primarily based on micro-mirror technology [3][4][5]. We reveal how affordable, high-speed, polarization insensitive solutions can be achieved over the visible spectrum - by demonstrating the tools themselves; as well as their application in investigating novel vector fields, performing birefringence measurements on a range of materials and even testing a novel communication scheme [6][7].

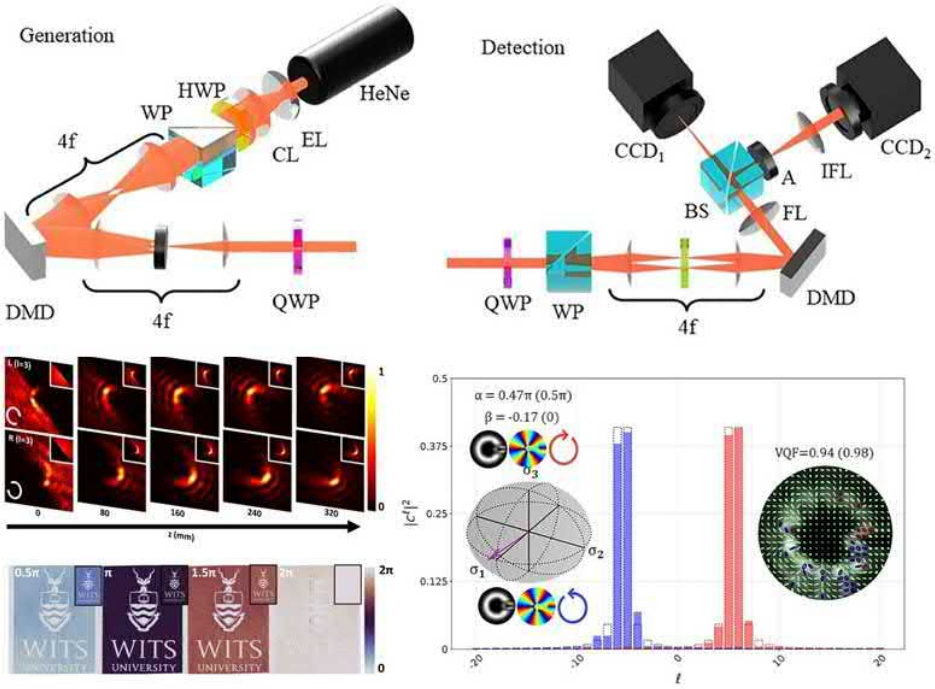


**Fig. 1:** Figure showing schematics of some micromirror based tools for structrued light generation and detection (top) and results obtained using these tools to probe light and matter (bottom).

## References

[1] A. Forbes, M. de Oliveira, M.R. Dennis, Nat. Phot. **15(4):253-61**, (2021).
[2] C. Rosales-Guzmán, B. Ndagano, A. Forbes, **20(12):123001** J. Opt. (2018).
[3] C. Rosales-Guzmán, XB. Hu, A. Selyem, P. Moreno-Acosta, S. Franke-Arnold, R. Ramos-Garcia, A. Forbes. Sci. Rep. **10(1):1-9**, (2020)
[4] K. Singh, N, Tabebordbar, A. Forbes, A. Dudley, JOSA A. **37(11):C33-44**. (2020).
[5] K. Singh, A. Dudley, Nanophot. **11(4):753-61**, (2022).
[6] K. Singh, W.T. Buono, M.A. Fernandes, A. Dudley, A. Forbes, Opt. Exp. **29(21):34616-28** (2021).
[7] K. Singh, W.T. Buono, S. Chavez-Cerda, A. Forbes, JOSA A. **38(9):1248-54**. (2021).

*Corresponding author: keshaanSingh@gmail.com

# OAM Mode Conversion using Two Dimensional Multimode Interference (2D MMI) Couplers

**Afsoun Soltani**[*1], **Zaker Hossein Firouzeh** [1], **S. Faezeh Mousavi** [3], **Rahman Nouroozi** [??]

*1. Department of Electrical and Computer Engineering, Isfahan University of Technology, Isfahan, Iran*
*2. Department of Physics, University of Trieste, Trieste, Italy*
*3. Department of Physics, Institute for Advanced Studies in Basic Sciences, Zanjan, Iran*

Recently, the implementation of rectangular waveguides for generation and manipulation of OAM modes, have been developed to exploit the outstanding features of these modes in more complex integrated devices. Multimode Interference (MMI) structures with many interesting features like their compact size, low sensitivity to fabrication parameters, and ease of fabrication, that are used in both 1D and 2D, are efficient candidates for OAM applications.

According to the imaging properties of OAM modes in 2D square cross sectional MMI waveguides, an incident OAM mode exhibit field splitting and OAM-maintaining image at lengths $3L_c/4$ and $3L_c/2$ of the waveguide, respectively. $L_c$ is the coupling length between the two lowest order modes, given by:

$$L_c = \frac{4n_g W_{eff}^2}{3\lambda_0}; \quad W_{eff} = W + \frac{\lambda_0}{\pi\sqrt{n_g^2 - n_c^2}}$$

where $n_g, n_c, \lambda_0$, and $W$ are the guide index, the cladding index, the working wavelength, and the waveguide width, respectively. It is worth mentioning that any order of OAM modes can be decomposed into odd- and even- mode field components as [1]: $f_{OAM}(x,y) = f_{odd}(x,y) \pm i f_{even}(x,y)$, where $\pm$ sign is determined by the sign of the OAM order $(\pm l)$. In accordance with Eq. (2), OAM modes with opposite topological charges have identical real parts and $\pi$ phase difference in imaginary parts. This fact has been used to design a 2D MMI switch between OAM modes with $l = \pm 1$ by applying $\pi$ phase shift between sided decomposed field components at $3L_c/4$ length of the MMI waveguide that correspond to the imaginary part of OAM mode. The proposed structure (Figure 1 .(a)) consists of three main parts including two MMI waveguides and four intermediate ports in between. The first MMI waveguide with field splitting length of $3L_c/4$ decomposes the input OAM mode. Figure 1.(b) and (c) display power distributions (left) and phase patterns (right) of the input OAM mode with $l = +1$ and the decomposed field at the field splitting length, respectively. Intermediate ports in the second part, guide up and down field patterns with no change in phase, and apply $\pi$ phase shift between the sided decomposed fields (Figure 1.(d)). The second MMI waveguide in the third part of the structure composes the manipulated fields in the last part and makes OAM mode with opposite topological charge (Figure 1.(e)). The simulation of the structure performance has been done using the commercially available simulation software package OptiBPM 13.1. All the simulations assume a vacuum wavelength of $\lambda_0 = 1550$ nm, and a silicon waveguide $(n_g = 3.45)$ surrounded by silica $(n_c = 1.45)$. The calculated purity of the output mode is 93%.

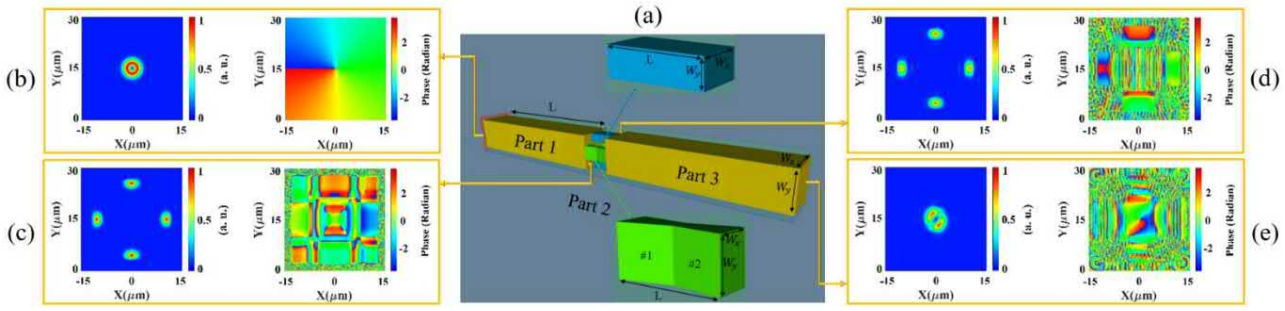


**Fig. 1:** (a) Schematic representation of the proposed structure: Part 1 (First MMI waveguide), Part 2 (Intermediate ports including the linear waveguides (up and down) and the tapered phase shifters (right and left)), and Part 3 (Second MMI waveguide). (b)-(e) Power distributions (left) and phase patterns (right) of the input OAM mode with $l = +1$, the decomposed field at the field splitting length, the decomposed field after the intermediate ports, and the output generated OAM mode with $I = -1$, respectively.

Table 1. Geometrical parameters of the proposed structure

| Components | | | $W_x(\mu m)$ | $W_y(\mu m)$ | $L(\mu m)$ |
|---|---|---|---|---|---|
| Part 1 and Part 3 | First and second MMI waveguide | | 25 | 25 | 1221 |
| Part 2 | Linear waveguides | | 10 | 6 | 189 |
| | Tapered phase shifters | #1 | 6~3 | 10 | 189/2=94.5 |
| | | #2 | 3~6 | 10 | 189/2=94.5 |

## References

[1] Z. Ma, H. Chen, K. Wu, Y. Zhang, Y. Chen, and S. Yu, Self-imaging of orbital angular momentum (OAM) modes in rectangular multimode interference waveguides, Optics Express, vol. 23, no. 4, pp. 5014-5026 (2015).

*Corresponding author: afsun.soltani@ec.iut.ac.ir

# Integrated orbital angular momentum mode sorters on vortex fibers

**Shlomi Lightman*** [1] **Lavi Somers**†[2], **Ilan Bleyhman**‡ [2], **Gilad Hurvitz** [1], **Raz Gvishi** [1], **Leslie A. Rusch** [3], **Ady Arie** [2]

*1. Applied Physics Division, Soreq NRC, Yavne 81800, Israel*

*2. School of Electrical Engineering, Tel Aviv University, Tel-Aviv 69978, Israel*

*3. Center for Optics, Photonics and Lasers, ECE Dept., Universitè Laval, Quèbec, Canada*

Light waves that carry orbital angular momentum (OAM) can be utilized to increase the channel capacity of classical optical communication systems by space division multiplexing, or as a multi-dimensional basis for quantum optical communication. These OAM modes can be carried in vortex fibers with minimum inter-modal coupling. In order to utilize the different OAM modes in the fibers, they need to be multiplexed and demultiplexed, but up until now this was primarily achieved by bulky and large devices.

Here we report on the design, fabrication and characterization of an integrated mode sorter for vortex fibers. It consists of three optical elements: a parabolic lens that collimates the OAM beams at the fiber exit, a transformer that unwraps the azimuthal phase and a corrector that corrects the residual phase deviations [1]. A focusing lens term corrects the residual phase deviations [1]. A focusing lens term was embedded into the corrector, so that the sorted modes will be focused at a desired output plane. These three elements, together with supporting posts, provide a miniature, well aligned, robust and polarization insensitive device that was printed directly on the exit tip of the vortex fiber [2]. The printing process was carried out using a commercial 3D-direct laser writing system (Photonic Professional GT, Nanoscribe GmbH, Germany) due to its high optical quality negative-tone IP-S photo-sensitive material.

We investigate two types of vortex fibers, RCF2 and RCF5 [3]. RCF 2 carries four relevant modes - two fundamental LP $L_{01}$ modes (hence with zero OAM), with either right circular polarization (RCP) or left circular polarization (LCP), and two $OAM_{\pm 1,1}$, each one carrying only one circular polarization and with orbital angular momentum of $+\hbar, -\hbar$. RCF5 carries four additional $OAM_{+2,1}$ modes, ie two modes that can have two orthogonal circular polarizations, and with OAM of $+2\hbar, -2\hbar$. The size of the polarizations, and with OAM of $+2h, -2h$. The size of the sorters with the supporting posts is
about $150\mu m \times 150\mu$mX$150\mu$m. There are some differences in the overall size and the structure of the supporting posts between the two sorter designs for the two fibers, as can be seen in figure 1 but the underlying design concept is identical.

The entire integrated system was characterized by injecting vortex beams carrying different OAM values, $-2\hbar \leq l\hbar \leq 2\hbar$ into the appropriate vortex fiber. By setting $l = 0$ state as a reference, other modes could be analyzed according to their transverse location on the camera. As can be seen in figure 2 and figure 3 , the sorters send each OAM mode to a different position at the output plane. The device is polarization insensitive, and operates in a similar manner for LCP and RCP states. The measurements are in good for LCP and RCP states. The measurements are in good agreement with the theoretical simulation. The sorters can now be readily used for applications in classical and quantum communication.

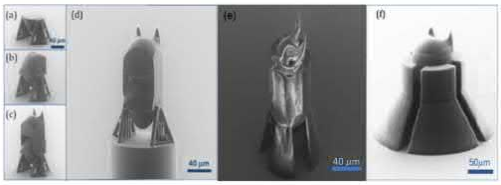


Figure 1: Figure 1: SEM images of the integrated mode sorter on a vortex fiber. (a-c) The elements during the printing process: a collimating lens, a transformer and a corrector. (d) A sorter on an RCF-2 OAM fiber. (e) Final design of a sorter for RCF-2 OAM fiber with additional protective and stabilizing support structure. (f ) A sorter for RCF-5 OAM fiber with additional protective and stabilizing support structure

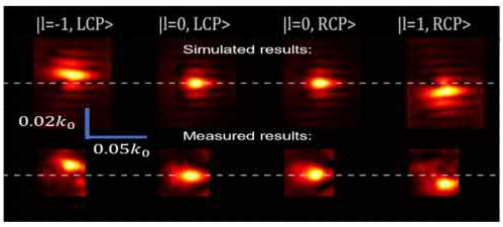


Figure 2: Figure 2: Simulation and measurement at the sorter output plane, for 4 different modes that propagated in RCF2 vortex fiber.

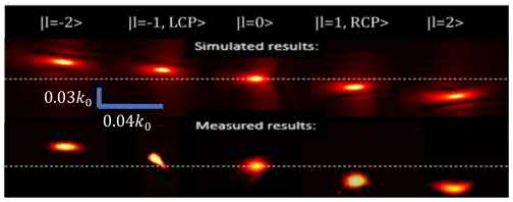


Figure 3: Figure 3: Simulations and measurements of 6 different modes that propagated in RCF-5 vortex fiber.

Acknowledgment. This work was supported by the Pazy Foundation.

## References

[1] E. Bolduc, N. Bent, E. Santamato, E. Karimi, and R.W. Boyd, "Exact solution to simultaneous intensity and phase encryption with a single phase-only hologram," Opt. Lett. 38, 3546-3549 (2013)

[2] S. Lightman, G. Hurvitz, R. Gvishi, and A. Arie, "Miniature wide-spectrum mode sorter for vortex beams produced by 3D laser printing," Optica 4, 605-610 (2017). [3] C. Brunet, B. Ung, L. Wang, Y. Messaddeq, LaRochelle, [3] C. Brunet, B. Ung, L. Wang, Y. Messaddeq, LaRochelle, OAM transmission studies," Opt. Express **23**, 10553 (2015).

*Corresponding author: shlomi.litman@gmail.com

†Corresponding author: lavisomers@tau.mail.ac.il

‡Corresponding author: ilan.bleyhman@gmail.com

# Transversal movement transfer of light carrying OAM to single trapped $^{40}Ca^{+}$ ions

**Felix Stopp**[*1], **Maurizio Verde**[1], **Milton Katz**[2], **Martín Drechsler**[2], **Sebastian Wolf**[1], **Christian T. Schmiegelow**[2], **Ferdinand Schmidt-Kaler**[1]

*1. QUANTUM, Institut für Physik, Johannes Gutenberg-Universität Mainz, Staudingerweg 7, 55128 Mainz*

*2. Departamento de Física and IFIBA, FCEN, Universidad de Buenos Aires, Ciudad Universitaria, Pabellón I, 1428 Ciudad de Buenos Aires*

We present measurements showing the transfer of the orbital angular momentum of a laser beam to the transversal movement of the center of mass of a trapped ion. For this, we rely on single $^{40}Ca^{+}$ ions confined in a segmented Paul trap with trap frequencies $\omega_{\mathrm{rad}} \approx 2\pi \cdot 2\,\mathrm{MHz}$ and $\omega_{\mathrm{ax}} \approx 2\pi \cdot 700\,\mathrm{kHz}$. An additional homogeneous magnetic field of $\sim 3\,\mathrm{G}$ splits the narrow $S_{1/2} \leftrightarrow D_{5/2}$ transition near 729 nm into Zeeman sublevels. The setup is designed in such a way that a laser beam, switchable between different structures through holographic pitch-fork pattern, is focused on the ion from the trap's radial direction. By using a lens with numerical aperture of NA $= 0.3$ we reach focus sizes of $< 3\mu$m for the OAM beam [1]. The extra angular momentum from the structure of the beam can be used to drive transitions forbidden for Gaussian beams, as shown in previous experiments [2].

Here we investigate the transfer to the center-of-mass motion in transversal direction to the **k** vector, impossible for a Gaussian beam. In particular, we drive the transition $|m_j = -1/2\rangle$ to $|m_{j'} - 3/2\rangle$, whose spectrum is extended by motional sidebands, see Fig 1. Cooling the transversal motional modes to $\langle n_{\mathrm{th}} \rangle \simeq 0.2$, we can demonstrate coherent Rabi oscillations on the sideband, parametrized by a new Lamb-Dicke parameter, which now depends on the extention of the transverse gradient to the size of the wavepacket. In future we plan the usage of OAM light on two-ion crystals to create a so-called two-ion rotor [3].

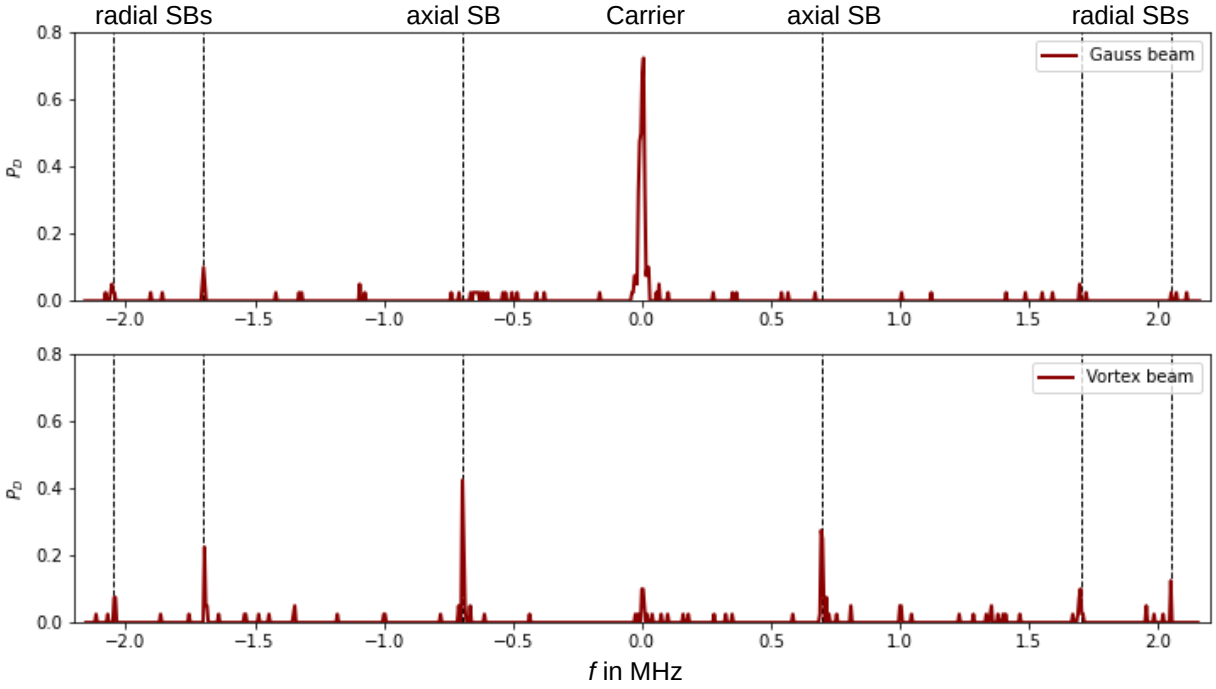


**Fig. 1:** Spectrum of the $S_{1/2}|-1/2\rangle \leftrightarrow D_{5/2}|-3/2\rangle$ transition for a) Gaussian beam and b) Laguerre-Gaussian beam with phase-singularity. Transversal motional modes at $\approx 700\,\mathrm{kHz}$ occur only for b) because of the additional OAM carried in the structure of the beam.

## References

[1] M. Drechsler et al., Phys. Rev. Lett. **127** 143602 (2021)
[2] C.T. Schmiegelow et al., Nat. Comm. **7** 12998 (2016)
[3] A. Afanasev, C. E. Carlson and A. Mukherjee, arXiv 09655v1 (2022)

*Corresponding author: felstopp@uni-mainz.de

# Inhomogeneous Dirac-Bloch Equations for Graphene Interacting with Structured Light

**Yaraslau Tamashevich**[*1], **Marco Ornigotti** [1]
*1. Faculty of Engineering and Natural Sciences, Tampere University, Tampere, Finland*

In this work, we extend the usual Dirac-Bloch equation approach [6] to study the nonlinear response of graphene [1] (and graphene-like materials) to an external electromagnetic pulse, to the case of an impinging structured light pulses [5], i.e., an optical pulse with a spatially inhomogeneous electric field and develop a framework that allows to calculate nonlinear current and nonlinear optical response of graphene-like materials when excited by structured light.

We start by considering the minimally coupled, low-energy Hamiltonian for graphene electrons interacting with an external electromagnetic field described by a vector potential $\mathbf{A}(\mathbf{r},t)$ in the Coulomb gauge, i.e., $\nabla\cdot\mathbf{A}=0$, which reads $\hat{H}(\mathbf{k})=\hbar v_f(\sigma_x k_x+\xi\sigma_y k_y)+H_i$, where $v_f$ is the Fermi velocity, and $\sigma_i$ are Pauli matrices, and $\xi=\pm1$ is the valley index, and $\hat{H}_I$ is the interaction Hamiltonian in the electric dipole approximation, whose explicit expression is given by $\mathbf{r}\cdot\mathbf{E}_T(\mathbf{r},t)$

Moreover, we also neglect the Coulomb interaction terms, since they don't contribute significantly for the case of graphene [1], and we assume that the standard electric dipole approximation for light-matter interaction holds.

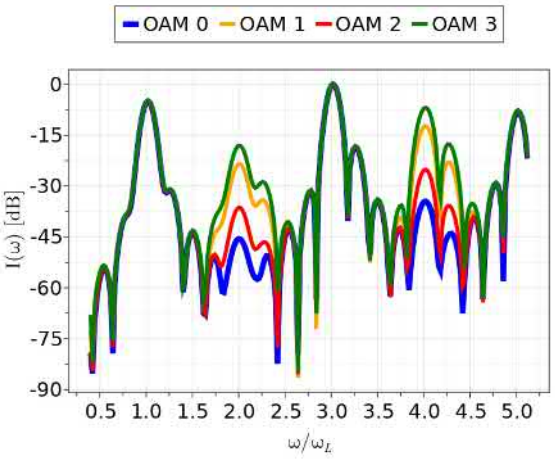


Figure 1: Nonlinear Optical Response $I(\omega)$ of graphene, as a function of the different harmonics of the carrier frequency $\omega_L$ of the impinging Laguerre-Gaussian

To calculate the explicit expression for the interaction Hamiltonian we use the Bloch Ansatz and assume, as usual, only nearest neighbour coupling, such that $\mathbf{R}_\ell=\mathbf{R}_m-\mathbf{R}_n$ is only significant for $\ell=\{0,\pm1\}$. Moreover, we make the extra assumption that the electric field is constant over a single unit cell [2], i.e., $\mathbf{E}_T(\mathbf{x}+\mathbf{R}_n,t)\simeq\mathbf{E}_T(\mathbf{R}_n,t)$. Taking these approximation into account, and describing everything in Fourier space, we get the following expression for the second quantized interaction Hamiltonian, in the lattice basis

$$\hat{H}_I=\sum_q \mathscr{E}_T(\mathbf{q},t)\mathbf{d}(\mathbf{k}-\mathbf{q})\hat{a}_k^\dagger\hat{b}_{k-q}, \tag{1}$$

where $\hat{a}_k^\dagger$ $\left(\hat{b}_k^\dagger\right)$ creates an electron on lattice A (B), $\mathscr{E}_T(\mathbf{q},t)$ is the angular spectrum of the impinging pulse, and $\mathbf{d}(\mathbf{k})$ is the (conduction-to-valence) electric dipole moment of graphene. We can transform the interaction Hamiltonian in the electron-hole representation by means of the unitary transformation given by diagonalisation of free Hamiltonian. To calculate the Dirac-Bloch equations, we introduce the following two-body populations and polarisation $n_e(\mathbf{k},\mathbf{q})=\langle\hat{e}_k^\dagger\hat{e}_q\rangle$, $n_h(\mathbf{k},\mathbf{q})=\langle\hat{h}_{-k}^\dagger\hat{h}_{-q}\rangle$, $p(\mathbf{k},\mathbf{q})=\langle\hat{h}_{-k}\hat{e}_q\rangle$, and calculate their time derivative with the help of the Heisenberg equation. To build the nonlinear optical responce of graphene, we need to calculate the induced (nonlinear) current. To do so, we use the usual definition of current, in terms of population and polarisation

$$\hat{\mathbf{j}}(t)=\sum_{k',k,q}\hat{\psi}_{k'}^\dagger U^\dagger(\mathbf{k}')\nabla_k h_I(\mathbf{k},\mathbf{q})U(\mathbf{k}-\mathbf{q})\hat{\psi}_{k-q}, \tag{2}$$

where we work in the interaction picture, so that the k-dependent interaction Hamiltonian, in the band representation,is $h_I(\mathbf{k},\mathbf{q})=\hbar\sigma\cdot\Omega$, where $\Omega$ is the generalized Rabi frequency. To characterize structured light impact on nonlinear optical response of graphene we solve Dirac-Bloch equation for external field defined by Laguerre-Gaussian beam with different orbital angular momentum (OAM). We then calculate the nonlinear signal with the relation $I(\omega)\sim|\omega\mathbf{J}(\omega)|^2$ [2]. The nonlinear optical response of the graphene for the case of impinging LG beams which carrier different OAM is shown in Fig. 1. We see that the presence of OAM breaks the centrosymmetry of graphene because under the influence of OAM, two valies differ from each other. And when we calculate current, generated by one of the valies, the absolute values of it differs from the current that a generated in another values more and more while we increase OAM of the impinging pulse.

## References

[1] Novoselov, K. S., Geim, A. K., Morozov, S. V., Jiang, D., Zhang, Y., Dubonos, S. V., Grigorieva, I. V., Firsov, A. A.,Science, **306**, 666–669. (2004)
[2] Kuklinski, J. R., Mukamel, S. Phys. Rev. B, **44**, 11253(1991)
[3] Ishikawa, K. L., Phys. Rev. B, **82**, 201402 (2010)
[4] Vozmediano, M. A. H., Katsnelson, M. I., Guinea, F. Physics Reports, **496**, 109–148. (2010).
[5] Allen, L., Beijersbergen, M. W., Spreeuw, R. J. C., Woerdman, J. P. Phys. Rev. A, **45**, 8185. (1992)
[6] Wallace, P. R. Physical review, **71**, 622. (1947)

*Corresponding author: yaraslau.tamashevich@tuni.fi

# Optical super-resolution sensing of a trapped ion's wave packet size

**Maurizio Verde**[*1], **Felix Stopp** [1] **Martín Drechsler**[†2], **Sebastian Wolf,** [1], **C. T. Schmiegelow,** [2], **Ferdinand Schmidt-Kaler** [1]

*1. QUANTUM, Institut für Physik, Universität Mainz, Staudingerweg 7, 55128 Mainz, Germany.*

*2. Departamento de Física and IFIBA, FCEN, Universidad de Buenos Aires, Ciudad Universitaria, Pabellón I, 1428 Ciudad de Buenos Aires, Argentina.*

The phase-singularity on the optical-axis gives rise to unique properties in single atom light-matter interaction. Here, we demonstrate super-resolution optical sensing of the size of the wave packet of a single trapped ion. Our method extends the well-known ground state depletion (GSD) technique to the coherent regime. We use a hollow beam to strongly saturate the coherently driven dipole-forbidden $|4S_{1/2}\rangle \leftrightarrow |3D_{5/2}\rangle$ transition near 729 nm around a sub-diffraction limited area at its center and observe state dependent fluorescence. By spatially scanning this laser beam over a single trapped $^{40}Ca^{+}$ ion, we are able to measure the wave packet sizes of cooled ions [1]. Using a depletion beam waist of 2.2(1) $\mu$m we reach a spatial resolution of about 50 nm. We use two different shape pulses giving rise to either Rabi oscillations or Rapid Adiabatic Passage (RAP) quantum dynamics, see Fig. 1. In order to search for the optimal geometry of light-matter interaction and maximize the achievable spatial resolution, we generalized the theoretical framework to predict space-dependent quadrupole transition amplitudes for different polarizations and for any relative orientation between the electronic eigenstates quantization axis and the laser beam optical axis. We used the spherical tensor decomposition for the multipoles expansion of the interaction Hamiltonian to account for a general vector electric field geometry beyond the paraxial approximation in order to quantify the role of the various electric field gradients terms driving the quadrupole transitions near the phase-singularity. The quadrupole transition $|4S_{1/2}, m = -\frac{1}{2}\rangle \leftrightarrow |3D_{5/2}, m = -\frac{3}{2}\rangle$ with parallel configuration between the magnetic field quantization axis and the vortex beam optical axis, results to be the more suitable geometry to maximize the spatial resolution while minimizing the perturbations from unavoidable magnetic field fluctuations and off-resonant transitions.

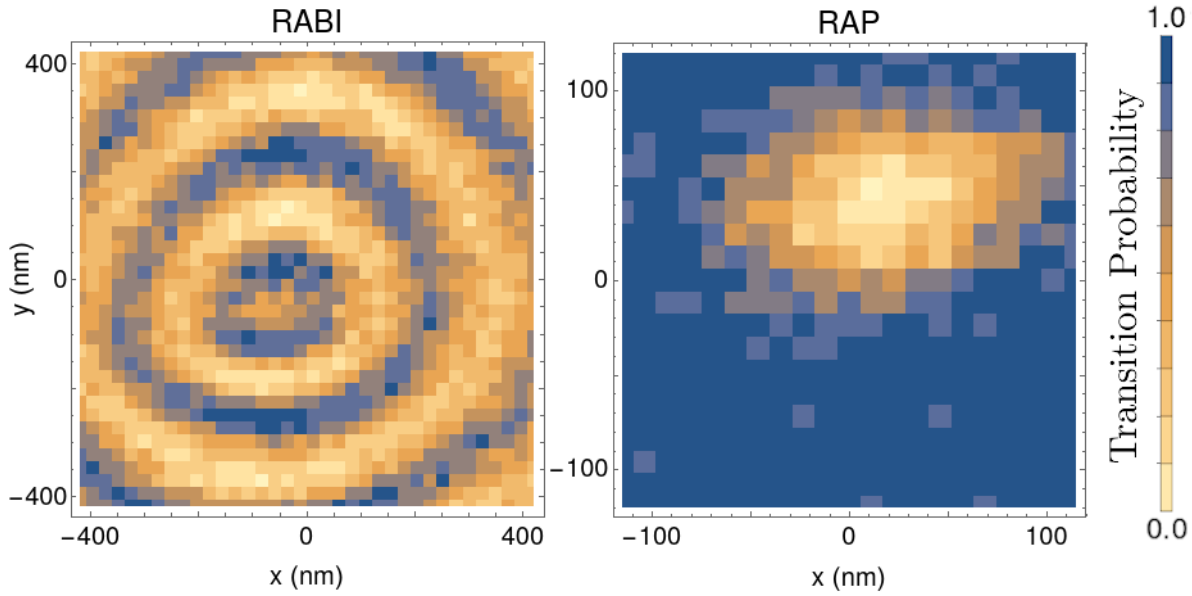


**Fig. 1:** Imaging the quantum wave packet of a single trapped ion in a thermal state at 0.5 mK temperature by using vortex light either driving Rabi flopping (on the left) or RAP single ion quantum dynamics (on the right).

We experimentally observed a single trapped ion thermal wave packet with both shape pulses reaching a sub-diffraction spatial resolution about 50 nm. By driving Rabi dynamics several rings are visible, while with RAP pulses the single ion is excited when it interacts out of the vortex beam dark spot. We are discussing the achievable resolution, that is dominated by thermal mechanical drifts of the setup, misalignment of the magnetic field and the occurrence of parasitic off-resonant transitions.

## References

[1] M. Drechsler, S. Wolf, C. T. Schmiegelow, F. Schmidt-Kaler Phys. Rev. Lett. **127** 143602 (2021)

[*]Corresponding author: mauverde@uni-mainz.de

[†]Corresponding author: martindrech@df.uba.ar

# Cold Spots: A Meeting Point for Polarisation Singularities, and their Complete

**Alexander J. Vernon**[*2], **Mark R. Dennis** [2], **Francisco J. Rodríguez-Fortuño**[† 1]
*1. Department of Physics, King's College London, Strand, London, WC2R 2LS, UK*
*2. School of Physics and Astronomy, University of Birmingham, Birmingham, B15 2TT, UK*

Cold spots are dark, three-dimensional, and sub-wavelength pockets which might emerge near a nanoantenna when all three electric field components cancel out at a single point. Similar regions of zero electric field are applied to diffraction limitbeating microscopy techniques [1,2], such as MINFLUX [3], and commonly delivered in two-dimensional form by a doughnut beam. An illuminated nanoantenna holds the potential for control of a more confined, three-dimensional zero in the form of a cold spot. Though previously explored in the literature, the current extent of cold spot position control is an ON/OFF switching behaviour between a few well-known locations or involves a physical change to the nanoantenna shape. We show that by changing only the polarisation, amplitude, and phase of two plane waves, a unique, zero-magnitude and highly sub-wavelength cold spot can be created and moved anywhere in the space around a nanoantenna of any arbitrary shape. The technique exploits the linearity of Maxwell's equations and could be adapted to manipulate any phenomena governed by the linear wave equation, including acoustic scattering. We prove that three-dimensional cold spots are a natural meeting point for threads of circular (Cline) and linear (L-line) polarisation. A general cold spot is shown to be an intersection of either zero or two C-lines and one or three L-lines. When the spatial derivatives of the electric field are also zero in the cold spot, the cold spot becomes an even more complicated polarisation singularity junction.

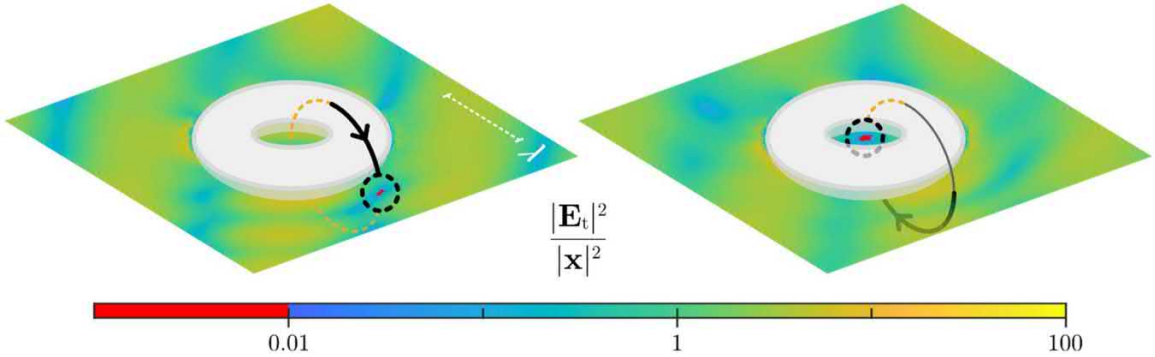


**Fig. 1:** Two frames of a cold spot as it moves along a circular path around a silver torus particle by changing, in a time-harmonic approximation, the polarisation, relative intensity, and phase of two plane waves with $\lambda = 800$ nm. The plot shows the local field intensity, $|\mathbf{E}_t|^2$, relative to the combined intensity of the plane waves, $|\mathbf{x}|^2 = |\mathbf{E}_{pw1}|^2 + |\mathbf{E}_{pw2}|^2$.

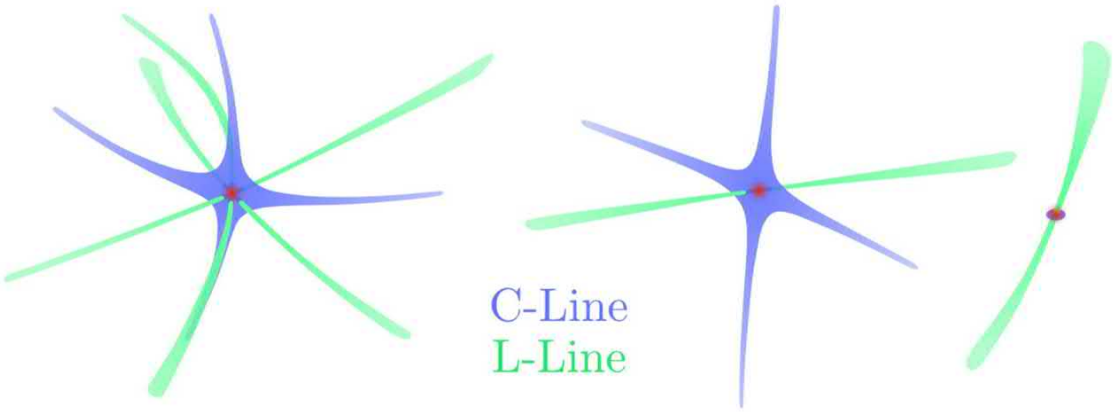


**Fig. 2:** Three examples of polarisation singularities meeting at a general cold spot (red) where $\mathbf{E} = \mathbf{0}$. Blue regions are C-lines, where $\mathbf{E} \cdot \mathbf{E} \approx \mathbf{0}$. Green regions are L-lines, where the Stokes parameter $S3 \approx 0$. Either zero or two C-lines and one or three L-lines cross.

## References

[1] Hell, S. W., & Wichmann, J. (1994). Opt. Lett. 19(11), 780 .
[2] Rust, M. J., Bates, M., & Zhuang, X. (2006). Nat. Methods, 3(10), 793-796.
[3] Betzig, E., et. al. (2006). Science, **313**(5793), 1642 – 1645.

[*]Corresponding author: alexander.vernon@kcl.ac.uk
[†]Corresponding author: francisco.rodriguez_fortuno@kcl.ac.uk

# Environment-modified Three-body Energy Transfer

**Maddie Waller**[*1], **Robert Bennett** [1]
*1. School of Physics Astronomy, University of Glasgow, Glasgow G12 8QQ, United Kingdom*

Resonant energy transfer from a donor to an acceptor is one of the most basic interactions between atomic and molecular systems. In real-life situations, the donor and acceptor are not isolated, but in fact coupled to their environment and to other atoms and molecules. The presence of a third body can modify the rate of energy transfer between donor and acceptor in distinctive and intricate ways, especially when the three-site system is itself interacting with a larger macroscopic background such as a solvent. The rate can be calculated perturbatively, which ordinarily requires the summation of very large numbers of Feynman-like diagrams. Here we demonstrate a method based on canonical perturbation theory that allows us to reduce the computational effort required. We use this technique to derive a formula for the rate of three-body resonance energy transfer in a background environment and apply this to some simple cases including for example enhanced transfer rates for atoms in angular momentum states.

[*]Corresponding author: m.waller.1@research.gla.ac.uk

# Helicity in a chiral Hopfield dielectric

**Neel Mackinnon**[1], **Jörg Götte**[1], **Niclas Westerberg**[*1]
*1. School of Physics and Astronomy, University of Glasgow, Glasgow, G12 8QQ, United Kingdom*

It is well known that helicity is closely linked to the Heaviside-Lorentz, or duality, symmetry of Maxwell's equations. Indeed, helicity is the conserved charge generated by duality symmetry. The generalisation of duality symmetry to the macroscopic Maxwell's equations can, however, take multiple forms, where the emphasis is either on the displacement and magnetic induction fields $(\mathbf{D},\mathbf{B})$ [1][2], or on the electric and magnetic fields $(\mathbf{E},\mathbf{H})$ [3][4]. Whilst the former has been investigated in the context of helicity, the latter is much less explored. In particular, by focusing on the electric ($\mathbf{E}$) and magnetic ($\mathbf{H}$) fields, we can explicitly treat duality transformations on the polarisation ($\mathbf{P}$) and magnetisation ($\mathbf{M}$) fields, and any associated internal material degrees of freedom. Here we study this and investigate the notion of helicity in a general lossless linear dielectric, where the medium polarisation and magnetisation are obtained through phenomenological microscopic degrees of freedom as in the Hopfield model [5]. The helicity is generated by the duality transform

$$\begin{pmatrix} \mathbf{E}' \\ \mathbf{H}' \end{pmatrix} = \begin{pmatrix} \cos\theta & \sin\theta \\ -\sin\theta & \cos\theta \end{pmatrix} \begin{pmatrix} \mathbf{E} \\ \mathbf{H} \end{pmatrix}, \tag{1}$$

where $\mathbf{D}$ and $\mathbf{B}$ transform analogously, and where we have the constitutive equations $\mathbf{D}=\mathbf{E}+\mathbf{P}$, and $\mathbf{B}=\mathbf{H}+\mathbf{M}$. Note that we work in units such that $c=1=\varepsilon_0$. A general medium is then described by

$$\begin{aligned} \mathbf{P} &= \alpha\mathbf{E}+(\gamma+iG)\mathbf{H} = \alpha\mathbf{X}+(\gamma+iG)\mathbf{Y}, \\ \mathbf{M} &= \beta\mathbf{H}+(\gamma-iG)\mathbf{E} = \beta\mathbf{Y}+(\gamma-iG)\mathbf{X}, \end{aligned} \tag{2}$$

where $\alpha$ and $\beta$ are the electric and magnetic polarisabilities, $\gamma$ is the electromagnetic coupling and $G$ is the chiral coupling. We have here introduced the phenomenological microscopic degrees of freedom $\mathbf{X}$ and $\mathbf{Y}$ in the Hopfield manner [5] in order to model a dispersive medium with a single resonance each for the electric and magnetic responses.

First of all, by Noether's theorem and a suitably chosen Lagrangian, we show that the in-medium helicity density and helicity-density current is given by

$$h = \frac{1}{2}\left(\mathbf{A}\cdot\mathbf{B}+\mathbf{C}\cdot\mathbf{D}\right)+\dot{\mathbf{X}}\cdot\mathbf{Y}-\dot{\mathbf{Y}}\cdot\mathbf{X}, \tag{3}$$

$$\mathbf{j} = \frac{1}{2}\left(\mathbf{E}\times\mathbf{A}-\mathbf{H}\times\mathbf{C}\right), \tag{4}$$

where the electric vector potential $\mathbf{C}$ is defined by $\nabla\times\mathbf{C}=\mathbf{D}$. We would note that this helicity density reduces to the usual expression in vacuum, and acts as a generator of the chosen duality transform. Interestingly, we find that the requirements for a medium to be 'duality symmetric' are similar to those obtained by purely macroscopic treatments such as [1]: we require that $\varepsilon(\omega)=\mu(\omega)$ and $\gamma=0$. Finally, when expressed in terms of the natural excitations of such a system, i.e. the polaritons, we find that the total helicity takes the satisfyingly simple form

$$\hat{h}_{\text{total}} = \sum_i \int d^3k\, \hat{n}_i(\mathbf{k},+)-\hat{n}_i(\mathbf{k},-), \tag{5}$$

where $\hat{n}_i(\mathbf{k},\pm)$ is the polariton number operator in the $i^{\text{th}}$ polariton mode and with right-handed $(+)$, or left-handed $(-)$, circular polarisation. In other words, akin to the free space expression, the total helicity is the difference between the number of polaritons in the right-hand circular and the left-hand circular polarisations. As such, we find that this is a natural extension to the notion of helicity in a linear dielectric.

## References

[1] K. Van Kruining, J. Götte, Journal of Optics **18**, 085601 (2016)
[2] F. Alpeggiani, K. Y. Bliokh, F. Nori, L. Kuipers, Phys. Rev. Lett. 120, 243605 (2018)
[3] N. Westerberg, A. Messinger, S. M. Barnett, arXiv:2112.05762 (2021)
[4] S. Y. Buhmann, *Macroscopic quantum electrodynamics and ground-state Casimir, Casimir-Polder and van der Waals forces*, Vol. 247, Springer.
[5] J. J. Hopfield, Phys. Rev. 112, 1555 (1958).

*Corresponding author: Niclas.Westerberg@glasgow.ac.uk

# Faraday effect for vector vortex beams

**Zhujun Ye**[*1], **Jörg B. Götte** [1], **Sonja Franke-Arnold** [1]
*1. School of Physics and Astronomy, University of Glasgow, Glasgow, G12 8QQ, Scotland*

In this work we show that the Faraday effect can be used to manipulate vector vortex beams. For example, it can turn radially polarized beams into azimuthally polarised ones. Owing to the difference in propagation for left and right circularly polarized light, this transformation is, however, not perfect, and additional effects occur. We characterise these smaller effects for both paraxial and highly focussed light, where they become much stronger.

When a linearly polarized light beam passes through a static magnetic field which is aligned along the direction of optical axis, the direction of polarization changes on propagation. For a plane wave this constitutes the well known Faraday effect, which is known to be the first experimental evidence revealing the relation between light and electromagnetism [1]. We investigate the Faraday effect for light beams of a more complicated structure, for example vector vortex beams. We show mathematically and by simulation that when passing through a Faraday medium, a paraxial vector vortex beam will experience small corrections to the Faraday effect, based on the differential propagation of circularly polarized light. We can increase the effect of these corrections by focussing the light beam strongly. We simulate the propagation of a strongly focussed light beam using the method by Richards and Wolff [2][3]

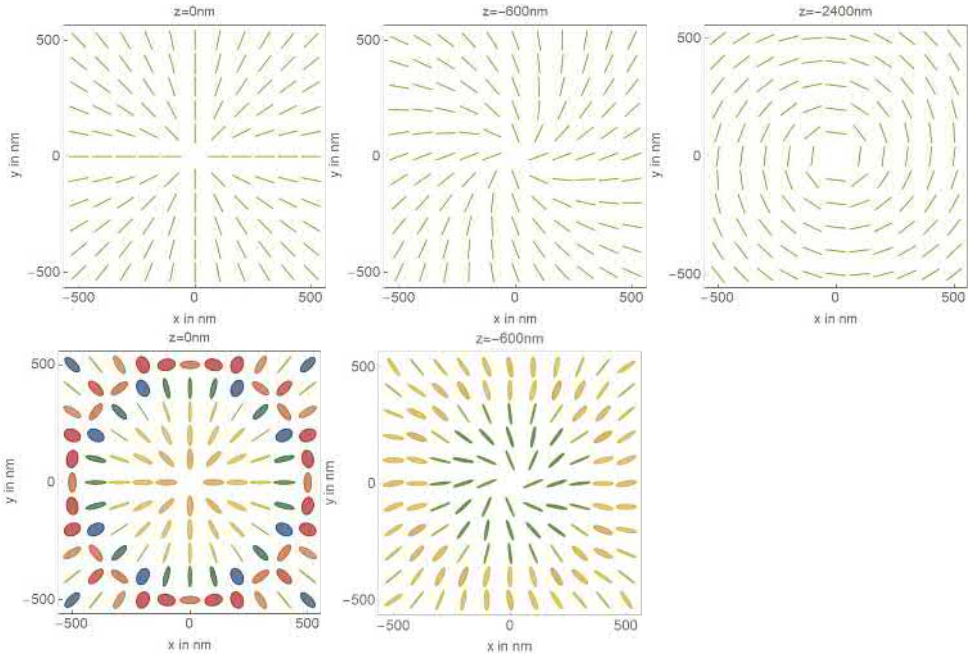


**Fig. 1:** Comparison between Faraday effect on paraxial beams (above) and highly focused field (below).

[1] Berman, P. (2010). Optical Faraday rotation. American Journal Of Physics, 78(3), 270-276. doi: 10.1119/1.3266970

[2] B. Richards and E. Wolf, "Electromagnetic diffraction in optical systems. II. Struc- ture of the image field in an aplanatic system," Proc. Roy. Soc. A 253, 358–379 (1959).

[3] Novotny, L., Hecht, B. (2019). Principles of nano-optics. Cambridge: Cambridge University Press.

*Corresponding author: 2423997y@student.gla.ac.uk

# A double-clad ytterbium-doped tapered fiber with circular birefringence as a gain medium for structured light

**Iuliia Zalesskaia**[*1], **Yuhao Lei** [2], **Peter G. Kazansky** [1,2], **Regina Gumenyuk** [1,3], **and Valery Filippov** [3]

*1. Tampere University, Tampere, Finland*

*2. Optoelectronics Research Centre, University of Southampton, Southampton, UK*

*3. Ampliconyx Ltd, Tampere, Finland*

The technology of active tapered double-clad fibers (T-DCF) has been developing rapidly during the last decades. Due to a special geometrical architecture, T-DCF supports only the launched mode propagation and enables elevation of the nonlinear effects threshold, which was widely explored for the development of high peak power/energy laser systems with pure Gaussian beam. Recently, our group has demonstrated a new type of T-DCF - so-call spun T-DCF (sT-DCF) supporting the propagation and amplification of radially polarized light becoming an attractive gain medium for high power structured beam [1]. Radially polarized beams with a doughnut-shaped intensity profile have attracted a great interest in recent years owing to a wide range of applications, such as particle acceleration and trapping, high-resolution microscopy, optical data storage and material processing driving a significant performance improvement [2]. In this work, we demonstrate the successful direct amplification of a radially-polarized beam carrying 10 ps pulses at 1030 nm.

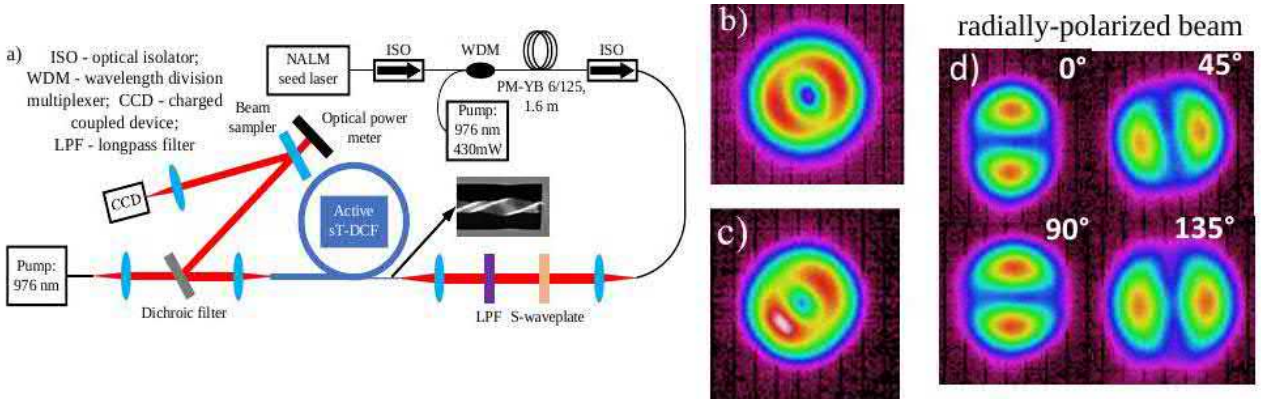


**Fig. 1:** (a) The Schematic of the experimental setup (inset: the side view of the sT-DCF); (b) experimental sT-DCF output intensity distributions in the near-field (b) without amplification and (c) for output power 20 W; d) beam profile after passage through a rotated polarizer.

Figure 1 (a) shows the experimental setup for amplification of a radially polarized beam in a Yb-doped sTDCF (inset Fig. 1(a)). The narrow side of the sT-DCF had a core diameter of 16.5$\mu$m and a numerical aperture (NA) of 0.1. The normalized frequency parameter for the narrow side of the sT-DCF was 5.05 at 1030 nm which enabled only the fundamental $LP_{01}$ mode and higher order $LP_{11}, LP_{21}$, and $LP_{02}$ modes to be propagated in the core. The linearly-polarized beam carrying 10ps pulses at a 15MHZ repetition was generated by a nonlinear amplifying loop mirror (NALM) seed laser and pre-amplified up to 50 mW. The radiallypolarized beam was formed by a spatially-variant waveplate (S-waveplate) and injected into the narrow side of sT-DCF. Pump light, provided by a laser diode at 976 nm, was launched through the dichroic filter into the sT-DCF from the wide side. The sT-DCF-based amplifier generated an output power of 20 W for the directly amplified short-pulsed signal at the 60 W pump power. Output sT-DCF beam profiles before and after amplification are shown in Figure 1$(b, c)$.

The progress in the development of high-power structured light will have a dramatic impact on all laserinduced technologies bringing an additional degree of process control. In the next steps, our research work will be focused on an increase in average output power and signal-to-background ratio.

## References

[1] J. Rissanen, A. Fedotov, T. Noronen, R. Gumenyuk, Yu. Chamorovskiy, A. Kolosovskii, V. Voloshin, I. Vorobev, M. Odnoblyudov, and V. Filippov, "Large-mode-area double clad ytterbium-doped tapered fiber with circular birefringence," Proc.SPIE 10897, pp. 342–394, 2019.

[2] K. Venkatakrishnan, and B. Tan, "Interconnect microvia drilling with a radially polarized laser beam," J Micromech Microeng 16, pp. 2603-2607, 2006.

*Corresponding author: iuliia.zalesskaia@tuni.fi

# ICOAM gift from IOP Publishing

Three free books from IOP!

Each book can be consulted online or downloaded for free during the whole ICOAM week, ONLY if the link is accessed through the Tampere University WiFi (all the TUNI/TAU internet connections should work).

It is possible to download the pdf, and one can keep it for personal use after the conference, but the links will expire at the end of ICOAM.

- D. S. Simon, A Guided Tour of Light Beams (Second Edition)
  https://iopscience.iop.org/book/978-0-7503-3467-9
- P. K. Khare, Orbital Angular Momentum States of Light
  https://iopscience.iop.org/book/978-0-7503-2280-5
- D. S. Simon, Topology in Optics (Second Edition)
  https://iopscience.iop.org/book/978-0-7503-3471-6

## Contact


Local organizers: Marco Ornigotti (marco.ornigotti@tuni.fi)

Robert Fickler (robert.fickler@tuni.fi)

Support Team: Subhajit Bej, Rafael F. Barros, Matias Eriksson, David T. Garcia, Markus Hiekkamäki, Matias Koivurova, Lea Kopf, Oussama Korichi, Madona Mekhael, Yaraslau Tamashevich

Practical arrangements: congress@tuni.fi


## Sponsors